

Exodermal Function and Suberin Chemistry

by

Christopher John Meyer

A thesis

presented to the University of Waterloo

in fulfilment of the

thesis requirement for the degree of

Doctor of Philosophy

in

Biology

Waterloo, Ontario, Canada, 2010

© Christopher John Meyer 2010

Author's Declaration

I hereby declare that I am the sole author of this thesis. This is a true copy of the thesis, including any required final revisions, as accepted by my examiners.

I understand that my thesis may be made electronically available to the public.

Abstract

The thesis work concerns the multiseriate exodermis (MEX), an outermost cortical layer (two or more cell layers thick) characterized by Casparian bands and suberin lamellae. Diverse aspects of *Iris germanica*'s MEX were examined including its maturation under differing growth conditions, and how this maturation affected water and solute permeability. Also, suberin metabolite profiles for the maturing MEX of *I. germanica* and the maturing uniseriate exodermis of *Allium cepa* were established. This multidisciplinary approach resulted in a comprehensive understanding of how anatomical and biochemical changes to the exodermis affect water and solute permeability of the MEX.

Most previous studies of exodermal development have involved species with a uniseriate exodermis. To extend this work, the MEX in *I. germanica* roots was investigated. The outermost exodermal layer matured first with normal Casparian bands and suberin lamellae. But as subsequent layers matured, the Casparian band extended into the tangential and anticlinal walls of their cells. This atypical Casparian band was continuous around the root circumference. MEX maturation was influenced by the roots' growth medium. Plants were grown in soil or hydroponics (with and without a humid air gap), and their roots were sectioned and stained with various dyes to detect Casparian bands and suberin lamellae. In soil-grown roots, the exodermis started maturing (with concurrent deposition of Casparian bands and suberin lamellae) 10 mm from the root tip, and two layers had matured by 70 mm. In hydroponically grown roots, exodermal maturation was delayed. However, in basal regions exposed to an air gap in the hydroponic tank, maturation of the second exodermal

layer was accelerated. Therefore, changes in growth conditions have striking effects on exodermal maturation in *I. germanica*.

With respect to radial water and solute transport, *I. germanica* roots with a mature MEX had lower permeability rates compared with uniseriate exodermal roots or roots in which the endodermis represents the major transport barrier. Transport studies were conducted on completely submerged roots and air gap-exposed root regions using a pressure chamber whereby water permeability ($L_{p_{pc}}$) was measured quantitatively across the entire root. This instrument proved to be preferable because in large diameter roots (up to 2.5 mm in *I. germanica*), root hydraulics were affected by the large water storage capacity of the central cortex. Compared with regions of roots with no mature exodermal layers, the mature MEX reduced $L_{p_{pc}}$ from 8.5×10^{-8} to $3.9 \times 10^{-8} \text{ m s}^{-1} \text{ MPa}^{-1}$. Puncturing the MEX increased $L_{p_{pc}}$ to $19 \times 10^{-8} \text{ m s}^{-1} \text{ MPa}^{-1}$, indicating that the MEX is an important hydraulically resistant tissue. A root pressure probe was used to measure the permeability of roots to NaCl and ethanol; solute permeability was reduced in the presence of two mature MEX layers. The MEX of *I. germanica* should play an important role in survival under conditions of drought and salt stress.

Suberin is a complex biopolymer with a poly(aliphatic) domain (SPAD) that, in the case of a suberin lamellae, is known to be located between the cell wall and plasma membrane. The location and lipophilic nature of the SPAD establishes it as a structure restrictive to radial water transport through the transcellular pathway. Synthesis of the SPAD in a maturing exodermis was not well understood. Hence, a suberin metabolite analysis during development was conducted on the maturing MEX of *I. germanica* grown in submerged and

air gap hydroponic conditions. Suberin monomers of the soluble (unpolymerized) and insoluble (polymerized) fractions were chemically isolated, then quantified and identified by GC-MS. Interestingly, in air gap-exposed regions, there was an increased synthesis and deposition of insoluble SPAD monomers in the first two exodermal layers, compared with submerged regions. The SPAD fraction included fatty acids, α,ω -dioic acids, ω -OH fatty acids, and ferulic acid, with C18:1 α,ω -dioic acid and ω -OH fatty acid being the two most abundant monomers. Also, in tissue that matured in the air gap, the composition of the soluble fraction changed significantly among exodermal maturation stages and between growth conditions. Of particular significance, increased amounts of alkanes, the major component of waxes, accumulated in the first exodermal layer. Other monomers of the soluble fraction included fatty acids, fatty alcohols, and ferulic acid, that were SPAD biosynthetic precursors. It was postulated that the localized and abundant deposition of C18:1 α,ω -dioic acid and ω -OH fatty acid, along with high accumulation of intercalated waxes in the first mature exodermal layer, were more important than the overall number of suberized exodermal layers for reducing water loss from the root during drought.

Lastly, hydroponically grown *Allium cepa* roots were used as models to analyze SPAD synthesis in a maturing uniseriate exodermis. Roots were divided into four maturation zones based on the growth rate and the deposition of suberin lamellae in maturing exodermal cells as determined by histochemical analyses. The chemical composition of the soluble fraction was essentially unchanged as the exodermis matured. In contrast, the SPAD composition differed during maturation, mainly due to significant increases in the deposition of C18:1 α,ω -dioic acids and C18:1 ω -OH fatty acids. It is proposed that the exodermal maturation

zones with corresponding suberin metabolite profiles be used as targets for the functional enzymatic characterization of suberin biosynthetic pathways.

Acknowledgements

I thank my supervisor Prof. Carol A. Peterson for mentoring me during this most challenging and rewarding period in my life. Carol's encouragement and direction were essential to my success. Her investment in my professional development has transformed me into a confident, well-rounded, and mature scientist.

Many thanks to my fantastic collaborators for providing the training and insight that made this thesis work exciting and multi-faceted. Prof. Mark A. Bernards (London, Ontario) for his in-depth knowledge of suberin chemistry, Prof. Ernst Steudle (Bayreuth, Germany) for his expertise in plant-water relations, and Prof. James L. Seago, Jr. (Oswego, New York) for his assistance with understanding the root apical meristem.

Life in the lab was always a hospitable experience thanks to the many colleagues and friends that I had the pleasure of working with. Waterloo: Daryl Enstone, Lynn Hoyles, Prof. Barb Moffatt, Dr. Fengshan Ma, Ishari Waduware. Bayreuth: Dr. Kosala Ranathunge, Dr. Lukasz Kotula, Burkhard Stumpf. London: Megan Haggitt, Dr. Raymond Thomas.

I thank my mother, father and sister for their unconditional love.

Lastly, I thank my partner and artistic director Jesseline Gough, whose love, support and mastery of illustration has made my life much more colourful.

Financial support was provided by an Alexander Graham Bell Canada Graduate Scholarship (Natural Sciences and Engineering Research Council), an Ontario Graduate Scholarship (Government of Ontario), and a President's Graduate Scholarship (University of Waterloo).

Table of Contents

Author's Declaration	ii
Abstract	iii
Acknowledgements	vii
Table of Contents	viii
List of Figures	xiii
List of Tables	xvi
List of Abbreviations.....	xviii

Chapter 1 - General introduction	1
1.1 Introduction	1
1.2 Root anatomy	2
1.2.1 Primary root tissue development and anatomy	2
1.2.2 Exodermal and endodermal cell ontogeny	3
1.2.3 Exodermal types, sub-types, and a variation	8
1.2.4 Multiseriate exodermal development	12
1.2.5 Growth conditions influence exodermal development.....	13
1.2.6 Research aims I	14
1.3 Root physiology.....	15
1.3.1 Root structure determines radial transport pathways	15
1.3.2 Water transport.....	18
1.3.3 Ion transport.....	19
1.3.4 Apoplastic tracers	22
1.3.5 Hydrostatic and osmotic pressure gradients	23
1.3.6 Pressure chamber.....	24
1.3.7 Root pressure probe.....	25
1.3.8 Quantitative measurements of water and solute permeability across the exodermis	31

1.3.9 Research aims II	36
1.4 Suberin chemistry and biosynthesis.....	37
1.4.1 What is suberin?.....	37
1.4.2 SPAD biosynthesis	40
1.4.3 SPPD biosynthesis.....	50
1.4.4 The role of glycerol	50
1.4.5 Physiological significance of suberin.....	51
1.4.6 Suberin deposition in maturing tissues	58
1.4.7 Suberin deposition in the exodermis of <i>Iris germanica</i> and <i>Allium cepa</i>	59
1.4.8 Research aims III.....	60
Chapter 2 - Environmental effects on the maturation of the endodermis and multiseriate exodermis of <i>Iris germanica</i> roots	63
2.1 Overview	63
2.2 Introduction	64
2.3 Materials and methods	68
2.3.1 Plant material and growth conditions	68
2.3.2 Root anatomy	72
2.3.3 <i>Iris germanica</i> root growth rate measurements.....	74
2.3.4 Apoplastic permeability.....	74
2.4 Results	77
2.4.1 <i>Iris germanica</i> root growth and anatomy	77
2.4.2 Ferrous sulphate toxicity in <i>Z. mays</i> roots	90
2.4.3 Root permeability to apoplastic tracers	91
2.4.4 Mature root anatomy of other soil-grown iris species	97
2.5 Discussion.....	98
2.6 Supplementary data.....	114

Chapter 3 - Permeability of <i>Iris germanica</i>'s multiseriate exodermis to water, NaCl and ethanol	115
3.1 Overview.....	115
3.2 Introduction.....	116
3.3 Materials and methods.....	121
3.3.1 Plant material and growth conditions.....	121
3.3.2 Root pressure probe experiments.....	123
3.3.3 Pressure chamber experiments.....	126
3.3.4 Resistance of the exodermis to water and solute flows.....	128
3.3.5 Statistical analyses.....	128
3.4 Results.....	129
3.4.1 Root anatomy.....	129
3.4.2 Measurements of hydraulic conductivity.....	134
3.4.3 Measurements of root permeability to solutes.....	148
3.5 Discussion.....	148
3.5.1 Root anatomy and cell viability.....	148
3.5.2 Measurements of radial water permeability.....	152
3.5.3 Solute permeability.....	157
3.5.4 Adaptive significance of the multiseriate exodermis in <i>I. germanica</i>	159
3.6 Conclusions.....	160

Chapter 4 - Suberin monomer analysis of <i>Iris germanica</i>'s multiseriate exodermis during maturation and under differing growth conditions	163
4.1 Overview.....	163
4.2 Introduction.....	164
4.3 Materials and methods.....	169
4.3.1 Growth conditions and plant material.....	169
4.3.2 Exodermal suberin extraction and analysis.....	170
4.4 Results.....	174

4.4.1 <i>I. germanica</i> exodermal anatomy.....	174
4.4.2 Suberin chemistry.....	175
4.5 Discussion.....	216
4.6 Supplementary data.....	223
Chapter 5 - Suberin biosynthesis in <i>Allium cepa</i>'s maturing exodermis.....	225
5.1 Overview.....	225
5.2 Introduction.....	226
5.3 Materials and methods.....	230
5.3.1 Growth conditions and plant material.....	230
5.3.2 Root growth rate measurements.....	231
5.3.3 Exodermal maturation.....	231
5.3.4 Root tissue isolation.....	234
5.3.5 Suberin monomer extraction and analysis.....	235
5.4 Results.....	238
5.4.1 <i>Allium cepa</i> root growth, anatomy, and exodermal maturation.....	238
5.4.2 Suberin chemistry.....	244
5.5 Discussion.....	269
Chapter 6 - General discussion.....	281
6.1 Exodermal development.....	281
6.2 Lateral root emergence.....	284
6.3 Hydraulic conductivity measurements.....	285
6.4 Exodermal suberin lamellae deposition reduces water permeability.....	286
6.5 The role of aquaporins.....	288
6.6 Cell viability and the symplastic pathway with respect to ion transport.....	288
6.7 How do roots tolerate salt stress?.....	290
6.8 Additional responses of roots to abiotic stress.....	293
6.9 The two-domain model of suberin lamellae.....	293

6.10 A revised chemical model for the Casparian band	294
6.11 Time course-based suberin metabolite analyses.....	296
6.12 Suberin biosynthetic enzymes	297
6.13 Conclusions	301
Appendices	
Appendix A - Supplementary Tables for Chapter 2	303
Appendix B - Supplementary Figures for Chapter 4	316
Appendix C - Declaration of research collaborations.....	332
References	333

List of Figures

Chapter 1

Figure 1.1 Cross section of an <i>Allium cepa</i> (onion) root.....	4
Figure 1.2 Illustrations of endodermal cells	6
Figure 1.3 Illustrations of four exodermal sub-types and one exodermal variation	10
Figure 1.4 Illustration of the three parallel, radial transport pathways	16
Figure 1.5 Drawing of the outer part of a root with a uniseriate exodermis.....	20
Figure 1.6 Illustration of the pressure chamber	26
Figure 1.7 Typical data obtained from pressure chamber experiments.....	28
Figure 1.8 Illustration of the root pressure probe.....	32
Figure 1.9 Typical data obtained from root pressure probe experiments.....	34
Figure 1.10 Chemical model of suberin lamellae	38
Figure 1.11 Transesterification of the poly(aliphatic) domain using MeOH/HCl.....	42
Figure 1.12 Depolymerization of the poly(phenolic) domain using NBO	44
Figure 1.13 Aliphatic monomers of suberin lamellae	46
Figure 1.14 Synthesis of two key aliphatic monomers.....	48
Figure 1.15 Pathway of the fatty acid elongation complex	52
Figure 1.16 Phenolic monomers of suberin lamellae	54
Figure 1.17 Synthesis of three key phenolic monomers.....	56

Chapter 2

Figure 2.1 Drawings of the hydroponic, air gap, and aeroponic systems.....	70
Figure 2.2 <i>Iris germanica</i> adventitious root tips in longitudinal and transverse sections	78
Figure 2.3 Outer part of <i>I. germanica</i> roots in cross and longitudinal section	82
Figure 2.4 Cross and longitudinal sections from <i>I. germanica</i> roots	84
Figure 2.5 Diagrams of key exodermal and endodermal developmental stages.....	88
Figure 2.6 The effect of FeSO ₄ exposure on the growth rates of <i>Z. mays</i> roots	92
Figure 2.7 Apoplastic permeability tests on <i>I. germanica</i> roots with berberine or FeSO ₄	94
Figure 2.8 Exodermis in transverse sections from roots of various iris species	100

Chapter 3

Figure 3.1 Drawing of the outer part of an <i>I. germanica</i> root in cross section.....	118
Figure 3.2 Drawings of two hydroponic systems with photomicrographs that represent typical effects of the growth conditions on the roots' epidermal viability and exodermal maturation.....	130
Figure 3.3 Sections of <i>I. germanica</i> roots grown in submerged or air gap hydroponic conditions	132
Figure 3.4 Water flow through roots during the pressure chamber experiments	136
Figure 3.5 Steady-state water flow per unit root surface area	138
Figure 3.6 Osmotic water and solute permeability graphs	150

Chapter 4

Figure 4.1 Cross sections of the outer part of <i>Iris germanica</i> roots.....	176
Figure 4.2 Total insoluble aliphatic suberin (SPAD) monomers in <i>Iris germanica</i> 's exodermis	178
Figure 4.3 Change in amounts of SPAD monomer classes in the maturing MEX.....	180
Figure 4.4 Deposition of α,ω -dioic acids in the SPAD	182
Figure 4.5 Deposition of ω -OH fatty acids in the SPAD	188
Figure 4.6 Deposition of fatty acids in the SPAD.....	190
Figure 4.7 Deposition of esterified ferulic acid in the SPAD.....	194
Figure 4.8 Total soluble fraction of <i>Iris germanica</i> 's exodermal suberin	198
Figure 4.9 Change in amounts of soluble monomer classes in the maturing MEX.....	200
Figure 4.10 Accumulation of fatty acids in the soluble fraction	202
Figure 4.11 Accumulation of alkanes in the soluble wax fraction	210
Figure 4.12 Accumulation of fatty alcohols in the soluble fraction.....	212
Figure 4.13 Accumulation of ferulic acid in the soluble fraction.....	214

Chapter 5

Figure 5.1 Illustration of the hydroponic system used to grow <i>Allium cepa</i> roots	232
Figure 5.2 Diagram of the key exodermal maturation zones in <i>Allium cepa</i> roots.....	240
Figure 5.3 <i>Allium cepa</i> roots in cross section and surface view	242
Figure 5.4 Total and individual insoluble SPAD monomers in <i>Allium cepa</i> 's exodermis ...	246
Figure 5.5 Total soluble monomer fraction of <i>Allium cepa</i> 's exodermal suberin.....	250
Figure 5.6 Accumulation of fatty acids in the soluble fraction.....	254
Figure 5.7 Accumulation of alkanes in the soluble fraction	256
Figure 5.8 Accumulation of fatty alcohols in the soluble fraction.....	260
Figure 5.9 Accumulation of ω -OH fatty acids in the soluble fraction	262
Figure 5.10 Accumulation of 2-OH fatty acids in the soluble	264
Figure 5.11 SPPD monomer deposition in <i>Allium cepa</i> 's exodermis.....	266

Appendix B - Supplementary Figures

Supp. Figure 4.1 Change in amount of α,ω -dioic acids in the SPAD in <i>I. germanica</i>	316
Supp. Figure 4.2 Change in amount of ω -OH fatty acids in the SPAD in <i>I. germanica</i>	318
Supp. Figure 4.3 Change in amount of fatty acids in the SPAD in <i>I. germanica</i>	320
Supp. Figure 4.4 Change in amounts of ferulic acid in the SPAD in <i>I. germanica</i>	322
Supp. Figure 4.5 Change in amount of soluble fatty acids in <i>I. germanica</i>	324
Supp. Figure 4.6 Change in amount of soluble alkanes in <i>I. germanica</i>	326
Supp. Figure 4.7 Change in amount of soluble fatty alcohols in <i>I. germanica</i>	328
Supp. Figure 4.8 Change in amounts of soluble ferulic acid in <i>I. germanica</i>	330

List of Tables

Chapter 2

Table 2.1 Rhizomatous <i>Iris</i> species' natural habitats are correlated with the type of exodermis they develop and whether aerenchyma is present or absent.....	96
Table 2.2 List of monocot species that have a multiseriate exodermis and inhabit well-drained or dry substrates.....	102
Table 2.3 List of monocot species that have a multiseriate exodermis and inhabit water-saturated substrates. All of these representatives are from the order Poales.....	109
Table 2.4 Number of species with a multiseriate exodermis that inhabit wet or well-drained/dry substrates.....	110
Table 2.5 Number of species with a uniseriate exodermis that inhabit wet or well-drained/dry substrates.	112

Chapter 3

Table 3.1 Hydraulic conductivity values calculated from pressure chamber and pressure probe experiments.....	140
Table 3.2 Resistance values calculated from pressure chamber and pressure probe experiments.....	143
Table 3.3 Fold change in resistance of the exodermis to water and solute flows.....	144
Table 3.4 The effect of puncturing the biseriate exodermis on hydraulic conductivity.....	145
Table 3.5 Osmotic data from root pressure probe experiments	146
Table 3.6 The effect of puncturing the biseriate exodermis on osmotic hydraulic conductivity	147

Chapter 4

Table 4.1 Percent composition of <i>Iris germanica</i> 's exodermal SPAD at different exodermal maturation zones.....	184
Table 4.2 Percent composition of the soluble fraction of <i>Iris germanica</i> 's exodermal suberin at different maturation zones	206

Chapter 5

Table 5.1 Percent composition of <i>Allium cepa</i> 's exodermal SPAD at the different exodermal maturation zones.	248
Table 5.2 Percent composition of the soluble monomer fraction of <i>Allium cepa</i> 's exodermal suberin at the different exodermal maturation zones.	252
Table 5.3 Percent composition of <i>Allium cepa</i> 's exodermal SPPD at the different exodermal maturation zones.	268

Appendix A - Supplementary Tables

Supp. Table 2.1 List of 25 <i>I. germanica</i> cultivars tested	303
Supp. Table 2.2 Monocot species with a uniseriate exodermis and growth substrates	304
Supp. Table 2.3 Eudicot species with a uniseriate exodermis and growth substrates	309

List of Abbreviations

A_r = root surface area

BSTFA+TMCS = *N,O*-bis(trimethylsilyl)trifluoroacetamide

ccCb = continuous circumferential Casparian band

GC-MS = gas chromatography-mass spectrometry

J_v = water flow

k = rate constant

$L_{p_{pc}}$ = root hydraulic conductivity measured with a pressure chamber

L_{p_r} = root hydraulic conductivity measured with a pressure probe

$L_{p_{ro}}$ = root osmotic hydraulic conductivity

MeOH/HCl = methanolic HCl

MEX = multiseriate exodermis

σ_{sr} = reflection coefficient

$\Delta\pi_s$ = change of external osmotic pressure

OPR = outer part of the root

ΔP = change in pressure

P_{sr} = solute permeability

Q_v = linear slope of a volume/time graph

SPAD = suberin poly(aliphatic) domain

SPPD = suberin poly(phenolic) domain

$T_{1/2}^w$ = half-time of the water phase

$T_{1/2}^s$ = half-time of the solute phase

ΔV = change in volume



“Until a man begins to work with plants, he is apt to grant them the word 'alive' in rather a meagre sense. But the more he works, the more vivid does the sense of their vitality become. The plant physiologist has much to learn from the worker who confined himself to animals. Possibly, however, the process may be partly reversed – it may be that from the study of plant physiology we can learn something about the machinery of our own lives.”

Francis Darwin. 1878. The analogies of plant and animal life.

Nature 17(438): 411-414.

“Roots - To know them is to Love them!!”

Dr. David T. Webb, University of Hawaii at Manoa.

[www.biologie.uni-hamburg.de/b-](http://www.biologie.uni-hamburg.de/b-online/library/webb/BOT410/Roots/roots.htm)

[online/library/webb/BOT410/Roots/roots.htm](http://www.biologie.uni-hamburg.de/b-online/library/webb/BOT410/Roots/roots.htm)

Image source:

Whitfield J. 2007. Nature 449: 136-138.

Chapter 1

General introduction

1.1 Introduction

Investigations of root structure, root function, and suberin biochemistry were conducted for the current thesis work. Much of this diverse, multidisciplinary study focused on the maturation and function of the root exodermis, a specialized cortical layer adjacent to the epidermis. An exodermis often acts as the outermost root layer, following sloughing off of the epidermis (Shishkoff 1986; McCully 1999), making first contact with soil particles, water, and dissolved minerals. The exodermis is an important “physiological sheath” (von Guttenberg 1968; Enstone et al. 2003) containing Casparian bands and suberin lamellae. These two cell wall-modifying structures are important for regulating radial solute and water transport across the root, and for tolerating abiotic stresses such as soil drought and high salt concentrations. Hence, the maturation of the exodermis, its permeability to water and solutes, and the chemistry and synthesis of the suberin monomers that comprise the Casparian bands and suberin lamellae were studied to better understand the role of the exodermis as a physiological sheath. *Iris germanica* was selected as the model species for most of this work because its exodermis is multiseriate (i.e., multi-layered); an exodermal type not thoroughly studied to date. *Allium cepa* was also used in the latter stages of this work as a model for suberin synthesis in a uniseriate (i.e., single-layered) exodermis.

1.2 Root anatomy

1.2.1 Primary root tissue development and anatomy

Primary roots are derived from sequential cell divisions in primary meristems followed by differentiation of primary tissues. The typical root apical meristem contains initials that produce three primary meristems. Each of these meristems gives rise to a primary tissue system, which later differentiates into the specific tissue types that comprise mature primary roots (Raven et al. 1999). 1) The protoderm gives rise to dermal tissue which differentiates into the epidermis. 2) The ground meristem gives rise to tissue that differentiates into parenchyma and sclerenchyma. All cells of the cortex originate from the ground tissue system. 3) The procambium gives rise to the pericycle, and vascular tissue which differentiates into the xylem and phloem within the stele. When mature primary roots are observed in transverse section, the tissue composition or anatomy becomes evident. For example, in *Allium cepa* roots (Fig. 1.1), the outermost layer of cells is the epidermis. Interior to the epidermis is the cortex, consisting normally of an exodermal layer (outermost), a multi-layered central cortex, and an endodermal layer (innermost). Intercellular air spaces are lacking in the exodermis and endodermis, but are present in the central cortex. Interior to the endodermis is the region of the stele which includes the pericycle (from which lateral roots originate), and the xylem and phloem (Fig. 1.1). In most monocot species, not including *A. cepa*, the stele has a central pith. The development and maturation of the exodermis and endodermis has been the focus of much research as these two tissue layers are of paramount importance to root physiology (see Enstone et al. 2003, and references therein).

1.2.2 Exodermal and endodermal cell ontogeny

Development of the exodermis and endodermis in primary roots is complex and involves the deposition of characteristic cell wall-modifying structures. The cells of these highly specialized tissue layers pass through two or sometimes three states of maturity as described by Van Fleet (1961), Esau (1965) and Robards et al. (1973). Usually, the endodermis starts to mature before the exodermis, but the sequence of development is roughly the same in both layers. The primary developmental state (State I) is reached when Casparian bands are deposited in the intermicrofibrillar spaces of radial and transverse cell walls (Fig. 1.2A,B). At this stage, a tight connection exists between the modified wall and the adjacent plasma membrane (Bonnert 1968; Karahara and Shibaoka 1992; Enstone and Peterson 1997; Ma and Peterson 2001a). Essentially, the exodermis is a hypodermis with Casparian bands (Peterson and Perumalla 1990); this definition corrected an earlier one by von Guttenberg (1968) who referred to the exodermis as a hypodermis with suberin lamellae. The Casparian band in the exodermis typically fills the majority of the anticlinal wall space, whereas in the endodermis the band can be dot-like in cross-sectional view and situated close to the inner tangential wall. Next, the secondary developmental state (State II) is marked by the deposition of a suberin lamella between the cell wall and plasma membrane (Fig. 1.2C,D). This lamella severs the tight connection between the Casparian band and plasma membrane (Robards et al. 1973; Haas and Carothers 1975; Ma and Peterson 2001a). Often, mature suberin lamellae are perforated at primary pit fields where plasmodesmata are located. The perforations are important because they leave the plasmodesmata intact and the cells remain alive. Such perforations have been observed in the exodermal cells of *Zea mays* (Clarkson et

Figure 1.1 Cross section of an *Allium cepa* (onion) root stained with Toluidine Blue O, 100 mm from the root tip. Abbreviations: ep = epidermis; ex = exodermis; cc = central cortex; en = endodermis; pe = pericycle; ph = phloem; xy = xylem; ixy = immature xylem. Scale bar = 100 μm .

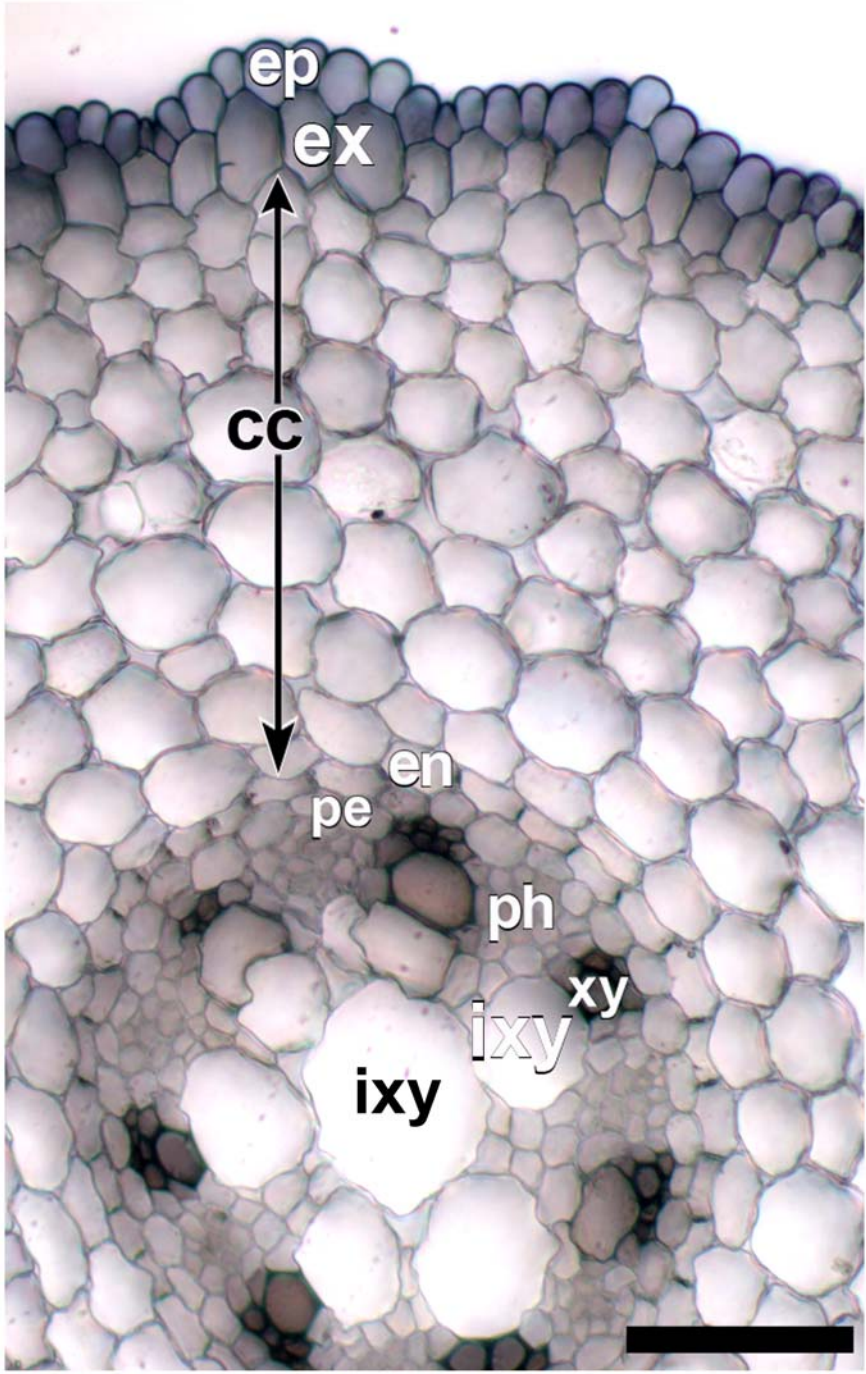
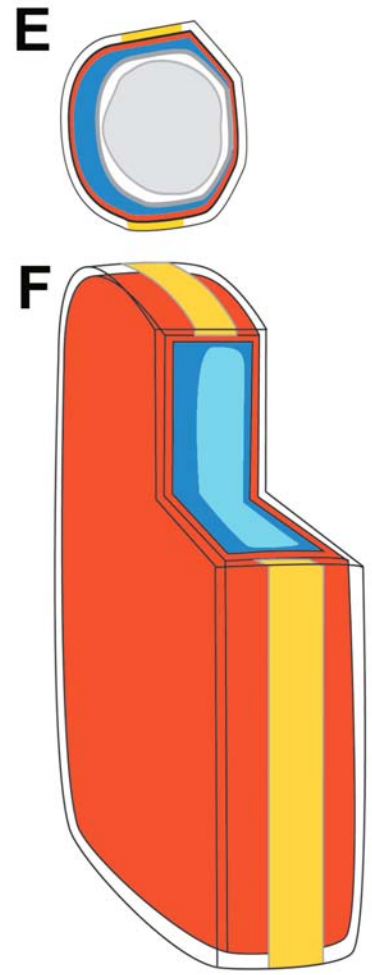
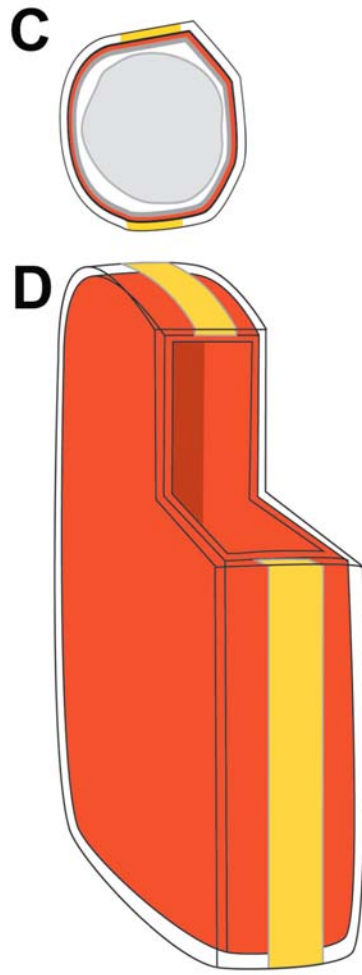
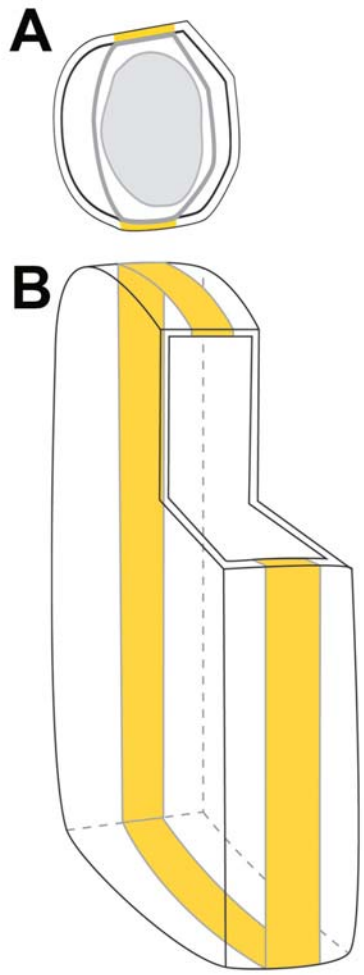


Figure 1.2 Illustrations of endodermal cells (not to scale) displaying the states of maturity in cross section (A,C,E) and in three-dimensions (B,D,F). (A,B) State I, Casparian bands in anticlinal walls. (A) Band plasmolysis is evident. (C,D) State II, suberin lamellae between the cell wall and plasma membrane. (E,F) State III, tertiary wall thickenings between the suberin lamellae and plasma membrane. Black lines = cell wall borders; dark grey lines = plasma membranes; light grey lines = tonoplasts; yellow shading = Casparian bands; red shading = suberin lamellae; blue shading = tertiary wall thickenings. Images (B,D,F) modified from Raven et al. (1999).



al. 1987; Wang et al. 1995) and in the endodermal cells of all species so far investigated (see Ma and Peterson 2000, and references therein). Conversely, in the long exodermal cells of *A. cepa*, suberin lamellae sever the plasmodesmata and these cells soon die (Ma and Peterson 2000). Lastly, in the tertiary developmental state (State III), tertiary cellulosic wall thickenings that are often embedded with lignin are deposited along the radial, tangential, and transverse walls (Fig. 1.2E,F). These tertiary walls are often U-shaped and thick enough to mask the Casparian bands and suberin lamellae (Van Fleet 1961; Esau 1965; Clarkson et al. 1987; Zeier and Schreiber 1998). Furthermore, the tertiary walls can be pitted, hence leaving plasmodesmata intact in the primary pit fields (Clarkson 1996; Ma and Peterson 2001a).

The rate of maturation through States I-III can vary in individual exodermal and endodermal cells. Often, a few cells located in older regions of roots will have only matured to State I whereas the others have matured to State III. While these State I cells have Casparian bands, they lack suberin lamellae and tertiary walls, and are referred to as passage cells (Esau 1965; von Guttenberg 1968; Peterson and Enstone 1996). Other variations in the development of the exodermis at the root apical meristem can lead to anatomical differences in the mature tissue, as described in the next section.

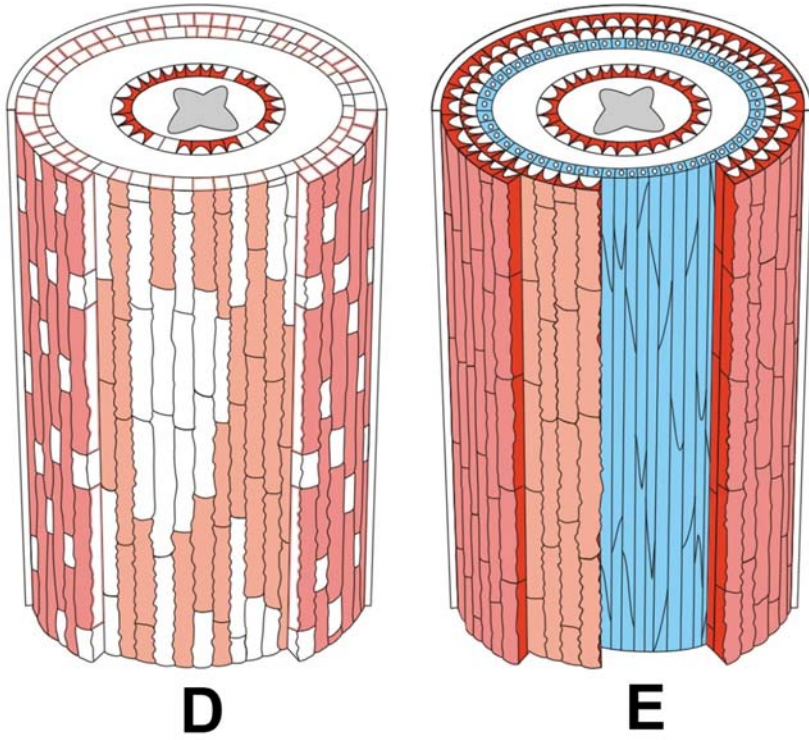
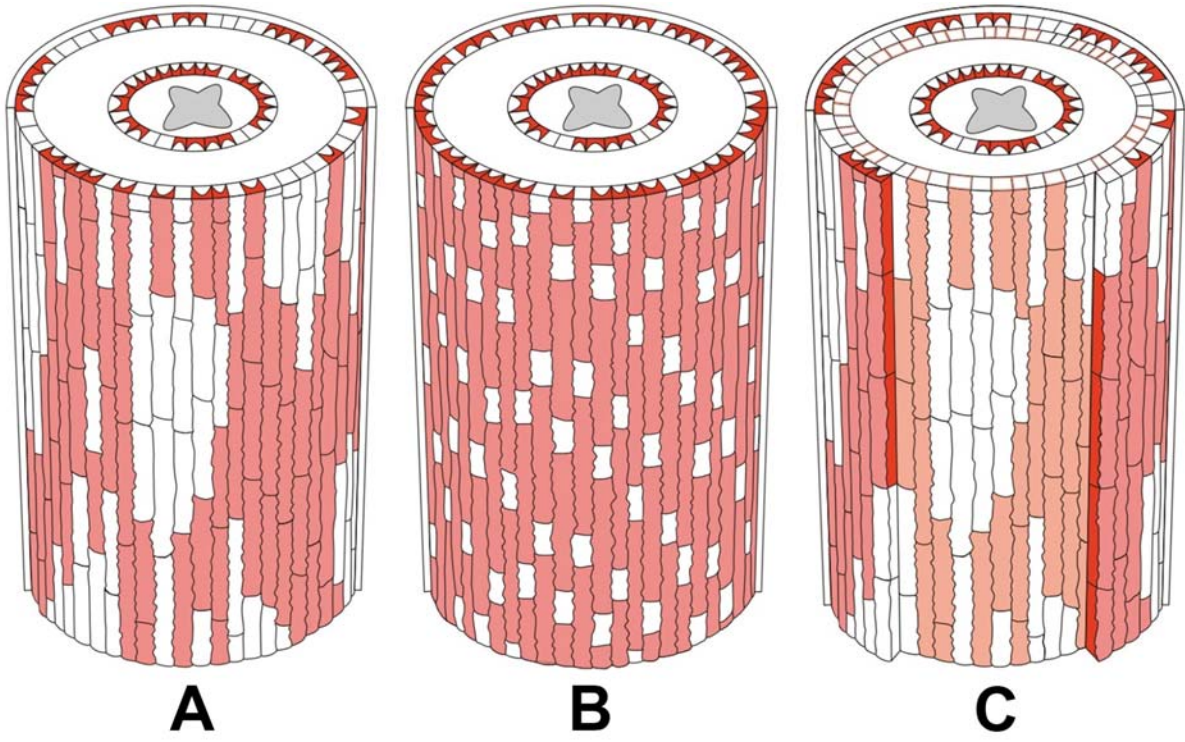
1.2.3 Exodermal types, sub-types, and a variation

The exodermis of roots is widespread and is structurally variable among species (Kroemer 1903; Perumalla et al. 1990; Peterson and Perumalla 1990; Hose et al. 2001; Enstone et al. 2003). In the more than 90% of tested angiosperm species that develop an exodermis, the majority have a single-layered (uniseriate) exodermis. This majority of species includes *A.*

cepa, *Oryza sativa*, and *Z. mays* (Perumalla et al. 1990; see Enstone et al. 2003, and references therein). Within the uniseriate type of exodermis there are two sub-types as originally described by Kroemer (1903). 1) A 'uniform exodermis' (Einheitliche Interkutis; after Kroemer [1903]) contains cells that are all of similar length, such as in *Z. mays* (Fig. 1.3A). In this case, exodermal cell maturation can be irregular resulting in regions containing a combination of immature cells and cells that have reached State II. The immature cells lack Casparian bands and, therefore, do not fit the definition of passage cells (Enstone and Peterson 1997). 2) A 'dimorphic exodermis' (Kurzzellen-Interkutis; after Kroemer [1903]) contains cells of two distinct lengths that are termed short and long cells, such as in *A. cepa* (Fig. 1.3B). In this case, the short cells can be passage cells because in mature root regions they contain Casparian bands but have delayed suberin lamella deposition compared with the long cells (von Guttenberg 1968; Kamula et al. 1994; Ma and Peterson 2001a).

A less common type of exodermis is the multi-layered (multiseriate) exodermis (MEX), which refers to an exodermis consisting of two or more layers. Species with a MEX include *Iris germanica* (Kroemer 1903; Shishkoff 1986; Peterson and Perumalla 1990; Zeier and Schreiber 1998), *Typha* spp. (Seago and Marsh 1989; Seago et al. 1999) and *Phragmites australis* (Armstrong et al. 2000; Soukup et al. 2002). Within the multiseriate type of exodermis there are two sub-types as originally classified by Kroemer (1903). 1) A 'uniform MEX' (Einheitliche mehrschichtigen Interkutis; after Kroemer [1903]) in which the cells in all layers have similar lengths (Fig. 1.3C). Examples of species that develop a uniform MEX are *Typha* spp. and *P. australis*. 2) A 'mixed MEX' (Gemischte mehrschichtigen Interkutis; after Kroemer [1903]) in which the outermost exodermal layer is dimorphic, but all

Figure 1.3 Illustrations of four exodermal sub-types and one exodermal variation, shown in cross and longitudinal section. (A) Uniseriate, uniform. (B) Uniseriate, dimorphic. (C) Multiseriate, uniform. (D) Multiseriate, dimorphic (or mixed). (E) Reinforced exodermal variation, with sclerenchyma (blue cells). Red shading = suberin lamellae in cells of the first exodermal layer; brownish-red shading = suberin lamellae in cells of the second exodermal layer; deep red shading = tertiary walls. (Images from Peterson 1997; reproduced with permission from the Copyright Clearance Center as the authorized agent for the American Society of Plant Biologists.)



underlying layers are uniform (Fig. 1.3D). To date, the mixed MEX has been observed in 14 species of various genera, but all within the order Asparagales. One such species is *I. germanica* (Kroemer 1903; Shishkoff 1986). Although several species are known to have a MEX, details of its development are not well known.

One notable variation to the exodermal types listed above is the 'reinforced exodermis' (verstärkte Interkutis), as described by Kroemer (1903). A reinforced exodermis refers to a uni- or multiseriate exodermis with an underlying layer of sclerenchyma (Fig. 1.3E). Such a variation has been observed for the uniseriate exodermis of *O. sativa* roots (Ranathunge et al. 2003). It is more appropriate to define the reinforced exodermis as a variation rather than a type or sub-type because the sclerenchyma layer lacks Casparian bands; hence this layer is not a true part of the exodermis. Instead the sclerenchyma layer can be considered a part of the hypodermis, which includes the exodermis.

1.2.4 Multiseriate exodermal development

Most studies of exodermal development have focussed on species with a uniseriate exodermis, with its typical Casparian band located only in the anticlinal walls (Perumalla et al. 1990; Enstone et al. 2003, and references therein). On the other hand, fewer studies have addressed MEX development with its unusual Casparian band. In an excellent set of examples, Seago and Marsh (1989) and Seago et al. (1999) followed MEX development in *Typha glauca* and *T. angustifolia*. From this work it was clear that the MEX developed centripetally from periclinal cell divisions of the outermost ground meristem layer. (Peterson and Perumalla [1990] also observed a centripetal development of the MEX in 21 other species.) This type of division results in exodermal cells that are arranged in radial files, and

consequently have an H-shaped cell wall continuum. The exodermal wall continuum acts as a scaffold for the subsequent deposition of the Casparian bands, which appear H-shaped when viewed in cross section. Additionally, this specialized Casparian band is continuous or unbroken around the root circumference, i.e. it forms a continuous circumferential Casparian band. Such an in-depth analysis of MEX development on other species was lacking. For the current thesis work, *I. germanica* roots were selected because, while brief descriptions of this species' root structure can be found in the literature, a detailed understanding of the development of its MEX and other tissues was unknown (Kroemer 1903; Shishkoff 1986; Peterson and Perumalla 1990; Zeier and Schreiber 1998). Furthermore, to the best of the author's current knowledge, the response of MEX maturation to different growth substrates has never been tested.

1.2.5 Growth conditions influence exodermal development

Although exodermal development is constitutive in many angiosperms, the timing and rate of development can be altered when plants are grown in different environmental conditions. In particular, alterations occur in the regulation of when and how quickly the exodermis and its wall-modifying structures are synthesized or modified. In one set of examples, Clarkson et al. (1987) and Enstone and Peterson (1998) exposed the basal parts of *Z. mays* roots to humid air inside hydroponic chambers. Within the region of humid air, a combination of the lower water potential and increased capacity for gas exchange, compared with completely submerged roots, led to an acceleration in exodermal suberin lamellae deposition. This was also observed when *Z. mays* was grown in aeroponics, vermiculite, or in a stagnant (oxygen-deficient) solution, compared with aerated nutrient solution (Zimmermann and Steudle 1998;

Enstone and Peterson 2005). When conducting experiments of this nature, it is necessary to measure root growth rates; what could be perceived as an acceleration in maturation may instead be a reduction in the root growth rate causing the exodermis to mature closer to the tip (Wilcox 1962; Perumalla and Peterson 1986). For instance, when roots are exposed to drought or salt-stress, their growth rates decline but the rate of exodermal maturation could remain steady. This would result in a greater exodermal surface area being suberized (see Enstone et al. 2003). The effect of different growth conditions on the maturation of *I. germanica*'s MEX had not been investigated prior to the present study.

1.2.6 Research aims I

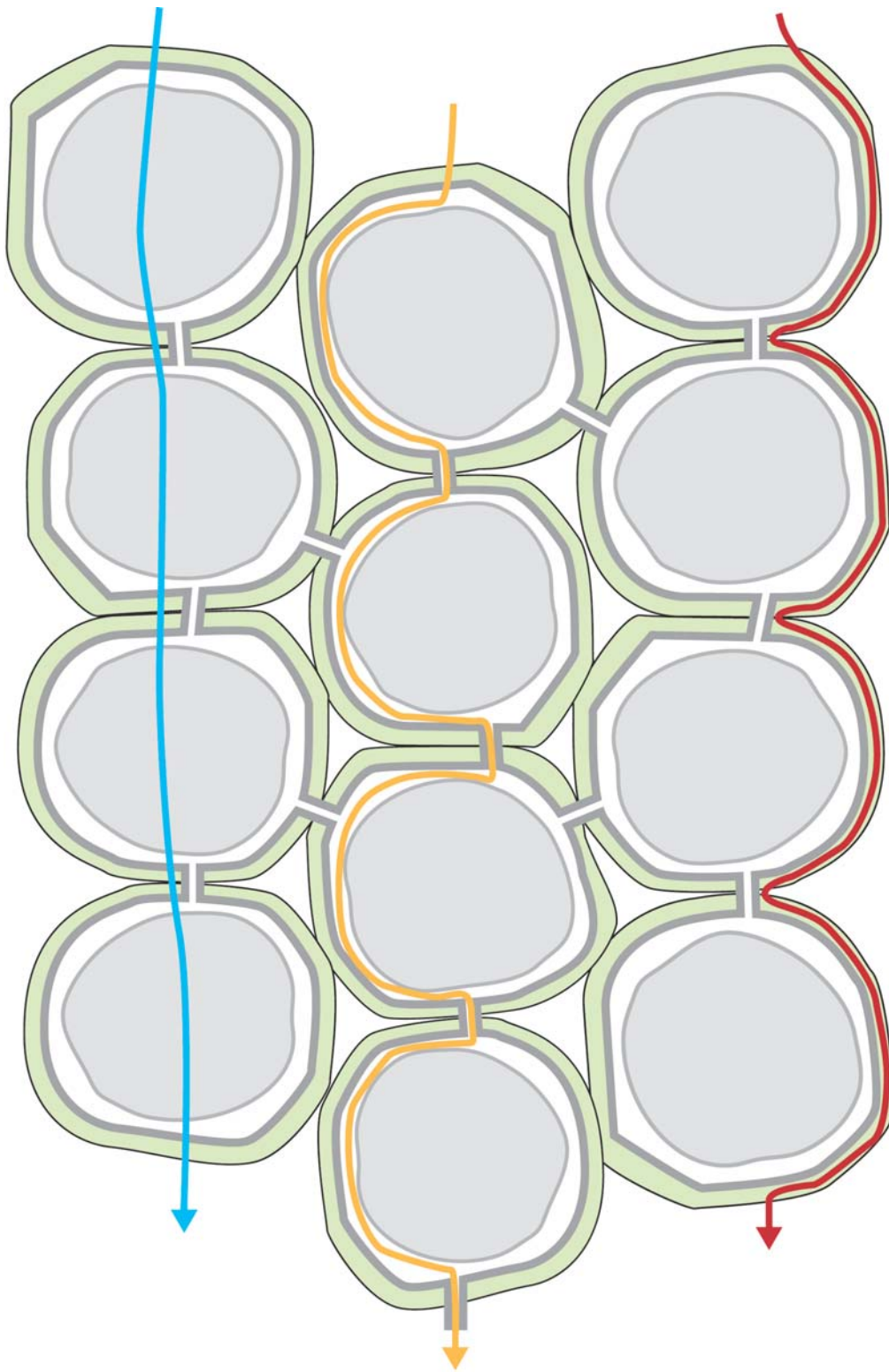
For the first phase of the current thesis work, the origin of *I. germanica*'s MEX was investigated (hypothesis: the exodermis originates from the division of the outermost layer of the ground meristem). Secondly, maturation of the MEX was observed when roots were grown in differing substrate conditions (hypotheses: exodermal maturation is delayed in hydroponically grown roots compared with soil-grown roots; exodermal maturation is accelerated when basal regions are exposed to a humid air gap). Furthermore, because members of the *Iris* genus occupy diverse substrates, roots from seven additional species were obtained to determine if correlations could be made between root anatomy and habitat (hypothesis: *Iris* spp. root anatomy is specific to its habitat).

1.3 Root physiology

1.3.1 Root structure determines radial transport pathways

Roots have been referred to as composite structures with several types of cell layers that all contribute to the radial transport properties of the organ (Steudle and Peterson 1998). There are three parallel, radial transport pathways (Fig. 1.4); 1) the apoplast – cell walls (intermicrofibrillar space diameter ranging from 5-30 nm [Nobel 2005]) and lumens of dead cells, 2) the symplast – cytoplasm of neighbouring cells connected by plasmodesmata (ranging from 60-90 nm in diameter [Ma and Peterson 2000]), and 3) the transcellular path – cell walls, cytoplasm and vacuoles. In the absence of wall-modifying structures, radial transport of dissolved solutes occurs mainly through the apoplast while the flow of water is through all three paths (Steudle and Peterson 1998). (The symplastic and transcellular pathways are often collectively referred to as the cell-to-cell pathway because, for water flow, it is not possible to differentiate the extent to which each pathway is being used.) Exodermal and endodermal cell layers (the outermost and innermost layers of the root cortex, respectively) have a pronounced ability to limit radial solute and water transport due to their characteristic wall-modifying structures. These structures are the Casparian bands which limit the apoplastic flow of solutes (de Rufz de Lavison 1910; Baker 1971; Peterson 1987; Enstone et al. 2003), and the poly(aliphatic) domain of suberin lamellae which may limit the transcellular flow of water and solutes (Evert et al. 1985; Zimmermann et al. 2000; Hose et al. 2001). Thus, development of the exodermis and endodermis has been studied in great detail for the purpose of understanding these layers' influence on radial water and solute transport.

Figure 1.4 Illustration of the three parallel, radial transport pathways across unmodified parenchyma cells. Green shaded regions = cell walls; white regions internal to the walls = cytoplasm; grey-shaded regions = vacuoles. Red line = apoplastic transport in cell walls. Orange line = symplastic transport in cytoplasm of neighbouring cells connected by plasmodesmata. Blue line = transcellular transport across cell walls, cytoplasm and vacuoles. Image modified from Steudle and Peterson (1998).



1.3.2 Water transport

Water is drawn into roots radially and then conducted axially as a bulk flow through the xylem in transpiring plants. The flow of water is mainly due to hydrostatic gradients created by tensional forces within tracheary elements (i.e., xylem vessels or tracheids) and less so by gradients in water potential (Steudle and Peterson 1998; see section 1.3.5 for more details).

To begin the process of radial transport, water enters the apoplast in the outer tangential walls of the epidermis. In the absence of an exodermis, the water can continue to flow nearly unrestricted inward through the apoplastic and cell-to-cell pathways of the central cortex to the endodermis. On the other hand, if a mature exodermis is present, presumably water enters the symplast and bypasses the exodermal Casparian bands and suberin lamellae (Fig. 1.5). (Water may still be able to flow through these structures – they may not be completely impermeable – but the path of least resistance is the symplast so it can be assumed that most water will flow through this pathway.) Entry into the symplast occurs across the plasma membrane of epidermal cells. Water will primarily flow through aquaporins to cross the plasma membrane, but it may also diffuse across. After traversing the exodermis, water will continue to flow radially inward through the central cortex mainly via the cell-to-cell pathway.

Upon reaching the mature endodermis, with Casparian bands in all cells and suberin lamellae in all but passage cells, the water will flow mainly through the cell-to-cell path of passage cells. Alternatively, some of the water may flow through the symplast of mature endodermal cells since the suberin lamellae does not sever their plasmodesmata (see Ma and Peterson 2000, and references therein). Once the water has reached the passage cell's inner

tangential wall, it will continue into the stele through a cell-to-cell path, but it must end up in the apoplast in order to enter the lumen of a tracheary element. Frequently, the endodermal passage cells are located adjacent to xylem poles so the water can flow efficiently into a tracheary element (Enstone et al. 2003).

Upon the entry of water into a mature tracheary element through the non-thickened pit membranes in its secondary walls, the water is conducted axially, with little resistance, according to the cohesion-tension theory. This theory was first proposed by Dixon and Joly (1894), and is widely accepted by the scientific community (Angeles et al. 2004). Briefly, the theory refers to the cohesion of water molecules and the tension within tracheary elements. Water molecules are bound together by hydrogen bonds forming an unbroken column of water in the lumens of tracheary elements. With the opening of leaf stomata, water vapour escapes into the atmosphere consequently creating a tension first in the walls of mesophyll cells and eventually in tracheary elements. The water column is drawn upward due to gradients of progressively decreasing hydrostatic pressure and decreasing water potential from the soil, into the plant, and out into the atmosphere (often referred to as the soil-plant-atmosphere continuum; Nobel 2005).

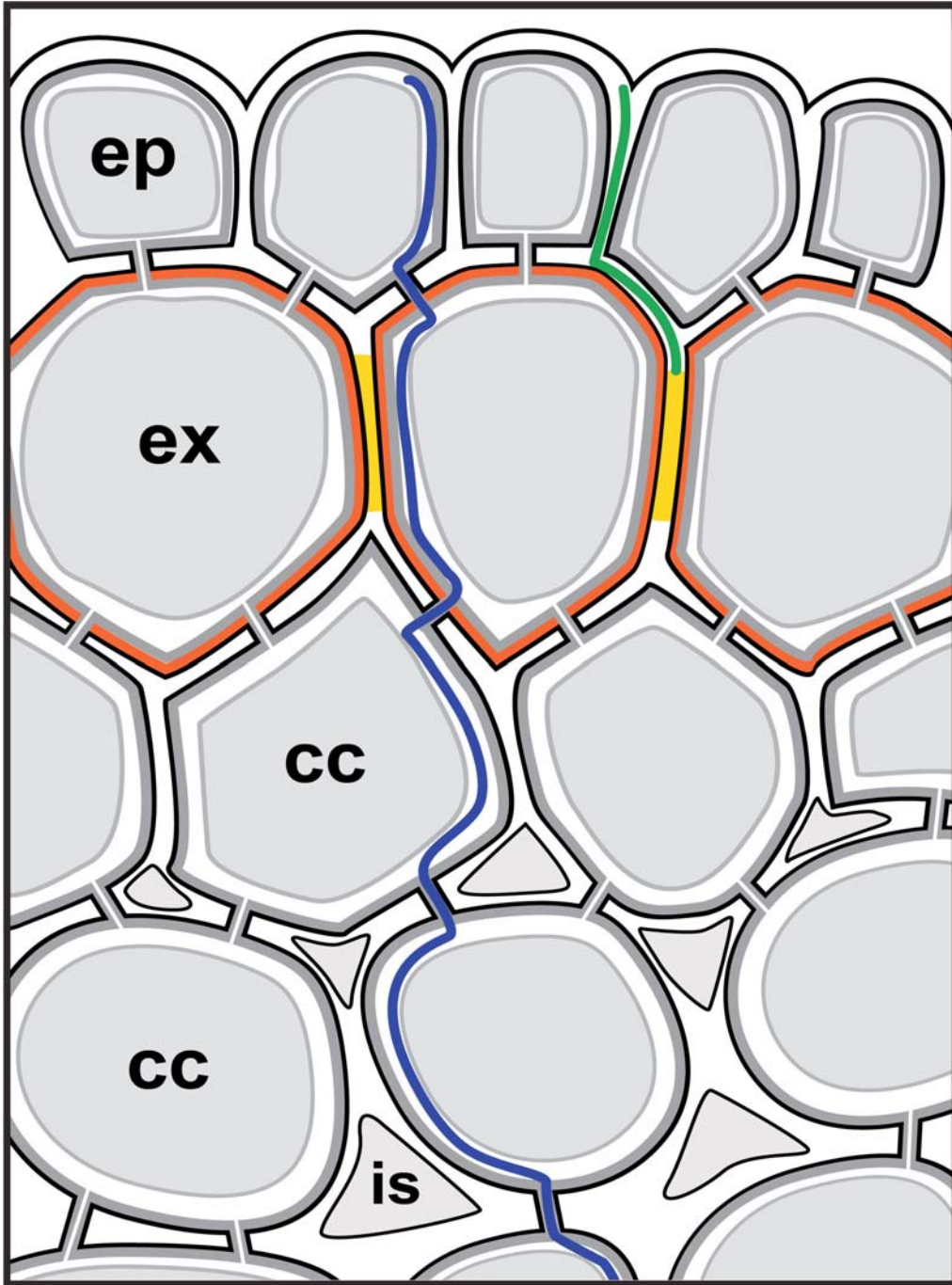
1.3.3 Ion transport

Under conditions of high transpiration, the radial transport of ions is influenced by the bulk flow of water, except in the presence of the exodermis and endodermis. Ion flow through the nearly non-restrictive apoplast of the central cortex may occur by solvent-drag, meaning that water moving by bulk flow 'drags' or pulls the dissolved ions through the intermicrofibrillar wall spaces (Aloni et al. 1998; Steudle and Peterson 1998). But, when a mature exodermis or

Figure 1.5 Drawing of the outer part of a root, with a uniseriate exodermis, in cross section.

Thicknesses of cell walls, cytoplasm, and plasmodesmata are exaggerated. Black lines = cell wall borders; dark grey lines = plasma membranes; light grey lines = tonoplasts; red lines = suberin lamellae; yellow lines = Casparian bands; blue line = symplastic transport through plasmodesmata; green line = apoplastic transport blocked by a Casparian band.

Abbreviations: ep = epidermis; ex = exodermis; cc = central cortex; is = intercellular space.



endodermis is present, the ions must bypass the Casparian bands and suberin lamellae by way of the symplast (Fig. 1.5). Ions enter the symplast via transmembrane transporters located in the plasma membranes of epidermal cells or in the membranes on the outer tangential walls of exodermal or endodermal passage cells. While in the symplast, ions will diffuse radially inward through plasmodesmata that connect living cells. Alternatively, if a transporter for a particular ion is not present in a plasma membrane, then the ion will be confined to the apoplast and its flow will be restricted by the Casparian band (Baker 1971; Peterson 1987; see Fig. 1.5). The radial flow of a solute toward future endodermal passage cells was observed using berberine as a fluorescent apoplastic tracer (Aloni et al. 1998). This method showed directly that tensional forces of the tracheary elements drew most of the dissolved solute (in this case berberine) toward the passage cells via solvent-drag. Since berberine is restricted to the apoplast and cannot permeate Casparian bands, it was prevented from crossing the endodermis. On the other hand, water can flow through the cell-to-cell pathway so it would have entered the stele. But, unlike berberine, water could not be visualized so the use of apoplastic tracers does not directly represent water transport (Steudle and Peterson 1998).

1.3.4 Apoplastic tracers

Apoplastic tracers are useful for providing clues about the efficacy of cell wall-modifying structures with regard to the potential limitation of the radial transport of water and ions. Qualitative apoplastic permeability tests have been conducted on the multiseriate exodermis (MEX) of *I. germanica* (Peterson and Perumalla 1990), *Typha* spp. (Seago et al. 1999) and *P. australis* (Soukup et al. 2002, 2007) using a suite of tracers (i.e., Cellufluor, berberine,

FeSO₄, and periodic acid). (To date, berberine is the best apoplastic tracer due to its high contrast as a fluorochrome and its reduced risk of toxicity when used within its concentration and exposure time limits [see Enstone and Peterson 1992].) For all species listed above, when the MEX was intact, and contained Casparian bands and suberin lamellae, there was little or no permeation of the tracers. From these results, it is proposed that a MEX can effectively restrict apoplastic solute permeability. But, can the thick MEX in *I. germanica* roots still allow water to permeate while preventing the influx of non-essential ions? To answer this question, direct and quantitative measurements of water and solute flow are necessary, as described below.

1.3.5 Hydrostatic and osmotic pressure gradients

There are two pressure gradients that are naturally-occurring in plants and function as the driving force for water flow. 1) A hydrostatic pressure gradient across the apoplast is the dominant driving force for radial water flow in transpiring plants (Steudle and Peterson 1998). Hydrostatic gradients result in a hydraulic water flow or conductivity; the hydrostatic gradients can be simulated and the hydraulic conductivity measured with quantitative devices such as a pressure chamber and a root pressure probe (see below). Water flows through the apoplast rapidly in the absence of wall-modifying structures. Furthermore, dissolved solutes are transported – nearly uninhibited – in the apoplast either by diffusion or solvent-drag due to the lack of selectively permeable membranes. 2) An osmotic potential gradient is the dominant driving force for water flow only when transpiration rates are reduced (Steudle and Peterson 1998). Specifically, the flow of water follows osmotic gradients along the cell-to-cell path, moving into regions where solutes have been either passively or actively

transported across plasma membranes. Osmotic gradients can be simulated and the osmotic hydraulic conductivity measured with a root pressure probe (see below). Osmotic hydraulic conductivity values are usually significantly lower than hydraulic conductivity values because the nature of the driving force results in flows across the cell-to-cell and apoplastic pathways, respectively (Steudle and Frensch 1989; Cruz et al. 1992; Steudle et al. 1993; Rüdinger et al. 1994; Steudle and Meshcheryakov 1996; Steudle and Peterson 1998).

1.3.6 Pressure chamber

The pressure chamber is a device that can be used to establish steady-state hydrostatic pressure gradients through roots in order to measure hydraulic water flow or conductivity ($L_{p_{pc}}$) (Fig. 1.6). When a root is excised from the rest of the plant, the solution within its tracheary elements will withdraw from the cut surface because the solution is under tension. If this excised root is attached to a pressure chamber filled with water, the pressure inside the chamber can be increased hydrostatically to force solution radially and axially through the root and toward the cut surface (Fig. 1.6). By gradually increasing the pressure of the external solution (ΔP in MPa), the volume that flows out of the cut end can be measured and plotted against time (Fig. 1.7A). The slopes from the linear parts of these volume/time graphs (Q_v in $m^3 \cdot s^{-1}$), along with the root surface area (A_r in m^2), are used to calculate the rate of water flow per unit root surface area (J_v in $m^3 \cdot m^{-2} \cdot s^{-1}$)

$$J_v = \frac{Q_v}{A_r} \quad (\text{Eq 1}).$$

When J_v is plotted against ΔP , the slope from the linear part of the $J_v/\Delta P$ graph gives $L_{p_{pc}}$ in $m \cdot s^{-1} \cdot MPa^{-1}$ (Fig. 1.7B). Root $L_{p_{pc}}$ (i.e., radial hydraulic water flow) is expected to be

reduced following the deposition of Casparian bands and suberin lamellae in endodermal and exodermal cells.

1.3.7 Root pressure probe

The root pressure probe is an instrument that can be used to establish transient changes in hydrostatic pressure across roots in order to measure radial hydraulic conductivity (Lp_r) (Fig. 1.8; Steudle et al. 1987; Steudle and Frensch 1989). Using the pressure probe, gradients in hydrostatic pressure between the root and its external solution are initiated by performing pressure-relaxations (Fig. 1.9A). A pressure-relaxation is started when the metal rod of the probe is quickly moved toward the attached root. This creates a pulse of increased pressure in the stele region due to water being forced into tracheary elements. Following a pulse in pressure, a relaxation occurs during which water flows radially out of the stele, across the cortex and out of the root, bringing the pressure back near to its original state (Fig. 1.9A). Pressure-relaxations can also be induced in the opposite direction by quickly moving the metal rod away from the root. This creates a pulse of tension on the tracheary elements, thereby drawing water from the outer bathing solution into the root (Fig. 1.9A). A transducer detects the pressure changes over time; these changes are directly related to the rate of hydraulic water flow through the root. From the recorded pressure/time graphs, a rate constant (k_{wr}) of water flow across the root, or the half-time of a relaxation ($T_{1/2}^w$), are used to calculate the root's hydraulic conductivity (Lp_r in $m \cdot s^{-1} \cdot MPa^{-1}$)

$$k_{wr} = \frac{\ln(2)}{T_{1/2}^w} = A_r \cdot \left(\frac{\Delta P_r}{\Delta V_s} \right) \cdot Lp_r \quad (\text{Eq 2}).$$

Figure 1.6 Illustration of the pressure chamber used in the current work. Image modified from Zimmermann and Steudle (1998).

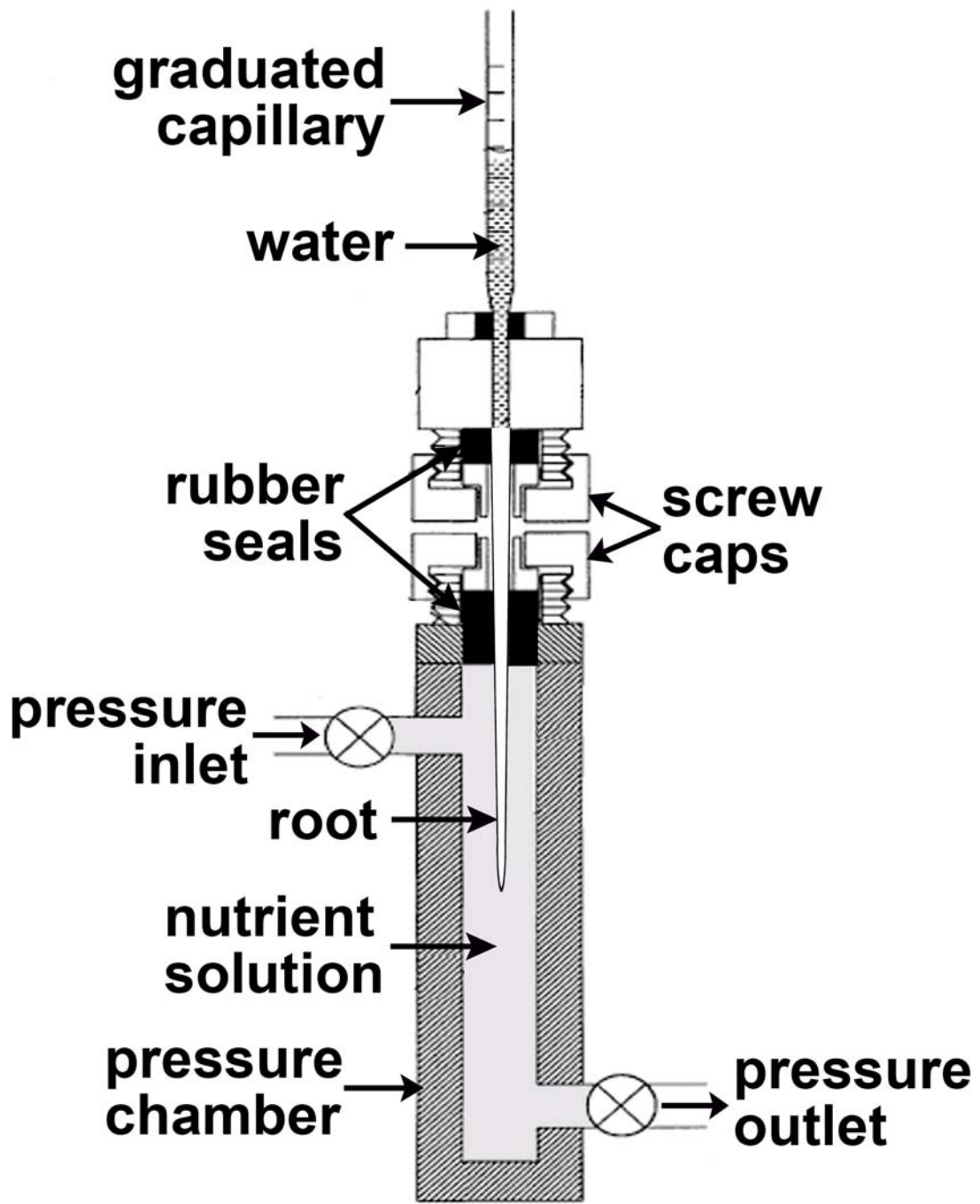
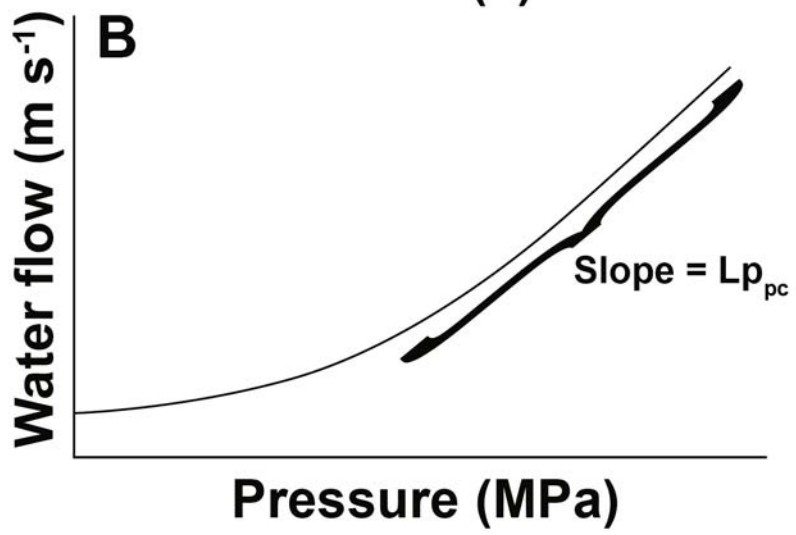
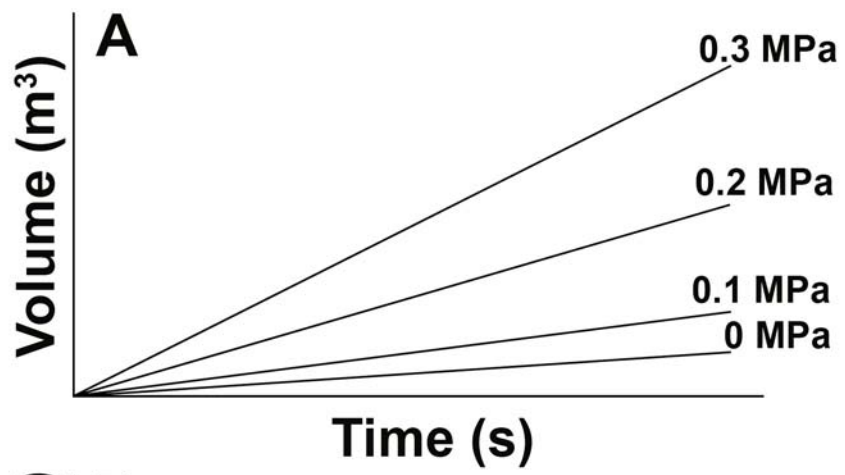


Figure 1.7 Typical data obtained from pressure chamber experiments. (A) Pressure within the chamber is gradually increased. At each step in pressure, the volume of water that flows through the root is recorded and plotted against time. The slopes of each graph are divided by the root surface area, to calculate the rate of water flow. (B) Water flow rates are plotted against their corresponding pressures. The slope of the linear part of this graph equals hydraulic conductivity ($L_{p_{pc}}$ in $\text{m s}^{-1} \text{MPa}^{-1}$).



Here, A_r refers to the surface area of the root (in m^2), and $\Delta P_r/\Delta V_s$ is the elastic coefficient (in $\text{MPa}\cdot\text{m}^{-3}$) which measures the rigidity of the pressure probe. Values of L_{p_r} are virtually the same when pressure-relaxations are induced in the forward or reverse direction. Root L_{p_r} is typically reduced with the deposition of suberin lamellae in the endodermis and exodermis (Melchior and Steudle 1993; Zimmermann et al. 2000; Enstone et al. 2003).

The root pressure probe can also be used to establish osmotic pressure gradients across root tissues in order to measure osmotic hydraulic conductivity ($L_{p_{ro}}$) and solute permeabilities (P_{sr}). Such gradients are created by introducing a test solute into the root's external bathing solution, thereby decreasing this solution's water potential (Fig. 1.9B). Consequently, a net efflux of water from the root occurs and is detected by the probe as a pressure decrease (i.e., the water phase). The net water efflux is followed by a net solute flow into the root which increases the root pressure back to its original state (i.e., the solute phase) (Fig. 1.9B). These reactions can be reversed by replacing the external bathing solute with water (Fig. 1.9B; Steudle and Tyerman 1983). The $T_{1/2}^w$ of the water phase is used to calculate $L_{p_{ro}}$ (as in Eq 2). The $T_{1/2}^s$ of the solute phase is used to calculate P_{sr} (in $\text{m}\cdot\text{s}^{-1}$) according to

$$k_{sr} = \frac{\ln(2)}{T_{1/2}^s} = A_r \cdot \left(\frac{P_{sr}}{V_x} \right) \quad (\text{Eq 3}),$$

where k_{sr} is the rate constant of solute permeability, and V_x is the volume of the tracheary element lumens.

In addition to measuring P_{sr} , a reflection coefficient (σ_{sr}) can be calculated from the pressure/time curves (Steudle and Tyerman 1983). The σ_{sr} refers to the selectivity of a membrane or tissue to a solute, and is calculated according to

$$\sigma_{sr} = \frac{(P_{ro} - P_{rmin})}{\Delta\pi_s} \times \exp(k_s \cdot t_{min}) \quad (\text{Eq 4}),$$

where P_{ro} and P_{rmin} are the original and minimum root pressures of pressure/time curves, respectively, $\Delta\pi_s$ is the change of external osmotic pressure caused by the solute, and t_{min} is the time required to reach P_{rmin} following a step change in the external concentration at $t = 0$. Values of σ_{sr} range from 0-1, where 0 means that there is no resistance or no selectivity to solute flow and 1 means there is a total blockage of solute flow.

1.3.8 Quantitative measurements of water and solute permeability across the exodermis

Quantitative instruments such as the pressure chamber and root pressure probe have yielded gross measurements of water and solute permeability across the exodermis. But, the majority of tests have been made with species with a uniseriate (single-layered) exodermis, such as *Z. mays* and *Oryza sativa*, and on roots with young regions that lack exodermal Casparian bands and suberin lamellae (Steudle and Peterson 1998; Zimmermann and Steudle 1998; Miyamoto et al. 2001; Ranathunge et al. 2005a, b). Although these model species are of agricultural and molecular genetic importance, their practicality for the precise testing of apoplastic barriers in roots is questionable. For example, in a typical uniseriate exodermis, Casparian bands are located in only the anticlinal walls, and suberin lamellae deposition can be “patchy” or irregular (von Guttenberg 1968; Enstone and Peterson 1997).

Figure 1.8 Illustration of the root pressure probe used in the current work. Image modified from Meyer et al. (2007).

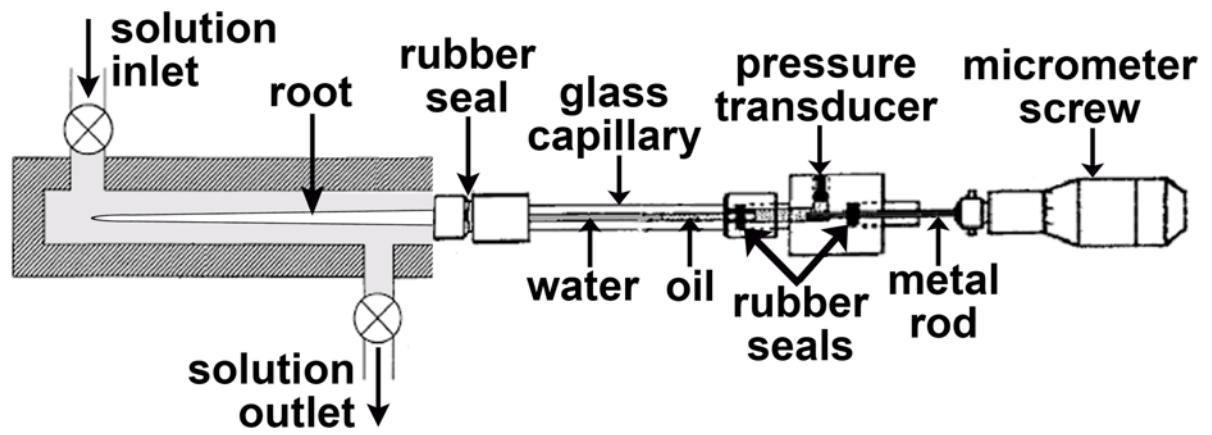
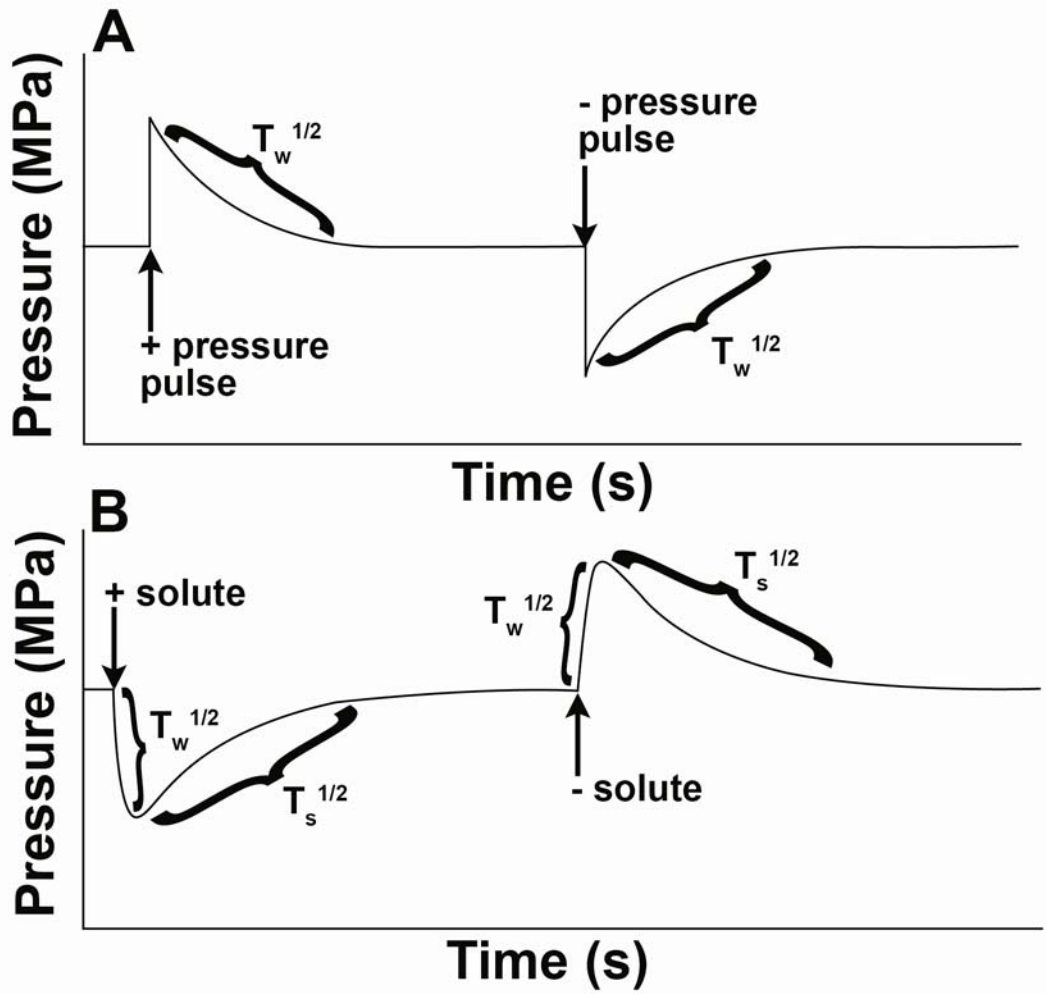


Figure 1.9 Typical data obtained from root pressure probe experiments. (A) Hydrostatic experiments. Internal root pressure is rapidly increased (+ pressure) by moving the metal rod of the probe toward the root. The subsequent relaxation in pressure is directly related to the efflux of water through the root. By measuring the half-time of this relaxation ($T_w^{1/2}$), hydraulic conductivity (Lp_r) can be calculated. The pressure-relaxation event is reversible; root pressure can be rapidly reduced by moving the rod away from the root (- pressure), and the $T_w^{1/2}$ of water influx is measured. (B) Osmotic experiments. A test solute is introduced to the root's bathing solution (+ solute). In the first phase, a decrease in pressure occurs due to water efflux. $T_w^{1/2}$ is measured to calculate osmotic hydraulic conductivity (Lp_{ro}). In the second phase, an increase in pressure is caused by solute influx. $T_s^{1/2}$ is measured to calculate solute permeability (P_{sr}). This biphasic reaction is reversible. When the test solute is replaced with water (- solute), water flows into the root and the solute flows out.



The irregularity in the formation of suberin lamellae means that it is not deposited in all exodermal cells at the same time or same distance from the root tip. Exodermal cells that lack suberin lamellae can provide low-resistance bypasses through the exodermis for water and solutes moving via the transcellular and symplastic pathways. Therefore *I. germanica* roots, with their MEX, lack of passage cells and unusual Casparian bands, offer the possibility of testing definitively the water and solute permeabilities of cell wall-modifying structures. Furthermore, permeability measurements are less variable with roots that develop few laterals, such as those of *I. germanica*, because the outgrowth of laterals temporarily disrupts the exodermis and endodermis (Peterson and Lefcourt 1990; Peterson and Moon 1993).

1.3.9 Research aims II

For this phase of the current thesis work, the water and solute permeability of *I. germanica*'s MEX was quantified for the first time. A pressure chamber was used to measure water permeability of root segments with exodermal Casparian bands and suberin lamellae. A root pressure probe was used to measure the water, NaCl, and ethanol permeability. The first hypothesis is that the permeability of *I. germanica* roots with a mature MEX is considerably lower than roots with an immature MEX. The second hypothesis is that the permeability of *I. germanica* roots with a mature MEX is lower than values obtained previously from other species with a uniseriate exodermis.

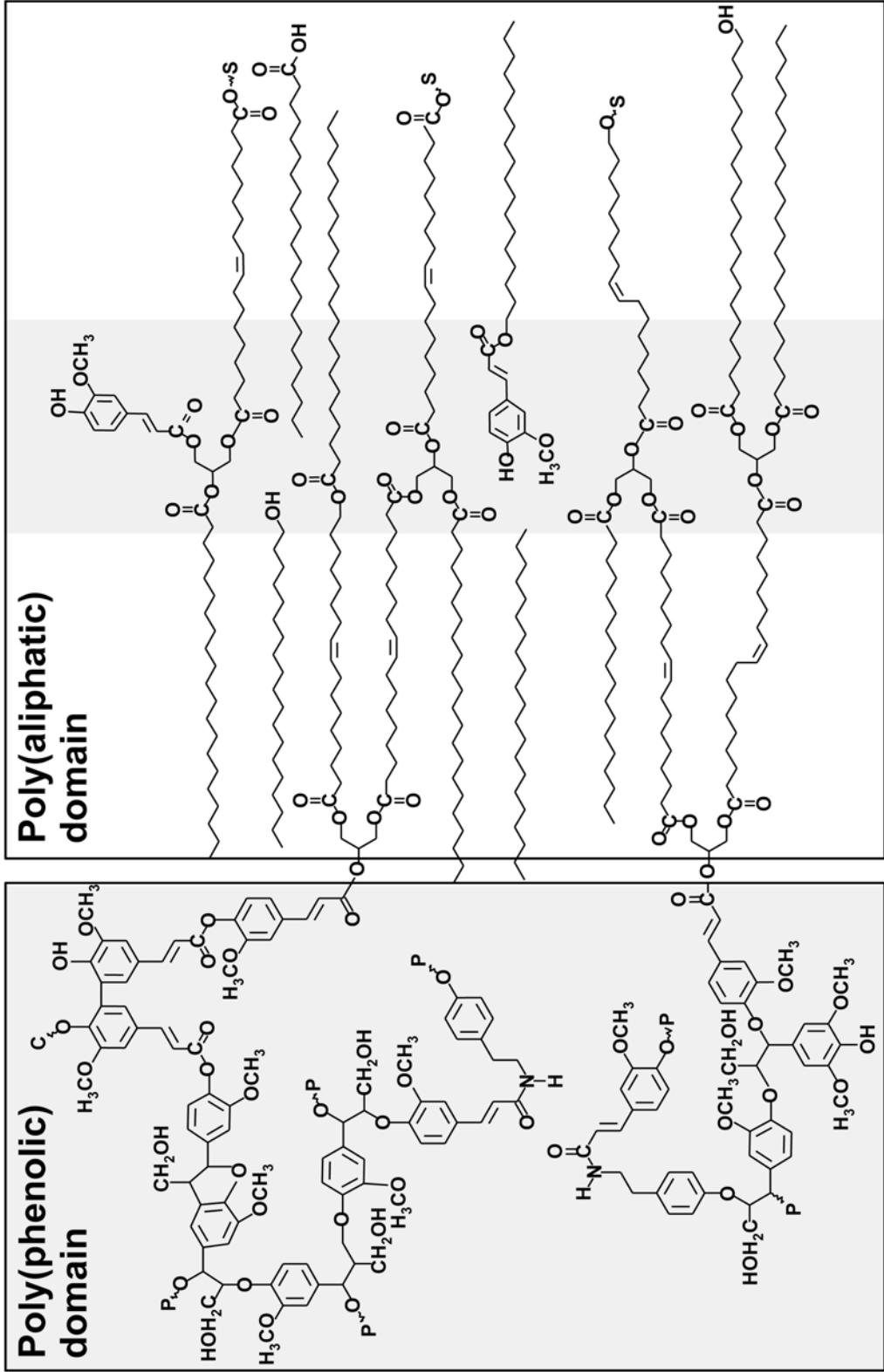
1.4 Suberin chemistry and biosynthesis

1.4.1 What is suberin?

Plants growing in natural habitats are able to tolerate desiccating conditions and resist pathogen attack, both above- and below-ground, due to the constitutive deposition of protective chemical compounds in specialized tissue layers. Suberin is one of these protective chemicals that functions, in part, to reduce the desiccation of organs. The cell wall localization and chemical composition of suberin has been well documented, providing clues as to its physiological properties (reviewed in Kolattukudy 1980, 1984; Bernards 2002). Examples of suberin-containing cells include the phellem of periderm in the skin of *Solanum tuberosum* (potato) tubers, the phellem of periderm in the bark of *Quercus suber* (cork oak) stem, the bundle sheath that surrounds vascular bundles in some grass leaves, and, of course, the exodermis and endodermis in the primary roots of angiosperms (see Esau 1965; Kolattukudy 1980, and references therein). Specifically, it is the wall modifying structures (i.e., the Casparian bands and/or suberin lamellae) of the cells listed above that are composed primarily of particular fatty acids and phenolics, the constituents of suberin.

Suberin is a complex biopolymer with a known morphology and monomeric profile that has been used to derive a model of its chemical structure (reviewed in Kolattukudy 1980, 1984; Bernards 2002) (Fig. 1.10). (The following descriptions were made possible primarily by analyses of suberin lamellae from *S. tuberosum* periderm.) Suberin is composed of two spatially distinct but covalently-linked domains; the poly(phenolic) domain (SPPD; after Bernards 2002) embedded in the primary cell wall, and the poly(aliphatic) domain (SPAD; after Bernards 2002) located between the cellulosic cell wall and plasma membrane (Fig.

Figure 1.10 Chemical model of suberin lamellae. The poly(phenolic) domain is embedded in the cell wall. The poly(aliphatic) domain is located between the cell wall and plasma membrane. Grey-shading = regions rich in phenolics and/or ester-linkages. Modified from Bernards (2002).



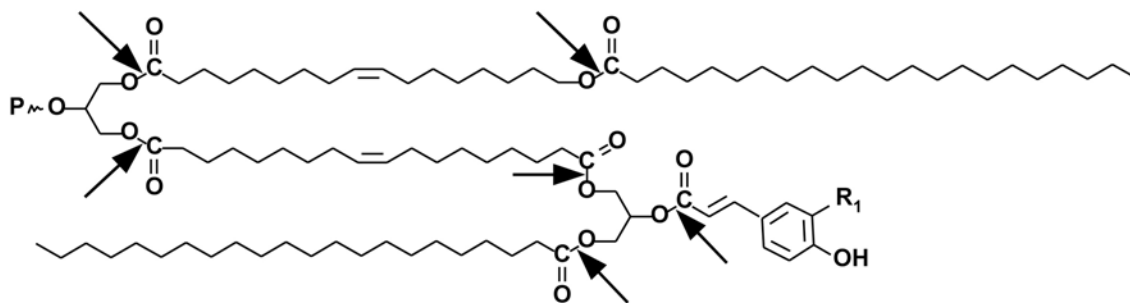
1.10). This two-domain model was previously inferred from histochemical (Lulai and Morgan 1992) and nuclear magnetic resonance studies (Stark and Garbow 1992; Lopes et al. 2000a, b), and more recently from differential scanning calorimeter measurements (Mattinen et al. 2009; see Chapter 6). When observing the SPAD with a transmission electron microscope, its lamellar structure is revealed as alternating bands of translucent, electron-light (aliphatic-rich) and opaque, electron-dense (aromatic or ester linkage-rich) compounds. The typical monomeric composition of the two domains has been determined through analysis of depolymerized compounds isolated from mature tissues (Kolattukudy 1980, 1984; Graça and Pereira 2000a, b; Bernardis 2002). To depolymerize the SPAD, transesterification is required using methanolic HCl (Fig. 1.11; Browse et al. 1986) or boron trifluoride in methanol (Riederer and Schönherr 1986). Depolymerization of the SPPD requires hydrolysis by alkaline nitrobenzene oxidation (Fig. 1.12; Meyer et al. 1998) or derivatization followed by reductive cleavage (Lu and Ralph 1997). Monomers are traditionally quantified and identified using gas chromatography coupled with mass spectrometry. Then the monomer profiles can be used, in conjunction with other information such as genetic and functional enzymatic processes, to predict how suberin lamellae are synthesized.

1.4.2 SPAD biosynthesis

The SPAD is hypothesized to be a glycerol-bridged, three dimensional polymer that is rich in fatty acid derivatives including ω -hydroxy fatty acids, α,ω -dicarboxylic acids, mid-chain oxidized fatty acids, and long-chain fatty acids (Fig. 1.13). Esterified hydroxycinnamic acids are also commonly found in the SPAD (Kolattukudy and Dean 1974; Kolattukudy 1980,

1984; Holloway 1983; Zeier and Schreiber 1998, 1999; Zeier et al. 1999a, b; Graça and Pereira 2000a, b; Bernards 2002, and references therein). The ω -hydroxy fatty acids and α,ω -dicarboxylic acids are typically deposited in abundance, but the overall composition and relative amounts of monomers can vary between different species (Holloway 1983; Matzke and Riederer 1991; Zeier and Schreiber 1998, 1999; Zeier et al. 1999a, b). Briefly, SPAD production begins with the plastidic synthesis of saturated C18 fatty acids driven by fatty acid synthases. Then these fatty acids are partitioned into two pools for further processing (Kolattukudy 1980, 1984; Yang and Bernards 2006). In one pool, the fatty acids are desaturated and ω -hydroxylated into 18:1 ω -hydroxy fatty acids (Fig. 1.14). Fatty acid ω -hydroxylation is catalyzed by NADPH-dependent cytochrome P450 monooxygenases (P450) from the CYP86 and CYP94 families (Duan and Schuler 2005). The ω -hydroxy fatty acids can then be oxidized into 18:1 α,ω -dicarboxylic acids by an ω -hydroxy fatty acid dehydrogenase (Fig. 1.14; Agrawal and Kolattukudy 1978a, b; Kurdyukov et al. 2006). In the second pool, the C18 fatty acids are first elongated to C20-C28 by means of a microsomal malonyl-CoA dependent pathway (Fig. 1.15; Schreiber et al. 2005b). This pathway is catalyzed by a fatty acid elongation complex (FAE) located on the endoplasmic reticulum. The FAE is composed of four enzymes in series. 1) The 3-ketoacyl CoA synthetase (KCS) which condenses a 2-carbon unit from malonyl-CoA to a long-chain acyl-CoA, producing 3-ketoacyl CoA. 2) The 3-ketoacyl CoA reductase (KCR) which reduces 3-ketoacyl CoA, resulting in 3-hydroxyacyl CoA. 3) The 3-hydroxyacyl CoA dehydratase which dehydrates 3-hydroxyacyl CoA, giving rise to trans-2,3-enoyl CoA. 4) The trans-2-enoyl CoA reductase which reduces trans-2,3-enoyl CoA, and generates a reduced and saturated long-chain acyl-

Figure 1.11 Transesterification of the poly(aliphatic) domain using MeOH/HCl. The polymeric structure is hypothetical and is based on the typical products that are released. Aliphatic monomers are analyzed as methyl ester or trimethylsilyl ether derivatives.



[1] MeOH/HCl (80°C, 2 h)
 [2] BSTFA+TMCS (70°C, 40 min)

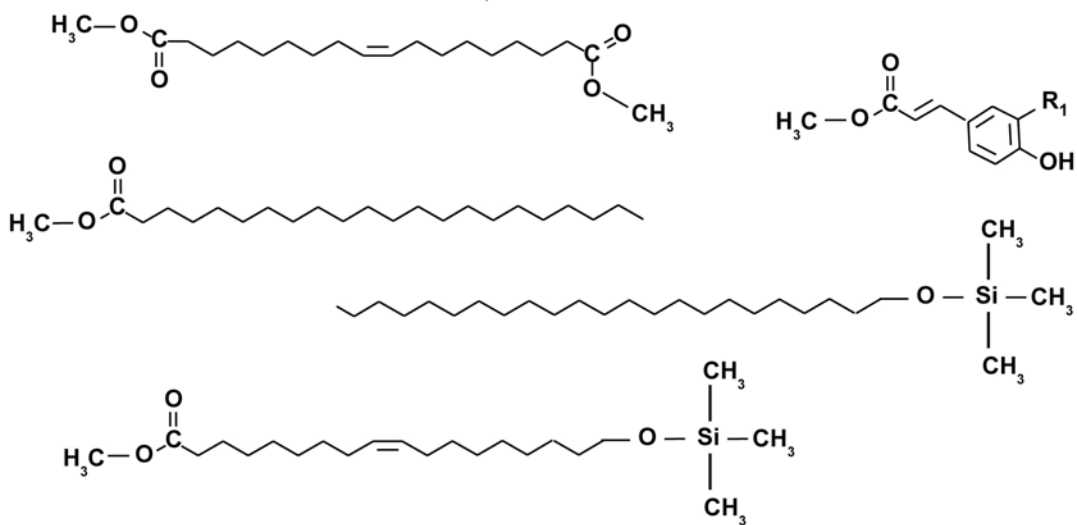
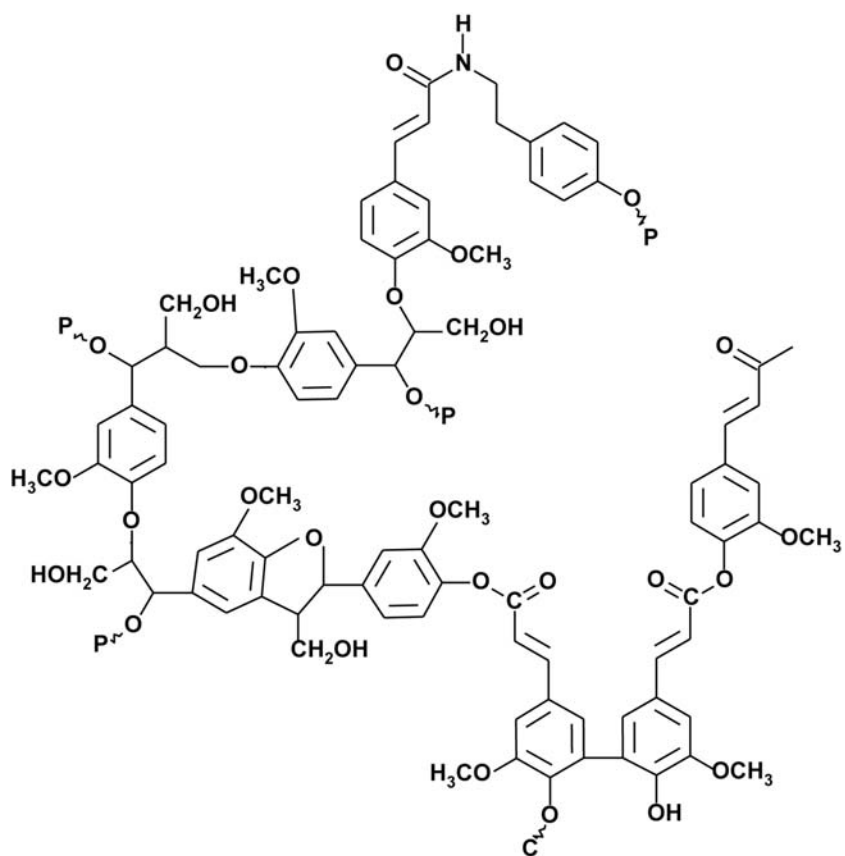


Figure 1.12 Depolymerization of the poly(phenolic) domain using alkaline nitrobenzene oxidation. The polymeric structure is hypothetical and is based on typical products that are released. Phenolic monomers are analyzed as trimethylsilyl ether derivatives.



[1] NaOH (37°C, 24 h)
 [2] Nitrobenzene (160°C, 3 h)
 [3] BSTFA+TMCS (70°C, 40 min)

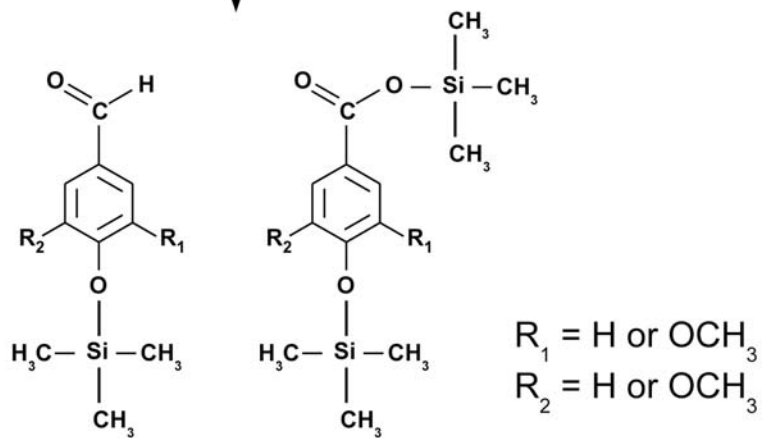


Figure 1.13 Aliphatic monomers of suberin lamellae. Modified from Bernards (2002).

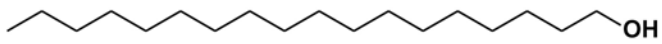
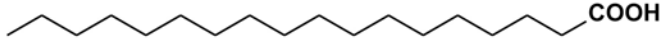
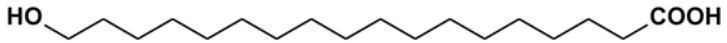
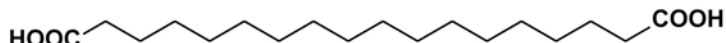
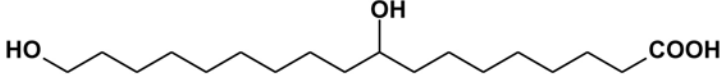
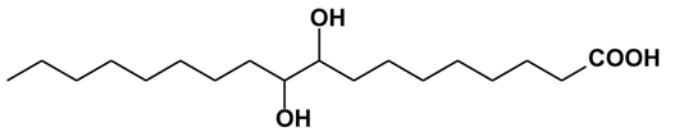
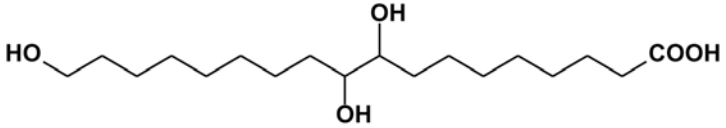
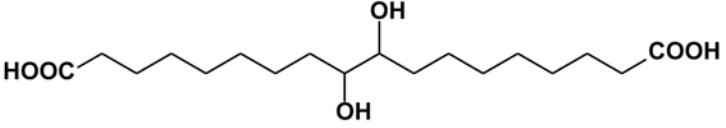
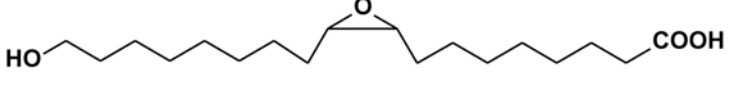

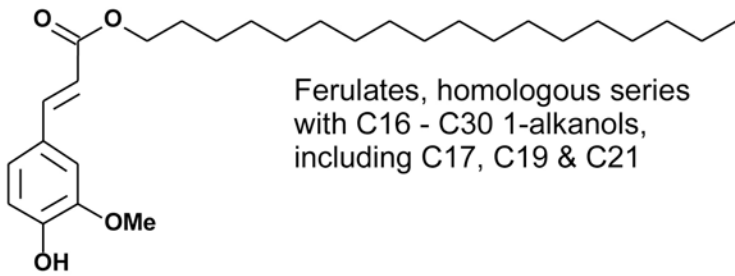
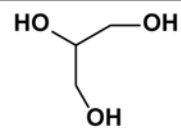
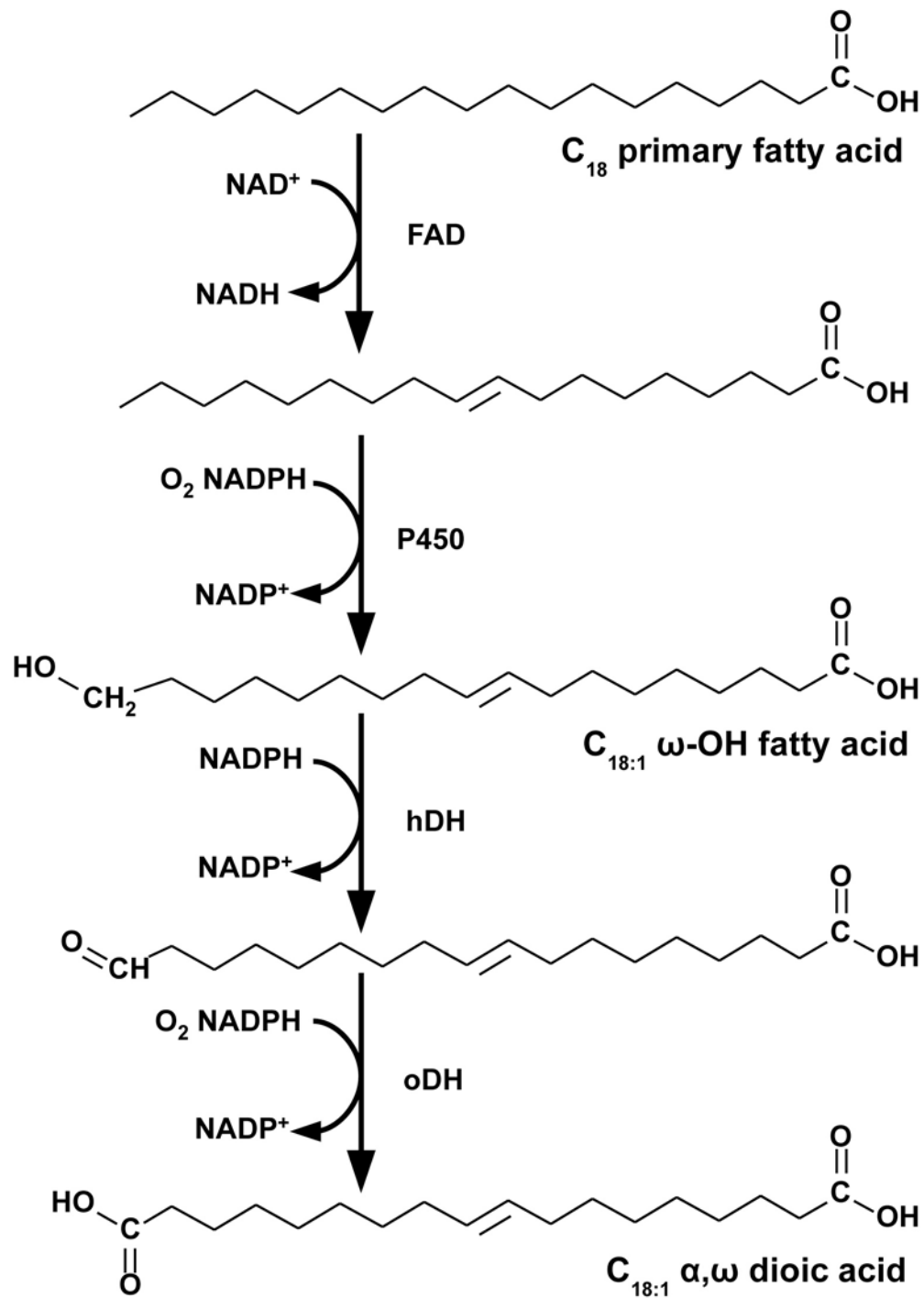
	Saturated 1-alkanols; 16:0 - 32:0
	Saturated alkanolic acids; 16:0 - 28:0
	ω-Hydroxyalkanoic acids; 16:0 - 24:0 & 18:1
	α,ω-Dioic acids; 16:0 - 24:0 & 18:1
	9(10),ω-Dihydroxyalkanoic acid; predominantly 18:0
	9,10-Dihydroxyalkanoic acids; 16:0 & 18:0
	9,10,18-Trihydroxyalkanoic acid; predominantly 18:0
	9,10-Dihydroxy-α,ω-dioic acid; predominantly 18:0
	9,10-Epoxy-ω- hydroxyalkanoic acid; predominantly 18:0
	9,10-Epoxy-α,ω-dioic acid; predominantly 18:0
 <p>Ferulates, homologous series with C16 - C30 1-alkanols, including C17, C19 & C21</p>	
 <p>Glycerol</p>	

Figure 1.14 Synthesis of two key aliphatic monomers. A C₁₈ primary fatty acid is desaturated, then ω-hydroxylated into C_{18:1} ω-hydroxy fatty acid, and oxidized into C_{18:1} α,ω-dioic acid. Abbreviations: FAD = fatty acid desaturase; P450 = cytochrome P450 monooxygenase; hDH = ω-hydroxyacid dehydrogenase; oDH = ω-oxoacid dehydrogenase. Modified from Kolattukudy (1980), Bernards (2002), and Franke and Schreiber (2007).



CoA that is two carbons longer than when it entered the FAE (Fig. 1.15; Kunst and Samuels 2003; Franke and Schreiber 2007; Samuels et al. 2008; Franke et al. 2009; Lee et al. 2009). Then the derivatives are either reduced into primary alcohols, decarboxylated into *n*-alkanes, or oxidized into ω -hydroxy and 2-hydroxy fatty acids (Yang and Bernards 2006).

1.4.3 SPPD biosynthesis

The SPPD is rich in mainly hydroxycinnamic acid derivatives with less relative amounts of monolignols and tyramine (Fig. 1.16; Borg-Olivier and Monties 1993; Bernards et al. 1995; Negrel et al. 1996). It is known that the synthesis of phenolic compounds is initiated within the shikimate pathway, which yields phenylalanine (Fig. 1.17). Phenylalanine is the precursor for most phenylpropanoids including hydroxycinnamic acids. The processing of hydroxycinnamic acids involves hydroxylation at the hydroxycinnamoyl-CoA derivative level (see Dixon et al. 2001) and methylation by a suberin-specific *O*-methyltransferase (Held et al. 1993), giving rise to key SPPD monomers including *p*-coumaric acid, caffeic acid, ferulic acid, and their amide derivatives (Fig. 1.17; see Bernards 2002).

1.4.4 The role of glycerol

Glycerol is hypothesized to act as the primary linker between the SPAD and SPPD, and also between monomers in the SPAD. The bonds are ester-linkages formed by a dehydration reaction between a hydroxyl group on glycerol and a carboxyl group on either α,ω -dioic acid, ω -hydroxy fatty acid, or ferulic acid (Graça and Pereira 2000a, b; Kolattukudy 2001; Bernards 2002). The presence of glycerol gives the domains a three-dimensional structure and indicates that glycerol-based compounds are substrates for oxidation and polymerization reactions (Beisson et al. 2007; Li et al. 2007).

1.4.5 Physiological significance of suberin

By coupling what is known about suberin chemistry with the location of suberin in the cell wall, one can further understand the physiological significance of suberin. In exodermal and endodermal cells, the suberin lamellae and Casparian bands both contain suberin monomers. In suberin lamellae, the SPAD, with its lipophilic nature and intercalated waxes, is located between the cell wall and plasma membrane. These features make the SPAD important for restricting radial water and solute transport (Kolattukudy and Dean 1974; Soliday et al. 1979; Vogt et al. 1983; Evert et al. 1985; Zimmermann et al. 2000; Hose et al. 2001; Schreiber et al. 2005a). The specific pathway that will be influenced by suberin lamellae is the transcellular pathway (Fig. 1.4) because of the location of the lamellae is between the cell walls and plasma membranes (Fig. 1.5). The SPPD consists of aromatic compounds that are linked covalently to primary cell wall carbohydrates. Such features make the SPPD important for limiting the penetration of pathogenic bacteria, fungi, and oomycetes (Kolattukudy 1980, 1984; Lulai and Corsini 1998). (Although resistance to microbe infection is an important function of suberin, the water and solute permeability properties of the suberin lamellae remain the focus of this thesis work.) Casparian bands are composed of mainly poly(phenolics) with less relative amounts of aliphatics, and are embedded within the intermicrofibrillar spaces of targeted cell walls (Schreiber et al. 1994; Schreiber 1996; see Steudle and Peterson 1998). These features allow Casparian bands to restrict the apoplastic flow of solutes (de Rufz de Lavison 1910; Baker 1971; Peterson 1987; Cholewa and Peterson 2004). The fundamental importance of suberin in root physiology has led to in-depth research on the dynamic metabolic processes involved in suberin synthesis.

Figure 1.15 Pathway of the fatty acid elongation complex (see text for details). (1) Condensation by 3-ketoacyl CoA synthetase. (2) Reduction by 3-ketoacyl CoA reductase. (3) Dehydration by 3-hydroxyacyl CoA dehydratase. (4) Reduction by trans-2-enoyl CoA reductase. Modified from Bernards (2002) and Franke and Schreiber (2007).

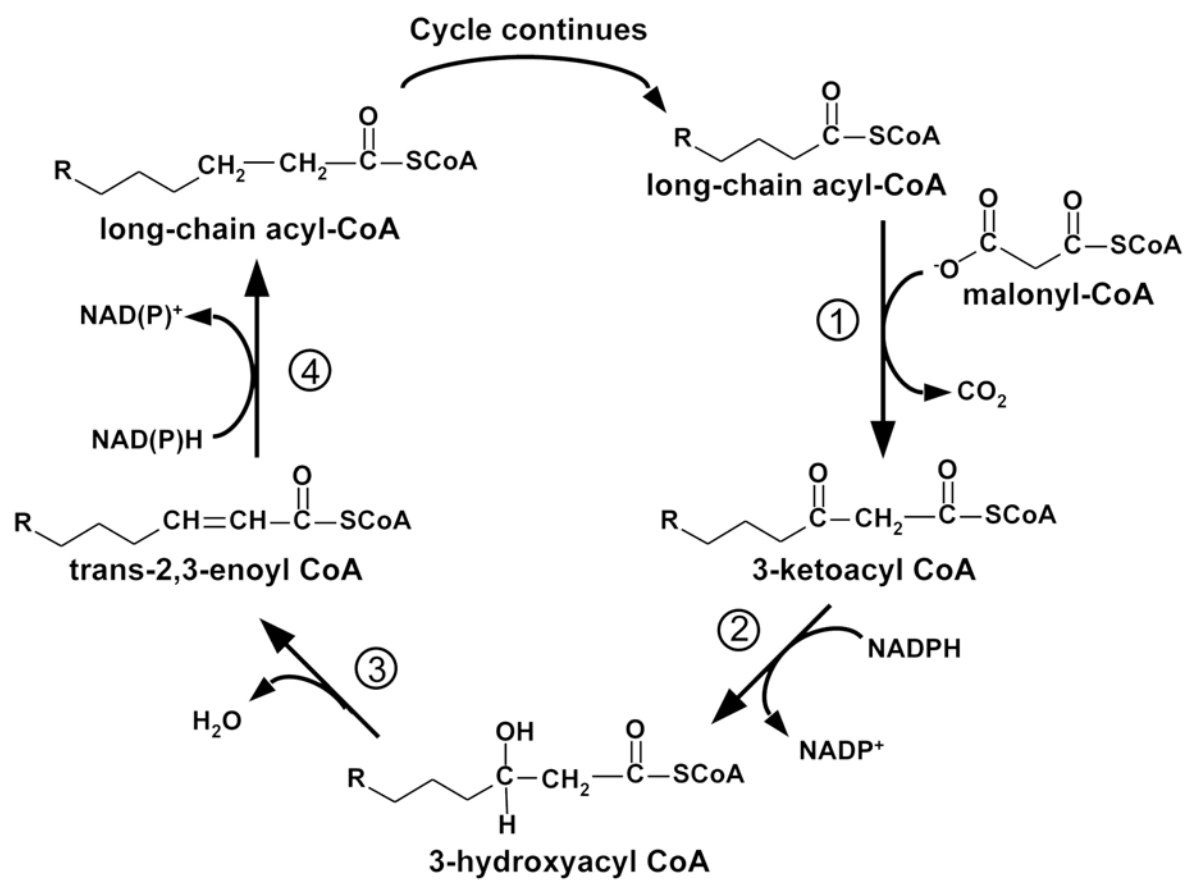


Figure 1.16 Phenolic monomers of suberin lamellae. Modified from Bernards (2002).

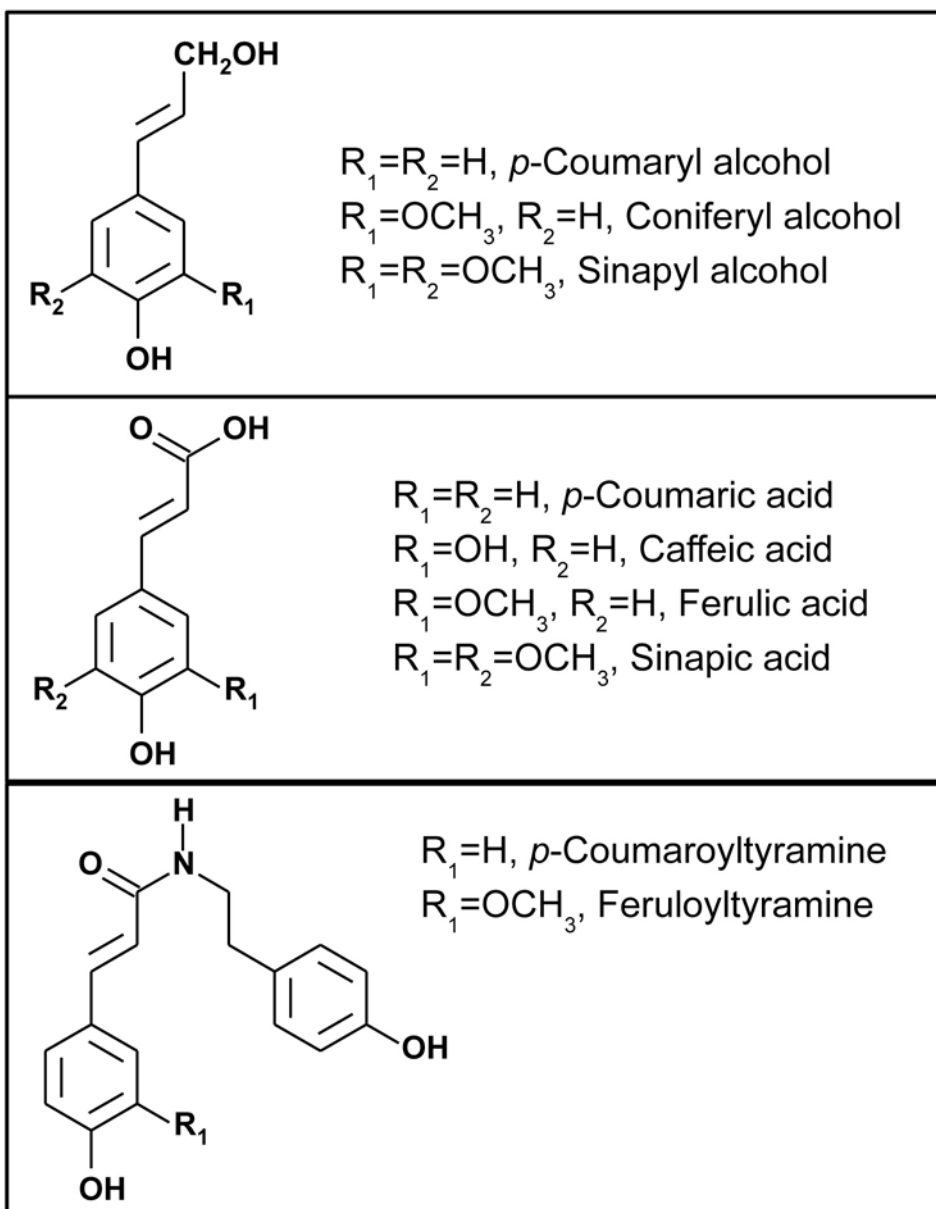
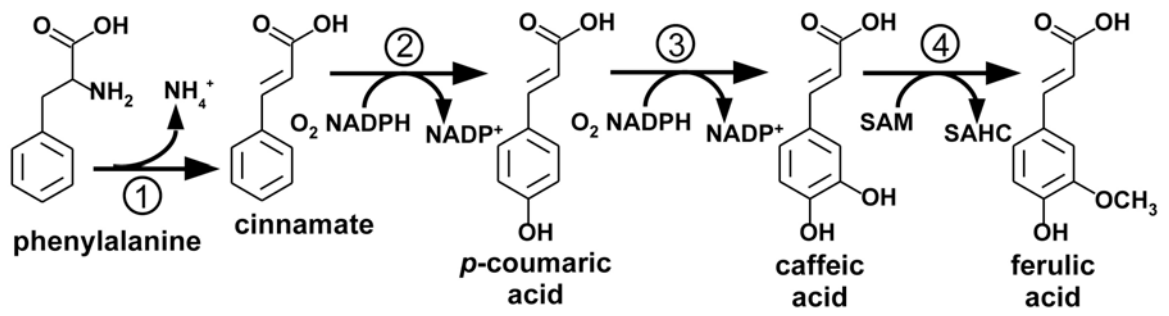


Figure 1.17 Synthesis of three key phenolic monomers (see text for details). (1) Deamination by phenylalanine ammonia-lyase. (2) Hydroxylation by cinnamate-4-hydroxylase. (3) Hydroxylation by *p*-coumaric acid 3-hydroxylase. (4) Methylation by caffeic acid 3-*O*-methyltransferase. Modified from Bernards (2002).



1.4.6 Suberin deposition in maturing tissues

Analysis of suberin monomeric composition and abundance during tissue maturation is necessary for understanding suberin biosynthesis. Early suberin research was directed toward 'end point-analyses', meaning the identification and quantification of monomers that were isolated as depolymerization products from suberin in mature tissues (see Bernards 2002; Yang and Bernards 2006, and references therein). With little or no turnover of the suberin polymer, and by using mature tissues that undoubtedly contained an abundance of suberin, much progress was made.

Fewer studies have been conducted where suberin composition and abundance during tissue maturation were analysed – but this approach is valuable in terms of understanding the dynamic metabolic processes of suberin biosynthesis. In an excellent example, Yang and Bernards (2006), inspired by Kolattukudy and Dean (1974) and Dean and Kolattukudy (1977), sampled wound-induced periderm in *S. tuberosum* tuber (as it developed over seven days) to identify and quantify polymerized (insoluble) and unpolymerized (soluble) SPAD monomers. The insoluble fraction consisted of ω -hydroxy fatty acids, α,ω -dioic acids, and primary fatty acids (>C20). These polymerized fatty acid derivatives were first detected three days after the initiation of wound-induced periderm development, and their abundances increased over three more days. The soluble fraction contained only trace amounts of ω -hydroxy fatty acids and α,ω -dioic acids, but >C20 fatty acids were detected in greater amounts. These results from Yang and Bernards (2006) could not have been predicted from an end point-analysis. In a second example, Höfer et al. (2008) identified and quantified insoluble SPAD monomers at three locations along the length of *Arabidopsis thaliana* roots.

They measured, from root tip to base, an increase in C18:1 ω -hydroxy fatty acid abundance, a steady quantity of C18:1 α,ω -dioic acids, and a decrease in the amount of primary fatty acids. While these authors had a good experimental approach, they unfortunately measured different tissue types – in the first zone closest to the root tip they measured endodermal suberin (primary growth), but in the two more basal locations they also measured peridermal suberin (secondary growth). In a third set of examples, Zeier et al. (1999a), Thomas et al. (2007), and Krishnamurthy et al. (2009) each measured increasing amounts of insoluble exodermal SPAD monomers (including ω -hydroxy fatty acids) along the length of *Z. mays*, *Glycine max*, and *O. sativa* roots, respectively (see Chapters 5 and 6 for further details). Such analyses of suberin composition and abundance in tissues undergoing maturation are valuable for determining the timing and regulation of suberin synthesis.

1.4.7 Suberin deposition in the exodermis of *Iris germanica* and *Allium cepa*

End point-analyses of the suberin from mature root tissues of *Iris germanica* and *Allium cepa* have been conducted previously. Zeier and Schreiber (1998) performed analyses of the exodermal and endodermal suberin content in a single mature region for roots of five species including *I. germanica* and *A. cepa*. While the authors presented the total yield of exodermal aliphatic suberin for *I. germanica* (approximately 40 $\mu\text{g mg}^{-1}$) and *A. cepa* (approximately 23 $\mu\text{g mg}^{-1}$), they did not report the number of mature exodermal layers nor the distance from the root tip of the analysed tissue. For *I. germanica*, the roots were soil-grown and the endodermis had matured to State III (meaning most cells contained Casparian bands, suberin lamellae and tertiary wall thickenings, as described by Van Fleet [1961], Esau [1965] and Robards et al. [1973]). Based on endodermal and MEX maturation patterns for soil-grown *I.*

germanica roots (Meyer et al. 2009; see Fig. 2.5, Chapter 2), it is currently assumed that Zeier and Schreiber (1998) tested tissue specimens were at least 100 mm from the root tip, and had contained at least three (but perhaps four) exodermal layers. For *A. cepa*, the roots were hydroponically grown and were at least 300 mm in length when harvested (Zeier and Schreiber 1998). Based on root growth rates and the sequence of exodermal maturation in *A. cepa* (Perumalla and Peterson 1986; Barrowclough and Peterson 1994; see Fig. 5.2, Chapter 5), it is currently assumed that the measured monomer amounts by Zeier and Schreiber (1998) corresponded to an exodermis that had been fully mature for about 14 days. These previously measured amounts of aliphatic suberin represent a metabolic snapshot of only mature exodermal layers. To build on this previous work, the objectives for the current study were to analyze the insoluble and soluble suberin monomer content and abundance at several stages of exodermal maturation, as well as under different growth conditions. The goal was to address how suberin is synthesized in maturing uniseriate and multiseriate exodermal layers.

1.4.8 Research aims III

For the current work with *I. germanica* roots, insoluble and soluble SPAD monomers were identified and quantified at key stages of MEX maturation and compared between submerged and humid air gap hydroponic growth conditions. The tested hypothesis was that root areas exposed to the lower humidity air gap have an increased abundance of key SPAD monomers as a response to the dehydrating growth condition compared with submerged root areas. Suberin monomeric data was then correlated with *I. germanica*'s structural (see Chapter 2) and functional data (see Chapter 3), to potentially reveal some of the traits that underlie a

coordinated response of the exodermis to drying growth conditions. In addition, the maturing uniseriate exodermis from hydroponically grown *A. cepa* roots was used as a model to analyse the insoluble and soluble monomer compositions and quantities for both the SPAD and SPPD. It was hypothesized that SPAD and SPPD monomer composition and quantities would increase gradually as the exodermis matured. Both *I. germanica* and *A. cepa* roots were amenable to such analyses because the sequence of exodermal maturation had been determined previously, and these roots generated very few or no lateral roots that could potentially alter the chemical analyses (Peterson and Perumalla 1984; Perumalla and Peterson 1986; Barrowclough and Peterson 1994; Ma and Peterson 2001a). The findings will lead to a more complete understanding of SPAD and SPPD biosynthesis during the maturation of uniseriate and multiseriate exodermal layers.

Chapter 2

Environmental effects on the maturation of the endodermis and multiseriate exodermis of *Iris germanica* roots

[Published in *Annals of Botany* 103: 687–702, 2009. Winner of the Canadian Botanical Association's 2009 Taylor Steeves Award - for the best plant development paper by a student.]

2.1 Overview

Most studies of exodermal structure and function have involved species with a uniseriate exodermis. To extend this work, the development and apoplastic permeability of *Iris germanica* roots with a multiseriate exodermis (MEX) were investigated. The effects of different growth conditions on MEX maturation was also tested. In addition, the exodermises of eight *Iris* species were observed to determine if their mature anatomy correlated with habitat. Plants were grown in soil, hydroponics (with and without a humid air gap), or aeroponics. Roots were sectioned and stained with various dyes to detect MEX development from the root apical meristem, Casparian bands, suberin lamellae, and tertiary wall thickenings. Apoplastic permeability was tested using dye (berberine) and ionic (ferric) tracers. The root apical meristem was open and MEX development non-uniform. In soil-grown roots, the exodermis started maturing (i.e., Casparian bands and suberin lamellae were deposited) 10 mm from the tip, and two layers had matured by 70 mm. In both hydro- and aeroponically grown roots, exodermal maturation was delayed. However, in areas of roots exposed to an air gap in the hydroponic system, MEX maturation was accelerated. In contrast, maturation of the endodermis was not influenced by the growth conditions. The

mature MEX had an atypical Casparian band that was continuous around the root circumference. The MEX prevented the influx and efflux of berberine, but had variable resistance to ferric ions due to their toxic effects. *Iris* species living in well-drained soils developed a MEX, but species in water-saturated substrates had a uniseriate exodermis and aerenchyma. MEX maturation was influenced by the roots' growth medium. The MEX matures very close to the root tip in soil, but much further from the tip in hydro- and aeroponic culture. The air gap accelerated maturation of the second exodermal layer. In *Iris*, the type of exodermis was correlated with natural habitat suggesting that a MEX may be advantageous for drought tolerance.

2.2 Introduction

An exodermis is present in the majority of angiosperm roots tested (Perumalla et al. 1990; Peterson and Perumalla 1990) and an endodermis is present in all roots so far tested except for some members of the Lycopodiaceae (see Clarkson 1996; Damus et al. 1997; DE Enstone, University of Waterloo, Canada, 'pers. comm.'). The development of the highly specialized cells of these two layers progresses through as many as three states as described by Van Fleet (1961), Esau (1965), and Robards et al. (1973). In roots of most species, the endodermis starts to mature before the exodermis, but the sequence of development is roughly the same in cells of both layers. The first developmental state (State I) is reached when Casparian bands are formed in the anticlinal walls. At this time, there is a tight connection between the modified wall and the adjacent plasmalemmas of the cells (Bonnett 1968; Enstone and Peterson 1997; Karahara and Shibaoka 1992; Ma and Peterson 2001a).

Isolated Casparian bands are composed predominantly of lignin phenolics, along with aliphatic suberin, cell wall carbohydrates and proteins (Zeier and Schreiber 1998). Next, during the second developmental state (State II), a suberin lamella is deposited around the protoplast (i.e., between plasmalemma and wall). This lamella severs the connection between the Casparian band and plasmalemma (Robards et al. 1973; Haas and Carothers 1975; Ma and Peterson 2001a). According to Kolattukudy (1980), Zeier and Schreiber (1998) and Bernards (2002), suberin lamellae consist mainly of poly(aliphatic) and poly(phenolic) suberin monomers, as well as glycerol and associated waxes; cell wall proteins and polysaccharides were also detected in their isolates of the lamellae. Lastly, in the third developmental state (State III), tertiary cellulosic walls that are often lignified (Zeier and Schreiber 1998) are laid down along the suberin lamellae. These depositions can be U-shaped and thick enough to mask the identification of Casparian bands and suberin lamellae (Van Fleet 1961; Esau 1965; Clarkson et al. 1987). In the endodermis, there is typically a gap between the development of the Casparian bands, suberin lamellae and tertiary walls, whereas in the exodermis the situation is more variable. In the uniform exodermis, the Casparian bands and suberin lamellae are normally deposited simultaneously. But in the dimorphic exodermis, development of suberin lamellae and tertiary walls is delayed in the short cells (von Guttenberg 1968; Peterson and Enstone 1996; Enstone and Peterson 1997). The rate at which individual cells mature within the exodermis and endodermis can vary; it is common to observe some cells of the dimorphic exodermis and endodermis in older parts of roots that have only matured to State I. These cells have Casparian bands but lack suberin lamellae and tertiary walls, and are called passage cells (Esau 1965; von Guttenberg 1968).

In the uniform exodermis, concurrent deposition of Casparian bands and suberin lamellae can be patchy or variable along the root. Since immature cells in the uniform exodermis lack Casparian bands, they are not referred to as passage cells (Enstone and Peterson 1997). In a broader context, this variation in maturation rates, in addition to other modifications, can allow a plant species to become specialized in order to exploit specific environmental conditions.

The exodermis is known to vary in structure among species (Kroemer 1903; Perumalla et al. 1990; Peterson and Perumalla 1990; Hose et al. 2001). To date, most root structure and function research has focussed on species with a single-layered (uniseriate) exodermis, including *Zea mays*, *Oryza sativa*, and *Allium cepa* (Perumalla et al. 1990; Miyamoto et al. 2001; see Enstone et al. 2003 and references therein, Ranathunge et al. 2003, 2004, 2005a, b). A less common type of exodermis that has received little attention is the multi-layered or multiseriate exodermis (MEX) such as that found in *Iris germanica* (Kroemer 1903; Shishkoff 1986; Peterson and Perumalla 1990; Zeier and Schreiber 1998), *Typha* spp. (Seago and Marsh 1989; Seago et al. 1999) and *Phragmites australis* (Armstrong et al. 2000; Soukup et al. 2002). The exodermal Casparian band in these species is atypical because, instead of being confined to the anticlinal walls, it also extends into the tangential walls of the adjacent layers of the exodermis. Since this Casparian band deposition follows the exodermal wall continuum, the band often appears H- or Y-shaped in cross section. Roots of *I. germanica*, in particular, are of interest as they have been the subject of some basic anatomical studies (Kroemer 1903; Shishkoff 1986; Peterson and Perumalla 1990) and biochemical work (Zeier and Schreiber 1998, 1999). In these articles, brief descriptions of exodermal ontogeny and

structure were provided, but a thorough investigation that combined the development of all root tissues was lacking. Furthermore, the distribution of *Iris* is global with many species inhabiting diverse natural habitats such as wetlands and well-drained soils, allowing observation of potential correlations between root anatomy and habitat.

The timing and rates at which exodermal and endodermal tissues mature depend on environmental cues and how these cues influence the regulation of expression of developmental genes (see Bray et al. 2000; Enstone et al. 2003). Plant species that are native to particular habitats have evolved constitutive resistances to local environmental stresses. However, if these stresses increase in severity or duration, or if a new stress is encountered, the species must acclimate or otherwise risk death (Bray et al. 2000). Acclimation occurs, in part, by regulation of the onset and rapidity of tissue development or its modification. In roots the exodermis, for example, is known to respond to changes in the substrate (see Enstone et al. 2003). Like Clarkson et al. (1987), Enstone and Peterson (1998) exposed basal parts of *Z. mays* roots to humid air inside hydroponic chambers. After 2 d, 92% of the exodermal cells in the exposed part of the root were in State II compared to 11% of the cells of the same age in submerged roots. Exodermal suberin lamellae formation was also accelerated in *Z. mays* grown in aeroponics, vermiculite, or in a stagnant (oxygen-deficient) solution compared to aerated hydroponics (Zimmermann and Steudle 1998; Enstone and Peterson 2005). In contrast, the developmental reactions of a MEX to various growth conditions have not been investigated.

The origin and maturation of *I. germanica*'s exodermis and endodermis, layers flanking the parenchymatous central cortex, were studied in the current work. The effects of varying

growth conditions on maturation of these layers were explored. Additionally, the apoplastic permeability of its MEX was tested using dye (berberine) and ionic (ferric) tracers. To establish a suitable treatment time and concentration for the latter, a toxicity test using *Zea mays* seedlings with rapid root growth was performed. *I. germanica* roots were amenable to permeability tests because they generated very few lateral roots leaving the exodermis intact, a trait not shared by *Typha* and *Phragmites*. Lastly, the mature root anatomy of seven other iris species was compared to that of *I. germanica* to determine if the root anatomy among species of this genus is correlated with their natural habitats.

2.3 Materials and methods

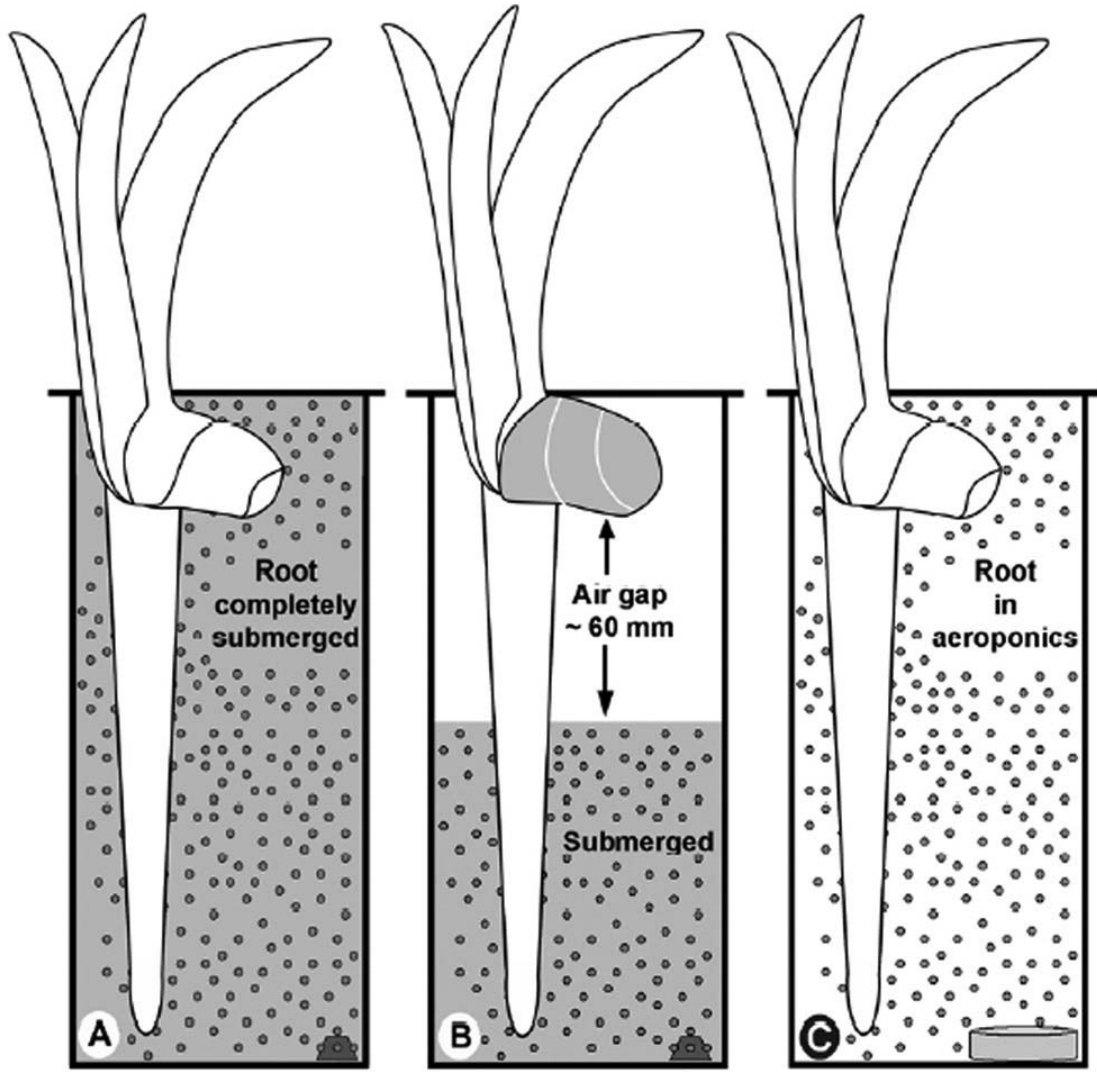
2.3.1 Plant material and growth conditions

Vegetative plants (rhizomes, with their leaves and subtending roots) of 25 *Iris germanica* L. cultivars [Supplementary table 2.1] and five additional species (*I. pumila* L. [origin], *I. pallida* Lam. [cv. Argenteo Variegata], *I. sibirica* L. [cvs. Super Ego and Violet Flare], *I. spuria* L. [cvs. Amber Ripples and White Olinda] and *I. versicolor* L. [cv. Blue Flag]) were collected from outdoor plots at the Royal Botanical Gardens in Burlington, Ontario in early August 2005. They were transplanted in potting soil (Pro-Mix, Premier Horticulture Inc., Dorval, Quebec) and placed in a growth chamber (light $300 \mu\text{mol m}^{-2} \text{s}^{-1}$ PAR, 16 h day period, 25°C day, 23°C night, R.H. 65%). To obtain roots for testing, the rhizomes and attached roots were carefully lifted from the soil after 30-45 d. Then healthy looking adventitious roots, between 150-200 mm in length, were excised from the rhizome under

water with a razor blade and rinsed to remove most of the soil. Roots used for anatomical analysis were stored in 70% ethanol and kept in a refrigerator (4°C). Roots that were tested for apoplastic permeability were used immediately after excision from the rhizome. Roots from two additional species, *I. hexagona* and *I. pseudacorus*, were preserved in 70% ethanol and obtained for anatomical observation (courtesy of S. Mopper, University of Louisiana, Lafayette, USA).

I. germanica plants were also collected from outdoor plots at the University of Bayreuth, Germany, in May 2006, transplanted into potting soil, and placed in a growth chamber. After 30-45 d, some were gently unearthed and transferred to hydroponic or aeroponic culture. The nutrient solution was 0.09 mM (NH₄)₂SO₄, 0.07 mM MgSO₄, 0.06 mM Ca(NO₃)₂, 0.05 mM KH₂PO₄, 0.05 mM KNO₃, 0.05 mM Fe(III)-EDTA, 0.03 mM K₂SO₄, 4.6 μM H₃BO₃, 1.8 μM MnSO₄, 0.3 μM ZnSO₄, 0.3 μM CuSO₄; pH = 5.5-6.0. All the hydroponic tanks were completely filled with solution until new roots, produced subsequent to transfer, were longer than 65 mm. Some tanks remained full of nutrient solution (control, Fig. 2.1A) while others were only partially filled during the weekly nutrient exchange to create an air gap of approximately 60 mm between the base of the rhizome and solution surface (Fig. 2.1B). These rhizomes were wrapped in paper towel saturated with nutrient solution to prevent them from drying. The humidity in the air gap was measured with a digital hygrometer/thermometer (Control Company; Friendswood, Texas). The nutrient solution was constantly aerated using a single bubbling stone and was replaced with fresh solution weekly. The aeroponic chamber was a cylinder (1 m diameter, 1 m high) that could hold two rhizomes. A humidifier ('Defensor'; Barth and Stöcklein, Garching, Germany) that

Figure 2.1 Drawings of the hydroponic (A), air gap (B), and aeroponic (C) systems used to expose iris roots to various conditions (not to scale). (A) Roots and rhizomes were completely submerged in hydroponic nutrient solution. (B) A partially filled hydroponic tank with an air gap between the base of the root (attached to the rhizome) and the surface of the solution. Nutrient solutions were constantly aerated with atmospheric air using bubbling stones (trapezoids). (C) Roots and rhizomes were completely saturated from continuous misting with a humidifier (grey cylinder) in an aeroponic tank.



continuously produced a mist of nutrient solution was placed in this chamber (Fig. 2.1C). A high humidity was thus obtained, and nutrient solution was observed dripping from the roots.

2.3.2 Root anatomy

To observe *I. germanica*'s root apical meristem and origin of the MEX, 4-10 mm long roots were used. After excising these roots from the rhizome, they were vacuum infiltrated with 4% formaldehyde in acetic acid (FAA), left submerged in FAA for 2-3 d, then rinsed and stored in 70% ethanol. The fixed root specimens were embedded in Paraplast Plus (Sherwood Medical Industries; DeLand, Florida) and cross-sectioned with a microtome at 8-10 μm increments from the root tip. Median longitudinal sections were also taken. Sections were stained with safranin/fast green and viewed with white light (Seago and Marsh 1989).

Root structure, especially key exodermal and endodermal developmental stages, was observed in detail along the length (all areas from the tip to 20 mm, and then at intervals of 10 mm up to 150-200 mm) of at least ten roots for *I. germanica*, grown in the different conditions described above. Additionally, the anatomy 150-200 mm from the tip was observed for at least three roots from each of the 25 *I. germanica* cultivars. For all other species, the anatomy of at least five roots each was observed at 90-120 mm from the tip. Roots were freehand sectioned transversely or longitudinally at various distances from the root tip and then subjected to several staining procedures. These were Sudan red 7B and Fluorol yellow 088 for lipids including suberin lamellae (Brundrett et al. 1991), berberine hemisulphate–aniline blue for Casparian bands (Brundrett et al. 1988), phloroglucinol-HCl for lignin (Jensen 1962), and TBO as a general polychromatic stain (O'Brien et al. 1964).

The removal or clearing of cellular protoplasts can be advantageous when studying cell

wall structure. Recently, Lux et al. (2005) reported new approaches for simultaneously clearing and staining tissue. Basically, the fluorochromes 0.1% berberine hemisulphate and 0.01% Fluorol yellow were dissolved in a clearing mixture consisting of pure lactic acid saturated with chloral hydrate. In the present study, iris root sections were incubated in either of the two dye solutions at 70°C for 1 h. In the case of berberine hemisulphate, sections were counterstained with 0.5% aniline blue (dissolved in dH₂O) at room temperature for 30 min. All specimens were viewed with ultraviolet (UV) light. In addition to the clearing, physical separation of the central region (endodermis and stele) from the rest of the root tissue was possible. To achieve this, root segments were cut longitudinally with a razor blade through the central cortex, and then the loosely adhering epidermal, exodermal and central cortical tissues were peeled off using fine-tipped forceps. This allowed a clear longitudinal view of the endodermal cells so that their passage cells and cell lengths could be observed.

Results of all staining procedures were compared to control, unstained sections. These were viewed with either white or UV light as appropriate.

Sulphuric acid digestion was also used which reportedly spares suberized and cutinized tissue (Johansen 1940). Sections of roots were bathed in a drop of concentrated sulphuric acid on a slide for 24 h at room temperature.

Specimens were examined with Zeiss epifluorescence microscopes with either white or UV light (filter set: exciter filter G 365, dichroitic mirror FT 395, and barrier filter LP 420; Carl Zeiss, Inc.). Photographs were taken with a Q-Imaging digital camera (Retiga 2000R, Fast 1394, Cooled Mono, 12-bit; Quorum Technologies Inc., Guelph, ON) or a Cool Snap digital camera (Visitron Systems, Puchheim, Germany).

2.3.3 *Iris germanica* root growth rate measurements

Growth rates were estimated for soil-grown roots (n = 9) and hydroponically grown roots that were completely submerged (n = 10) or exposed to the air gap (n = 10). An initial measurement of root length was made (length = 40-70 mm), and five or six days later a second measurement was taken. Root tips did not contact the sides or bottoms of either the pots or hydroponic chambers during the growth measurement period. Data were analyzed with a one-way Analysis of Variance (ANOVA) at $p \leq 0.05$ (Statistix Student Ed., v. 2.0). The ages of root regions where key maturation processes occurred were calculated by assuming the roots grew uniformly during the period of measurement.

2.3.4 Apoplastic permeability

Soil-grown *I. germanica* roots were excised from the rhizome under water and then cut into 30-40 mm long segments. The cut ends were blotted dry with tissue paper and then sealed with molten sticky wax (Kerr Manufacturing Canada, Mississauga, ON) prior to treatment. Two apoplastic tracers were employed to test the permeability of the exodermis. At least five roots were used for each tracer test. Several controls were run, 1) unstained sections (to observe native pigmentation or autofluorescence), 2) sections stained with the tracers (to confirm that cells exposed to the tracers would be stained), and 3) peripheral layers (i.e., epidermis, exodermis, and part of the central cortex) severed by a longitudinal cut prior to tracer application (to test the permeability of the central cortex).

Berberine hemisulphate. As described by Enstone and Peterson (1992) excised, sealed roots were bathed in 0.05% berberine hemisulphate for 1 h followed by 0.05 M potassium thiocyanate for 1 h. In some cases, a short, longitudinal incision was made with a razor blade

through the peripheral layers so that the dye could bypass the exodermis and enter the central cortex. This allowed for exodermal permeability from the inside to be tested. Roots were freehand-sectioned and viewed with UV light as described above.

Ferrous sulphate toxicity test. Thirty germinated kernels of *Zea mays* L. (cv. Seneca Horizon; Ontario Seed Co., Waterloo, ON) with root lengths of 30-40 mm and emerged coleoptiles were transferred to aerated hydroponic culture in a glasshouse under ambient lighting. The culture solution consisted of 0.7 mM K_2SO_4 , 0.5 mM $Ca(NO_3)_2$, 0.5 mM $MgSO_4$, 0.1 mM KCl, 0.1 mM KH_2PO_4 , 0.01 mM Fe(III)-EDTA, 1.0 μM H_3BO_3 , 0.5 μM $MnSO_4$, 0.5 μM $ZnSO_4$, and 0.2 μM $CuSO_4$. The hydroponic system (with light-proof walls) was assembled as previously described (Enstone and Peterson 1998). Kernels were placed on a floating styrofoam sheet with holes to accommodate the roots. This was then covered with two sheets of cheesecloth that hung into the solution to keep the kernels hydrated. The top of each hydroponic tank was covered with two layers of shading cloth to reduce light transfer from above into the tank. After 2 d in the hydroponic solution, the root lengths of all seedlings were measured. The roots were then exposed to ferrous sulphate ($FeSO_4 \cdot 7 H_2O$) at different concentrations. Six large, glass test tubes (60 mL) were jacketed with aluminium foil and completely filled with a desired concentration of $FeSO_4$ (0.25 mM in 1 tube, 0.5 mM in 3 tubes, and 1.0 mM in 1 tube) or with nutrient solution (1 tube). The top of each tube was covered with flexible, laboratory film (Parafilm) in which small slits had been made to allow the roots to enter the solution while supporting the kernels above. Five seedlings were placed in each tube. Roots were exposed to the nutrient solution, 0.25 and 1 mM $FeSO_4$ treatments for 2 h; the duration of the 0.5 mM $FeSO_4$ treatment was 1, 2, or 3 h (hence the need for 3

tubes containing this concentration). Following the intended exposure time, the seedlings were transferred back to the original hydroponic tank and grown for three more days during which the root lengths were measured daily. This toxicity experiment was conducted twice. Growth rate data were analyzed using a one-way ANOVA with a Least Significant Differences (LSD) post-hoc test at $p \leq 0.05$ (Statistix Student Ed., v. 2.0).

Ferrous sulphate permeability. This method was modified from de Rufz de Lavison (1910), Soukup et al. (2002) and Armstrong and Armstrong (2005), considering the results from the toxicity test above. *I. germanica* roots were incubated in 0.5 mM FeSO₄ for 1 h. To test exodermal permeability from the inside, the peripheral layers of some roots were cut open as described above, allowing the FeSO₄ to enter the central cortex. After treatment, all roots were rinsed with running water for 30 min and then freehand-sectioned. The sections were placed in a drop of 1 mM potassium ferrocyanide (K₄[Fe(CN)₆]·3 H₂O) dissolved in 0.5% HCl on a slide for 2-3 min. During this time, a ‘Prussian blue’ precipitate of ferric ferrocyanide (Fe₄[Fe(CN)₆]₃) formed in the areas where the ferric ions had entered (Pearse 1968). (According to Guerinot and Yi [1994], in the eudicots and non-graminaceous monocots [such as *I. germanica*], ferric ions are restricted to the apoplast while ferrous ions can be transported across the plasmalemma.) Sections were observed using the microscope described above (with white light).

The potential toxicity of FeSO₄ and its effect on the apoplastic permeability of *I. germanica* roots were tested. Sealed root segments were incubated in 0.5 mM FeSO₄ or water (i.e., control) for 1 h, followed by rinsing with running water for 30 min. These root

segments were then submerged in 0.05% berberine hemisulphate for 1 h, rinsed with water, cross sectioned, and viewed with UV light.

2.4 Results

2.4.1 *Iris germanica* root growth and anatomy

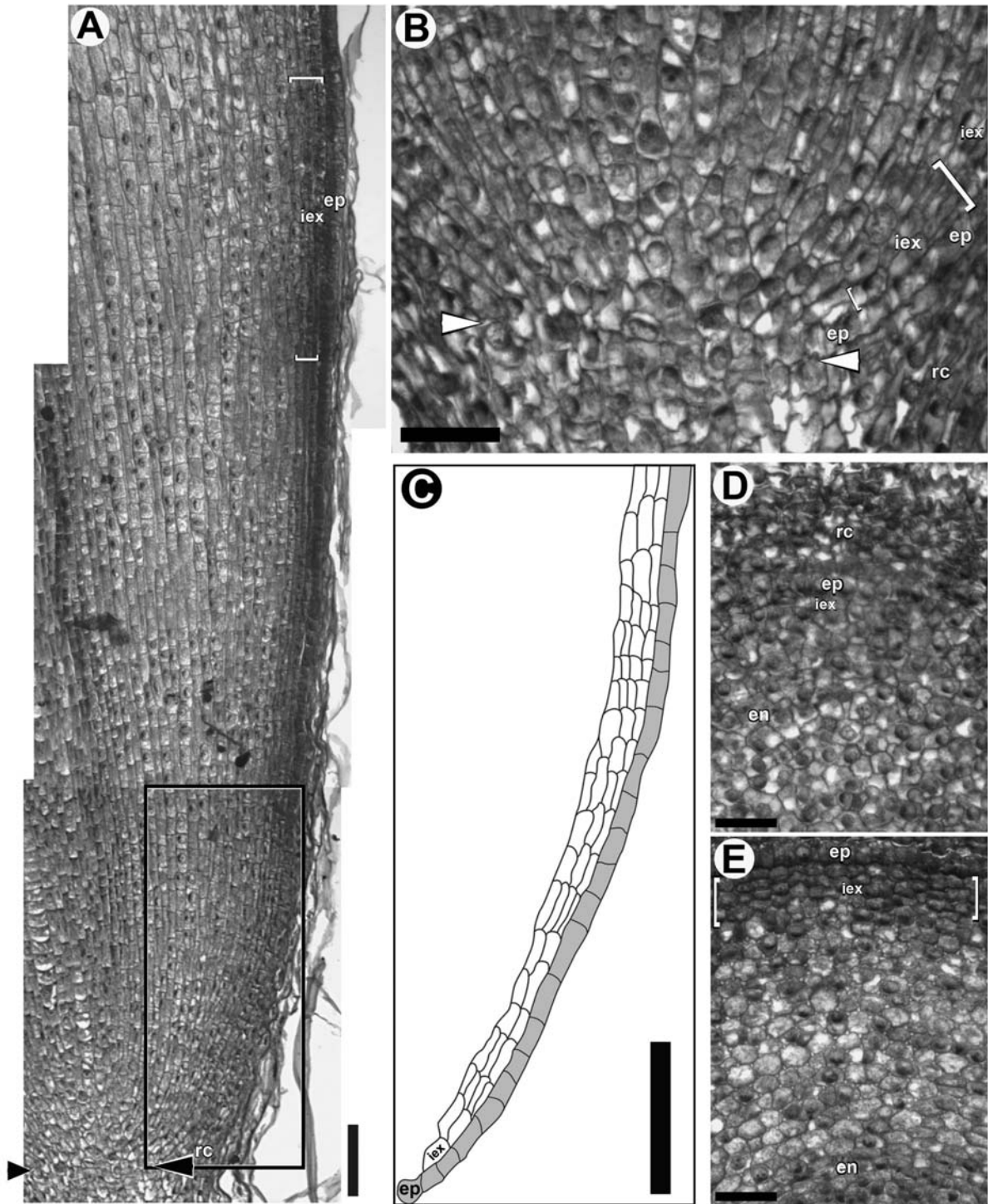
Root growth rates (mean \pm standard deviation) for soil-grown roots (14.7 ± 1.9 mm d⁻¹), submerged hydroponically grown roots (14.7 ± 2.3 mm d⁻¹), and air gap roots (14.8 ± 1.9 mm d⁻¹), were the same statistically (ANOVA; $p=0.99$). With these data, it was possible to relate the age of specific root regions to their distances from the tip.

Root anatomy was virtually identical among the 25 cultivars of *Iris germanica* observed [listed in Supplementary Table 2.1]. The following data is from the cultivar 'Paradise'.

Unless otherwise noted, data are from primary, adventitious roots originating in the rhizome.

Root apical meristem. Close examination of *I. germanica*'s root apical meristem revealed that it was an open type with multiple files of cortex cell precursors (Fig. 2.2A-C). There was no temporal regularity of increase in the number of immature exodermal cell files. After differentiation from the exodermal initial, subsequent immature exodermal cell divisions were irregular over time, forming files ranging from two to four near the root tip (Fig. 2.2A, C). Furthermore, there were no apparent radial cell alignments across the central cortex, i.e. between the immature exodermis and the endodermis (Fig. 2.2D, E); this was related to the open nature of the root apical meristem as well as to the non-uniform anticlinal and periclinal cell divisions within it.

Figure 2.2 *Iris germanica* adventitious root tips in longitudinal (A, B) and transverse (D, E) sections. (A) Tip of a 4-mm-long adventitious root. Arrowheads indicate the distal extremity of the root apical meristem. (B) Enlargement of the apical meristem area (arrowheads as in A). The epidermis is immature and the number of developing immature exodermal cell files varies (within brackets). (C) Tracing of the immature epidermal (grey) and exodermal (white) cells, located in the black rectangle in (A). Note the variable number of immature exodermal cell files in this region. (D) 50 μm from the tip of the root proper. Note the lack of regular radial alignments of cells across the young cortex. The root cap is thick at this distance. (E) 200 μm from the tip of the root proper. A boundary between the epidermis and immature exodermis is noticeable at this distance. There are 2-4 layers of cells in the immature exodermis, which are characterized by a lack of intercellular air spaces (within brackets). Abbreviations: rc = root cap; ep = epidermis; iex = immature exodermis; en = endodermis. Scale bars: (A, C) = 100 μm ; (B, D, E) = 50 μm .



Soil-grown roots; outer layers. In the outermost layer of the exodermis, Casparian bands in the anticlinal walls and suberin lamellae formed concurrently and were first detected 10-15 mm from the root tip (Fig. 2.3A, B). Initially, Casparian bands appeared in two separate locations in each radial and transverse wall, but they rapidly extended through these walls to form one continuous band. By 20 mm from the root tip, most of the exodermal cells contained typical Casparian bands and suberin lamellae. At 30 mm from the tip, a second exodermal layer started to differentiate centripetal to the first layer. The first indication of this was the extension of the Casparian band into the inner tangential walls of the first layer and the outer tangential walls of the second layer. As the root aged, the band extended into the anticlinal walls of the second layer. While the second exodermal layer continued to mature, very thin lignified tertiary walls formed in the first layer. It was not until 70 mm from the tip that the second exodermal layer had completed its maturation (Fig. 2.3C, D). At this bi-layered stage, the extension of the Casparian bands through adjoining tangential walls created a continuous circumferential Casparian band (ccCb). Depending on the arrangement of the exodermal cells, this Casparian band was either Y- or H-shaped when viewed in cross-section (Fig. 2.3C). Maturation of the third exodermal layer was complete at 100 mm from the tip with continued extension of the Casparian band through the tangential and anticlinal walls of the adjacent cells (Fig. 2.3E), as well as suberin lamella deposition (Fig. 2.3F, G) and lignification of the thin tertiary walls (Fig. 2.3H) of this third cell layer. Proximal to this area, an ultimate fourth exodermal layer could mature in the sequence described above. When the tissue was digested with sulphuric acid, all walls of the mature exodermis were

retained (data not shown). To observe cell lengths, it was necessary to use longitudinal views because in transverse view long and short cells would be indistinguishable. In the MEX, an irregular dimorphy was observed in the first layer (i.e., short cells were present but did not regularly alternate with long cells), but not in the underlying layers (Fig. 2.3J). The shorter cells differed from the longer cells only in length; all cells had Casparian bands, suberin lamellae and thin tertiary wall thickenings.

In the epidermis, the cells were tabular and uniform (data not shown). Their walls did not stain for lipids (Fig. 2.3G) but did stain positively for lignin (Fig. 2.3H) in addition to being faintly autofluorescent under UV light (Fig. 2.3I) at all distances from the root tip that were investigated. All epidermal walls were digested by sulphuric acid (not shown).

Soil-grown roots; inner parts. In the endodermis, the initial Casparian bands formed 10-15 mm from the root tip (i.e., the same distance as did the exodermis). These bands appeared as small dots in cross-section and were located very close to the pericycle. Also at this distance, lignin was detected in the outer tangential walls of all the endodermal cells and in the walls of protoxylem vessels. Suberin lamellae were first detected in the endodermis 20 mm from the root tip. At 30 mm, cells with suberin lamellae possessed Casparian bands that had started to extend through the anticlinal walls (Fig. 2.4A, B). This extension did not occur in unsuberized passage cells that were usually located near the protoxylem poles. At 50 mm from the tip, U-shaped tertiary wall thickenings were first observed and were present only in suberized endodermal cells. Also at this distance, early metaxylem vessel walls and those in the pith region became lignified. The U-shaped wall thickenings continued to enlarge (Fig. 2.4C, D) and by 100 mm from the tip, they had reached their maximum size; few passage

Figure 2.3 Photomicrographs of the outer part of *I. germanica* roots in cross (A-I) and longitudinal (J) section. Values in mm refer to distances from the root tips. (A) 15 mm. Stained with berberine hemisulphate–aniline blue. Casparian bands (white arrows) fluoresced yellow and occupied the anticlinal walls of the outermost exodermal layer. (B) 15 mm. Stained with Sudan red 7B. Suberin lamellae (black arrowheads) appeared as red rings in the walls of the outermost exodermal layer. (C) 70 mm. Stained with berberine hemisulphate–aniline blue. The ccCb (white arrows) was Y-shaped (in cells labelled with †) or H-shaped (in cells labelled with ‡). (D) 70 mm. Stained with Sudan red 7B. Cells in the two mature exodermal layers contained suberin lamellae (black arrowheads). (E) 100 mm. Stained with berberine hemisulphate–aniline blue. The ccCb (white arrows) filled the anticlinal and tangential walls of cells in the multiseriate exodermis. (F) 100 mm. Stained with Sudan red 7B. Cells in the multiseriate exodermis all contained suberin lamellae (black arrowheads). (G) 100 mm. Stained with Fluorol yellow 088. Suberin (white arrowheads) fluoresced yellow in exodermal cell walls. (H) 100 mm. Stained with phloroglucinol-HCl. Lignin (black arrows) appeared reddish-orange in the walls of epidermal and exodermal cells. (I) 70 mm. Autofluorescence with UV light. Walls of the epidermis and exodermis autofluoresced faint blue (light blue arrowheads). (J) 70 mm. Epidermal cells containing berberine thiocyanate crystals (yellow) and a dimorphic, biseriate exodermis with blue, autofluorescent walls. Asterisks = short cells. Abbreviations: epi = epidermis; ex = mature exodermis; iex = immature exodermis. Scale bars = 100 μ m.

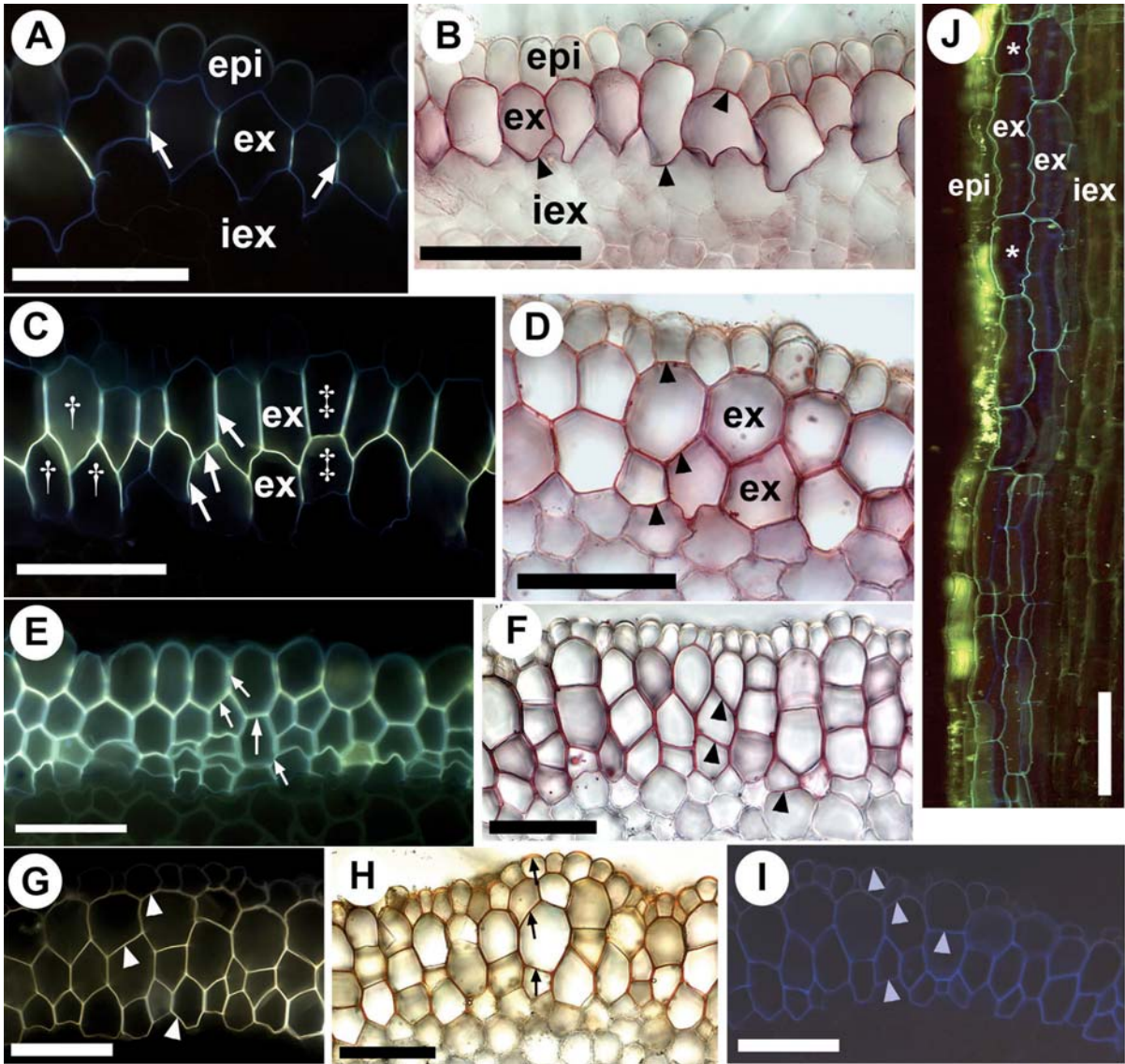
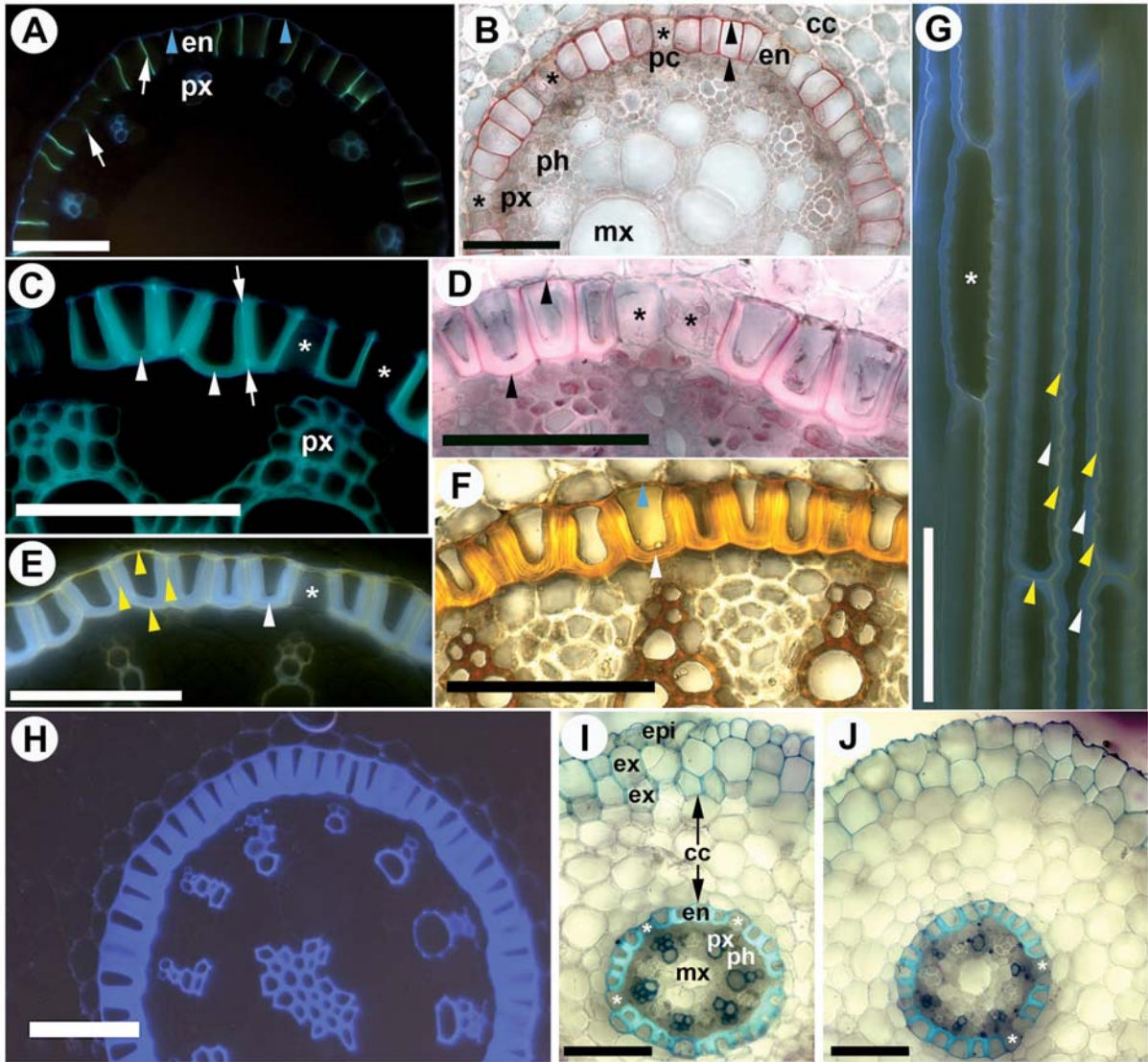


Figure 2.4 Photomicrographs of cross (A-F, H-J) and longitudinal (G) sections from *I. germanica* roots. Values in mm refer to distances from the root tips. (A) 30 mm. Stained with berberine hemisulphate–aniline blue. The endodermis had Casparian bands (white arrows) that either appeared dot-like or extended throughout the anticlinal walls. Autofluorescence (blue arrowheads) was observed in the outer tangential walls of the endodermal cells and in protoxylem vessel walls. (B) 30 mm. Stained with Sudan red 7B. Endodermal cells contained suberin lamellae (black arrowheads) when the Casparian band had extended through their anticlinal walls. (C) 90 mm. Stained with berberine hemisulphate–aniline blue. Mature endodermis with U-shaped wall thickenings (white arrowheads) and Casparian bands (between arrows). (D) 90 mm. Stained with Sudan red 7B. Mature endodermis with suberin lamellae (black arrowheads) that were exterior to the U-shaped wall thickenings. (E) 100 mm. Stained with Fluorol yellow 088. Mature endodermis with suberin lamellae (yellow arrowheads) surrounding the wall thickenings (white arrowhead). (F) 100 mm. Stained with phloroglucinol-HCl. Lignin appeared reddish-orange in the wall thickenings (white arrowhead), the outer tangential cell walls of the endodermis (blue arrowhead), and in xylem vessel walls. (G) 100 mm. Stained with Fluorol yellow 088. Suberin lamellae (yellow arrowheads) were positioned in between wall thickenings (white arrowheads). A short passage cell (*) without suberin lamellae or wall thickenings was evident. (H) 90 mm. Unstained and viewed with UV light. Note autofluorescence of endodermal wall thickenings, and walls of xylem vessels and modified parenchyma in the pith. (I) Lateral root in cross section, stained with TBO. Lignified walls stained blue. (J) Same as (I), but the epidermis had been sloughed off. Asterisks = passage cells. Abbreviations: epi = epidermis; ex = exodermis; cc = central cortex; en = endodermis; pc = pericycle; px = protoxylem; mx = metaxylem; ph = phloem. Scale bars = 100 μ m.



cells remained. These U-shaped thickenings stained positively for lignin (Fig. 2.4F) and autofluoresced with UV light (Fig. 2.4H). Although suberin was detected as a lamella in each of these cells, it was absent from the U-shaped thickenings (Fig. 2.4D, E, G). By this stage, the late metaxylem vessel walls had lignified. After digesting the tissue with sulphuric acid, the walls of the endodermis, mature xylem vessels, and modified parenchyma in the pith were retained. Dissolved structures included the U-shaped wall thickenings, pericycle, phloem and immature vessels (data not shown). Observing the inner part of the root longitudinally revealed its three-dimensional structure. Dimorphy was seen in the endodermis, where the shorter cells were without suberin lamellae and tertiary wall thickenings and, thus, were passage cells (Fig. 2.4G). Mature xylem vessels had reticulate wall thickenings and simple perforation plates (data not shown).

Soil-grown lateral roots. Some observations of lateral root development and anatomy were also made. Lateral root primordia initiated from the pericycle grew through the central cortex in the wake of a digestive pocket. However, they physically broke through the exodermis. The area of the exodermis thus wounded was sealed shut with a collar of modified cells that were suberized and lignified (data not shown). In general, lateral root anatomy was similar to that of the adventitious roots, except that laterals were substantially thinner, and their late metaxylem vessels were located in the center of the root instead of a pith (Fig. 2.4I). The epidermis of lateral roots was not always present; it could be sloughed off (Fig. 2.4J).

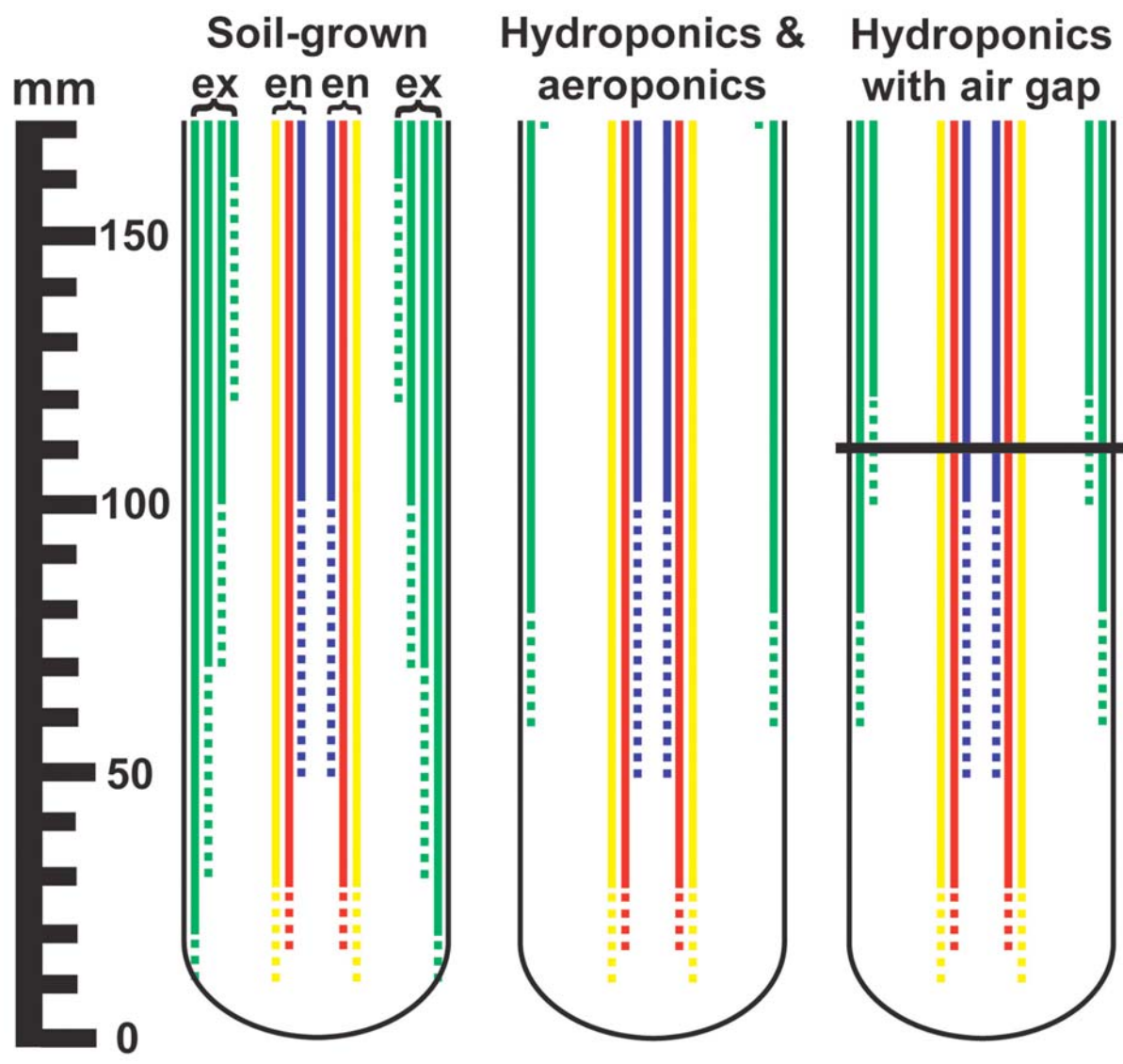
Hydroponically grown roots. When *I. germanica* plants were grown with their roots completely submerged in nutrient solution, the onset of exodermal maturation occurred

further from the root tip compared to soil-grown roots (Fig. 2.5). Exodermal Casparian bands and suberin lamellae were first detected in some cells of the outermost cortical cell layer of hydroponically grown roots 60 mm from the root tip compared to 10 mm in soil-grown roots. All cells of the first exodermal layer of hydroponically grown roots had formed typical Casparian bands and suberin lamellae at 80 mm (between 5 and 6 days old) compared to 20 mm (between 1 and 2 days old) in soil-grown roots (Fig. 2.5; see Fig. 2.3A, B). In the maturing second exodermal layer of hydroponic roots, Casparian bands and suberin lamellae were found in some cells 170 mm from the root tip compared to 30 mm in soil (Fig. 2.5). All cells of the second exodermal layer of hydroponically grown roots matured to State II 200 mm from the tip (about 14 days old) compared to 70 mm (between 4 and 5 days old) in soil-grown roots (see Fig. 2.3C, D). In hydroponics, no cells of the third exodermal layer had begun to mature by 200 mm from the tip whereas in soil some cells of this layer had begun to mature at 70 mm. Unlike the exodermis, endodermal maturation occurred as close to the tip in hydroponic roots as in soil roots.

Air gap-treated roots. The submerged part of air gap treated roots had an exodermal anatomy like that of completely submerged roots with maturation of the first exodermal layer finishing at 80 mm from the tip (between 5 and 6 days old; Fig. 2.5). In air gap treated roots, the second exodermal layer matured close to the air gap-solution interface, 100-120 mm from the tip. The second exodermal layer, with a ccCb and suberin lamellae, completed maturing by 120 mm (between 8 and 9 days old). Exodermal anatomy was nearly identical in the region of root exposed to the humid air gap (120-170 mm from the tip, between 9 and 12 days old). This 50-mm long root zone had been exposed to humid air for 7 d (Fig. 2.5). The

Figure 2.5 Diagrams of key exodermal and endodermal developmental stages in *I.*

germanica roots that were grown in different conditions. According to the growth rates, the proximal ends of the illustrated roots were 12 days old. The vertical scale refers to distance from the root tip. Green lines – concurrent exodermal Casparian band and suberin lamellae development. Yellow lines – endodermal Casparian bands. Red lines – endodermal suberin lamellae. Blue lines – endodermal tertiary wall thickenings. Dashed coloured lines – the structure had not yet completely developed in all cells. Solid coloured lines – the structure had completed developing in all exodermal cells or the majority of endodermal cells (i.e., few passage cells remained). The horizontal line across the air gap root marks the interface between the air gap and nutrient solution. Abbreviations: ex = exodermis; en = endodermis.



third layer had not begun to mature by 200 mm. The air gap treatment brought about a precocious maturation of the second exodermal layer, more resembling the soil-grown root than the control hydroponically grown root (Fig. 2.5). Since the endodermis had already reached State III of maturity 100 mm from the tip in the air gap growth condition, as well as in the other two growth conditions (Fig. 2.5), it was not surprising that endodermal anatomy in the part of the root exposed to the air gap was similar to roots grown in the other conditions. The average relative humidity in the air gap was 92%.

Aeroponically grown roots. As with completely submerged, hydroponically grown roots, the exodermal maturation of aeroponically grown roots occurred further from the root tip compared to soil-grown roots (Fig. 2.5). In fact, the maturation sequence was similar in aeroponically and hydroponically grown roots (data combined in Fig. 2.5). For example, two complete exodermal layers were not observed until 200 mm from the tip (about 14 days old). This anatomy resembled that of soil-grown roots at 70 mm from tip (between 4 and 5 days old; see Fig. 2.3C, D). Endodermal maturation in aeroponic roots occurred at a similar distance from the tip as in roots grown in all other conditions (Fig. 2.5).

2.4.2 Ferrous sulphate toxicity in *Z. mays* roots

Zea mays roots that were exposed to FeSO_4 had reduced growth rates compared to the control (Fig. 2.6). For the 0.5 mM FeSO_4 for 2 and 3 h and 1.0 mM FeSO_4 for 2 h exposures, there were little or no measurable increases in root length. Roots exposed to 0.25 mM FeSO_4 for 2 h had growth rates that were initially minimal, but increased over the next two days. Roots exposed to 0.5 mM FeSO_4 for 1 h had growth rates greater than roots exposed to any

of the other FeSO₄ treatments, but still significantly lower than the control until day 3 (Fig. 2.6).

2.4.3 Root permeability to apoplastic tracers

Using berberine as a tracer necessitated the observation of two controls. Firstly, unstained root sections were irradiated with UV light. Faint blue autofluorescence was observed in the walls of the exodermis, endodermis, lignified xylem vessels, and modified parenchyma in the stele (Fig. 2.7A, see Figs. 2.3I, 2.4H). Secondly, root sections were stained directly with berberine hemisulphate. Then all cell walls of the epidermis and cortex (including those of the exodermis and endodermis) took up the fluorochrome and fluoresced yellow (Fig. 2.7B). When an intact root was treated externally with berberine, the dye entered the cortex and stele close to the tip where the first exodermal layer had not yet matured (< 20 mm from the tip; Fig. 2.7C). Beyond 20 mm, the dye penetrated and stained the walls of the epidermis and the outer tangential walls of the first layer of exodermis, but its further entry was blocked by the Casparian band in the first exodermal cell layer (Fig. 2.7D). When berberine was applied simultaneously to the epidermis and central cortex, it moved freely in the epidermal cell walls, walls of cortical parenchyma, walls of immature exodermal layers, and the inner tangential walls of the innermost mature exodermal layer. However, the dye did not penetrate the anticlinal walls of a mature exodermis (Fig. 2.7E).

When FeSO₄ was used as a tracer, both unstained and stained controls were necessary. Unstained cross sections lacked blue pigmentation (data not shown). When cross sections were exposed to FeSO₄ and mounted in K₄[Fe(CN)₆] many, but not all, contained blue Fe₄[Fe(CN)₆]₃ in every cell wall (Fig. 2.7F). When intact roots were exposed to FeSO₄,

Figure 2.6 The effect of FeSO₄ exposure on the growth rates of *Z. mays* roots. Values are averages (n=10) ± standard deviation that were pooled from two independent trials. Root growth per day refers to the time following the FeSO₄ treatment. Different letters within each day indicate significant differences (ANOVA with LSD, p≤0.05). Bracketed letters are shared by the 0.5 mM FeSO₄ for 2 and 3 h exposures and 1.0 mM FeSO₄ for 2 h exposure.

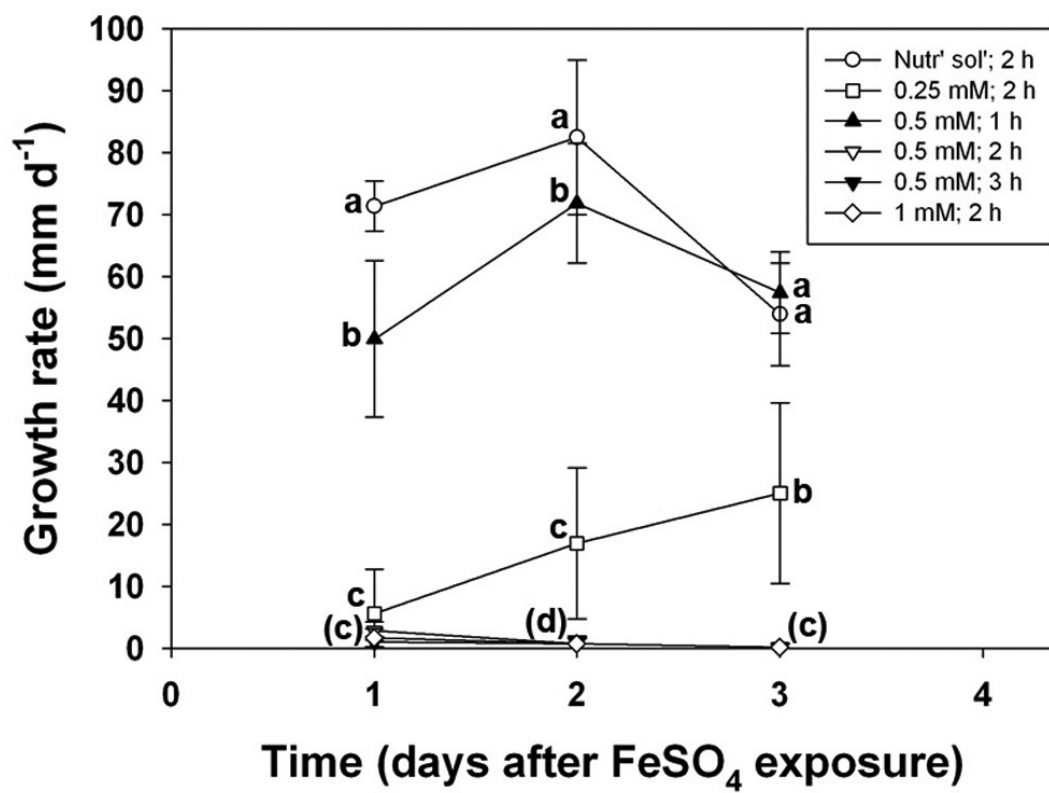


Figure 2.7 Apoplastic permeability tests on *I. germanica* roots with berberine or FeSO₄. The photomicrographs show cross sections of the roots unless otherwise stated. Values in mm refer to distances from the root tips. (A) 90 mm. Unstained, UV autofluorescent control. All exodermal walls were faint blue. (B) 60 mm. Entire section stained with berberine. Epidermal, exodermal and central cortical cell walls fluoresced yellow (white arrowheads). (C) Longitudinal section of a root tip treated externally with berberine. The walls of all cells near the tip fluoresced yellow. (D) 70 mm. The outermost Casparian bands of an intact multiseriate exodermis prevented externally applied berberine (white arrowheads) from permeating the exodermis and central cortex. (E) 70 mm. A punctured multiseriate exodermis allowed berberine to stain the walls of epidermal, immature exodermal and central cortical cells (white arrowheads). (F) 80 mm. Entire section treated with FeSO₄ followed by K₄[Fe(CN)₆]·3 H₂O. Ferric ions precipitated in all epidermal and exodermal walls and appeared blue (black arrowheads). (G) 70 mm. Following an external treatment, ferric ions were detected in mature exodermal walls (black arrowheads). (H) Longitudinal section of a root tip treated externally with FeSO₄ followed by K₄[Fe(CN)₆]·3 H₂O. The ferric ions entered the cortex of the tip readily. (I) 90 mm. Ferric ions, as evidenced by blue precipitates (black arrowheads), were blocked from permeating the exodermal Casparian bands. (J) 90 mm. A punctured multiseriate exodermis allowed the ferric ions limited entry to the central cortex (black arrowheads). (K) 70 mm. Intact root incubated in water and then berberine. Berberine (white arrowheads) did not permeate the Casparian bands in the first exodermal layer. (L) 100 mm. Intact root incubated in FeSO₄ and then berberine. Berberine stained the walls of all mature and immature exodermal cells, and walls of cortical parenchyma (white arrowheads). Scale bars: cross sections = 50 μm; longitudinal sections = 500 μm.

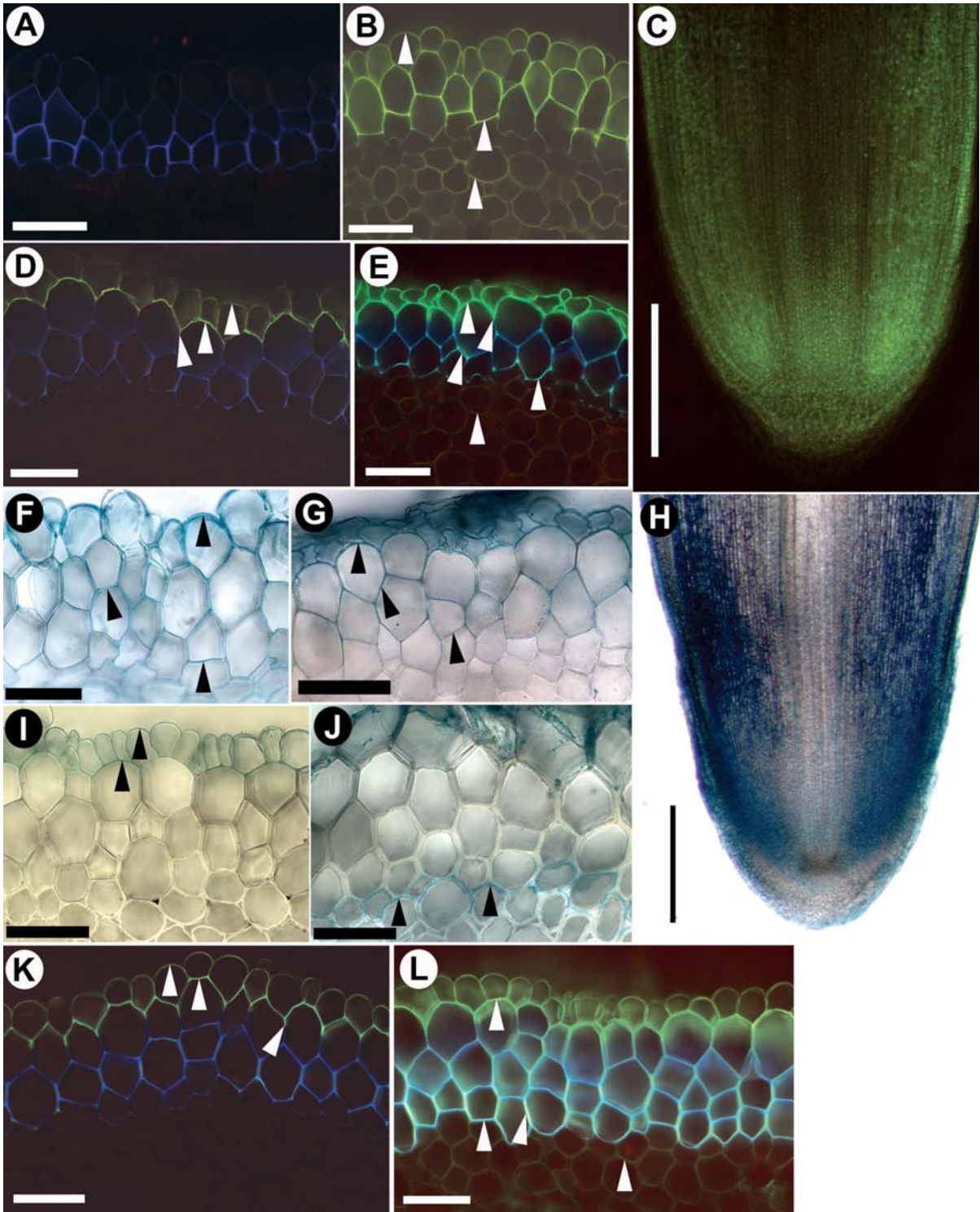


Table 2.1 Rhizomatous *Iris* species' natural habitats are correlated with the type of exodermis they develop and whether aerenchyma is present (+) or absent (-).

<i>Iris</i> species	Natural habitat	Type of exodermis	Aerenchyma
¹ <i>I. germanica</i> L.	Well-drained soil	Multiseriate	-
¹ <i>I. pumila</i> L.	Well-drained soil	Multiseriate	-
¹ <i>I. pallida</i> Lam.	Well-drained soil	Multiseriate	-
¹ <i>I. sambucina</i> L.*	Well-drained soil	Multiseriate	?
² <i>I. sibirica</i> L.	Water-saturated soil	Uniseriate	+
² <i>I. spuria</i> L.	Water-saturated soil	Uniseriate	+
² <i>I. versicolor</i> L.	Water-saturated soil	Uniseriate	+
² <i>I. hexagona</i> Walt.	Water-saturated soil	Uniseriate	+
² <i>I. pseudacorus</i> L.	Water-saturated soil	Uniseriate	+
² <i>I. virginica</i> L. †	Water-saturated soil	Uniseriate	+

¹ = 'bearded irises'; ² = 'beardless irises'; * = observed by Kroemer (1903); † = observed by Stevens (2003).

variable results were obtained. In areas of the root within 20 mm from the tip, the ferric ions entered the central cortex and stele (Fig. 2.7H). As the MEX matured, the outermost Casparian band did not always prevent the ions from permeating through the apoplast. For example, instances were seen where the ion penetrated through the anticlinal walls of the first and second mature exodermal layers (Fig. 2.7G). Ferric ions were not detected permeating deeper than two exodermal layers. Frequently, however, ferric ions were blocked at the location of the Casparian band in the first exodermal cell layer (Fig. 2.7I). When the root segments' peripheral layers were cut, an unexpected result was observed. In the majority of cases, ferric ions were detected penetrating the walls of only two cortical cell layers. In the few instances where the ions were observed entering deeper into the central cortex, their transport was restricted to the cell walls subjacent to the mature exodermis. The ions did not penetrate the anticlinal walls of the innermost mature exodermal layer (Fig. 2.7J).

To understand the reason for the variable FeSO_4 permeability results, a third apoplastic tracer experiment was performed. When root segments were exposed to water and then berberine, the fluorochrome did not penetrate the first exodermal layer (Fig. 2.7K). However, exposing root segments initially to FeSO_4 for 1 h followed by berberine altered the exodermis such that berberine was able to permeate through the exodermal walls and into the central cortex (Fig. 2.7L).

2.4.4 Mature root anatomy of other soil-grown iris species

Of the other species observed, *I. pumila* (Fig. 2.8A, B) and *I. pallida* (Fig. 2.8C, D) were very similar to *I. germanica*. On the other hand, the remaining five species each had a uniseriate exodermis and aerenchyma in the central cortex (Table 2.1). These species include

I. sibirica (Fig. 2.8E, F), *I. spuria* (Fig. 2.8G, H), *I. versicolor* (Fig. 2.8I, J), *I. hexagona* (Fig. 2.8K, L), and *I. pseudacorus* (Fig. 2.8M, N).

2.5 Discussion

The current detailed investigation of *I. germanica* root structure, development, and apoplastic permeability extended the information contained in past reports (Kroemer 1903; Shishkoff 1986; Peterson and Perumalla 1990; Zeier and Schreiber 1998). *I. germanica*'s multiseriate exodermis (MEX) was classified by Kroemer (1903) as a 'Gemischte Interkutis' (mixed exodermis) which referred to the outermost exodermal layer as being dimorphic (i.e., having long and short cells) while all underlying layers had uniform cell lengths. Both Kroemer (1903) and Shishkoff (1986) observed this mixed exodermis in 14 species of various genera, all of which are members of the Asparagales (Table 2.2). In species with a dimorphic uniseriate exodermis, such as *Allium cepa* (von Guttenberg 1968; Ma and Peterson 2001a), the shorter cells are typically passage cells with delayed suberin lamella deposition compared to the long cells. The lack of suberin lamellae allows passage cells to function as the least restrictive pathways for the radial transport of water and solutes across the exodermis. However, in the present study of *I. germanica*, suberin lamellae were deposited in the short cells as early as in the long cells. Thus, the short cells were not passage cells. This type of dimorphic layer may have evolved from the more common type with passage cells. *I. germanica*'s MEX began developing from the outermost cortical layer and each subsequent layer developed centripetal to the previous one, a feature also observed by Peterson and Perumalla (1990), to a maximum of four layers.

I. germanica's specialized exodermal Casparian band, located in the anticlinal and tangential walls as illustrated earlier by Peterson and Perumalla (1990), was termed a continuous circumferential Casparian band (ccCb; see Results above). It is proposed that ccCb be used as the standard term when referring to this type of Casparian band, which was also detected in the roots of *Typha* spp. and *P. australis* (Seago et al. 1999; Soukup et al. 2002). The shape of the ccCb is dependent on that of the exodermal wall continuum (i.e., apoplast) which is governed by the orientation of MEX cells. Their orientation is related to how they are generated at the root tip. For example, formation of the MEX of *Typha glauca* is initiated when the outermost layer of the ground meristem continues to divide periclinally to form multiple exodermal layers centripetally (Seago and Marsh 1989). When *T. glauca* root is viewed in transverse section, one can observe that the periclinal divisions gave rise to an H-shaped wall continuum; hence the ccCb is also H-shaped. However, in *I. germanica* roots, the ccCb can be both H- and Y-shaped. This means that in *I. germanica*, and presumably other species with a Y-shaped ccCb, generation of the MEX at the root apical meristem differs from that of *Typha* spp. which has a tiered apex (Seago and Marsh 1989; Heimsch and Seago 2008). In *I. germanica*, the immature exodermal layers were not derived by a unified set of periclinal and anticlinal divisions. This was shown in transverse sections where uniform radial files were not present in the 3-4 cell layers across much of the immature exodermis. These ambiguous patterns of MEX development are what led to the variable ccCb shapes found in the exodermal layers. In other words, the irregular sequences of cell files derived from the open root apical meristem are reflected in the cross sectional patterns of the later developing and mature exodermis.

Figure 2.8 Exodermis in transverse sections from soil-grown roots of various iris species. Tissue displayed in the left column was stained with Sudan Red 7B; tissue displayed in the right column was stained with phloroglucinol–HCl. Values in millimetres refer to distances from the root tips. (A, B) *Iris pumila*, 100 mm; multiseriate exodermis. (C, D) *Iris pallida*, 100 mm; multiseriate exodermis. (E, F) *Iris sibirica*, 120 mm; uniseriate exodermis. (G, H) *Iris spuria*, 90 mm; uniseriate exodermis. (I, J) *Iris versicolor*, 100 mm; uniseriate exodermis. (K, L) *Iris hexagona*, 100 mm; uniseriate exodermis. (M, N) *Iris pseudacorus*, 100 mm; uniseriate exodermis. Abbreviations: epi = epidermis; ex = exodermis; cc = central cortex. Red arrowheads = suberin lamellae (stained red); black arrowheads = wall thickenings; white arrowheads = lignified walls (stained reddish-orange). Scale bars = 50 mm.

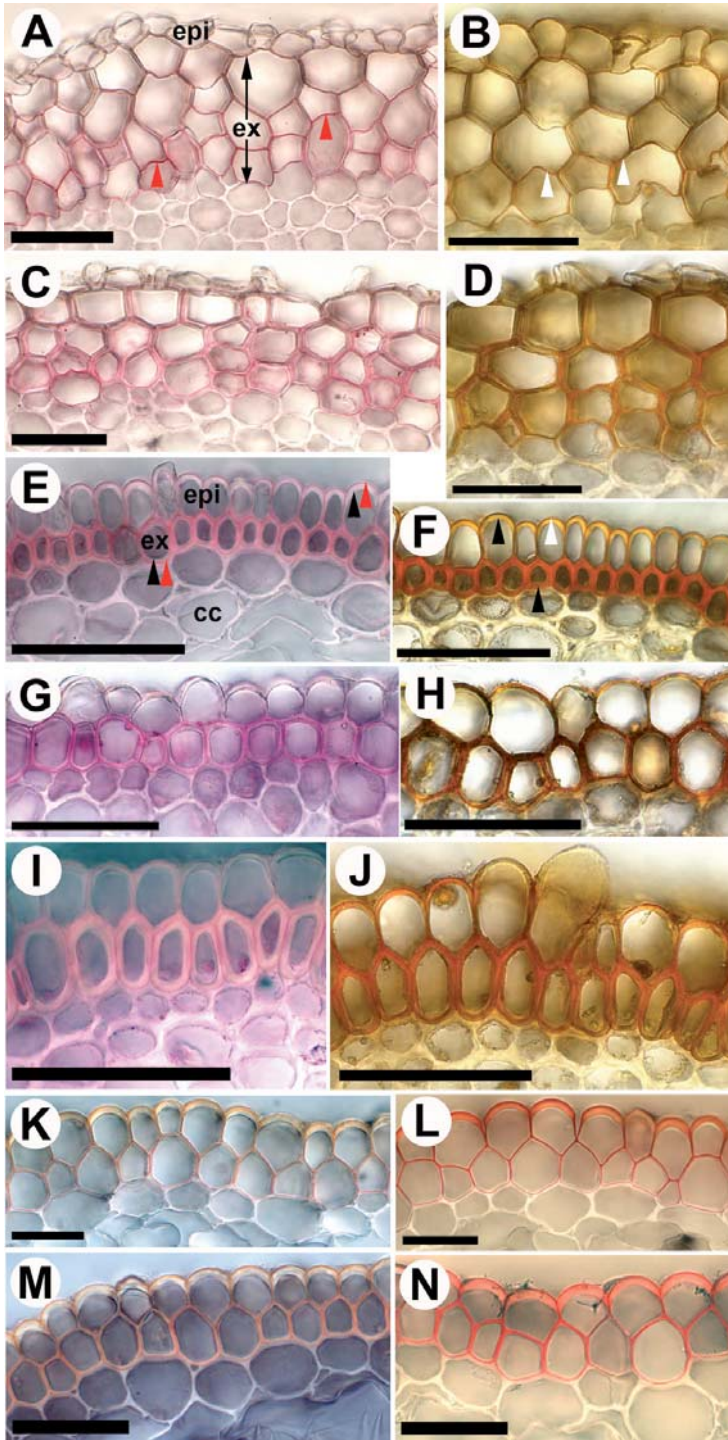


Table 2.2 List of monocot species (class Liliopsida) that have a multiseriate exodermis and inhabit well-drained or dry substrates.

Order	Family	Genus and species	
Alismatales	Araceae	^ <i>Philodendron wendlandii</i> Schott	
Arecales	Arecaceae	*^ <i>Phoenix dactylifera</i> L.	
		^ <i>Phoenix roebelinii</i> O'Brien	
		^ <i>Trachycarpus fortunei</i> (Hook.) H.Wendl.	
		^ <i>Washingtonia filifera</i> (Lindl.) H.Wendl.	
Asparagales	Agavaceae	* <i>Yucca recurvifolia</i> Salisb. [me] * <i>Yucca gloriosa</i> L. [me]	
	Asparagaceae	^ <i>Asparagus asparagoides</i> (L.) Druce	
		^ <i>Asparagus densiflorus</i> (Kunth) Jessop	
		*^† <i>Asparagus officinalis</i> L. [me] * <i>Asparagus setaceus</i> (Kunth) Jessop	
		*† <i>Asparagus sprengeri</i> Regel. [me]	
		*† <i>Asparagus verticillatus</i> L. [me]	
	Asphodelaceae	*† <i>Asphodeline lutea</i> (L.) Reichenb. [me] ^ <i>Gasteria disticha</i> (L.) Haw.	
	Hemerocallidaceae	*^† <i>Hemerocallis fulva</i> L. [me] *^ <i>Phormium tenax</i> Forst. & Forst. f.	
		Iridaceae	*^† <i>Iris germanica</i> L. [me] *† <i>Iris pallida</i> Lam. [me] *^† <i>Iris pumila</i> L. [me] *† <i>Iris sambucina</i> L. [me]
	Orchidaceae		^ <i>Brassavola subulifolia</i> Lindl. ^ <i>Cattleya aurantiaca</i> (Bateman ex Lindl.) P.N.Don
Ruscaceae			^† <i>Aspidistra elatior</i> Blume [me] * <i>Dracaena cannifolia</i> Hort. [me] *† <i>Dracaena draco</i> L. [me] ^ <i>Sansevieria cylindrica</i> Bojer
	Commelinales		Commelinaceae

Pandanales	Pandanaceae	* <i>Pandanus stenophyllus</i> Kurz
Poales	Bromeliaceae	*† <i>Ananas macrodontes</i> E.Morr. * <i>Aechmea longifolia</i> (Rudge) L. B.Sm. & M.A.Spencer
	Juncaceae	* <i>Luzula sylvatica</i> (Huds.) Gaudin
	Poaceae	* <i>Chrysopogon zizanioides</i> (L.) Roberty
Zingiberales	Cannaceae	*† <i>Canna indica</i> L. * <i>Canna tuerckheimii</i> Kraenzl.
	Marantaceae	* <i>Maranta arundinacea</i> L. ^ <i>Maranta leuconeura</i> C.J.Morren
	Strelitziaceae	* <i>Strelitzia augusta</i> Thunb.
	Zingiberaceae	*† <i>Curcuma longa</i> L. *† <i>Globba marantina</i> L. * <i>Hedychium coccineum</i> Buch.- Ham. ex Sm. *† <i>Hedychium gardnerianum</i> Sheppard ex Ker Gawl. *† <i>Zingiber officinale</i> Roscoe

*Kroemer (1903); †Shishkoff (1986); ^Peterson and Perumalla (1990); [me] = mixed exodermis identified by Kroemer (1903) and Shishkoff (1986).

Taxonomic information referenced from the Angiosperm Phylogeny Group's website (Stevens 2001 onwards) and Tropicos.org.

Development of the endodermis in *I. germanica* was also observed progressing through States I, II and III. Casparian bands were offset toward the pericycle in cells lacking suberin lamellae, a feature also observed in *Hordeum vulgare* (barley, Robards et al. 1973), *Z. mays* (Haas and Carothers 1975), and *Triticum aestivum* (wheat, Grymaszewska and Golinowski 1987). The presence of endodermal passage cells in mature regions far from the root tip is also common. Three striking characteristics of *I. germanica*'s endodermal cells were i) dimorphy, ii) their palisade-like shape when viewed in cross section, and iii) their thick, lignified tertiary walls that may function in mechanical stabilization of the stele. In the dimorphic endodermis, short cells were passage cells. To the best of our knowledge, this is the first report of dimorphy in the endodermis of any species. Features ii) and iii) were also noted by Zeier and Schreiber (1998) who observed *I. germanica*'s mature (i.e., State III) endodermis with white light, fluorescence and scanning electron microscopy, pointing out the presence of mature wall-modifying structures.

It is well known that environmental conditions can influence plant organ growth and tissue maturation. In the current work, this was evident with regard to the timing of exodermal maturation in *I. germanica* roots that were grown in soil, hydroponics or aeroponics. Complete exodermal development, i.e., through States I-III, occurred closer to the root tip in soil-grown roots relative to hydroponically and aeroponically grown roots. Generally, the faster a root grows in length, the further from the tip its exodermis and endodermis will develop (Wilcox 1962; Perumalla and Peterson 1986). Mechanical impediment of *Hordeum vulgare* non-nodal root growth was shown to induce exodermal development (Lehmann et al. 2000) and limit root elongation resulting in accelerated

endodermal maturation (Wilson and Robards 1978). However, in the present study, growth rates were remarkably similar for *I. germanica* roots grown in the various environments, indicating that factors other than growth rate were responsible for the differences in the onset of exodermal maturation. In roots grown in hydroponic and aeroponic conditions, the exodermis matured at a similar distance from the tip, and the same was true for endodermal maturation. It could be argued that these two conditions were essentially the same since the roots were always saturated with solution. Also, having a thin (10-100 μm) unstirred layer of water on the root surface, sheltered between epidermal hairs, is possible even if roots are grown in an aerated solution (Nye and Tinker 1977; Clarkson 1996). Miyamoto et al. (2001) also observed no difference in tissue development in *O. sativa* roots grown in hydroponics and aeroponics. In contrast, Zimmermann and Steudle (1998) reported that exodermal development in *Z. mays* was promoted by aeroponic conditions. In the present study, exposing hydroponically grown *I. germanica* roots to an air gap for seven days accelerated the maturation of the second exodermal layer. Similarly, Clarkson et al. (1987) and Enstone and Peterson (1998) found that an air gap accelerated exodermal suberization in *Z. mays* roots within two days. The lower humidity levels and increased gas exchange capability within the air gap, similar to that of well-drained soil but in contrast to completely submerged conditions, may have played a role (Enstone and Peterson 1998). The essence of all these findings is that developmental responses by plants to environmental conditions can vary depending on the species and type of condition (see Enstone et al. 2003). The past and current work reveals that these responses are species-specific, making it necessary to test the reactions in each case; they cannot be assumed.

Apoplastic tracers were used to test the permeability of *I. germanica*'s exodermis. It is known that Casparian bands can limit the apoplastic flow of solutes (Enstone et al. 2003) and possibly also water (Hose et al. 2001). In the present study, berberine entered the root cortex and stele close to the tip where the exodermis and endodermis were immature. However, once the Casparian bands were deposited, the dye could not penetrate even a uniseriate exodermis. The current berberine tracer results are the same as those obtained with *Typha* spp. and *P. australis* (Seago et al. 1999; Soukup et al. 2002). Similar results were also observed by Peterson and Perumalla (1990) who used Cellufluor to test the apoplastic permeability of *I. germanica*'s mature exodermis; Cellufluor did not pass the outermost Casparian bands.

The permeability of the exodermis was also tested with ferrous sulphate. In solution, some of the ferrous ions were oxidized to ferric ions that could be precipitated in place by a subsequent application of potassium ferrocyanide (Ranathunge et al. 2005a). This test has the advantage of using an ion of physiological interest that has a smaller molecular size than berberine. Others have used FeSO_4 as an apoplastic tracer. Soukup et al. (2002) exposed *P. australis* roots to 1 or 10.75 mM FeSO_4 for 1–24 h. Ferric ions permeated close to the tip (where the exodermis had not yet matured), but were blocked at the first mature exodermal layer (see Fig. 6 in Soukup et al. [2002]). Soukup et al. (2002) also observed toxicity in the form of leaky plasmalemmas when tracer exposure times exceeded 1 h. Armstrong and Armstrong (2005) exposed *Oryza sativa* roots to 2 mM FeSO_4 for 1-2 h. The corresponding images display a young (5-25 mm from the tip) exodermis (situated between the epidermis and hypodermal sclerenchyma layer) that was permeated by ferric ions. In roots grown in

sulphide, permeation of ferric ions was reduced but not completely blocked by the exodermis as accumulation of the ions is noticeable in the sclerenchyma layer (see Fig. 8 in Armstrong and Armstrong [2005]). Unfortunately, they did not stain for Casparian bands or suberin lamellae and it is possible that the exodermis had not matured 5-25 mm from the root tip.

In the present work, the toxicity of FeSO_4 was investigated since Soukup et al. (2002) and Ranathunge et al. (2005a) had expressed concern in using it as an apoplastic tracer. Because of the necessity of forming crystals, a minimum concentration of 0.5 mM FeSO_4 had to be used; preliminary tests showed that this was the lowest concentration that would form crystals when mixed with 1 mM $\text{K}_4[\text{Fe}(\text{CN})_6] \cdot 3 \text{H}_2\text{O}$ (unpublished data). In the toxicity test consisting of monitoring the growth rate of *Z. mays* roots, the time of exposure to FeSO_4 proved to be very important. Times longer than 60 min were harmful to root vitality causing significant decreases in root growth and even the complete arrest of growth at concentrations above 0.25 mM. Thus, a one hour treatment with 0.5 mM FeSO_4 was used with *I. germanica* roots. Even with these precautions, ferric ion entry into the central cortex was restricted but not always prevented by the intact exodermis, indicating a possible toxic reaction. Toxicity became evident when root segments were pretreated with FeSO_4 followed by berberine, resulting in permeation of the latter tracer into all exodermal walls and the walls of cortical parenchyma. When introduced into the central cortex, ferric ions rarely permeated further than two cortical cell layers. This result was unexpected because the hydrated ionic radius of ferric (0.457 nm; Nightingale 1959) should be much smaller than the diameter of the cell wall intermicrofibrillar spaces (5-30 nm; Nobel 2005). It is possible that the concentration of ferric ions was diluted as they diffused into the free water in the cell walls, thus preventing

detection by precipitation in deeper cell layers. Alternatively, attraction of the positively charged ferric ions to the walls of the first two cortical cell layers may have been strong enough to prevent deeper permeation. The problems discussed above with using FeSO₄ as an apoplastic tracer outweigh its benefits; hence, it is recommended that use of this tracer procedure be discontinued.

After observing the mature root anatomy from other rhizomatous iris species, a correlation between exodermal anatomy and habitat was noted. Those species that formed a MEX and lacked aerenchyma (*I. germanica*, *I. pumila* and *I. pallida*) live in habitats with well-drained soils. On the other hand, species that had a uniseriate exodermis and aerenchyma (*I. sibirica*, *I. spuria*, *I. versicolor*, *I. hexagona* and *I. pseudacorus*) preferably inhabit water-saturated areas. Additionally, Stevens (2003) described the root anatomy of three wetland-living species, *I. virginica*, *I. pseudacorus*, and *I. versicolor*, all of which have a uniseriate exodermis and aerenchyma. This correlation between root anatomy and habitat, however, does not extend to other taxa. From a review of the current and published data, it became clear that the majority (83%) of species known to have a MEX are perennial monocots (eudicot exception: *Codiaeum variegatum*; Peterson and Perumalla 1990) that inhabit well-drained substrates, and are from diverse orders within the class Liliopsida (Tables 2.2, 2.4; Kroemer 1903; Peterson and Perumalla 1990). The remaining 17% of these species are aquatic, e.g., *Typha* spp. (Seago et al. 1999), *P. australis* (Soukup et al. 2002), and an additional 6 species listed by Kroemer (1903), Peterson and Perumalla (1990), and Soukup et al. (2007); all of these members are of the order Poales (Tables 2.3, 2.4). Within the Poales, the families Cyperaceae, Poaceae, Sparganiaceae, and Typhaceae are positioned

Table 2.3 List of monocot species (class Liliopsida) that have a multiseriate exodermis and inhabit water-saturated substrates. All of these representatives are from the order Poales.

Family	Genus and species
Cyperaceae	* <i>Carex hirta</i> L.
	* <i>Schoenoplectus lacustris</i> (L.) Palla
Poaceae	» <i>Glyceria maxima</i> (Hartm.) Holmb.
	*» <i>Phragmites australis</i> (Cav.) Trin. ex Steud.
	^ <i>Stenotaphrum secundatum</i> (Walter) Kuntze
	* <i>Sparganium emersum</i> Rehmman
Typhaceae	‡ <i>Typha angustifolia</i> L.
	‡ <i>Typha glauca</i> Godr.
	*† <i>Typha latifolia</i> L.

*Kroemer (1903); †Shishkoff (1986); ^Peterson and Perumalla (1990); ‡Seago *et al.* (1999); »Soukup *et al.* (2007).

Taxonomic information referenced from the Angiosperm Phylogeny Group's website (Stevens 2001 onwards) and Tropicos.org.

Table 2.4 Number of species with a multiseriate exodermis that inhabit wet or well-drained/dry substrates.*

Plant	Growth substrate		Total (%)
	# wet (%)	# well-drained or dry (%)	
Monocots	9 (17)	43 (83)	52 (100)

*See Tables 2.2 and 2.3 for species lists.

in three different major phylogenetic clades (see Stevens 2001 onwards) and have variable amounts of mixed-linkage (1→3),(1→4)-β-glucans in their cell walls (see Trethewey et al. 2005). Species with a uniseriate exodermis also occupy both wet and well-drained habitats. From the known cases, 23% of the monocots and 16% of the eudicots inhabit water-saturated soils while the remaining majority of monocots (77%) and eudicots (84%) inhabit well-drained or dry soils (Table 2.5; Supplementary Tables 2.2 and 2.3).

It is possible that the type of exodermis confers particular advantages to aquatic plants as well as those preferring well-drained habitats. In waterlogged soils, an exodermis can restrict radial oxygen loss from the root. Radial oxygen loss occurs readily where the exodermis has not matured, such as near the root tip and in ‘windows’ where lateral roots will emerge, but is reduced in regions with a mature exodermis. Decreases in radial oxygen loss were measured across the suberized uniseriate exodermis of *O. sativa* (Armstrong and Armstrong 2001) and *Tabernaemontana juruana* (De Simone et al. 2003), and the suberized MEX of *P. australis* (Armstrong et al. 2000; Armstrong and Armstrong 2001) and *Glyceria maxima* (Soukup et al. 2007). In well-drained or dry soils, the (poly)aliphatic domain of suberin lamellae in the exodermis may contribute variably to the apoplastic retention of water (Hose et al. 2001). Reductions, but not blockage, in radial water permeability have been measured in roots with a mature exodermis, including *Agave deserti* (North and Nobel 1991, 1995), *Z. mays* (Zimmermann and Steudle 1998; Zimmermann et al. 2000), *A. cepa* and *Helianthus annuus* (Taleisnik et al. 1999). While a uniseriate exodermis will restrict oxygen and water from being lost to the substrate to some degree, it is presumed that multiple exodermal layers containing Casparian bands and suberin lamellae, with the correct molecular arrangements

Table 2.5 Number of species with a uniseriate exodermis that inhabit wet or well-drained/dry substrates.*

Plant	Growth substrate		Total (%)
	# wet (%)	# well-drained or dry (%)	
Monocots	24 (23)	80 (77)	104 (100)
Eudicots	21 (16)	108 (84)	129 (100)
Sum	45 (19)	188 (81)	233 (100)

*See Supplementary Tables 2.2 and 2.3 for species lists.

and precisely localized cell wall depositions (Bernards 2002; Schreiber et al. 2005a), should provide roots with a greater resistance to oxygen loss and drought. Drought stress would occur more often to plants growing in well-drained soils than in submerged conditions. Hence, in lieu of secondary growth, perennial monocots with roots that have a MEX should be able to effectively withstand periods of drought that may be common to their natural environments. This postulate is supported in part by quantitative measurements of water permeability (see section 3.5, Chapter 3) and suberin chemical modifications (see section 4.5, Chapter 4).

In conclusion, a MEX, with a continuous ccCb and suberin lamellae in all cells, matured close to the root tip of soil-grown *I. germanica* roots. However, its maturation occurred much further from the tip when the roots were grown in hydroponic or aeroponic conditions. When roots were exposed to an air gap in the hydroponic chamber, maturation of the second exodermal layer was accelerated. The distance from the root tip in which the endodermis matured was not affected by the growth conditions. The root apical meristem was open and development of MEX cell files was irregular. Root growth rates were similar among the different growth conditions. Regions of the root with an intact MEX were impenetrable to berberine but slightly permeable to ferric ions, which was likely the result of a toxic reaction. Lastly, iris species that inhabit well-drained soils have roots with a MEX while those that inhabit water-saturated substrates have a uniseriate exodermis and cortical aerenchyma. Future investigations should focus on the direct influence that a MEX may have on water and solute permeabilities and radial oxygen loss using quantitative approaches. It would also be

instructive to test the mechanical strength of the lignified (and suberized) exodermis and endodermis, and to test their antimicrobial properties.

2.6 Supplementary data

See Appendix A for Supplementary Tables 2.1 – 2.3. Supplementary Table 2.1 - List of the 25 *Iris germanica* cultivars observed for their root anatomy. All cultivars had identical root anatomy. Supplementary Table 2.2 - Monocot species with a uniseriate exodermis and various growth substrates. Supplementary Table 2.3 - Eudicot species with a uniseriate exodermis and various growth substrates.

Chapter 3

Permeability of *Iris germanica*'s multiseriate exodermis to water, NaCl and ethanol

3.1 Overview

The exodermis of *Iris germanica* roots is multiseriate. The outermost layer matures first with normal Casparian bands and suberin lamellae. But as subsequent layers mature, the Casparian band extends into the tangential and anticlinal walls of the cells. With respect to water and solute transport, roots with a developed multiseriate exodermis (MEX) should have much lower permeability rates than those in which the endodermis represents the major transport barrier. Precocious maturation of the exodermis was induced with a humid air gap inside a hydroponic chamber. Epidermal cells were unusually robust; most remained alive during the 14 d air gap exposure. Transport studies were conducted on completely submerged roots with an immature exodermis and on air gap-exposed root regions where two exodermal layers had matured. Hydraulic conductivity (L_{pc}) results were obtained with a pressure chamber. This instrument was used because in thick roots (diameters up to 2.5 mm in *I. germanica*), root hydraulics were affected by the high storage capacity of the central cortex. Compared with regions of roots with no mature exodermal layers, the mature MEX reduced L_{pc} from 8.5×10^{-8} to $3.9 \times 10^{-8} \text{ m s}^{-1} \text{ MPa}^{-1}$. Puncturing the MEX increased L_{pc} to $19 \times 10^{-8} \text{ m s}^{-1} \text{ MPa}^{-1}$, indicating that the MEX is an important hydraulically resistant tissue (75% of the total). Alternatively, a root pressure probe was used to measure hydraulic conductivity which tended to be related to the endodermis. The permeability of roots to NaCl and ethanol

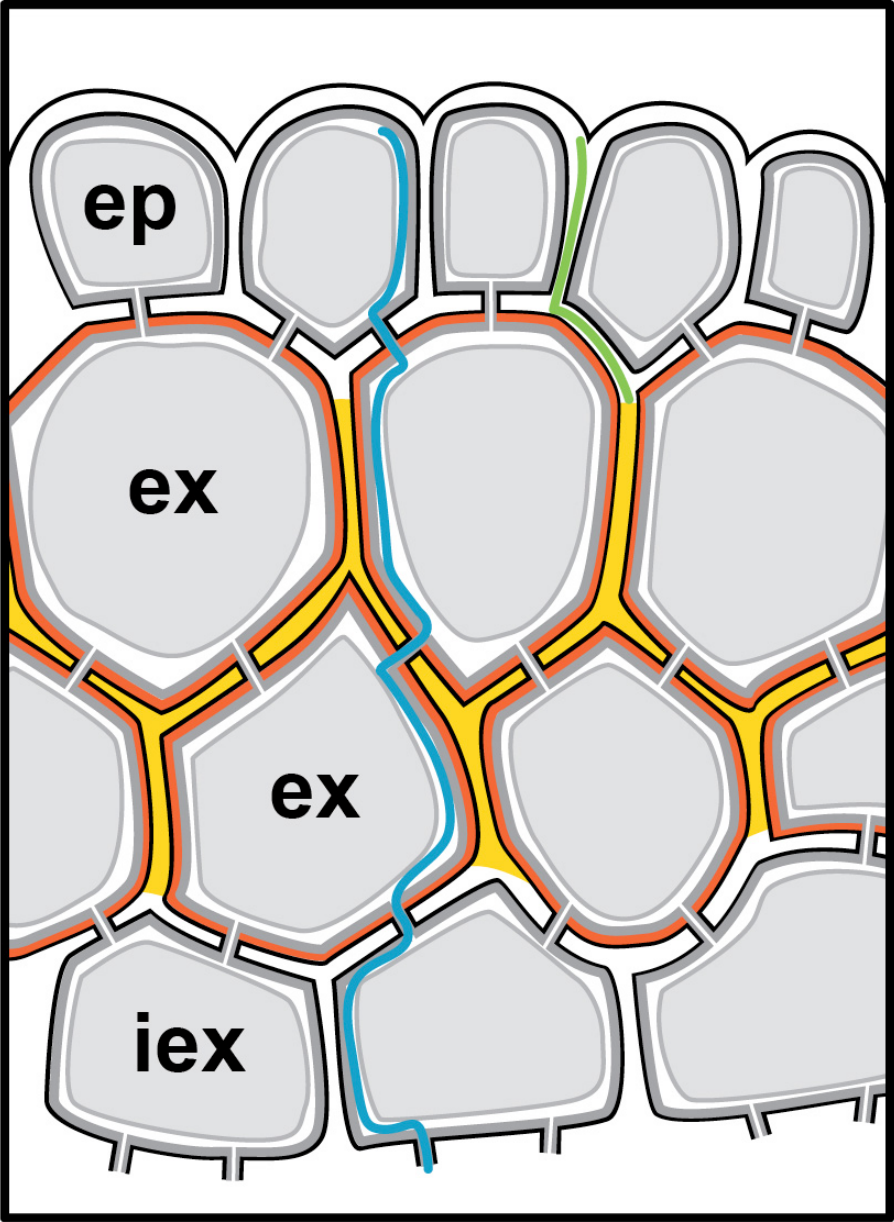
was reduced in the presence of two mature MEX layers, as obtained from pressure probe measurements. The data are discussed in terms of the validity of current root models and in terms of a potential role of *I. germanica*'s MEX in survival under conditions of drought and salt stress.

3.2 Introduction

Roots of *Iris germanica* have a number of unusual anatomical features that make them instructive for modelling and permeability and studies (Kroemer 1903; Peterson and Perumalla 1990; Zeier and Schreiber 1998; Meyer et al. 2009; see Chapter 2). 1) The root diameter is wide (up to 2.5 mm), as is the central cortex. 2) The endodermis is conspicuous with its palisade-like cells that have Casparian bands, suberin lamellae, and thick, lignified tertiary walls as close as 20-30 mm from the root tip in optimal growing conditions. 3) The multiseriate exodermis (MEX), composed of up to four centripetally maturing layers, has Casparian bands in the tangential walls of adjoining layers in addition to the anticlinal walls of the cells (Fig. 3.1). Meyer et al. (2009) (see Chapter 2) termed this structure a continuous circumferential Casparian band. 4) Immature areas (windows) in the exodermis through which lateral roots emerge are absent. Such windows occur in *Phragmites australis* and *Oryza sativa* (Soukup et al. 2002; Armstrong and Armstrong 2005). 5) Passage cells are absent from mature exodermal layers; thus, all cells have suberin lamellae (Fig. 3.1). These substantial wall modifications of the MEX can be expected to increase resistance to the radial movement of water and solutes through the transcellular and apoplastic pathways. (For a complete description of transport pathways, see section 1.3.1, Chapter 1.)

Roots have been referred to as composite structures since they have several types of cell layers that all contribute to the radial transport properties of these organs (Steudle and Peterson 1998). In spite of this, roots have been largely treated as osmometers with a membrane-equivalent barrier comparable to the membrane found in a cell; the 'root membrane' was assumed to be the endodermis (Dainty 1963; Steudle and Brinckmann 1989; Steudle and Jeschke 1983). This may be a reasonable approach for young, thin, non-exodermal roots with a diameter of a millimetre or less, or to the fine roots of trees that contribute most of the surface area responsible for the uptake of water and nutrients (Steudle and Jeschke 1983; Rüdinger et al. 1994; Tyree et al. 1994, 1995; Steudle and Meshcheryakov 1996). In thin roots, the storage of water in the central cortex may be negligible, allowing one to measure root hydraulics from transients in the flow of small volumes of water. Such transients are produced with a root pressure probe or a high pressure flow meter (HPFM) (Knipfer and Steudle 2008; Joshi et al. 2009). However, the situation may be different in thicker roots in which there is substantial water storage in the central cortex. The existence of an exodermis also complicates root models in that its hydraulic resistance in series to that of the endodermis would add to the overall resistance of the root. When roots are thin, this may reduce the water flow accordingly as derived from transient water flow (Zimmermann and Steudle 1998). However, a significant hydraulic capacity of the tissue between the endodermis and exodermis (i.e., a large central cortex) would tend to complicate the interpretation of transients in water flow as produced by the root pressure probe and HPFM.

Figure 3.1 Drawing of the outer part of an *I. germanica* root in cross section. Thicknesses of cell walls, cytoplasm, and plasmodesmata are exaggerated. Black lines = cell wall borders; dark grey lines = plasma membranes; light grey lines = tonoplasts; red lines = suberin lamellae; yellow lines = continuous circumferential Casparian band; blue line = symplastic transport through plasmodesmata; green line = apoplastic transport blocked by the continuous circumferential Casparian band. Abbreviations: ep = epidermis; ex = exodermis; iex = immature exodermis.



It may well be impossible to use these techniques to measure root hydraulic conductivity from pressure-relaxations or initial water flow. Instead, instruments that apply steady-state flows such as the pressure chamber may prove to be more suitable.

Ion movement into the root is profoundly affected by the endodermis and exodermis. Passage of ions through the apoplast is essentially prevented by Casparian bands (de Rufz de Lavison 1910; Baker 1971; Peterson 1987; Enstone et al. 2003). Ions are also virtually blocked from contacting the plasma membranes by suberin lamellae (Evert et al. 1985). Thus, for ion uptake into the symplast to occur in regions of *I. germanica* roots with a mature exodermis, some epidermal cells must be alive. Subsequent inward symplastic transport of ions through the exodermis requires at least some of its cells to be alive and connected by plasmodesmata (Fig. 3.1). Ions unable to traverse cell membranes should be efficiently blocked by the cell wall-modifying structures of the multiseriate exodermis (Fig. 3.1).

In the present study, the suitabilities of the root pressure probe and the pressure chamber were assessed for measuring the hydraulic conductivity of *I. germanica* roots. To ascertain the effect of the exodermis on hydraulic conductivity, a comparison was made between roots with an immature exodermis versus root segments in which two exodermal layers had matured. Similarly, the effect of the exodermis on Na^+ (a membrane-impermeant ion) and ethanol (a membrane-permeant molecule) permeability were made. The extent to which a symplastic pathway across the exodermis might be present was determined by testing epidermal cell viability.

3.3 Materials and methods

3.3.1 Plant material and growth conditions

Soil-grown *Iris germanica* L. plants were carefully removed from outdoor plots at the University of Bayreuth, Germany, in early May 2006. Rhizomes and their subtending adventitious roots were rinsed clean of adhering soil and then transferred to a 10 L hydroponic tank completely filled with nutrient solution (macronutrients in mM: 0.09 (NH₄)₂SO₄, 0.07 MgSO₄, 0.06 Ca(NO₃)₂, 0.05 KH₂PO₄, 0.05 KNO₃, 0.05 Fe(III)-EDTA, 0.03 K₂SO₄; micronutrients in μM: 4.6 H₃BO₃, 1.8 μMnSO₄, 0.3 μZnSO₄, 0.3 CuSO₄; pH = 5.5-6.0). The tank was placed inside a growth cabinet (25/23 °C [day/night]; 16 h photoperiod, 300 μmol m⁻² s⁻¹ PAR), and the solution was continuously aerated and exchanged with fresh solution weekly (Fig. 3.2A). During culturing, new adventitious roots emerged from each rhizome and grew into the nutrient solution.

It was known from previous work that the maturation of *I. germanica*'s second exodermal layer was delayed in fully submerged roots (up to 170 mm in length), but accelerated in regions exposed to an air gap (110-170 mm from tip; Meyer et al. 2009; see Chapter 2). In the current work, once several new adventitious roots (> 60 mm in length) had formed, some of the hydroponic tanks were only partially filled so that a 60-mm air gap was present between the solution surface and the base of the rhizome (Fig. 3.2F). The relative humidity in the air gap measured with a digital hygrometer/thermometer was 92% (Control Company; Friendswood, Texas). To prevent the rhizomes from dehydrating in this area, they were wrapped in paper towel saturated with nutrient solution. To ensure that two exodermal layers had matured, roots were exposed to the air gap condition for 14 d. Casparian bands and

suberin lamellae in the exodermis and endodermis were detected by staining freehand cross sections of the roots with berberine hemisulphate followed by aniline blue for Casparian bands, or with Sudan red 7B for lipids (Brundrett et al. 1988, 1991). Cell vitality was assessed by placing intact roots in uranin (disodium fluorescein) or Evan's blue (Stadelmann and Kinzel 1972; Taylor and West 1980; Barrowclough and Peterson 1994). For the former, specimens were viewed with ultraviolet light (UV filter set: excitation filter BP 365, dichroitic mirror FT 395, barrier filter LP 397) and for the latter, white light using an epifluorescence microscope (Carl Zeiss, Oberkochen, Germany). Photographs were taken with a digital camera (Cool Snap; Visitron Systems, Puchheim, Germany).

For physiological tests, adventitious, primary roots that had grown either fully submerged (control; Fig. 3.2A) or with the air gap (Fig. 3.2F) were excised from the rhizome under water with a razor blade. Submerged roots were then mounted directly into either a root pressure chamber or onto a pressure probe. To test the permeability of just the part of the root that had been exposed to the air gap, this portion was cut away and its distal end sealed using a combination of polyacrylamide glue (UHU, Bühl, Germany) and beeswax:colophony (1:3, w/w; Ranathunge et al. 2003). To apply the seal, the cut end of the root was first dipped in a pool of glue, the glue was allowed to dry and then this process was repeated, followed by dipping the same end into molten beeswax:colophony once. During the sealing process, the remainder of the root segment was kept hydrated by gently wrapping it with water-saturated tissue paper. Once the wax mixture had cooled and hardened, the segment was mounted into either the pressure chamber or pressure probe. In the latter case, the effectiveness of the glue-wax seal was confirmed when a positive internal root pressure was attained.

3.3.2 Root pressure probe experiments

Measurements using the root pressure probe (see Fig. 1.8, Chapter 1) were conducted as described previously (Steudle et al. 1987; Steudle and Frensch 1989). The base of each excised root was tightly mounted into the probe with a custom-made silicone seal. To minimize effects due to unstirred layers along the root surface, roots were bathed in a turbulent nutrient solution (the same solution as in the hydroponic tank). For roots of *I. germanica*, stable root pressures were rather low ($P_{ro} = 0.05-0.08$ MPa) and 8-10 h were required before this pressure developed. Once the pressure was stable, 4 - 6 hydrostatic pressure relaxations were conducted by increasing or decreasing the xylem pressure with the rod of the probe. Responses in pressure by the root were recorded; in accordance with previous studies, the fast phase was used, which occupied about 75% of the total change in pressure (Steudle and Frensch 1989; Knipfer et al. 2007; Joshi et al. 2009; see Fig. 1.9A, Chapter 1). The rate constants (k_{wr}), or the half-times of the pressure relaxations ($T_{1/2}^w$), were determined and used to calculate the root's hydraulic water conductivity (Lp_r in $m \cdot s^{-1} \cdot MPa^{-1}$), referred to the surface area of the root, A_r (in m^2)

$$k_{wr} = \frac{\ln(2)}{T_{1/2}^w} = A_r \cdot \left(\frac{\Delta P_r}{\Delta V_S} \right) \cdot Lp_r \quad (\text{Eq 1}).$$

Here, $(\Delta P_r / \Delta V_S)$ is the elastic modulus of the system (in $MPa \cdot m^{-3}$). The elastic modulus was measured by inducing a rapid change in volume (ΔV_S) with the rod of the probe and measuring the corresponding change in root pressure (ΔP_r).

Osmotic hydraulic conductivity (Lp_{ro}) and solute permeability (P_{sr} in $m \cdot s^{-1}$) were measured using the root pressure probe, but the force was applied by changing the osmolarity

of the external medium with nutrient solution amended with either ~40 mOsmol of NaCl or ~200 mOsmol of ethanol (EtOH). The precise osmolarities of these solutions were measured cryoscopically with an osmometer (Osmomat 030; Gonotec, Berlin, Germany). These solutes and concentrations have been used in the past, and are not toxic (Steudle and Frensch 1989; Ranathunge et al. 2003). External application of the test solute solutions created an osmotic pressure gradient between the outside and inside of the root. The reduced external water potential resulted in a net flow of water out of the root as measured by a decrease of the internal root pressure (see Fig. 1.9B, Chapter 1). The half-time of this recorded pressure change was used to calculate $L_{p_{ro}}$ (as in Eq 1). In some cases, a net flow of the solute into the root occurred in response to a concentration gradient, causing transients in root pressure. From the second phase of transients, the permeability coefficients (P_{sr}) of the solutes (NaCl or ethanol) were worked out assuming a membrane-equivalent barrier in the root (Steudle et al. 1987; see Fig. 1.9B, Chapter 1). Analogous to Eq 1, the rate constant of solute permeability (k_{sr}) was related to P_{sr} by

$$k_{sr} = \frac{\ln(2)}{T_{1/2}^s} = A_r \cdot \left(\frac{P_{sr}}{V_x} \right) \quad (\text{Eq 2}),$$

where V_x is the volume of the vessel lumens (= 0.13-0.4% of total root volume, which was estimated from cross sections). The biphasic reaction described above was reversible, i.e., when the external solute solution was changed back to the original, there was a net flow of water into the root and of solute out (exosmotic) (see Fig. 1.9B, Chapter 1). Again, $L_{p_{ro}}$ and P_{sr} were calculated from the recorded changes in pressure. Reflection coefficients (σ_{sr}) of the two solutes were calculated from pressure/time curves using the following equation

$$\sigma_{sr} = \frac{(P_{ro} - P_{rmin})}{\Delta\pi_s} \times \exp(k_s \cdot t_{min}) \quad (\text{Eq 3}),$$

where P_{ro} and P_{rmin} are the original and minimum root pressures of pressure/time curves, respectively, $\Delta\pi_s = RT \cdot \Delta C_s$ is the change of external osmotic pressure caused by the osmoticum (NaCl or ethanol), and t_{min} the time required to reach P_{rmin} following a step change in the external concentration at $t = 0$.

For experiments involving roots from the air gap growth condition, the complete hydrostatic and osmotic methods described above were conducted twice per root. The first series of measurements were done when the root was intact. The second series were taken after the multiseriate exodermis had been punctured so that its role in permeability could be determined (Steudle et al. 1993). Each root was punctured eight times using a glass microcapillary 100 μm in diameter. Since air gap-exposed root segments were relatively thick (average diameter of 2.5 mm), puncturing was easily accomplished with the endodermis remaining unscathed the majority of the time. Puncturing caused the root pressure to drop slightly, but it remained stable. Wounds were observed following the experiments by staining with Evan's blue to detect dead cells (Taylor and West 1980) and making cross-sections to view the puncture depth. Additional cross-sections were stained with berberine-hemisulphate and aniline blue to detect the presence of the continuous circumferential Casparian band (Brundrett et al. 1988). These sections were viewed and photographed with the microscope and camera described above.

For the submerged and air gap growth conditions, 5-6 roots were tested. Submerged roots used for permeability testing had an average length of 100 mm. Air gap-exposed root

segments used for permeability testing were, on average, 220-260 mm from the root tip. The exodermis of the latter segments was punctured using the method described above. In cases where the endodermis was accidentally wounded, root pressure dropped to zero, and no further permeability tests could be conducted. The effect of puncturing the biseriate exodermis on hydraulic and osmotic water flow was established by taking the ratio between the L_p of intact vs. punctured air gap-exposed root segments for each case.

3.3.3 Pressure chamber experiments

A small custom-made pressure chamber (see Fig. 1.6, Chapter 1) was used as an alternate instrument for measuring the hydraulic conductivity of *I. germanica*'s adventitious roots. This chamber had a volume of $6 \times 10^{-5} \text{ m}^3$ and was filled with nutrient solution (as above). It was equipped with a screw cap that had a small hole in the center (3.2 mm diameter) where a single root could be mounted using a silicone seal. At the same time, the excised end of the root was mounted by means of a silicone seal into a small chamber into which a narrow, graduated capillary had been sealed. Initially, water was injected into the chamber until the liquid entered the capillary. Roots from both the submerged and air gap treatments were mounted in this way. Pneumatic pressure was applied to the chamber and water flow (in $\text{m}^3 \cdot \text{s}^{-1}$) was monitored. Pressure was increased in steps of 0.05 MPa up to a maximum of 0.30 MPa. Measurements were taken at following pressures: 0.00, 0.10, 0.20 and 0.30 MPa. After reaching each of these pressures, the system equilibrated for 60 min during which readings were taken every 10 or 15 min. At each pressure, rates of water flow were plotted against time (see Fig. 1.7A, Chapter 1), and the slopes from the linear parts of the lines (Q_v in $\text{m}^3 \cdot \text{s}^{-1}$) were used to calculate the rate of water flow (J_v in $\text{m}^3 \cdot \text{m}^{-2} \cdot \text{s}^{-1}$)

$$J_v = \frac{Q_v}{A_r} \quad (\text{Eq 4}).$$

By plotting J_v against ΔP , the contribution of the osmotic component was observed as an initial slow phase. Once the solutes in the xylem were diluted, $J_v/\Delta P$ became linear.

Hydraulic conductivity ($L_{p_{pc}}$ in $\text{m}\cdot\text{s}^{-1}\cdot\text{MPa}^{-1}$) was determined from the slope of the linear part of the $J_v/\Delta P$ curve (see Fig. 1.7B, Chapter 1). In the pressure chamber experiments, effects of unstirred layers due to a concentration polarization of nutrient ions at the exodermis or endodermis could be neglected because of the low concentration of these solutes in the nutrient medium.

Experiments involving puncturing of the biseriate exodermis of air gap-exposed roots were also conducted. Two series of increasing pneumatic pressures were conducted per root – first before puncturing the biseriate exodermis and then after puncturing. Following the first set of measurements, the pressure in the chamber was released through a valve. Then the chamber was separated from the screw cap and graduated capillary, which held the mounted root, by fixing the cap and capillary in a stationary position and unscrewing the chamber from the cap. The exodermis of the exposed root was punctured using the technique described above. Then the chamber was re-filled with nutrient solution and screwed back on to the cap so that water flow measurements could be repeated. Five or six roots were used for the submerged and air gap growth conditions. From the punctured air gap roots, a complete data set was obtained for repetitions that did not have a damaged endodermis. The effect of puncturing the biseriate exodermis on hydraulic water flow was established by taking the ratio between the L_p of intact vs. punctured, air gap-exposed root segments for each case.

3.3.4 Resistance of the exodermis to water and solute flows

Hydraulic resistances (R_w) were calculated from Lp_r , Lp_{ro} , Lp_{pc} , and the respective surface area (A). Likewise, resistances to solute flow (R_s) were obtained from P_{sr} :

$$R_w = \frac{1}{Lp \times A} \text{ and } R_s = \frac{1}{P_{sr} \times A} \quad (\text{Eq 5}).$$

Lp values were typically calculated with the root surface area. However, in some cases the Lp was calculated with the endodermal surface area (Eq 1 and 4; see Results). Resistance values were used to determine the fold change in the resistance of the root to hydraulic or solute flow between completely submerged roots with an immature exodermis and air gap-exposed roots with a biseriate exodermis. Similarly, the fold change in resistance was determined between the intact biseriate exodermis and its punctured counterpart.

3.3.5 Statistical analyses

To test whether or not root water and solute permeabilities were significantly different with the maturation of the biseriate exodermis, two-tailed, unpaired t-tests ($\alpha = 0.05$) were employed. Similar tests were conducted to test if the permeabilities were significantly different between roots with an immature exodermis and root segments with a punctured biseriate exodermis. On the other hand, one-tailed, paired t-tests ($\alpha = 0.05$) were used to determine if the water and solute permeabilities of the intact root segment with a biseriate exodermis increased significantly after it was punctured. The t-tests described above were also used to determine differences in hydraulic and solute resistances.

3.4 Results

3.4.1 Root anatomy

Development of the exodermis in submerged and air gap-exposed roots was followed by staining for Casparian bands and suberin lamellae. Differences were evident when comparing roots of similar lengths that had been grown in these conditions. In completely submerged roots with lengths of 200 mm or less, the first exodermal layer usually matured 80 mm from the root tip. This layer had typical Casparian bands occupying its anticlinal walls (Figs. 3.2A,E, 3.3A). Submerged roots 100 mm in length were used for both pressure chamber and pressure probe experiments. In the case of the pressure chamber, the proximal 30 mm of the root was sealed into the instrument so that the exposed part on which measurements were made had a uniformly immature exodermis (0EX). In the case of the pressure probe, approximately 15 mm were sealed into the instrument so that 94% of the exposed root had an immature exodermis (0EX). In contrast, the basal part of roots exposed to a humid air gap (average relative humidity = 92%) for 14 d had a uniformly developed biseriate exodermis with its characteristic continuous circumferential Casparian band (2EX) (Figs. 3.2C,F, 3.3B). (It was this region that was used to test radial water and solute permeability.) On these same roots, the part that remained submerged (i.e., below the air gap) exhibited a gradual exodermal maturation, similar to the completely submerged roots (see Fig. 3.2E). Exodermal cells that had Casparian bands also had suberin lamellae as the two structures were deposited concurrently (Fig. 3.3C).

Epidermal cell viability was also examined in submerged and air gap-exposed roots using uranin. In the submerged epidermis, uranin accumulated in all cells; hence, they were all

Figure 3.2 Drawings of two hydroponic systems (not to scale) with photomicrographs that represent typical effects of the growth conditions on the roots' epidermal viability and exodermal maturation. (A) Control growth condition: rhizomes and roots were submerged in nutrient solution. (B) Surface view of the epidermis from a uranin-treated, air gap-exposed region of the root. Uranin was trapped in the cytoplasm and nuclei of living epidermal cells, but was absent from dead epidermal cells (*). (C) Cross section from an air gap-exposed region of a root, stained with berberine-aniline blue, showing a mature biseriate exodermis with continuous circumferential Casparian band (arrows). (D) Surface view of the epidermis from a uranin-treated, submerged region of the root. Uranin was observed in all epidermal cells. (E) Cross section from a submerged, basal region of a root, stained with berberine-aniline blue, showing a mature uniseriate exodermis with typical Casparian bands (arrows). (F) Air gap growth condition: the hydroponic chamber was partially filled leaving a 60 mm gap between the solution surface and the rhizome base. These rhizomes were wrapped in paper towel saturated with nutrient solution. Scale bars = 100 μ m. Abbreviations: ex = exodermis; grey rectangle = aeration stone.

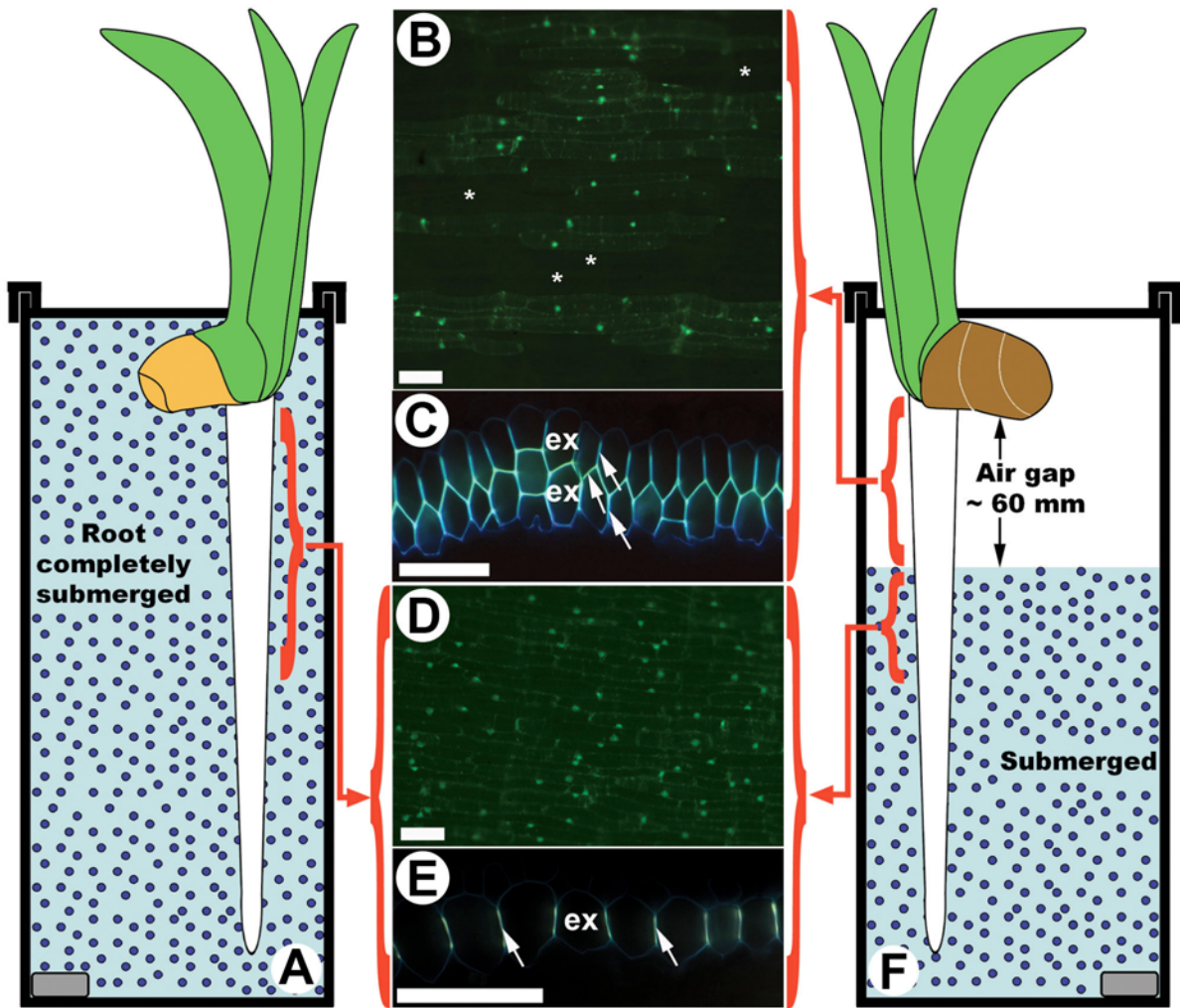
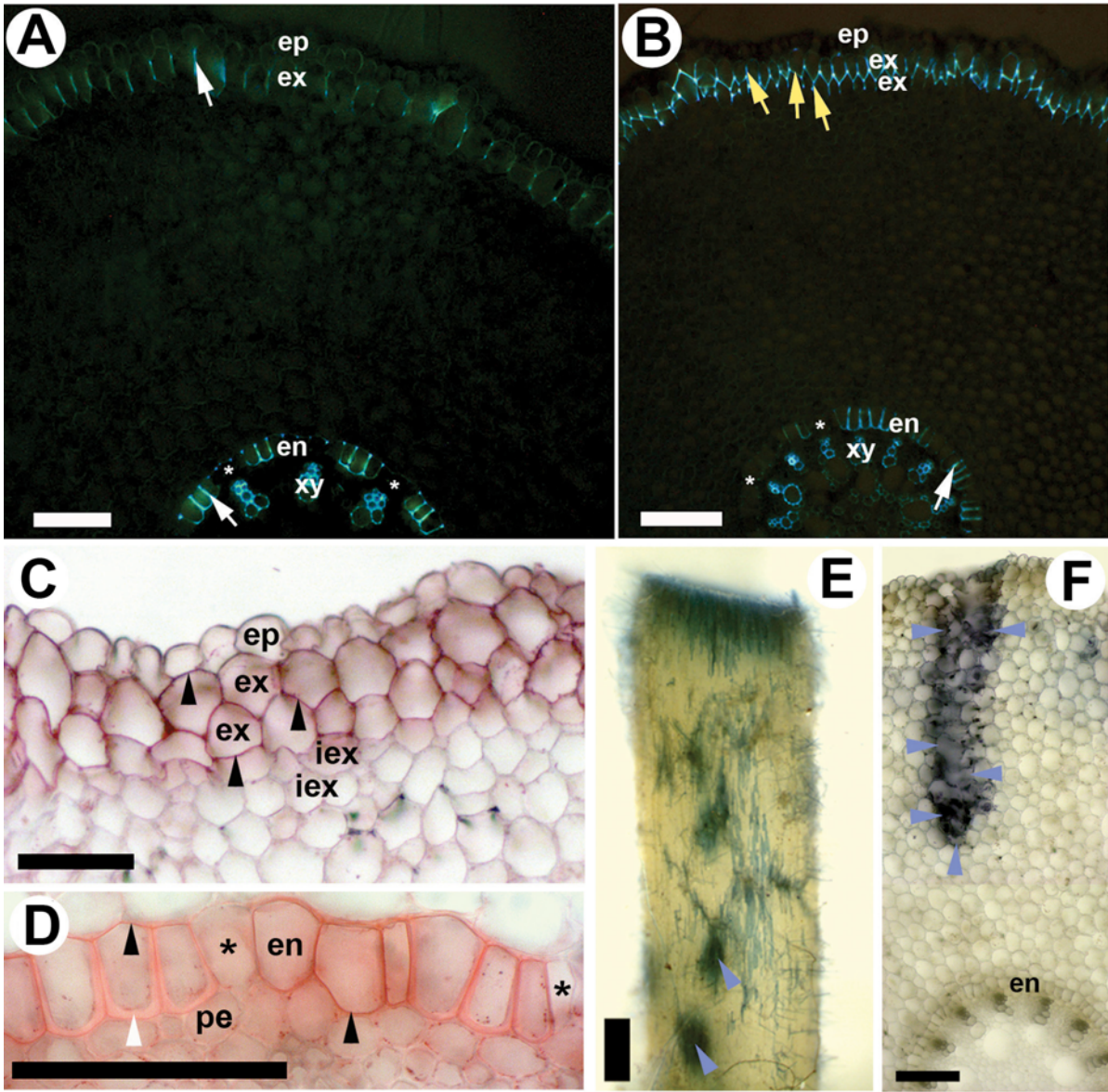


Figure 3.3 Photomicrographs from *I. germanica* roots grown in submerged or air gap hydroponic conditions showing cross sections of the roots unless otherwise stated. Values in mm refer to distances from the root tips. (A) 100 mm. Stained with berberine-aniline blue. This specimen typifies the basal region of submerged roots, exhibiting a typical Casparian band in the endodermis (arrow) and in the outermost cells of the exodermis (arrow). (B) 100 mm. Stained with berberine-aniline blue. This specimen typifies the air gap-exposed root region, exhibiting a continuous circumferential Casparian band in the multiseriate exodermis (yellow arrows) and a typical Casparian band in the endodermis (white arrow). (C) 120 mm. Stained with Sudan red 7B. The outer part of a root with two mature exodermal layers that contain suberin lamellae (arrowheads). (D) 80 mm. Stained with Sudan red 7B. Endodermis with suberin lamellae (black arrowheads) in all cells except the passage cells (*). Suberin was not deposited in the U-shaped wall thickenings (white arrowhead). (E) 255-247 mm. Treated with Evan's blue. Whole mount of an air gap-exposed root with a punctured exodermis (arrowheads). Scale bar = 1 mm. (F) 220 mm. Cross section treated with Evan's blue. This specimen demonstrates the depth of a puncture within the root (arrowheads). The wound penetrated the epidermis, exodermis, and half of the central cortex; the endodermis was unscathed. Scale bars [except for (E)] = 100 μ m. Asterisks = passage cells.

Abbreviations: ep = epidermis; ex = exodermis; iex = immature exodermis; en = endodermis; pe = pericycle; xy = xylem pole.



alive (Fig. 3.2D). On the other hand, in the air gap-exposed epidermis, uranin accumulated in approximately 50% of the cells indicating that half remained alive (Fig. 3.2B).

Endodermal development was not noticeably affected by the growth conditions (Fig. 3.3A,B). By 100 mm from the tip, the majority of endodermal cells had reached full maturity (State III), and some passage cells remained irrespective of growth conditions. Casparian bands in the endodermis were initially small and offset toward the pericycle. Later, in many endodermal cells the Casparian bands extended through the anticlinal walls, suberin lamellae were deposited, and U-shaped tertiary wall thickenings were formed (Fig. 3.3D). However, in the few passage cells of the endodermis where suberin lamellae were not deposited, Casparian bands were not elongated (Fig. 3.3D).

To visualize the location and depth of the wounds after puncturing, air gap-exposed roots that had their two exodermal layers punctured (2EX-P) were stained with Evan's blue (Fig. 3.3E). The 40-mm-long root segments had a surface area that ranged from 2.1×10^{-4} to $3.2 \times 10^{-4} \text{ m}^2$. The surface area of the punctured tissue was $6.3 \times 10^{-8} \text{ m}^2$, equalling 2×10^{-2} to $3 \times 10^{-2} \%$ of the total root surface area. From the cross-sections of punctured tissue, one could observe that the wound penetrated only about half way through the central cortex, leaving the endodermis intact (Fig. 3.3F).

3.4.2 Measurements of hydraulic conductivity

Water flow, as measured with the pressure chamber, was established for three cases of interest: 1) roots with no mature exodermal layers (0EX), 2) root segments with two mature exodermal layers (2EX), and 3) roots with two mature exodermal layers that had been punctured (2EX-P). In all cases, at each step in chamber pressure, the cumulative volume of

solution that was transported across the root increased linearly with time (Fig. 3.4). To demonstrate steady-state water flow, the slopes from the cumulative water flow graphs were plotted against the changes in pressure (Fig. 3.5). Generally, as pressure increased, water flow through the roots also increased. A typical trend was observed for the 0EX roots; the flow rate was initially slow but accelerated at greater pressures, resulting in a curvilinear response previously explained by Fiscus (1975) as a dilution effect. This effect refers to a decrease in the concentration of xylem sap as the inflow of water increased, hence the osmotic contribution to the driving force becomes negligible (Sands et al. 1982; Zimmermann and Steudle 1998). However, for 2EX the rate of water flow increased only linearly with increasing pressures. Such a linear increase may be due to the fact that both xylem sap concentration and water inflow were low, tending to reduce the dilution effect. Even more unusual was the water flow for 2EX-P which was initially very rapid, but then began to plateau at 0.3 MPa. Such a trend suggested that water flow was reaching a maximum in the plateauing region, similar to the plateau in water flow measured for *Picea mariana* roots (see Colombo and Asselstine 1989). The slopes of the linear parts of each curve yielded the hydraulic conductivity ($L_{p_{pc}}$).

A comparison of the $L_{p_{pc}}$ of roots with an immature exodermis versus those with a biseriate exodermis, and the latter roots versus those with a punctured exodermis indicated the effect of the exodermis on water flow. The average $L_{p_{pc}}$ of 0EX roots was $8.5 \times 10^{-8} \text{ m s}^{-1} \text{ MPa}^{-1}$. Maturation of the 2EX significantly reduced $L_{p_{pc}}$ to $3.9 \times 10^{-8} \text{ m s}^{-1} \text{ MPa}^{-1}$ (Table 3.1). Thus, the hydraulic resistance of roots with a biseriate exodermis was, on average, 3.1-fold greater than that of 0EX roots (Tables 3.2, 3.3). In every case, puncturing the

Figure 3.4 Cumulative water flow through roots during the pressure chamber experiments.

Each graph represents typical results. (A) 0EX roots. (B) 2EX roots. (C) 2EX-P roots.

Legends inset in graphs.

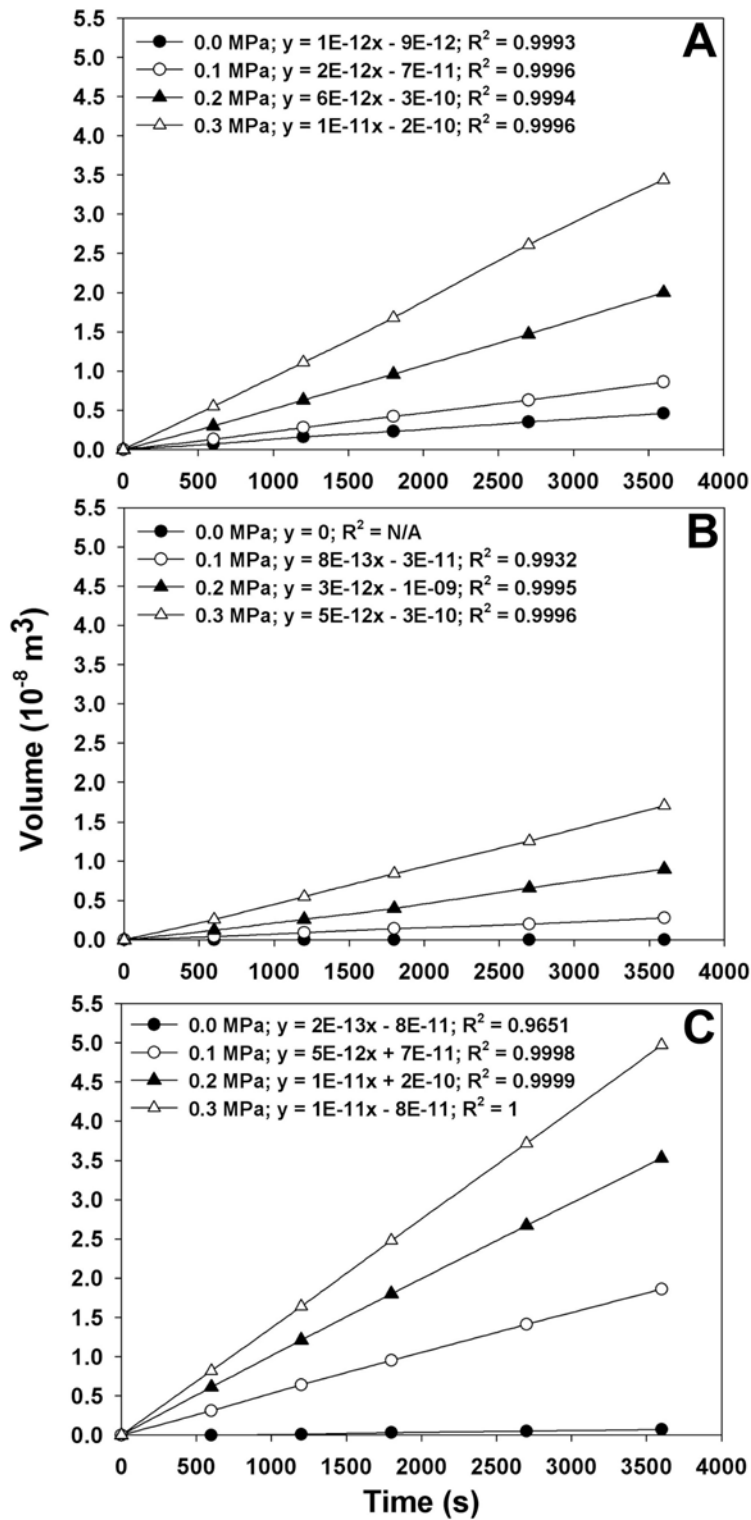


Figure 3.5 Steady-state water flow per unit root surface area with an increasing driving force (i.e., induced hydrostatic pressure changes). This graph displays typical results. Legend inset in graph.

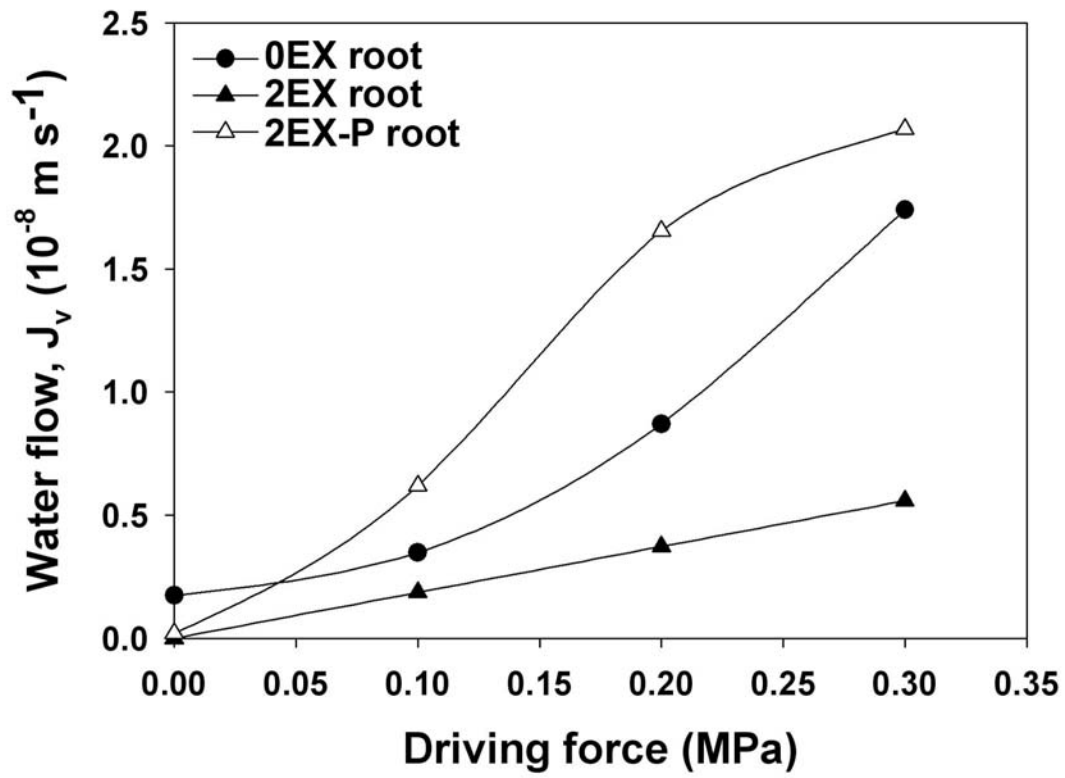


Table 3.1 Hydraulic conductivity values calculated from pressure chamber and pressure probe experiments. Conductivity data are means \pm standard deviations, and the number of replicates are in parentheses. Different superscripted letters indicate a significant difference within each row ($p \leq 0.05$). 0EX, roots with no mature exodermal layers; 2EX, root segments with 2 mature exodermal layers; 2EX-P, root segments with 2 mature exodermal layers that were punctured.

Instrument	L_p ($10^{-8} \text{ m s}^{-1} \text{ MPa}^{-1}$)		
	0EX	2EX	2EX-P
Pressure chamber	^a 8.5 ± 0.9 (5) ¹	^b 3.9 ± 2.1 (5) ¹	^a 18.6 ± 16.2 (5) ¹
			^a 92.8 ± 90.8 (5) ²
Pressure probe ¹	^a 39.1 ± 12.7 (6)	^b 23.3 ± 9.1 (6)	^a 40.6 ± 24.1 (6)
Pressure probe ²	^a 242 ± 103 (6)	^b 127 ± 55.5 (6)	^a 219 ± 137 (6)

¹ L_p values calculated using root surface area. ² L_p values calculated using endodermal surface area. L_{p_r} 2EX and $L_{p_{pc}}$ 2EX-P are statistically similar (result not shown in Table).

exodermis of 2EX roots (2EX-P) increased $L_{p_{pc}}$. Individual ratios of values for 2EX:2EX-P varied from 1:1.9 to 1:7.9 (average = 1:4.7). These ratios indicated a 4.7-fold increase in $L_{p_{pc}}$, or a 4.1-fold loss of resistance, when the exodermis was punctured (Tables 3.3, 3.4). Since puncturing the exodermis essentially nullified its hydraulic resistance, it was assumed that the endodermis then became the most hydraulically resistant tissue. For this case, $L_{p_{pc}}$ 2EX-P data was re-calculated using the endodermal surface area instead of the surface area for the outer part of the root. This re-calculation dramatically increased $L_{p_{pc}}$ 2EX-P (Table 3.1) by on average 23-fold compared with $L_{p_{pc}}$ 2EX (Table 3.4). Nonetheless, the percent loss of exodermal resistance was still 4.1-fold (the same as measured before $L_{p_{pc}}$ 2EX-P re-calculation) because when calculating resistance, L_p values are multiplied by the corresponding surface area (see Eq 5; Tables 3.2, 3.3).

When the root pressure probe was used to measure hydraulic conductivity (L_{p_r}), it was found that maturation of the biseriate exodermis reduced L_{p_r} significantly (Table 3.1); this was equivalent to a 2.8-fold increase in resistance (Tables 3.2, 3.3), which may have also been due to differences in the maturation state of the endodermis. Puncturing the biseriate exodermis resulted in a ratio (2EX:2EX-P) ranging from only 1:1 to 1:2.5 (average = 1:1.7), indicating a rather small increase in L_{p_r} , or a 1.4-fold loss of resistance (Tables 3.3, 3.4). Interestingly, the absolute values of L_{p_r} were markedly greater than those of $L_{p_{pc}}$. This indicated that, because of the large storage capacity of the root's central cortex, the pressure probe measured the hydraulic resistance of mainly the endodermis rather than the entire root. For a proper comparison in this situation, L_{p_r} was re-calculated on the basis of the surface area of the endodermis instead of the outer part of the root. Consequently, the L_{p_r} values

increased tremendously (Table 3.1), but there was essentially no change in the ratio comparison of 2EX:2EX-P (Table 3.4) and no change in the fold change in resistance (Tables 3.2, 3.3).

The statistical comparison between the values of L_{p_r} for 2EX and of $L_{p_{pc}}$ for 2EX-P was based on the rationale that only the endodermal hydraulic conductivity was measured with the pressure probe and that the same was true when punctured root segments were tested with the pressure chamber. The compared L_p values were statistically similar (Table 3.1), further proving that only the endodermis was tested in these specific cases.

The third method of measuring hydraulic conductivity ($L_{p_{ro}}$) was using osmotic gradients as the driving force. In this case, values of $L_{p_{ro}}$ were lower by one to two orders of magnitude than those of L_{p_r} and $L_{p_{pc}}$ (compare Tables 3.1 and 3.5). This indicated that, in the presence of osmotic gradients, water flow was from cell-to-cell rather than apoplastic, which is in line with earlier results of root hydraulics (see Discussion). As expected, with the maturation of 2EX, the average $L_{p_{ro}}$ for both NaCl- and EtOH-treated roots decreased, compared with 0EX (Table 3.5). Accordingly, when the 2EX was punctured, the NaCl- $L_{p_{ro}}$ increased an average of 11-fold (or an 11-fold loss of resistance), while the EtOH- $L_{p_{ro}}$ increased an average of 4.1-fold (or a 2.6-fold loss of resistance) (Tables 3.2, 3.3, 3.6). When the $L_{p_{ro}}$ 2EX-P data was re-calculated with the endodermal surface area, the values increased as expected (Table 3.6). Now, in punctured root segments, NaCl- $L_{p_{ro}}$ was an average of 58-fold greater and EtOH- $L_{p_{ro}}$ an average of 20-fold greater than their intact counterparts.

Table 3.2 Root hydraulic (above) and solute (below) resistances. Values of hydraulic resistance were calculated from L_p values obtained from pressure chamber and pressure probe experiments (Table 3.1; resistance = $1/[L_p \cdot \text{surface area}]$). Values of solute resistance were calculated from P_{sr} values obtained from pressure probe experiments (Table 3.5; resistance = $1/[P_{sr} \cdot \text{surface area}]$). Data are means \pm standard deviations. Different superscripted letters indicate a significant difference within each row ($p \leq 0.05$). PC, pressure chamber; RPP, root pressure probe; P_{sr} , solute permeability; 0EX, roots with no mature exodermal layers; 2EX, roots with 2 mature exodermal layers; 2EX-P, roots with 2 exodermal mature layers that had been punctured; n.m., not measurable.

Type of measurement	Hydraulic resistance ($10^{10} \text{ MPa}\cdot\text{s}\cdot\text{m}^{-3}$)		
	0EX	2EX	2EX-P
PC	^a 2.2 ± 0.27	^b 6.9 ± 3.5	^a 1.7 ± 0.76
RPP	^a 0.61 ± 0.30	^b 1.7 ± 0.92	^{ab} 1.2 ± 0.57
RPP (NaCl)	^a 29 ± 5	^b 220 ± 98	^a 19 ± 10
RPP (EtOH)	^a 47 ± 12	^b 310 ± 110	^a 118 ± 99
	Solute resistance ($10^{10} \text{ s}\cdot\text{m}^{-3}$)		
RPP, P_{sr} (NaCl)	^a 1050 ± 230	^b n.m.	^c 60 ± 51
RPP, P_{sr} (EtOH)	^a 140 ± 38	^b 1070 ± 430	^a 160 ± 140

Table 3.3 Fold change in resistance of the root to water and solute flows after maturation of the biseriate exodermis, or after puncturing the exodermis. These fold change values were calculated from the resistance values (see Table 3.2). PC, pressure chamber; RPP, root pressure probe; P_{sr} , solute permeability; 0EX, roots with no mature exodermal layers; 2EX, roots with 2 mature exodermal layers; 2EX-P, roots with 2 exodermal mature layers that had been punctured; n.m., not measurable.

Type of measurement	Fold change in resistance	
	0EX vs 2EX	2EX vs 2EX-P
Hydraulic resistance		
PC	+3.1	-4.1
RPP	+2.8	-1.4
RPP (NaCl)	+7.4	-11
RPP (EtOH)	+6.7	-2.6
Solute resistance		
RPP, P_{sr} (NaCl)	n.m.	n.m.
RPP, P_{sr} (EtOH)	+7.6	-6.8

Table 3.4 Effect of puncturing the biseriate exodermis on hydraulic conductivity. For all roots, L_p was calculated using the root surface area (values not within parentheses). It was assumed that after puncturing, the endodermis dominated the hydraulic resistance. Plus, the pressure probe primarily measured L_p of the endodermis. Therefore, the pressure chamber 2EX-P values and all pressure probe values were also calculated using the surface area of the endodermis (values within parentheses). This calculation resulted in increased L_p and ratio values compared with the former calculated values. For paired experiments, different superscripted letters within each row indicate a significant difference between 2EX and 2EX-P ($p \leq 0.05$). 2EX L_p = conductivity before puncturing; 2EX-P L_p = conductivity after puncturing the same root segment.

Instrument	Rep	L_p ($10^{-8} \text{ m s}^{-1} \text{ MPa}^{-1}$)		Ratio comparison
		2EX	2EX-P	2EX : 2EX-P
Pressure chamber	1	4.1	10 (49)	1:2.5 (1:12)
	2	4.0	7.6 (38)	1:1.9 (1:9.5)
	3	1.9	9.3 (47)	1:5.0 (1:25)
	4	2.4	19 (78)	1:7.9 (1:32)
	5	7.3	47 (250)	1:6.4 (1:35)
	Avg	^a 3.9±2.1	^b 19±16 (^b 93±91)	1:4.7 (1:23)
Pressure probe	1	11 (55)	11 (50)	1:1 (1:0.9)
	2	13 (59)	25 (113)	1:1.9 (1:1.9)
	3	23 (141)	28 (153)	1:1.2 (1:1.1)
	4	30 (165)	50 (258)	1:1.7 (1:1.6)
	5	30 (166)	52 (337)	1:1.7 (1:2.0)
	6	32 (175)	79 (406)	1:2.5 (1:2.3)
Avg	^a 23±9 (^a 127±55)	^b 41±24 (^b 219±137)	1:1.7 (1:1.6)	

Table 3.5 Osmotic data from root pressure probe experiments. Values are means \pm standard deviations, with the number of replicates in parentheses. Different superscripted letters within each row indicate a significant difference between 0EX and 2EX ($p \leq 0.05$). $L_{p_{ro}}$, osmotic hydraulic conductivity; P_{sr} , solute permeability; σ_{sr} , reflection coefficient. 0EX, roots with no mature exodermal layers; 2EX, roots with 2 mature exodermal layers.

Solute	$L_{p_{ro}} (10^{-8} \text{ m s}^{-1} \text{ MPa}^{-1})$		$P_{sr} (10^{-8} \text{ m s}^{-1})$		σ_{sr}	
	0EX	2EX	0EX	2EX	0EX	2EX
NaCl	^a 0.62 \pm	^b 0.21 \pm	^a 0.0084 \pm	^b 0.00 (5)	^a 0.92 \pm	^b 1.0 \pm
	0.08 (5)	0.08 (5)	0.012 (5)		0.22 (5)	0.00 (5)
EtOH	^a 0.40 \pm	^b 0.12 \pm	^a 0.14 \pm	^b 0.027 \pm	^a 0.16 \pm	^b 0.69 \pm
	0.09 (5)	0.05 (5)	0.04 (5)	0.027 (5)	0.12 (5)	0.39 (5)

Table 3.6 The effect of puncturing the biseriate exodermis on the roots' osmotic hydraulic conductivity. Values not within parentheses were calculated using root surface area. Values within parentheses were calculated using endodermal surface area. Paired experiments where different superscripted letters within each row indicate a significant difference between 2EX and 2EX-P ($p \leq 0.05$). 2EX $L_{p_{ro}}$ = conductivity before puncturing; 2EX-P $L_{p_{ro}}$ = conductivity after puncturing the same root segment.

Solute	Rep	$L_{p_{ro}} (10^{-8} \text{ m s}^{-1} \text{ MPa}^{-1})$		Ratio comparison
		2EX	2EX-P	2EX : 2EX-P
NaCl	1	0.11	1.2 (6.5)	1:11 (1:57)
	2	0.15	1.9 (8.6)	1:13 (1:57)
	3	0.19	2.4 (12)	1:12 (1:64)
	4	0.27	2.9 (15)	1:11 (1:57)
	5	0.30	3.1 (16)	1:11 (1:55)
	Avg	^a 0.21±0.08	^b 2.3±0.8 (^b 12±4.3)	1:11 (1:58)
EtOH	1	0.069	0.11 (0.58)	1:1.5 (1:8.4)
	2	0.080	0.18 (0.93)	1:2.2 (1:12)
	3	0.11	0.38 (1.9)	1:3.6 (1:18)
	4	0.14	0.83 (3.7)	1:6.0 (1:27)
	5	0.20	1.4 (7.1)	1:7.2 (1:36)
	Avg	^a 0.12±0.05	^a 0.58±0.54 (^b 2.8±2.7)	1:4.1 (1:20)

3.4.3 Measurements of root permeability to solutes

The root pressure probe was employed to measure the permeability (P_{sr}) and reflection coefficient (σ_s) for NaCl and ethanol (Table 3.5) using the membrane-equivalent root model (see section 3.2). NaCl permeated extremely slowly through 0EX roots ($8 \times 10^{-11} \text{ m s}^{-1}$) and for 2EX roots, NaCl permeation was reduced to an undetectable level (Fig. 3.6A). In contrast, for 2EX-P roots, NaCl permeated rapidly and variably ($1.3 \pm 0.6 \times 10^{-8} \text{ m s}^{-1}$; Fig. 3.6B). These same trends were observed for the NaCl σ_s values (Table 3.5).

In contrast to NaCl, EtOH permeated all roots regardless of maturity or treatment. For 0EX roots, EtOH P_{sr} was $0.14 \times 10^{-8} \text{ m s}^{-1}$. This was reduced significantly to $0.027 \times 10^{-8} \text{ m s}^{-1}$ in 2EX roots (Table 3.5), bringing about a 7.6-fold increase in resistance (Tables 3.2, 3.3; Fig. 3.6C). Puncturing the exodermis increased EtOH P_{sr} to $0.64 \times 10^{-8} \text{ m s}^{-1}$, lowering the resistance by 6.8-fold (Tables 3.2, 3.3). The trends observed for the EtOH σ_s values were similar to their corresponding P_{sr} trends (Table 3.5).

3.5 Discussion

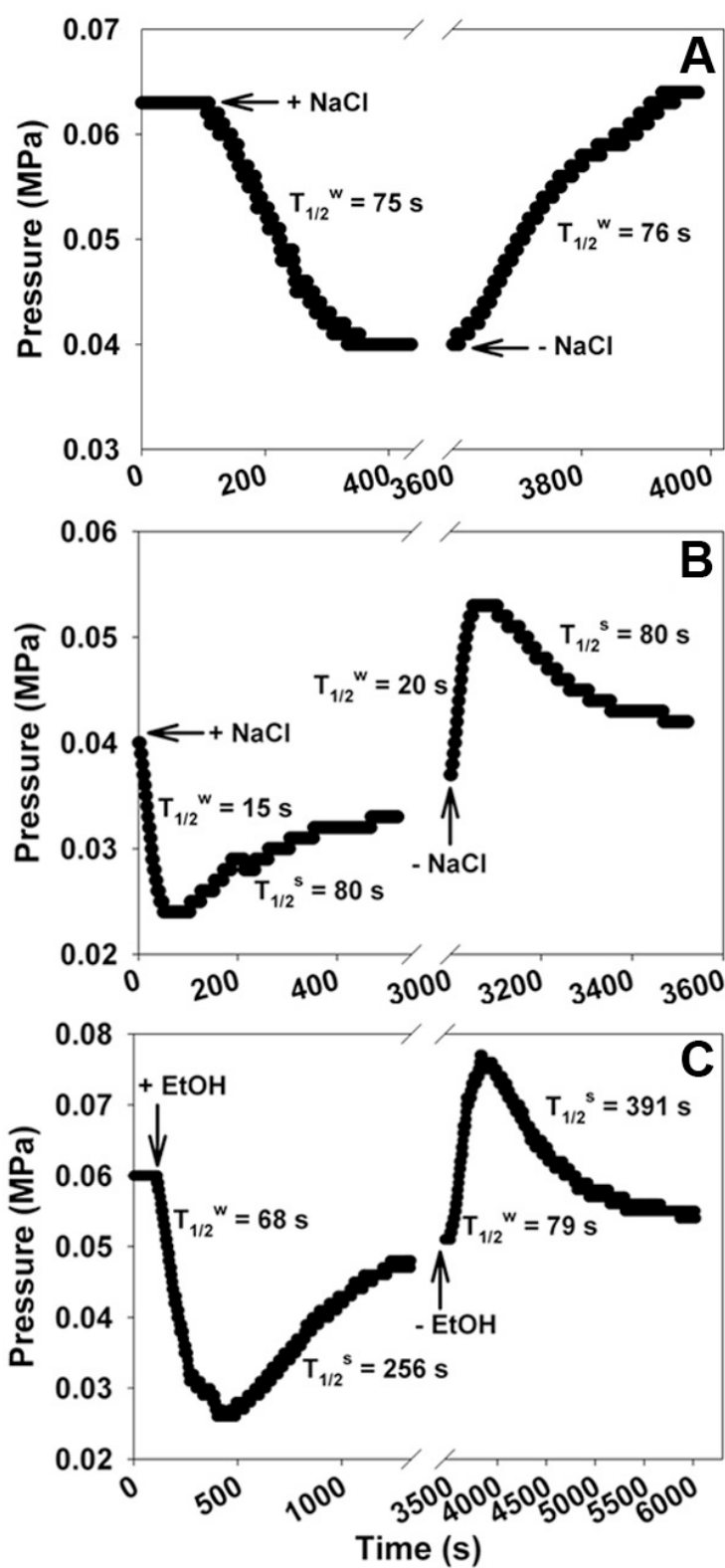
3.5.1 Root anatomy and cell viability

Adventitious roots of *Iris germanica* were chosen for testing radial water and solute permeabilities because the multiseriate exodermis, with its continuous circumferential Casparian band and suberin lamellae, would form a complete structure restrictive to both apoplastic and transcellular flows (see Introduction; Fig. 3.1). As more exodermal cell layers became encrusted with Casparian bands and suberin lamellae, the apoplastic and transcellular paths would become more restricted. However, the symplastic path would still have been

open if plasmodesmata linked the epidermal, exodermal and central cortical cells. There were two indicators that these plasmodesmata did, in fact, remain intact. First, half of the epidermal cells remained alive, even after the 14 day air gap exposure. This means that the plasmodesmata were connected to living exodermal cells. Interestingly, even under drought stress, ions could still be transported across the plasma membrane of a living epidermal cell, entering the symplast to traverse the exodermis, and continue flowing through the plasmodesmata of other living cortical cells (see section 6.6, Chapter 6 for further details). Second, exodermal cells also remained alive as they could eventually develop to State III, in which they had deposited lignified tertiary cellulosic walls (Meyer et al. 2009; see Fig. 2.3, Chapter 2). Thus, in *I. germanica* roots the symplast would be available as a path for radial transport across the multiseriate exodermis (Fig. 3.1).

Hydroponically grown roots of *I. germanica* had anatomies similar to those previously described in detail by Meyer et al. (2009) (see Chapter 2). Roots completely submerged in hydroponic solution had delayed exodermal maturation so that 94% of the tested root length lacked mature exodermal layers while the remaining 6% had one mature exodermal layer. Root regions exposed to a humid air gap had two uniformly matured exodermal layers. According to the anatomical data of Meyer et al. (2009) (see Chapter 2) and those of the present paper, endodermal maturation was not visibly affected by these growth conditions. (Specifically, tertiary wall deposition in the endodermis was not affected by the differing growth conditions. The endodermal Casparian bands and suberin lamellae had already been deposited prior to the air gap exposure.) The observed changes in the overall permeability of

Figure 3.6 Osmotic water and solute permeability graphs from air gap-exposed root segments with two mature exodermal layers. (A) 2EX root segment. Typical osmotic reaction when NaCl was added (+NaCl) and then removed (-NaCl) from the external solution. Since NaCl permeability was immeasurable, there was only a water phase in both the endosmotic and exosmotic tests. (B) 2EX-P root segment. After puncturing the biseriate exodermis, water (1st phase) and NaCl (2nd phase) permeated rapidly for both endosmotic and exosmotic tests. (C) 2EX root segment. Typical osmotic reaction when ethanol was added (+EtOH) and then removed (-EtOH) from the external solution. EtOH permeation is depicted in the 2nd phase of both the endosmotic and exosmotic tests, creating a biphasic reaction. $T_{1/2}^w$ = half-time of the water phase; $T_{1/2}^s$ = half-time of the solute phase.



roots grown in the two hydroponic culture conditions allowed separation of exodermal from endodermal permeabilities. In experiments where the exodermis was punctured (without affecting the endodermis) the propensity of this structure to reduce both water and solute permeability were demonstrated.

3.5.2 Measurements of radial water permeability

The radial water permeability of *I. germanica* roots was measured using three different approaches. 1) With a pressure probe to measure osmotic hydraulic conductivity, 2) with a pressure probe to measure hydraulic conductivity, and 3) with a pressure chamber to measure hydraulic conductivity. Water permeability values varied amongst each of these approaches (see below).

3.5.2.1 Osmotic hydraulic conductivity

Osmotic hydraulic conductivity ($L_{p_{ro}}$) of 2EX roots, as measured with the pressure probe (NaCl: $0.21 \times 10^{-8} \text{ m s}^{-1} \text{ MPa}^{-1}$; EtOH: $0.12 \times 10^{-8} \text{ m s}^{-1} \text{ MPa}^{-1}$), was 19 or 33-fold lower than the hydraulic conductivity as measured with the pressure chamber ($3.9 \times 10^{-8} \text{ m s}^{-1} \text{ MPa}^{-1}$) (see Tables 3.1 and 3.5). This was expected since osmotic permeabilities for water have typically been reported as being lower than hydraulic values due to the nature of the forces driving flows (Steudle and Frensch 1989; Cruz et al. 1992; Steudle et al. 1993; Rüdinger et al. 1994; Steudle and Meshcheryakov 1996; Steudle and Peterson 1998; see section 1.3.5, Chapter 1). Osmotic water flow has to occur from cell layer to cell layer across all root tissue layers, including the exodermis, in order for a net equilibrium in water potential to be attained. When *I. germanica* roots were bathed in ethanol or NaCl, water traversed both 0EX and 2EX roots slowly. Water flow may have occurred primarily through the symplastic

pathway, bypassing the continuous circumferential Casparian band and suberin lamellae (see Fig. 3.1). When the exodermis was punctured, its selective properties were diminished and, as expected, $L_{p_{ro}}$ increased dramatically. In transpiring plants, a hydrostatic gradient across the apoplast is the dominant driving force for radial water flow, but water can still flow through the parallel symplast and through aquaporins along the transcellular path (Maurel 1997; Steudle and Peterson 1998; Tyerman et al. 1999; Steudle 2001; Javot and Maurel 2002; Tyerman et al. 2002). When transpiration rates are reduced or even stopped, osmotic gradients across the symplastic and transcellular pathways become more important for radial water flow (Steudle and Peterson 1998). However, when EtOH or NaCl were applied externally to *I. germanica* roots, a hyperosmotic shock from the sharp increase in external solute concentration may have caused some of the aquaporins to close (Ye et al. 2004; Boursiac et al. 2005). Such an aquaporin closure may have contributed to the lower osmotic water conductivity measurements compared with the hydraulic conductivity measurements.

3.5.2.2 Hydraulic conductivity

Pressure probe. Pressure probe experiments yielded hydraulic conductivity values (L_{p_r} : $23.3\text{-}39.1 \times 10^{-8}$ or $127\text{-}242 \times 10^{-8} \text{ m s}^{-1} \text{ MPa}^{-1}$) that were markedly greater than data obtained with the pressure chamber ($3.9\text{-}8.5 \times 10^{-8} \text{ m s}^{-1} \text{ MPa}^{-1}$) (see Table 3.1). Measurements of L_{p_r} depended on transient flows of relatively small volumes of water. When water was injected into the root xylem as a pulse in pressure probe experiments, it should not pass through the entire root, but should be stored in *I. germanica*'s large central cortex with 12-18 cell layers. The storage capacity should also be increased by the existence of air-filled intercellular

spaces in the central cortex. Hence, in cases like the roots of *I. germanica*, it is concluded that the pressure probe largely measured the endodermal L_p .

Pressure chamber. The hydraulic conductivity of *I. germanica* roots was also measured with a pressure chamber ($L_{p_{pc}}$) whereby large volumes of water were induced to flow through the roots. Under these conditions, water storage areas in the stele and cortex should have been filled and a steady state accomplished. Problems with unstirred layers may have been relatively small because water flow was directed from outside the root to the xylem, tending to dilute the xylem sap (Zimmermann and Steudle 1998; Knipfer et al. 2007). Hence, the pressure chamber technique measured the $L_{p_{pc}}$ across both the endodermis and exodermis.

Which device is best for measuring the hydraulic conductivity of I. germanica roots?

There are several indications from the results that the pressure chamber measured flow across the whole root (including the exodermis), while the pressure probe measured flow across primarily the endodermis. The volume flow of water is large and steady with the pressure chamber, but low and transient with the pressure probe. Also, puncturing *I. germanica*'s exodermis caused a 4.1-fold loss of hydraulic resistance as measured with the pressure chamber, whereas it caused only a 1.4-fold loss as measured with the pressure probe (see Table 3.3). Furthermore, pressure chamber L_p values for punctured 2EX segments (18.6 or $92.8 \times 10^{-8} \text{ m s}^{-1} \text{ MPa}^{-1}$) were statistically equivalent to pressure probe L_p values for intact 2EX root segments (23.3 or $127 \times 10^{-8} \text{ m s}^{-1} \text{ MPa}^{-1}$) (see Table 3.1). Clearly, use of the pressure chamber is necessary when one wishes to measure total root hydraulic conductivity in thick roots such as those of *I. germanica*. (The pressure probe is suited for measuring

hydraulic water flow across thinner roots.) It should be stated that a high-pressure flowmeter (HPFM) could not be used as an alternative to the pressure chamber since the HPFM measures transient changes rather than steady flow (see Discussion in Joshi et al. 2009). Also, the use of the HPFM should be affected by internal unstirred layers which are negligible when using the pressure chamber or even the pressure probe (Knipfer et al. 2007).

3.5.2.3 Key hydraulic conductivity values from pressure chamber experiments

According to the hydraulic conductivity values as measured with the pressure chamber ($L_{p_{pc}}$), the maturation of two exodermal layers significantly reduced the permeability of roots to water. Deposition of a continuous circumferential Casparian band and suberin lamellae resulted in a 3.1-fold average increase of the overall hydraulic resistance, corresponding to a reduction in $L_{p_{pc}}$ from 8.5×10^{-8} to $3.9 \times 10^{-8} \text{ m s}^{-1} \text{ MPa}^{-1}$ (see Tables 3.1 and 3.3). Although the multiseriate exodermis reduced radial water flow, it was not completely blocked. Some water would have moved through the symplast and possibly also through the continuous circumferential Casparian band or suberin lamellae if pores existed in these structures (Ranathunge et al. 2005a,b; Waduwara et al. 2008). Puncturing the biseriate exodermis, but not the endodermis, separated the direct contribution for both the exodermis and endodermis to hydraulic resistance. According to the results of these experiments, the exodermis accounted for an average of 75% of the root's resistance to water flow ($L_{p_{pc}}$ increased from 3.9×10^{-8} to $18.6 \times 10^{-8} \text{ m s}^{-1} \text{ MPa}^{-1}$) (see Tables 3.1 and 3.3). In other words, the hydraulic resistance of the remaining undamaged tissues contributed 25% to the overall resistance. Assuming that the majority of this 25% refers to the endodermis, with an average diameter of 0.5 mm (whereas the diameter of the exodermis was on average 2.5 mm), then the exodermal

hydraulic resistance was about 23-fold greater than that of the endodermis (see Table 3.4). These results highlight the importance of *I. germanica*'s exodermis as a very hydraulically resistant structure.

To the best of the author's knowledge, there are, in the literature, only two quantitative comparisons of the overall vs. exodermal hydraulic resistances. 1) In young *Zea mays* roots, a comparison of the hydraulics of roots grown either in hydroponics or mist culture (similar to the conditions in the present study) led Zimmermann and Steudle (1998) to conclude that the development of the exodermis reduced hydraulic conductivity from 26×10^{-8} to 7.3×10^{-8} $\text{m s}^{-1} \text{MPa}^{-1}$. This decrease is equivalent to a 3.6-fold increase of the overall hydraulic resistance, which is within the range of the change in resistance measured for *I. germanica* (from 0EX to 2EX = 3.1-fold increase in resistance, see Table 3.3). In contrast, for *Oryza sativa* roots, Ranathunge et al. (2003) concluded that the endodermis was the major resistance to water flow; although the hydraulic conductivity for the whole root was low ($4 \times 10^{-8} \text{ m s}^{-1} \text{MPa}^{-1}$), the conductivity across only the outer part of root containing a uniseriate exodermis was 30-fold greater (or $120 \times 10^{-8} \text{ m s}^{-1} \text{MPa}^{-1}$). It was shown previously by Armstrong and Armstrong (2005) that *O. sativa* roots have "windows" in the exodermis, which are regions that lack suberin lamellae and where lateral roots emerge: these "windows" would be less resistant to water flow compared with suberized regions. Also, lateral root production in *O. sativa* is prolific and quite damaging to the exodermis. Lastly, since *O. sativa* roots were hydroponically grown, it is probable that there was reduced production of key suberin lamellae aliphatic monomers (particularly ω -OH fatty acids) in the

exodermis compared with growth in soil or in humid air (Krishnamurthy et al. 2009; see Chapter 4).

Like *I. germanica*, *Carex arenaria* has a 3-4 layered multiseriate exodermis and Robards et al. (1979) measured its water permeability. The permeability of *C. arenaria*'s isolated exodermis to water ($7\text{--}15 \times 10^{-11} \text{ m s}^{-1} \text{ MPa}^{-1}$) was lower by three orders of magnitude than that of *I. germanica*. Hence, while *C. arenaria*'s water conductivity values differ from that of *I. germanica* and *Z. mays*, the exodermis appears to function similarly with regard to the increase in hydraulic resistance. In view of these results, the present findings demonstrate a dominating effect of *I. germanica*'s multiseriate exodermis on hydraulic resistance, which is related to the deposition of a continuous circumferential Casparian band and suberin lamellae in all exodermal cells. In addition, this high hydraulic resistance may also be the result of an up-regulation in the production of suberin-associated fatty acids and waxes in the exodermal layers (see Chapter 4 for details).

3.5.3 Solute permeability

Solute permeability (P_{sr}) of *I. germanica* roots was measured concurrently with measurements of osmotic hydraulic conductivity (see Fig. 3.6). The permeability of ethanol (a small, uncharged, lipophilic solute) was reduced by nearly an order of magnitude with maturation of the biseriate exodermis, compared with 0EX (see Table 3.5). Assuming that the symplastic pathway did not change with maturation of the exodermis, this reduction in permeability reflects the importance of the apoplastic and transcellular pathways for permeation of this solute. After some of the exodermal cells were punctured, ethanol

permeation increased 28-fold, indicating that the exodermis provided a major resistance to ethanol entry into the root.

Reflection coefficients (σ_{sr}) refer to the selectivity of a membrane or tissue to a solute, and are used to express, in a quantitative way, the ability of membranes or cell wall-modifying structures to resist the flow of solutes. Values of σ_{sr} range from 0-1, where 0 means that there is no resistance or no selectivity to solute flow and 1 means there is a total blockage of solute flow. In the present study, the ethanol σ_{sr} was quite high for *I. germanica*'s intact multiseriate exodermis ($\sigma_{sr} = 0.69$; see Table 3.5). In contrast, Miyamoto et al. (2001) and Ranathunge et al. (2003) measured substantially lower ethanol σ_{sr} across the outer part of *O. sativa* roots, a region that included the uniseriate exodermis ($\sigma_{sr} = 0.04$ to 0.13). This is in line with the greater hydraulic resistance of *I. germanica*'s exodermis compared with that of *O. sativa*.

When *I. germanica* roots were exposed to NaCl, a small amount penetrated the 0EX roots but was effectively excluded from the 2EX region (see Table 3.5). These results explain the earlier findings of Wang (2002) for *Iris hexagona*, a species with a uniseriate exodermis (Meyer et al. 2009; see Fig. 2.8, Chapter 2). In this species, salt accumulated primarily in the roots but some was also transported to the leaves. Presumably in young root zones where the exodermis is immature, the majority of NaCl flow was blocked by the Casparian band in the endodermis. In older zones, however, based on the current puncturing experiments with the 2EX region, it is predicted that apoplastic NaCl flow was prevented by the Casparian band in the exodermis (see Fig. 3.1).

The NaCl σ_{sr} in *I. germanica* was high regardless of the exodermal maturation stage (0EX = 0.92; 2EX = 1.0; see Table 3.5). Based on these results, it is unlikely that Na^+ is being

transported across the epidermal plasma membranes; hence, the ions are isolated to the apoplast and come into direct contact with the Casparian bands (see section 6.7, Chapter 6 for further details). The current NaCl σ_{sr} values are much greater than those of other species. For example, in young *Z. mays* roots with an immature exodermis, NaCl σ_{sr} was 0.64 and puncturing the endodermis reduced it to 0.41 (Steudle et al. 1993). Using *O. sativa* roots it was possible to measure the NaCl σ_{sr} of the uniseriate exodermis ($\sigma_{sr} = 0.10$) as well as the entire root ($\sigma_{sr} = 0.20-0.30$) (Ranathunge et al. 2003). Interestingly, *Arabidopsis thaliana*, which has non-exodermal roots, had a NaCl σ_s of 0.77 (Boursiac et al. 2005). Apparently in certain species, the endodermis itself can be quite effective at restricting NaCl flow. On top of this, the presence of exodermal Casparian bands may function as additional apoplastic solute filters that could be of interest when determining a species' tolerance to salt.

3.5.4 Adaptive significance of the multiseriate exodermis in *I. germanica*

The multiseriate exodermis in *I. germanica*'s thick roots may be a special adaptation to drought conditions, and would tend to reduce water loss from the root to a relatively dry soil. This is achieved by having the highest resistance to radial water flow in the outer part of the root rather than at the endodermis, thus preserving the central cortex. According to Meyer et al. (2009) (see Chapter 2) the majority of species with a multiseriate exodermis (including *I. germanica*) inhabit well-drained soils suggesting that this type of exodermis may play a role in tolerating periodic drought stress. Under favourable growth conditions with abundant water, there will be exodermal developmental zones along the root length beginning with the outermost layer near the root tip and developing centripetally until four layers are mature (Meyer et al. 2009; see Chapter 2). Therefore, one would expect less resistance to radial

water flow closer to the root tip. In the event of a drought, root growth would slow but maturation of the multiseriate exodermis would continue (Perumalla and Peterson 1986), consequently increasing the number of exodermal layers and the resistance to water loss in younger root regions. This anatomical change could prevent excessive water loss from the root to the dry soil. As extreme examples, *C. arenaria* and *A. deserti*, two species that inhabit dry, sandy substrates and have roots with a multiseriate exodermis, are not very permeable to water (Robards et al. 1979; North and Nobel 1991, 1995). Hence, the capacity to produce a multiseriate exodermis is likely to be one of many important evolutionary specializations that allow some species to tolerate drought-prone habitats.

3.6 Conclusions

Hydraulic conductivity measured with the pressure chamber revealed a significant resistance of *I. germanica*'s intact multiseriate exodermis to radial water flow which was, in fact, dominating when two layers of the exodermis were fully developed. Due to the large water storage capacity of the central cortex, the measurement of transients by the root pressure probe resulted in estimates of the endodermal rather than the overall radial hydraulic conductivity. In agreement with the composite transport model of the root, the osmotic permeability of water was much smaller than the hydrostatic. Osmotic water permeability was greatly reduced in the presence of a multiseriate exodermis, as were the permeabilities of the two test solutes ethanol and NaCl. When the multiseriate exodermis was punctured, its limiting influence on radial water and solute transport was lost. The multiseriate exodermis

should be considered as one possible trait within a suite of specializations that evolved to enable plants to tolerate drought-prone habitats.

Chapter 4

Suberin monomer analysis of *Iris germanica*'s multiseriate exodermis during maturation and under differing growth conditions

4.1 Overview

More than 90% of tested angiosperm species have roots with an exodermis and approximately 18% of these, including *Iris germanica*, develop a multilayered exodermis (MEX). All of this species' mature MEX cells contain suberin lamellae with a poly(aliphatic) domain (SPAD) located between the wall and plasma membrane. The location and lipophilic nature of the SPAD establishes it as a biochemical structure restrictive to radial water and solute transport through the transcellular pathway. The objective of the current work was to analyze SPAD biosynthesis, by identifying and quantifying suberin-associated monomers, at particular stages of MEX maturation and under differing growth conditions. Roots were grown in hydroponic culture wherein MEX maturation was delayed in submerged root regions but accelerated in regions exposed to a humid air gap. Monomers of the soluble, unpolymerized fraction of suberin were soxhlet-extracted from maturing exodermal tissue with chloroform/methanol. Then the SPAD, still within the extractive-free exodermal tissue, was hydrolyzed and transesterified of ester-linked fatty acids using methanolic HCl. Monomers were quantified and identified by GC-MS. Resolving the monomer profiles at specific maturation stages revealed spatial and temporal patterns of SPAD synthesis. Interestingly, in air gap-exposed root regions, there was an up-regulation in the synthesis and

deposition of SPAD monomers in the first two exodermal layers, compared with submerged regions. The SPAD fraction included fatty acids, α,ω -dioic acids, ω -OH fatty acids, and ferulic acid, with C18:1 α,ω -dioic acid and ω -OH fatty acid being the two most abundant monomers. Also in air gap tissue, the composition of the soluble fraction changed significantly between exodermal maturation stages and between growth conditions, exemplified by an increased alkane accumulation in the first exodermal layer of air gap-exposed tissue. The soluble suberin fraction included alkanes, fatty acids, fatty alcohols, and ferulic acid. It is postulated that the localized and abundant deposition of C18:1 α,ω -dioic acid and ω -OH fatty acid, along with high accumulation of intercalated alkanes in the first mature exodermal layer, are more important than the overall number of suberized exodermal layers for reducing water loss from the root during drought.

4.2 Introduction

Suberin is a complex biopolymer that is deposited constitutively in a subset of specialized plant tissues. The presence and chemical composition of suberin in specific cell types has been well documented. Suberin-containing cells include the phellem of periderm (such as in *Solanum tuberosum* tuber, *Quercus suber* stem, and secondary growth of eudicot roots), bundle sheath cells (such as in grass leaves), cells in the hilum/chalazal region of seed coats, and exodermal and endodermal cells (in roots of angiosperms) (Esau 1965). In much of the past work, the chemical composition of suberin was analyzed by isolating monomers from a complete polymer located in cells of mature tissues. In the cells of the exodermis tissue (as well as the endodermis) there are two key wall-modifying structures that contain suberin;

these structures are the Casparian bands and suberin lamellae. In general, Casparian bands are composed primarily of lignin-like monomers with some aliphatic suberin (Schreiber et al. 1994; Schreiber 1996; Zeier and Schreiber 1997, 1998). Their location within intermicrofibrillar spaces of the cell wall allow them to restrict apoplastic flow of solutes (de Rufz de Lavison 1910; Baker 1971; Peterson 1987; Enstone et al. 2003). On the other hand, suberin lamellae are composed of two domains; the poly(aliphatic) (SPAD) and poly(phenolic) (SPPD) domains (after Bernards 2002; Mattinen et al. 2009; see Fig. 1.10, Chapter 1). The SPAD is rich in ω -hydroxy fatty acids, α,ω -dicarboxylic acids and intercalated waxes, but the relative amounts of these compounds can vary between species (Kolattukudy and Dean 1974; Kolattukudy 1980, 1984; Holloway 1983; Matzke and Riederer 1991; Bernards and Lewis 1998, and references therein; Zeier and Schreiber 1998, 1999; Zeier et al. 1999a, b; Graça and Pereira 2000a, b). The lipophilic nature of the SPAD, along with its location between the wall and plasma membrane, establishes it as a structure restrictive to radial water and solute transport through the transcellular pathway (Kolattukudy and Dean 1974; Soliday et al. 1979; Vogt et al. 1983; Evert et al. 1985; Zimmermann et al. 2000; Hose et al. 2001; Schreiber et al. 2005a; see Chapter 3). Such fundamental information has provided a basis for continued research into understanding suberin biosynthesis. In particular, the dynamic metabolic processes involved in suberin synthesis are starting to be revealed.

Analyzing suberin metabolite data at several key stages of tissue development is required to fully profile suberin biosynthesis. For example, like Kolattukudy and Dean (1974) and Dean and Kolattukudy (1977), Yang and Bernards (2006) used developing *S. tuberosum*

tuber periderm to identify and quantify polymerized (insoluble) and unpolymerized (soluble) SPAD monomers. In the insoluble fraction, ω -hydroxy fatty acids, α,ω -dioic acids, and primary fatty acids ($>C_{20}$) were detected three days after the start of wound-induced periderm development. Monomer abundances continued to increase for an additional three days. In the soluble fraction, ω -hydroxy fatty acids and α,ω -dioic acids were detected in only trace amounts, whereas $>C_{20}$ fatty acids were detected in considerable amounts. In another example, Höfer et al. (2008) measured the amount and composition of the insoluble SPAD at three developmental stages along the length of *Arabidopsis thaliana* roots. In the first zone closest to the root tip, endodermal suberin (primary growth) was measured. However, in the two more basal locations, peridermal suberin (secondary growth) was also measured. Monomer abundance – moving away from the root tip – increased for C18:1 ω -hydroxy fatty acids, was steady for C18:1 α,ω -dioic acids, and decreased for primary fatty acids. Lastly, Zeier et al. (1999a), Thomas et al. (2007), and Krishnamurthy et al. (2009) each measured progressively increasing amounts of insoluble SPAD monomers along the length of *Zea mays*, *Glycine max*, and *Oryza sativa* roots, respectively; in all cases, the most abundant monomers were ω -hydroxy fatty acids. It is clear from the above results that achieving a complete understanding of suberin biosynthesis necessitates analyses of both polymerized and unpolymerized monomers from tissue that is in the process of developing and/or maturing. Data collected in this way can provide clues as to when the various suberin monomers are synthesized, and how rapidly these monomers are polymerized into the suberin complex.

More than 90% of examined angiosperm species have roots with an exodermis (Perumalla et al. 1990; Peterson and Perumalla 1990). Of these species, approximately 18% develop a multilayered exodermis (MEX), including roots of *Iris germanica* (Meyer et al. 2009; see Chapter 2). Although a considerable number of species have MEX roots, research into MEX development, function and biochemistry is limited. (For work on *Typha* spp. see Seago and Marsh [1989] and Seago et al. [1999]; for work on *Phragmites australis* see Armstrong et al. [2000] and Soukup et al. [2002, 2007].) But, such comprehensive research has been conducted recently on roots of *I. germanica* (Meyer et al. 2009; see Chapters 2 and 3). When *I. germanica* roots are grown in well-drained soil, MEX maturation (i.e., the concurrent deposition of Casparian bands and suberin lamellae) begins at 10 mm from the root tip. When roots are grown submerged in hydroponic culture, MEX maturation is delayed, beginning at 60 mm from the root tip. Conversely, if basal parts of roots are exposed to a humid air gap inside a hydroponic chamber, then MEX maturation in these parts is accelerated. Every cell of the mature MEX is encrusted with a suberin lamella – there are no passage cells. This thick and suberized MEX is able to retain water and prevent NaCl from entering the root. Previously, Zeier and Schreiber (1998) calculated the total yield of aliphatic suberin in *I. germanica*'s MEX (approximately 40 $\mu\text{g mg}^{-1}$). Based on the facts that the roots were soil-grown and the endodermis had matured to State III (meaning most cells contained Casparian bands, suberin lamellae and tertiary wall thickenings, as described by Van Fleet [1961], Esau [1965] and Robards et al. [1973]), it is currently assumed that roots were sampled at least 100 mm from the root tip, and contained at least three but perhaps four mature exodermal layers (Meyer et al. 2009; see Chapter 2). Hence, the measured amount of

exodermal aliphatic suberin represents a snapshot in developmental time. One question that arises from this previous work is: how does SPAD composition and quantity change during MEX maturation? For the current work, a developmental time-course analysis was conducted to test whether or not insoluble and soluble SPAD monomer compositions and quantities changed during MEX maturation and under differing growth conditions.

The objectives of the current research were to identify and quantify the monomers that comprised the insoluble and soluble fractions of the SPAD in *I. germanica*'s maturing MEX. In addition, SPAD composition was compared between roots either grown submerged or exposed to a humid air gap in hydroponic culture. It was hypothesized that root areas exposed to the humid air gap would have an increased abundance of key SPAD monomers compared with submerged root areas. The rationale for this hypothesis was based on the known acceleration of exodermal maturation in root tissue exposed to lower humidity (Meyer et al. 2009; see Chapter 2). *Iris germanica* roots were amenable to such tests because the sequence of MEX maturation was well-known from previous work (Meyer et al. 2009; see Chapter 2), and the roots generated very few or no lateral roots (unlike the prolific lateral root formation by *Typha* and *Phragmites*). The findings will lead to a more complete understanding of SPAD biosynthesis during MEX maturation.

4.3 Materials and methods

4.3.1 Growth conditions and plant material

Iris germanica plants were grown in hydroponic conditions as described previously (see Meyer et al. 2009; see Chapter 2). When several adventitious roots longer than 60 mm had developed, the volume of solution inside some of the hydroponic chambers was reduced, hence lowering the solution surface and creating a 60 mm humid air gap between the rhizome base and solution surface. This air gap condition is known to accelerate the maturation of *I. germanica*'s multiseriate exodermis (Meyer et al. 2009; see Chapter 2). Maturation refers to the concurrent deposition of exodermal Casparian bands and suberin lamellae.

Roots that were totally submerged (control) or exposed to the air gap for 7-21 d were cut individually from the base of the rhizome. To determine the number of exodermal layers that had matured in the segment of root exposed to the air gap and in the equivalent segment in submerged roots (30-50 mm in length), freehand cross sections were made at the proximal and distal ends of each segment. Sections were then stained with berberine hemisulphate–aniline blue for Casparian bands (Brundrett et al. 1988), and Sudan Red 7B or Fluorol yellow 088 for lipids including aliphatic suberin (Brundrett et al. 1991). Sections were observed using a Zeiss Axiophot epifluorescence microscope with either white or UV light (filter set: exciter filter G 365, dichroitic mirror FT 395, and barrier filter LP 420; Carl Zeiss Inc., Canada). Photomicrographs were taken with a Q-Imaging digital camera (Retiga 2000R, Fast 1394, Cooled Mono, 12-bit; Quorum Technologies Inc., Canada).

Roots were grown in the submerged or air gap growth conditions long enough to produce 1, 2, or 3 fully mature exodermal layers. Then the roots were cut individually from the base of the rhizome. For each submerged or air gap-exposed segment, the distance from the root tip was recorded and segment length and diameter were measured so the surface area could be calculated. Each segment was slit superficially with a razor blade along most of its length at 2 or 3 evenly spaced locations. Then 2 or 3 sheets containing the exodermal layers, with adhering epidermal and some central cortex cells, were physically peeled from the central cortex and all underlying layers using fine-tipped forceps. Peeled sheets were placed quickly into a 1.5 mL eppendorf tube and flash frozen with liquid nitrogen. Frozen tissue was stored at -20°C until needed for suberin monomer extraction. (Regions that remained unpeeled above and below the peeled root segment were freehand cross sectioned and stained (as above) to verify the number of mature exodermal layers.) The 2 or 3 pooled exodermal sheets from each root segment represented one replicate. Three to six replicates were collected for each exodermal maturation stage within each growth condition.

4.3.2 Exodermal suberin extraction and analysis

Soluble compound extraction. The soluble fraction was extracted from the isolated exodermis. (This fraction included primarily unpolymerized suberin monomers, waxes, and membrane components.) Frozen exodermal tissue was placed into a cellulose extraction thimble (Whatman Ltd., Maidstone, England) that was saturated with chloroform/methanol (2:1). Using a micro-soxhlet extractor, solubles were extracted from the tissue by treating it with chloroform/methanol (2:1) for 3.5 h. This extraction was repeated, and then followed by an overnight extraction with chloroform. Extracted exodermal tissue was washed with

acetone, air-dried at room temperature, and stored at 4°C to be used later for insoluble compound extraction. The soluble extracts were pooled and concentrated by evaporating off the solvent using a rotary evaporator (Buchi, Switzerland) under vacuum and at 50°C. The dried residue was re-dissolved in 2 M MeOH/HCl (Supelco/Sigma-Aldrich, USA) and heated at 80°C for 2 h to hydrolyze esters and methylate the free carboxylic acids. Next, vials were cooled and NaCl-saturated water added to stop the reaction. Triacontane (10 µL, 1 mg/mL) was added as the internal standard. To extract the compounds from the aqueous phase, hexane was added to each vial and the contents shaken vigorously. The upper hexane phase was pipetted off and placed into a clean vial. This hexane partitioning step was repeated two more times. Pooled hexane phases were dried down with N₂ gas. The dried residue was re-dissolved with 50 µL each of pyridine and 99% BSTFA + 1% TMS (Supelco/Sigma-Aldrich, USA), and was incubated at 70°C for 40 min to trimethylsilylate (TMS) the remaining free alcohols.

Insoluble compound extraction. Next, the insoluble aliphatic suberin fraction was depolymerized and extracted from the dried exodermal tissue. (This fraction included primarily polymerized suberin monomers; the depolymerization technique employed was effective in degrading the SPAD, with little effect on the SPPD.) The exodermal tissue was weighed (1-4 mg), and then submerged in 0.5 mL of 2 M MeOH/HCl and incubated at 80°C for 2 h to allow hydrolysis and transesterification of ester-linked fatty acids (adapted from Browse et al. 1986). The remainder of the extraction method was identical to that used for the soluble fraction, including the organic partitioning and TMS derivatization steps (see above).

Gas chromatography-mass spectrometry. Soluble and insoluble monomer fractions that contained methyl ester/TMS ether derivatives were analyzed with a Varian CP-3800 Gas Chromatograph equipped with a flame ionization detector (GC-FID) and a Saturn 2000 ion trap Mass Spectrometer (GC-MS). The pair of columns installed in the GC were CP-Sil 5 CB low bleed MS columns (WCOT silica 30 m x 0.25 mm ID), with one directed to the FID and the other to the MS. Temperature for the injector oven was set to 250°C, and the FID oven was set to 300°C. After the injection of a sample (1 μL) into each column in splitless mode, compounds were eluted using the following program: 70°C held for 2 min, ramped up to 200°C at 40°C min^{-1} and held for 2 min, ramped up to 300°C at 3°C min^{-1} and held for 9.42 min, for a total run time of 50 min. The carrier gas was high purity helium flowing at a rate of 1 mL min^{-1} .

Data analysis. Compound identification was accomplished using a combination of retention time, retention index, and comparison of the obtained mass spectra to spectra from authentic standards. Compound abundance was quantified from the GC-FID chromatograms using the internal standard and standard calibration curves.

Monomer quantities were calculated and reported in three ways. 1) Monomer amount per dry tissue weight ($\mu\text{mol mg}^{-1}$). This calculation revealed information about monomer abundance as more exodermal layers matured, and was termed ‘monomer production’. 2) Monomer amount per root segment surface area ($\mu\text{mol mm}^{-2}$). This second calculation provided information about the distribution of monomer deposition across multiple exodermal layers, and was termed ‘monomer deposition’. The surface area dimension was corrected by multiplying by the number of mature exodermal layers; compared to a uniseriate

exodermis, a biseriate exodermis had double the suberized surface area while a triseriate exodermis had triple the suberized surface area. For calculations 1) and 2), the accumulative monomer production and deposition was measured. For example, when two exodermal layers were mature (i.e., all cells of the two layers contained Casparian bands and suberin lamellae), monomer measurements included layers one and two. Nonetheless, it was assumed that at each maturation stage, most of the new monomer production and deposition occurred in the most recently matured layer. Histochemical tests verified that aliphatic suberin was present in all mature exodermal layers. (It was not possible to observe differences in suberin abundance from the histochemical tests.) Furthermore, it is known that all cells of an exodermal layer become fully mature prior to the visible start of the maturation of an underlying immature exodermal layer (Meyer et al. 2009; see Chapter 2). 3) A third calculation revealed information about the change in the deposition of monomers in each exodermal layer per root segment surface area ($\mu\text{mol mm}^{-2}$), resolving the accumulative parameter. This calculation was termed 'change in monomer deposition'. According to calculations 1) and 2), the measured monomer amounts are accumulative; this means the amount in 2EX is actually the sum total of 1EX + 2EX, and that the amount in 3EX is, in fact, the sum total of 1EX + 2EX + 3EX. Hence, to determine how many more or fewer monomers were deposited in each newly matured exodermal layer relative to the previous layer(s), the difference between the 2EX sum total and 1EX represented the change in monomer deposition between the first and second exodermal layers. Similarly, the difference between the 3EX sum total and the 2EX sum total constituted the change in monomer deposition between exodermal layers 1 + 2 and the third layer. These difference values could be positive or negative. For example, in most

cases the accumulative value of 2EX was greater than 1EX, so the difference was positive. On the other hand, if a particular monomer was deposited in the first layer but not the second layer and the root diameter continued to increase, the accumulative value of 2EX would be less than 1EX hence the difference would be negative.

Differences in monomer amounts between the number of mature exodermal layers and between growth conditions were analyzed. Data were first analyzed by an Analysis of Variance. Where significance was noted, a Least Significant Difference post-hoc test was used with a significance value of $P \leq 0.05$. Also calculated was the percent contribution of each monomer class to the total compound fraction within growth conditions and for each stage of exodermal maturity.

4.4 Results

4.4.1 *I. germanica* exodermal anatomy

Exodermal structure and maturation was as expected according to Meyer et al. (2009) (see Chapters 2 and 3). Briefly, in submerged roots, maturation (i.e., concurrent deposition of Casparian bands and suberin lamellae) of the first exodermal layer was complete 80 mm from the root tip (5-6 d old; Fig. 4.1A,B). The second exodermal layer was fully mature by 200 mm from the tip (14 d old; Fig. 4.1C,D). Then the third exodermal layer had matured by 300 mm (21 d old; Fig. 4.1E,F). For air gap-exposed roots, the first exodermal layer had already matured in the submerged area (80 mm from the tip). As expected, in the 50-mm-long root area exposed to the air gap, the second exodermal layer had matured uniformly

after only a 7 d exposure (120–170 mm from the tip, between 9 and 12 d old). Then the third exodermal layer matured following a 14 d air gap exposure (220–270 mm from the tip, between 16 and 19 d old). Both submerged and air gap-exposed roots grew at an average rate of 14.7 mm d⁻¹ (data not shown).

4.4.2 Suberin chemistry

4.4.2.1 Insoluble fraction

Total insoluble fraction. The total insoluble fraction is the sum of all the monomers that were released from the suberin polymer following depolymerization (transesterification) with MeOH/HCl. In both submerged and air gap-exposed tissue, insoluble monomer production increased steadily as more exodermal layers matured (Fig. 4.2A). This trend suggested a uniform monomer deposition in each exodermal layer. However, when monomer amounts were calculated on a unit surface area basis, the deposition appeared greater in the first two layers of air gap-exposed tissue compared with submerged tissue (Figs. 4.2B). Similar deposition trends were also observed for the changes in monomer deposition between exodermal maturation stages (Fig. 4.3). In submerged tissue, most monomers were deposited in the third layer, followed by the first layer and then the second layer. In air gap-exposed tissue, deposition was fairly consistent in each exodermal layer; but, deposition in the first two layers was greater than the deposition in counterpart layers of submerged tissue (Fig. 4.3). The composition of the insoluble fraction was α,ω -dioic acids (C18:1 - C28), ω -hydroxy fatty acids (C18:1, C24), fatty acids (C16 - C28), and ferulic acid (Table 4.1, Figs. 4.3-4.7).

α,ω -Dioic acids. The α,ω -dioic acids were the most abundant insoluble monomers, accounting for an average of 53% of the total insoluble fraction (Table 4.1). Not surprisingly,

Figure 4.1 Photomicrographs of the outer part of *Iris germanica* adventitious roots in transverse section. (A) One mature exodermal layer. Stained with berberine hemisulfate–aniline blue. Casparian bands (white arrows) located in the radial walls, fluoresced yellow. (B) One mature exodermal layer. Stained with Sudan red 7B. Suberin lamellae (black arrows) appeared as red outlines in the radial and tangential walls. (C) Two mature exodermal layers. Stained with berberine hemisulfate–aniline blue. A continuous circumferential Casparian band (white arrows) filled the radial and tangential walls. (D) Two mature exodermal layers. Stained with Sudan red 7B. Suberin lamellae (black arrows) were located in the walls of all exodermal cells of both layers. (E) Three mature exodermal layers. Stained with Fluorol yellow 088. Suberin lamellae fluoresced yellow, located in the walls of all exodermal cells. (F) Three mature exodermal layers. Stained with Sudan red 7B. Suberin lamellae were located in the walls of all exodermal cells. Abbreviations: epi = epidermis; ex = mature exodermis; iex = immature exodermis. Scale bars = 100 μm .

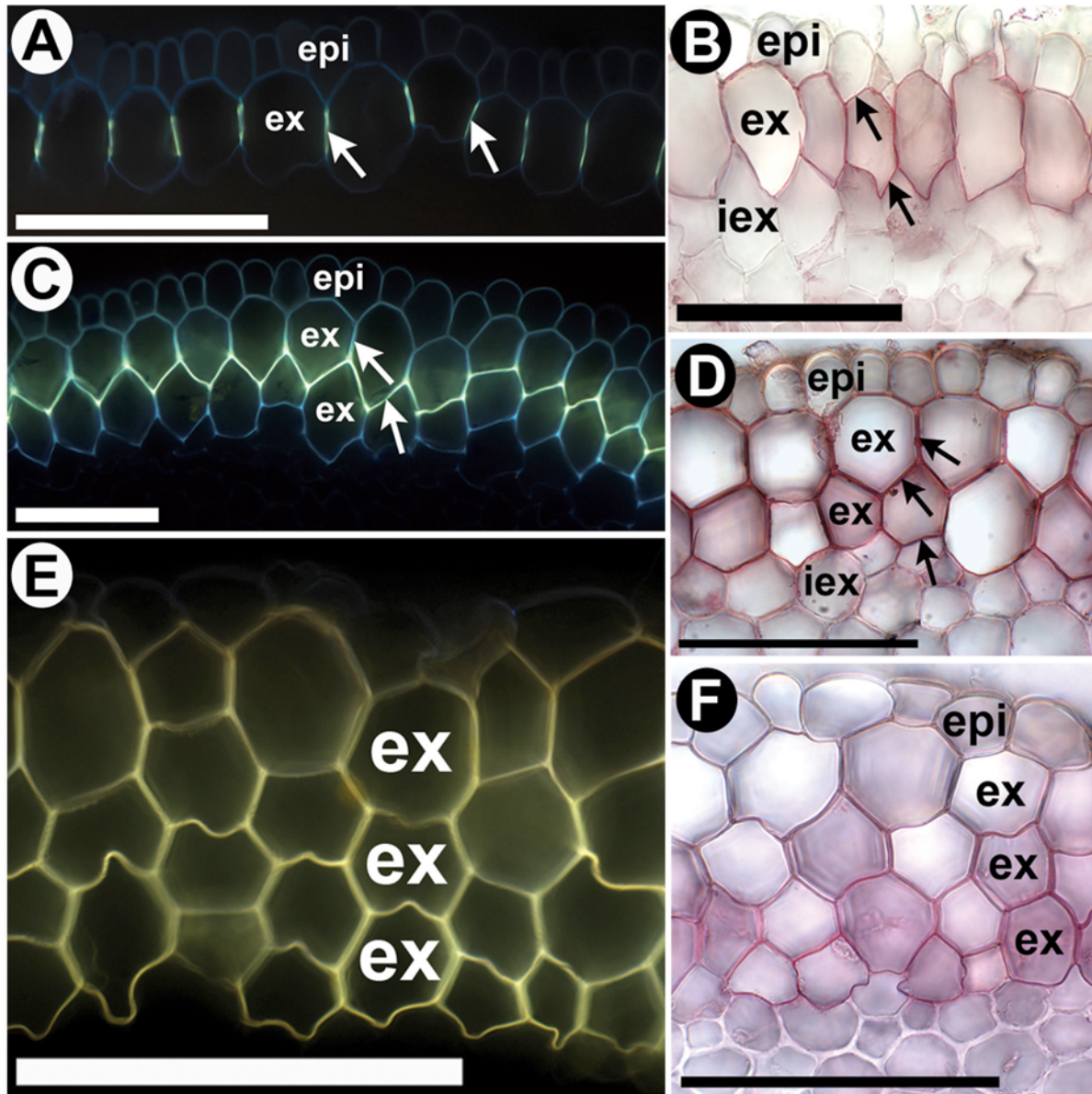


Figure 4.2 Total insoluble aliphatic suberin (SPAD) monomers in *Iris germanica*'s exodermis. Data are displayed per unit of tissue mass (A, in $\mu\text{mol mg}^{-1}$) and per unit of suberized surface area (B, in $\mu\text{mol mm}^{-2}$) for each mature exodermal layer under different growth conditions (legends inset). Values are means \pm standard deviation. Different lowercase letters within each graph indicate a significant difference ($P \leq 0.05$) across all values. Abbreviations: Sub1EX = submerged tissue with one mature exodermal layer; Sub2EX = submerged tissue with two mature exodermal layers; Sub3EX = submerged tissue with three mature exodermal layers; AG1EX = air gap-exposed tissue with one mature exodermal layer; AG2EX = air gap-exposed tissue with two mature exodermal layers; AG3EX = air gap-exposed tissue with three mature exodermal layers.

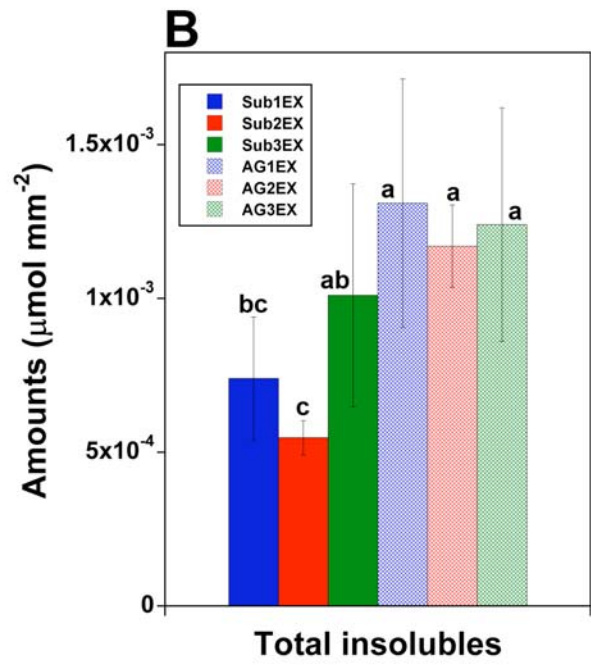
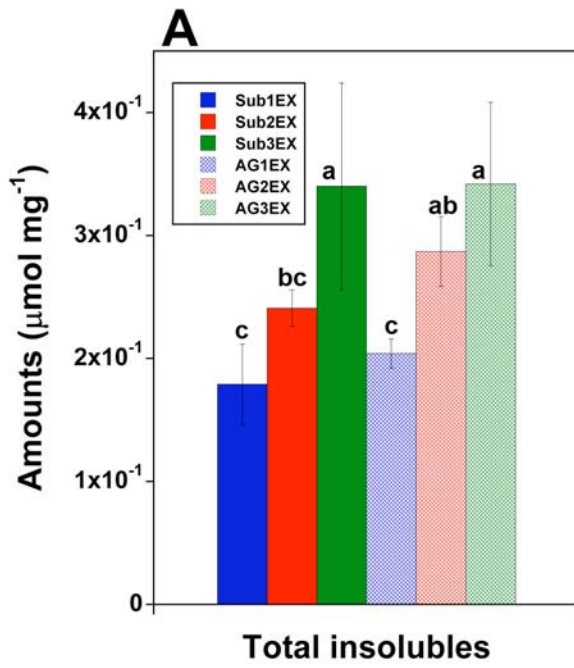


Figure 4.3 Change in amounts of SPAD monomer classes in the maturing MEX of *Iris germanica*. Data are displayed per root segment surface area ($\mu\text{mol mm}^{-2}$), and refer to the change in monomer amounts from one exodermal maturation stage to the next, under different growth conditions (legend inset). See materials and methods for data calculation details. Abbreviations: Sub 0EX-1EX = submerged tissue, monomer amounts in the first exodermal layer; Sub 1EX-2EX = submerged tissue, change in amounts between exodermal layers one and two; Sub 2EX-3EX = submerged tissue, change in amounts between exodermal layers two and three; AG 0EX-1EX = air gap-exposed tissue, monomer amounts in the first exodermal layer; AG 1EX-2EX = air gap-exposed tissue, change in amounts between exodermal layers one and two; AG 2EX-3EX = air gap-exposed, change in amounts between exodermal layers two and three.

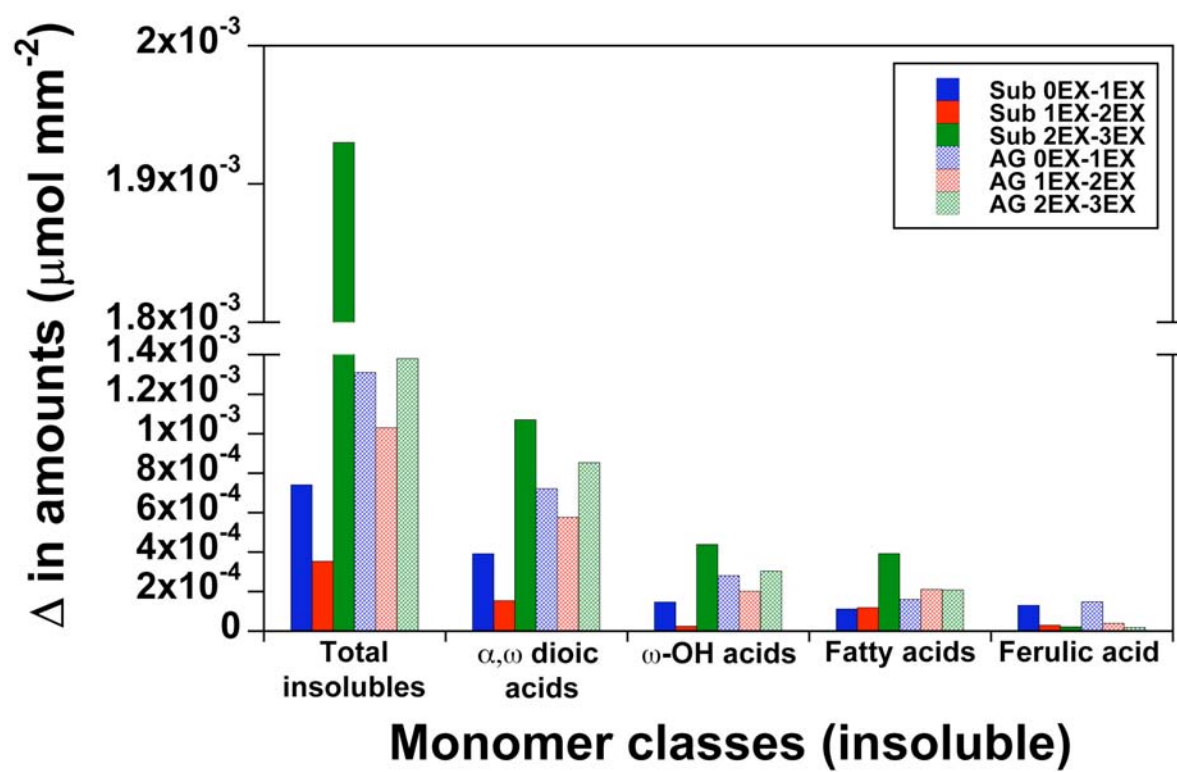


Figure 4.4 Deposition of α,ω -dioic acids in the aliphatic suberin (SPAD) of *Iris germanica*'s exodermis. Data are displayed per unit of tissue mass (A & C, in $\mu\text{mol mg}^{-1}$) and per unit of suberized surface area (B & D, in $\mu\text{mol mm}^{-2}$) for each mature exodermal layer under different growth conditions (legends inset). (A,B) Total α,ω -dioic acids. (C,D) Individual α,ω -dioic acid monomers. Values are means \pm standard deviation. Different lowercase letters within the total α,ω -dioic acids (A,B) or within each monomer chain length (C,D) indicate a significant difference ($P \leq 0.05$). Abbreviations: Sub1EX = submerged tissue with one mature exodermal layer; Sub2EX = submerged tissue with two mature exodermal layers; Sub3EX = submerged tissue with three mature exodermal layers; AG1EX = air gap-exposed tissue with one mature exodermal layer; AG2EX = air gap-exposed tissue with two mature exodermal layers; AG3EX = air gap-exposed tissue with three mature exodermal layers.

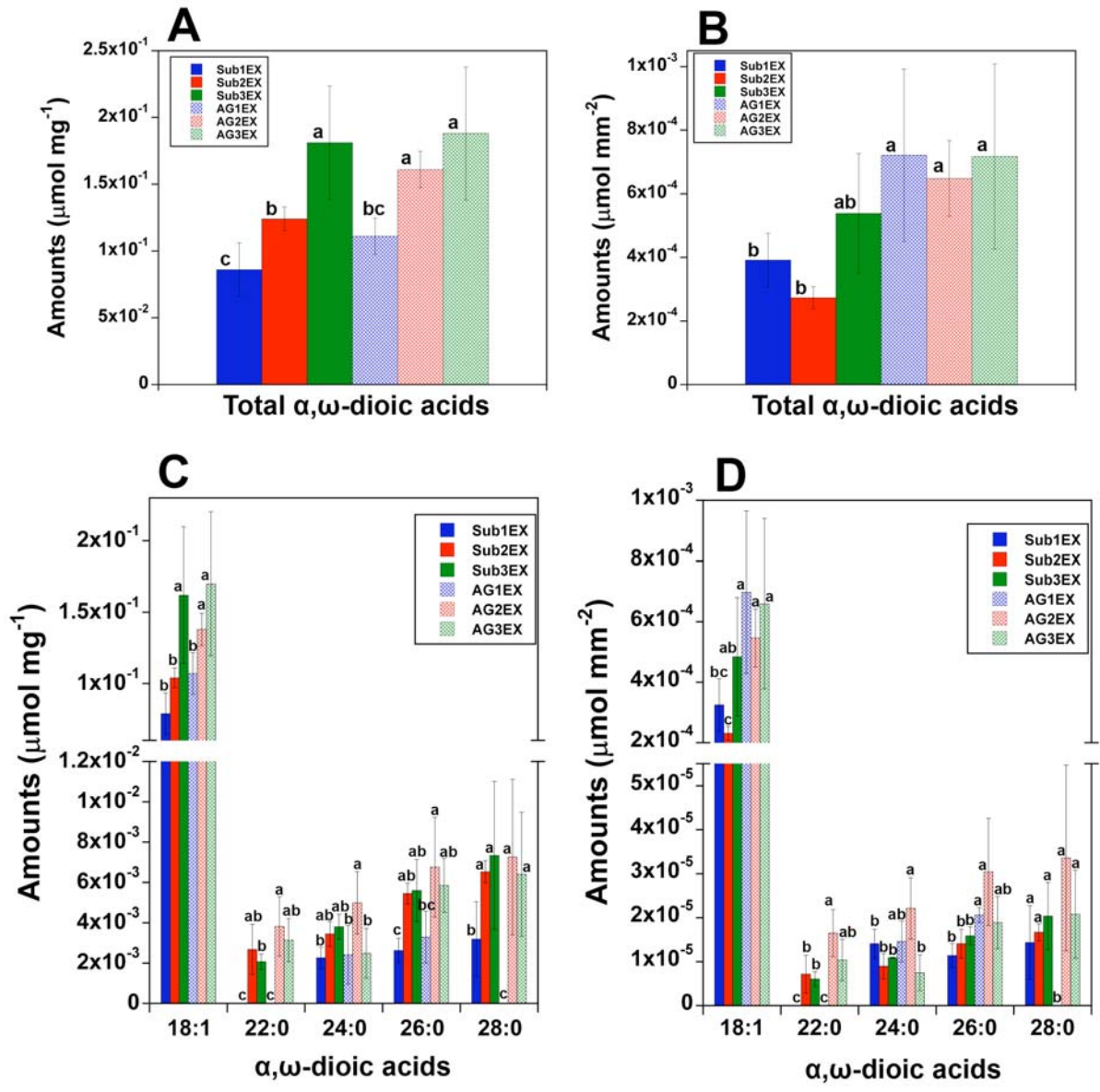


Table 4.1 Percent composition of *Iris germanica*'s exodermal SPAD at different exodermal maturation zones. Sub 1EX = submerged tissue with 1 mature exodermal layer; Sub 2EX = submerged tissue with 2 mature exodermal layers; Sub 3EX = submerged tissue with 3 mature exodermal layers; AG 1EX = air gap-exposed tissue with 1 mature exodermal layer; AG 2EX = air gap-exposed tissue with 2 mature exodermal layers; AG 3EX = air gap-exposed tissue with 3 mature exodermal layers.

Monomer class	Sub 1EX (%)	Sub 2EX (%)	Sub 3EX (%)	AG 1EX (%)	AG 2EX (%)	AG 3EX (%)	Avg. (%)
α,ω -dioic acids	48.5	50	53	55	56	56	53
ω -OH fatty acids	19.5	15	20	21	20	21	19
Fatty acids	14.5	21	21	12	16	16	17
Ferulic acid	17.5	14	6	12	8	7	11
Sum	100	100	100	100	100	100	100

α,ω -dioic acid production increased as more exodermal layers matured (Fig. 4.4A).

Furthermore, the pattern of deposition for α,ω -dioic acids resembled the pattern for the total insoluble fraction. In submerged and air gap-exposed tissue, α,ω -dioic acids were deposited uniformly across three exodermal layers. Interestingly, deposition in the first two exodermal layers of air gap tissue was significantly greater than the deposition in the counterpart layers of submerged tissue (Fig. 4.4B). The change in α,ω -dioic acid deposition between maturing exodermal layers in submerged tissue was greatest in the third layer, with reduced amounts deposited in the first and second layers. However, in air gap-exposed tissue, deposition amounts were similar in each exodermal layer. Interestingly, α,ω -dioic acid deposition in the first two layers was greater than the deposition in counterpart layers of submerged tissue (Fig. 4.3).

The most abundant α,ω -dioic acid was the unsaturated C18:1. In submerged tissue, C18:1 α,ω -dioic acid production progressively increased (Fig. 4.4C) and its distribution across three exodermal layers was uniform (Fig. 4.4D). But, when root tissue was exposed to the air gap, significantly greater amounts of the C18:1 α,ω -dioic acid were deposited in its first and second exodermal layers compared with the corresponding layers in submerged tissue. With maturation of the third exodermal layer, monomer abundance and deposition became equivalent between growth conditions (Fig. 4.4C,D). For all the less abundant α,ω -dioic acids (C22-C28), the trend in monomer production and distribution across exodermal layers and between growth conditions were similar to that of C18:1, but at a reduced scale. (For the changes in deposition between maturing exodermal layers for the different α,ω -dioic acid monomers, see Supplementary Fig. 4.1.)

ω-OH fatty acids. The ω-OH fatty acids accounted for an average of 19% of the insoluble fraction (Table 4.1). The trends in monomer production and distribution were similar to that measured for the total insoluble fraction and the α,ω-dioic acids, except at a reduced scale (Fig. 4.5A,B). Importantly, the deposition of ω-OH fatty acids was significantly greater in the first two exodermal layers of air gap tissue compared with submerged tissue. These deposition trends resembled trends in the changes to ω-OH fatty acid deposition between maturing exodermal layers (Fig. 4.3).

The most abundant ω-OH fatty acid was the unsaturated C18:1. In submerged tissue, C18:1 ω-OH fatty acid production increased as more exodermal layers matured (Fig. 4.5C) and its distribution was uniform across the layers (Fig. 4.5D). When root areas were exposed to an air gap, monomer distribution was steady across exodermal layers, but significantly greater in the first two layers compared with the equivalent layers in submerged tissue. Upon maturation of the third exodermal layer, C18:1 ω-OH fatty acid abundance and deposition were similar between roots exposed to either growth condition (Fig. 4.5C,D). For the less abundant C24 ω-OH fatty acid, the greatest production and deposition were measured in the first exodermal layer, with significant decreases as more exodermal layers matured. (For the changes in deposition between maturing exodermal layers for the different ω-OH fatty acid monomers, see Supplementary Fig. 4.2.)

Fatty acids. Fatty acids comprised an average of 17% of the insoluble fraction (Table 4.1). Fatty acid abundance increased as more exodermal layers matured (Fig. 4.6A), and deposition was fairly uniform across exodermal layers (Fig. 4.6B). These deposition trends

were similar to trends in the changes to fatty acid deposition between maturing exodermal layers (Fig. 4.3).

The fatty acid group contained eight different monomers, ranging from C16 to C28, with C28 being the most abundant. In submerged tissue, fatty acid abundance typically increased as more exodermal layers matured as observed for C17, C18:1, C22, and C28, but the abundance was steady for the other three (Fig. 4.6C). Fatty acid deposition was, in general, lower in the first exodermal layer but increased as the second and third layers matured (Fig. 4.6D). When root tissue was exposed to an air gap, the abundance of C16, C26 and C28 fatty acids tended to increase slightly as more exodermal layers matured, while amounts of the other five monomers remained steady (Fig. 4.6C). Fatty acid deposition was uniform across the exodermal layers for all chain lengths but C18:1, the majority of which was deposited in the first exodermal layer (Fig. 4.6D). (For the changes in deposition between maturing exodermal layers for the different fatty acid monomers, see Supplementary Fig. 4.3.)

The differences in monomer production and deposition between growth conditions were not as clear for the fatty acids as for the α,ω -dioic acids and ω -OH fatty acids. Fatty acid abundance was, for the most part, similar between growth conditions within corresponding exodermal layers. However, in submerged tissue, the deposition of C24 fatty acids was greater in the second exodermal layer and the C17 and C18:1 fatty acids were greater in the third layer compared with air gap tissue (Fig. 4.6C). The deposition of C17, C18:2, C18:1, and C26 fatty acids was significantly greater in the second exodermal layer of air gap exposed tissue compared with the same layer in submerged tissue (Fig. 4.6D). On the other hand, deposition of C18:1 fatty acids was significantly greater in the third exodermal layer of

Figure 4.5 Deposition of ω -OH fatty acids in the aliphatic suberin (SPAD) of *Iris germanica*'s exodermis. Data are displayed per unit of tissue mass (A & C, in $\mu\text{mol mg}^{-1}$) and per unit of suberized surface area (B & D, in $\mu\text{mol mm}^{-2}$) for each mature exodermal layer under different growth conditions (legends inset). (A,B) Total ω -OH fatty acids. (C,D) Individual ω -OH fatty acid monomers. Values are means \pm standard deviation. Different lowercase letters within the total ω -OH fatty acids (A,B) or within each monomer chain length (C,D) indicate a significant difference ($P \leq 0.05$). Abbreviations: Sub1EX = submerged tissue with one mature exodermal layer; Sub2EX = submerged tissue with two mature exodermal layers; Sub3EX = submerged tissue with three mature exodermal layers; AG1EX = air gap-exposed tissue with one mature exodermal layer; AG2EX = air gap-exposed tissue with two mature exodermal layers; AG3EX = air gap-exposed tissue with three mature exodermal layers.

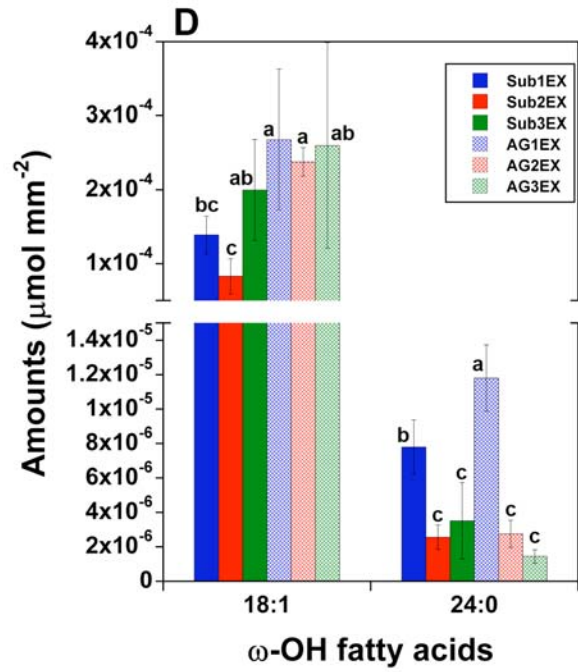
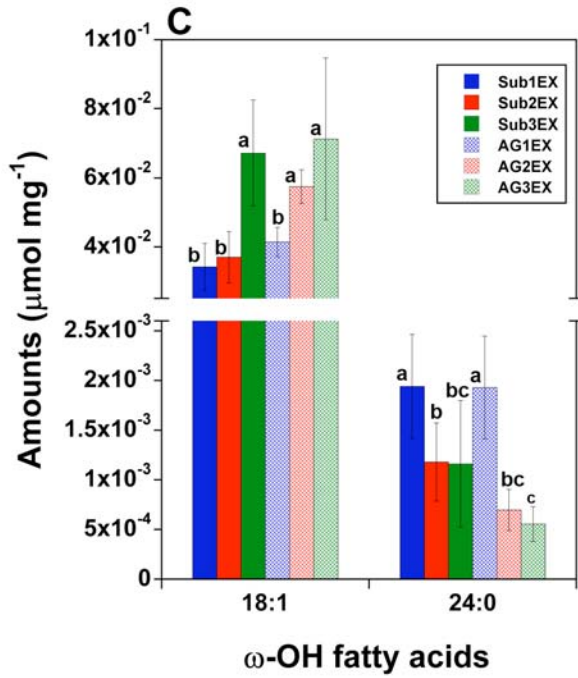
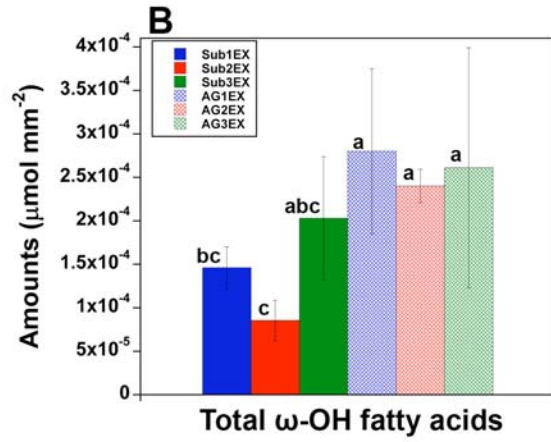
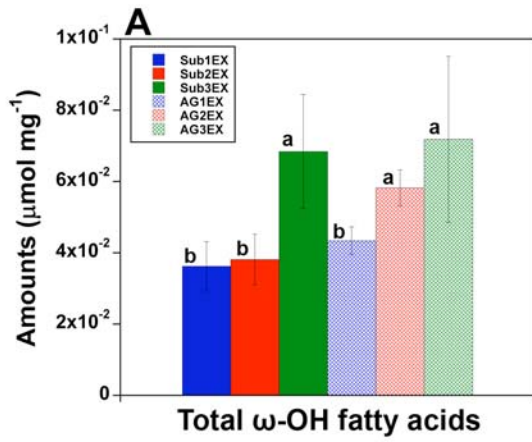


Figure 4.6 Deposition of fatty acids in the aliphatic suberin (SPAD) of *Iris germanica*'s exodermis. Data are displayed per unit of tissue mass (A, in $\mu\text{mol mg}^{-1}$) and per unit of suberized surface area (B, in $\mu\text{mol mm}^{-2}$) for each mature exodermal layer under different growth conditions (legend insets). (A,B) Total fatty acids. Values are means \pm standard deviation. Different lowercase letters within each graph indicate a significant difference ($P \leq 0.05$). Abbreviations: Sub1EX = submerged tissue with one mature exodermal layer; Sub2EX = submerged tissue with two mature exodermal layers; Sub3EX = submerged tissue with three mature exodermal layers; AG1EX = air gap-exposed tissue with one mature exodermal layer; AG2EX = air gap-exposed tissue with two mature exodermal layers; AG3EX = air gap-exposed tissue with three mature exodermal layers.

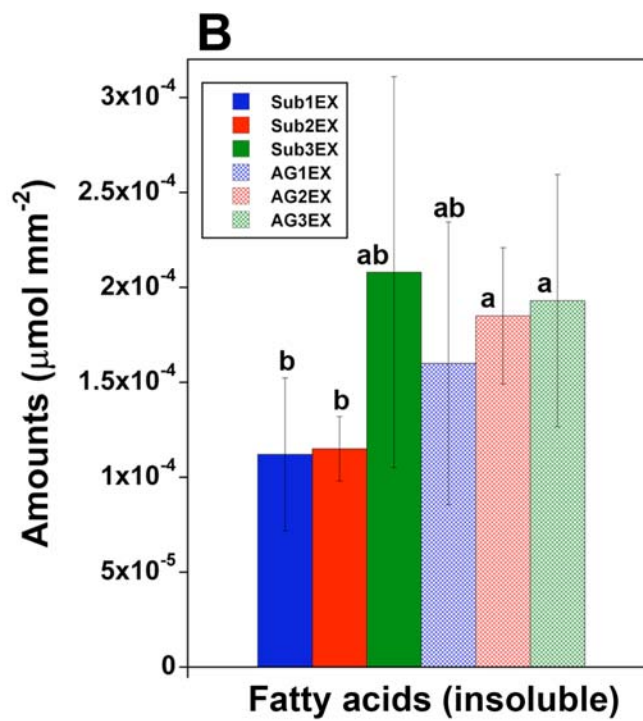
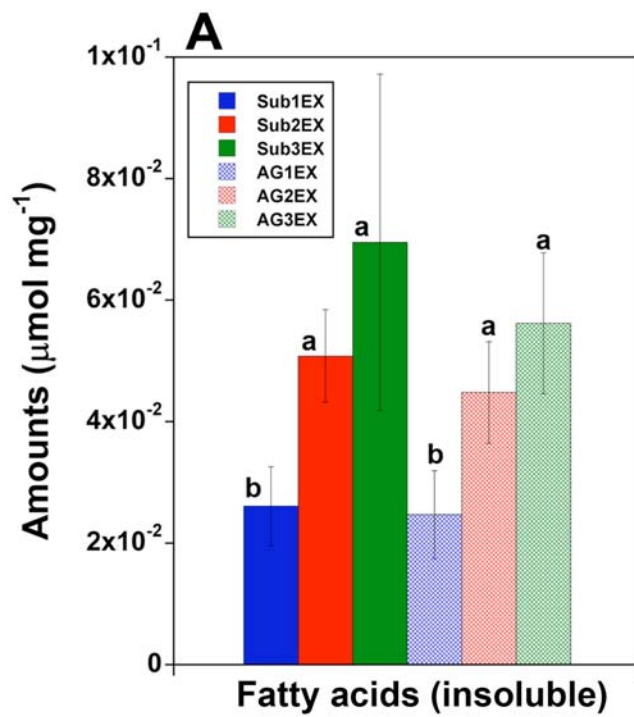


Figure 4.6 Deposition of fatty acids in the aliphatic suberin (SPAD) of *Iris germanica*'s exodermis. Data are displayed per unit of tissue mass (C, in $\mu\text{mol mg}^{-1}$) and per unit of suberized surface area (D, in $\mu\text{mol mm}^{-2}$) for each mature exodermal layer under different growth conditions (legend insets). (C,D) Individual fatty acid monomers. Values are means \pm standard deviation. Different lowercase letters within each monomer chain length indicate a significant difference ($P \leq 0.05$). Abbreviations: Sub1EX = submerged tissue with one mature exodermal layer; Sub2EX = submerged tissue with two mature exodermal layers; Sub3EX = submerged tissue with three mature exodermal layers; AG1EX = air gap-exposed tissue with one mature exodermal layer; AG2EX = air gap-exposed tissue with two mature exodermal layers; AG3EX = air gap-exposed tissue with three mature exodermal layers.

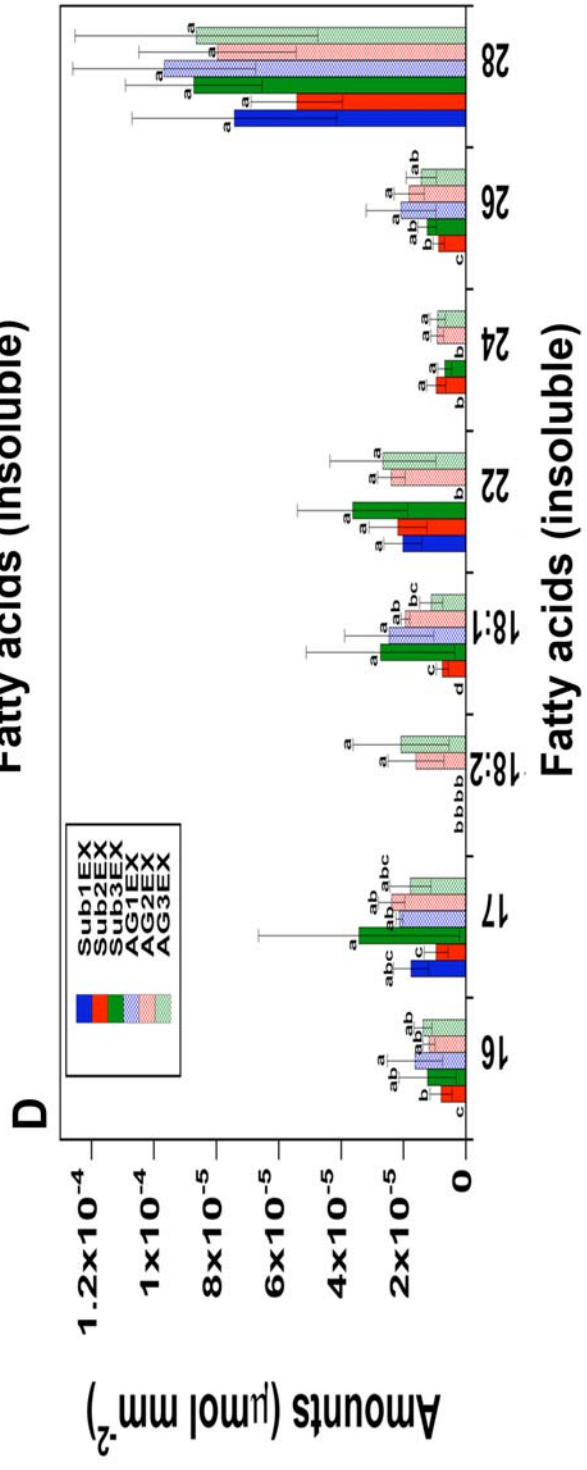
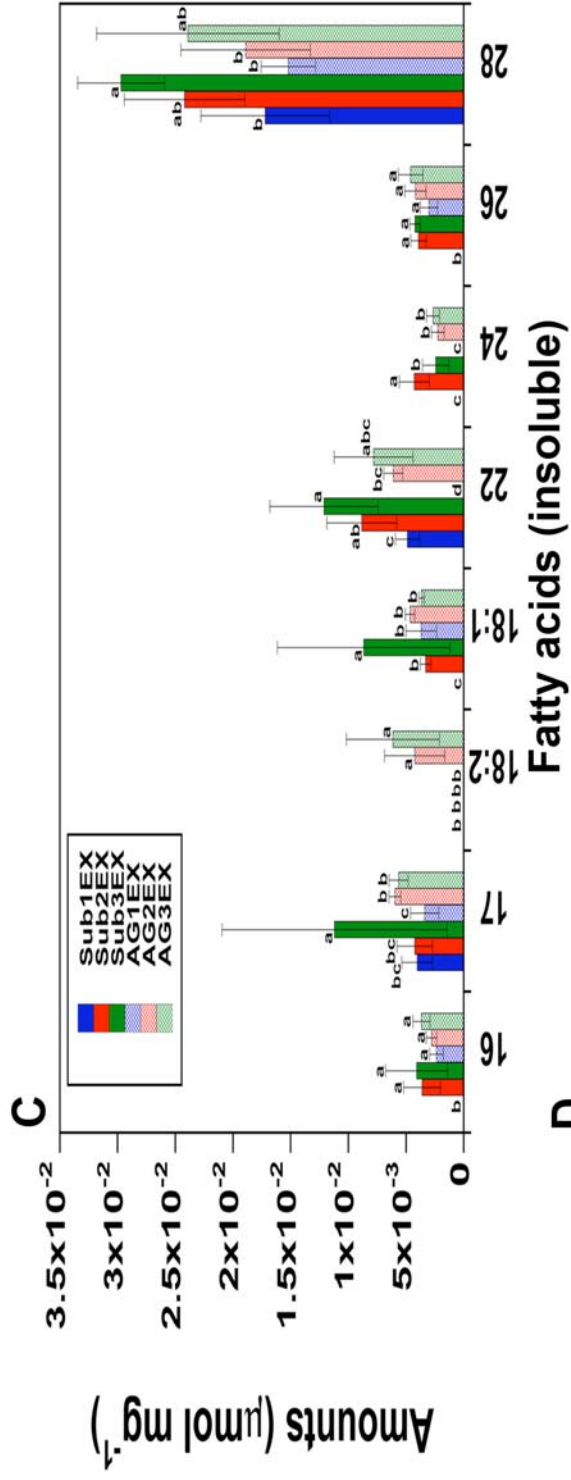
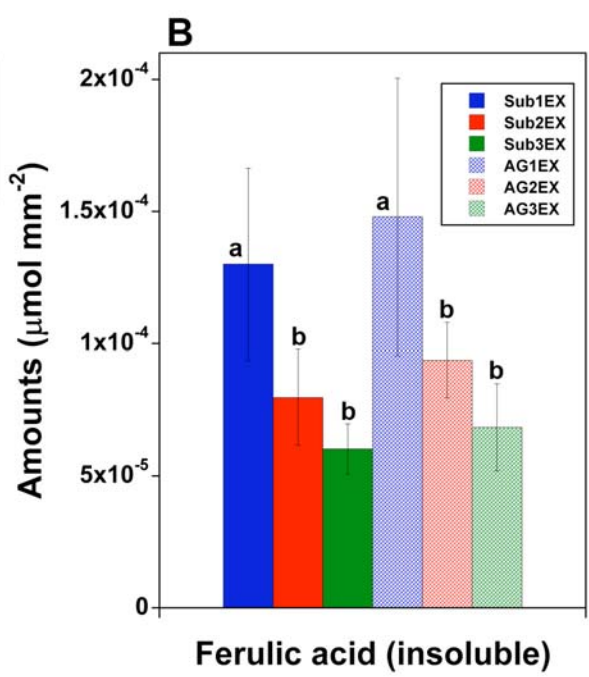
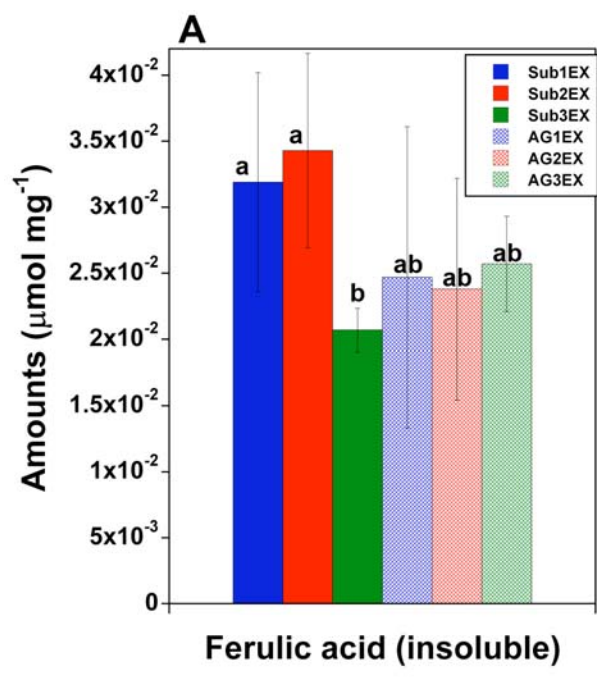


Figure 4.7 Deposition of esterified ferulic acid in the aliphatic suberin (SPAD) of *Iris germanica*'s exodermis. Data are displayed per unit of tissue mass (A, in $\mu\text{mol mg}^{-1}$) and per unit of suberized surface area (B, in $\mu\text{mol mm}^{-2}$) for each mature exodermal layer under different growth conditions (legend insets). Values are means \pm standard deviation. Different lowercase letters within each graph indicate a significant difference ($P \leq 0.05$).

Abbreviations: Sub1EX = submerged tissue with one mature exodermal layer; Sub2EX = submerged tissue with two mature exodermal layers; Sub3EX = submerged tissue with three mature exodermal layers; AG1EX = air gap-exposed tissue with one mature exodermal layer; AG2EX = air gap-exposed tissue with two mature exodermal layers; AG3EX = air gap-exposed tissue with three mature exodermal layers.



submerged tissue compared with the corresponding layer in air gap exposed tissue (Fig. 4.6D). The only other notable differences in monomer amounts between growth conditions included samples where the monomer was undetectable. One striking example of this was for C18:2, which was only detected in the second and third exodermal layers of air gap-exposed tissue.

Ferulic acid. Esterified ferulic acid comprised an average of 11% of the insoluble fraction (Table 4.1). The production of ferulic acid was steady as more exodermal layers matured, although there was a sharp decrease with maturation of the third layer in submerged tissue (Fig. 4.7A). Deposition was abundant in the outermost exodermal layer, regardless of growth condition, but was significantly reduced in the second and third layers (Fig. 4.7B). There were no statistical differences in production or deposition between exodermal layers of differing growth conditions. Similar trends were observed for the change in ferulic acid deposition between maturing exodermal layers. For both submerged and air gap-exposed tissue, the majority of the ferulic acid was deposited in the first layer with less amounts deposited in the second and third layers (Fig. 4.3; see Supplementary Fig. 4.4).

4.4.2.2 Soluble fraction

Total soluble fraction. The total soluble fraction is the sum of all monomers that were released by soxhlet extraction, and does not include monomers that were cross-linked to the suberin polymer. In submerged roots, soluble monomer amounts were steady as more exodermal layers matured. However, in air gap-exposed roots, soluble monomer amounts decreased with more exodermal layers (Fig. 4.8A). Soluble monomer accumulation in submerged tissue was uniform across exodermal layers (Fig. 4.8B). In marked contrast, the

accumulation of soluble monomers in air gap-exposed tissue was heavy in the first exodermal layer but significantly reduced in the second and third layers (Fig. 4.8B). Similar accumulation trends were also observed for the changes in soluble monomer accumulation between maturing exodermal layers (Fig. 4.9). In submerged tissue, most monomers accumulated in the first and third exodermal layers. In air gap-exposed tissue, nearly all of the soluble monomers accumulated in the first exodermal layer, while vastly reduced amounts were measured in all underlying layers. Notably, monomer accumulation in the first exodermal layer was greater in air gap tissue compared with submerged tissue (Fig. 4.9). The composition of the soluble fraction included fatty acids (C14 - C30), alkanes (C23 - C28), ferulic acid, and fatty alcohols (C12 - C18) (Table 4.2; Figs. 4.9-4.13).

Fatty acids. Fatty acids were the most abundant soluble monomers, accounting for an average of 68% of the total soluble fraction (Table 4.2). Hence, the pattern of fatty acid accumulation resembled the pattern for the total soluble fraction. Briefly, submerged tissue had a steady amount of fatty acids across exodermal layers (Fig. 4.10A). Conversely, in air gap-exposed tissue, fatty acid amounts were abundant in the first exodermal layer, but dwindled in the second and third layers (Fig. 4.10A). In submerged root tissue, fatty acid accumulation was uniform across the first and third exodermal layers, but was reduced in the second exodermal layer (Fig. 4.10B). In air gap-exposed root tissue, fatty acids were abundant in the first exodermal layer, with reduced accumulation in the second and third layers (Fig. 4.10B). The change in fatty acid accumulation between maturing exodermal layers was greatest in the first and third layers but vastly reduced in the second layer for both submerged and air gap-exposed tissue (Fig. 4.9).

Figure 4.8 Total soluble fraction of *Iris germanica*'s exodermal suberin. Data are displayed per unit of tissue mass (A, in $\mu\text{mol mg}^{-1}$) and per unit of suberized surface area (B, in $\mu\text{mol mm}^{-2}$) for each mature exodermal layer under different growth conditions (legend insets). Values are means \pm standard deviation. Different lowercase letters within each graph indicate a significant difference ($P \leq 0.05$). Abbreviations: Sub1EX = submerged tissue with one mature exodermal layer; Sub2EX = submerged tissue with two mature exodermal layers; Sub3EX = submerged tissue with three mature exodermal layers; AG1EX = air gap-exposed tissue with one mature exodermal layer; AG2EX = air gap-exposed tissue with two mature exodermal layers; AG3EX = air gap-exposed tissue with three mature exodermal layers.

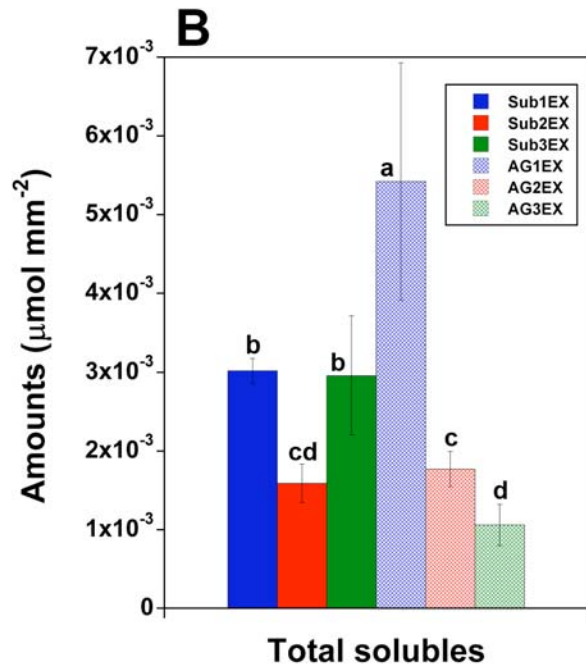
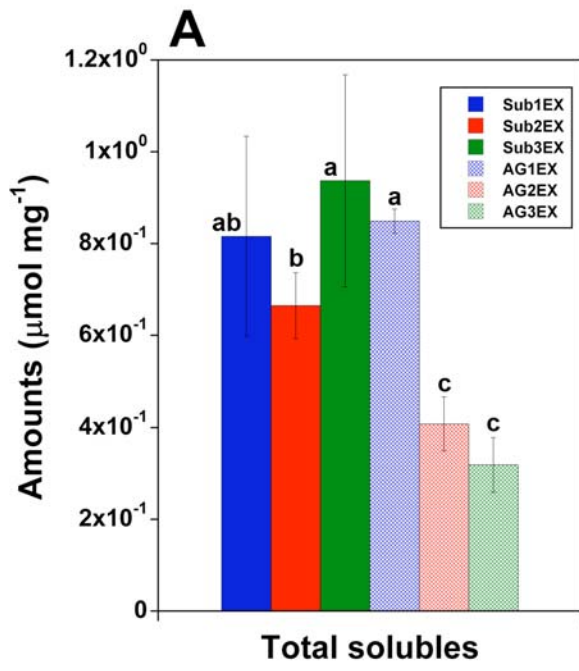


Figure 4.9 Change in amounts of soluble monomer classes in the maturing MEX of *Iris germanica*. Data are displayed per root segment surface area ($\mu\text{mol mm}^{-2}$), and refer to the change in monomer amounts from one exodermal maturation stage to the next, under different growth conditions (legend inset). See materials and methods for data calculation details. (A) Total soluble fraction, total fatty acids, and total alkanes. (B) Total fatty alcohols and ferulic acid. Abbreviations: Sub 0EX-1EX = submerged tissue, monomer amounts in the first exodermal layer; Sub 1EX-2EX = submerged tissue, change in amounts between exodermal layers one and two; Sub 2EX-3EX = submerged tissue, change in amounts between exodermal layers two and three; AG 0EX-1EX = air gap-exposed tissue, monomer amounts in the first exodermal layer; AG 1EX-2EX = air gap-exposed tissue, change in amounts between exodermal layers one and two; AG 2EX-3EX = air gap-exposed, change in amounts between exodermal layers two and three.

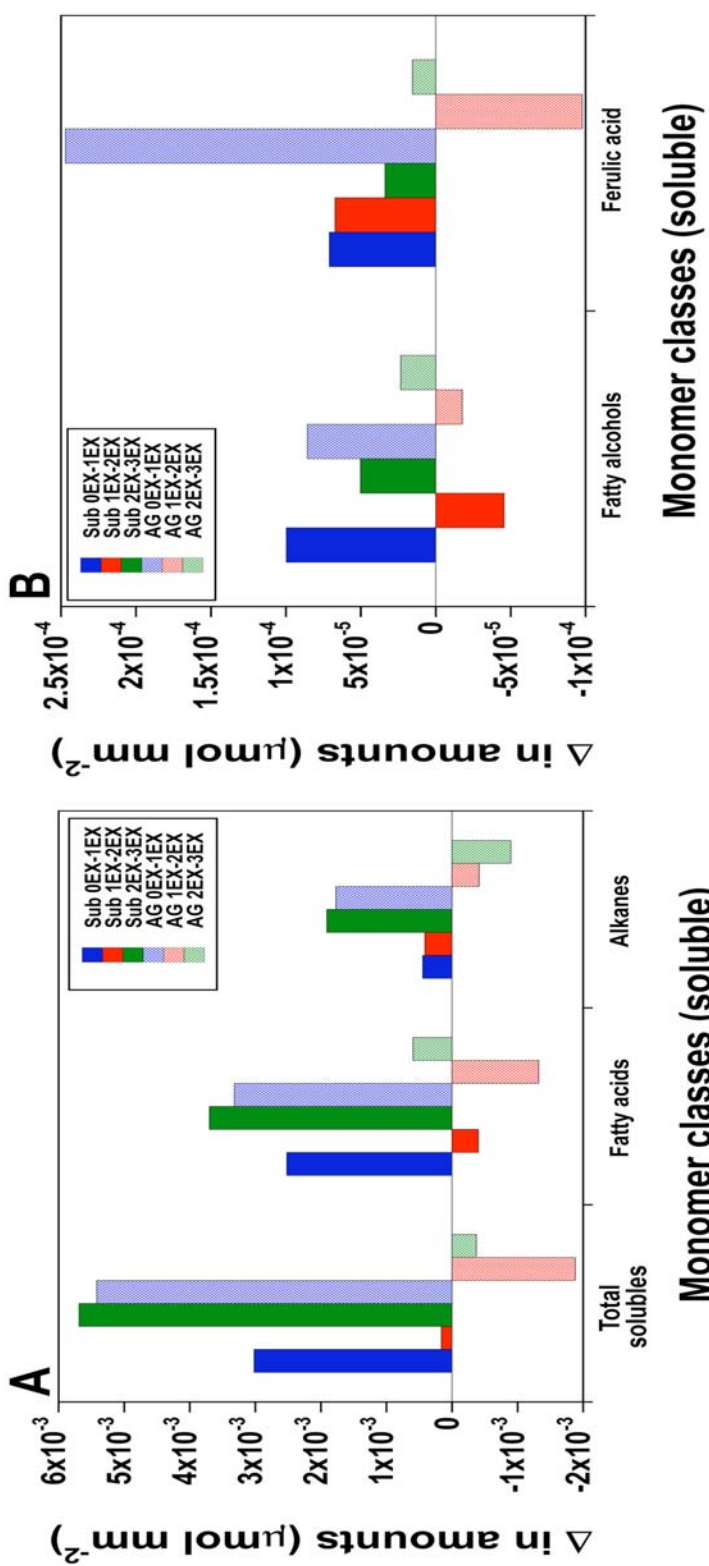


Figure 4.10 Accumulation of fatty acids in the soluble fraction of *Iris germanica*'s exodermal suberin. Data are displayed per unit of tissue mass (A, in $\mu\text{mol mg}^{-1}$) and per unit of suberized surface area (B, in $\mu\text{mol mm}^{-2}$) for each mature exodermal layer under different growth conditions (legend insets). (A,B) Total fatty acids. Values are means \pm standard deviation. Different lowercase letters within each graph indicate a significant difference ($P \leq 0.05$). Abbreviations: Sub1EX = submerged tissue with one mature exodermal layer; Sub2EX = submerged tissue with two mature exodermal layers; Sub3EX = submerged tissue with three mature exodermal layers; AG1EX = air gap-exposed tissue with one mature exodermal layer; AG2EX = air gap-exposed tissue with two mature exodermal layers; AG3EX = air gap-exposed tissue with three mature exodermal layers.

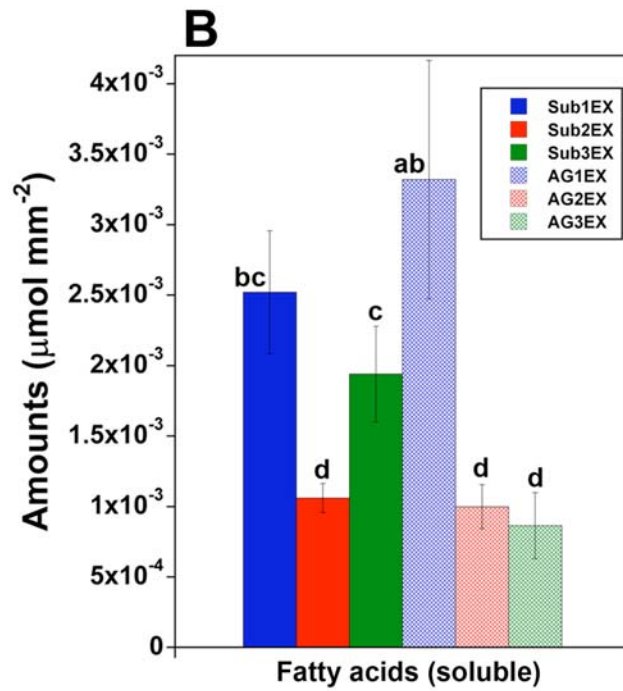
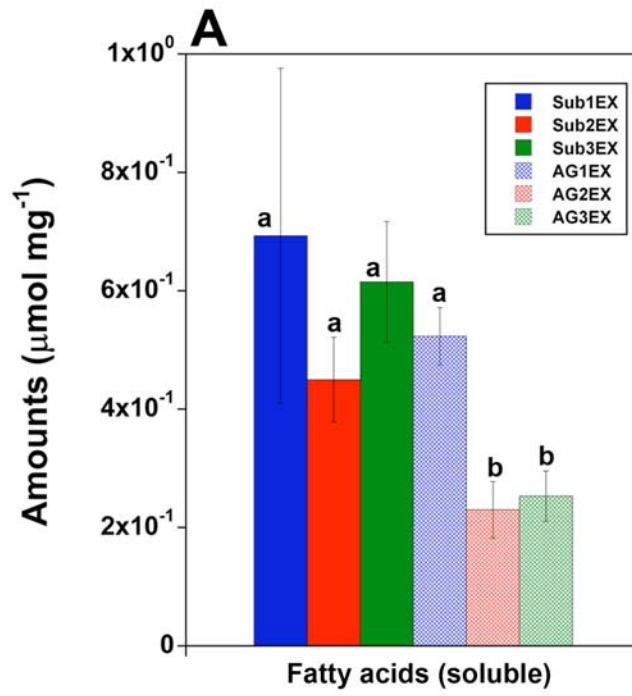


Figure 4.10 Accumulation of fatty acids in the soluble fraction of *Iris germanica*'s exodermal suberin. Data are displayed per unit of tissue mass (C, in $\mu\text{mol mg}^{-1}$) and per unit of suberized surface area (D, in $\mu\text{mol mm}^{-2}$) for each mature exodermal layer under different growth conditions (legend insets) (C,D) Individual fatty acid monomers. Values are means \pm standard deviation. Different lowercase letters within each monomer chain length indicate a significant difference ($P \leq 0.05$). Abbreviations: Sub1EX = submerged tissue with one mature exodermal layer; Sub2EX = submerged tissue with two mature exodermal layers; Sub3EX = submerged tissue with three mature exodermal layers; AG1EX = air gap-exposed tissue with one mature exodermal layer; AG2EX = air gap-exposed tissue with two mature exodermal layers; AG3EX = air gap-exposed tissue with three mature exodermal layers.

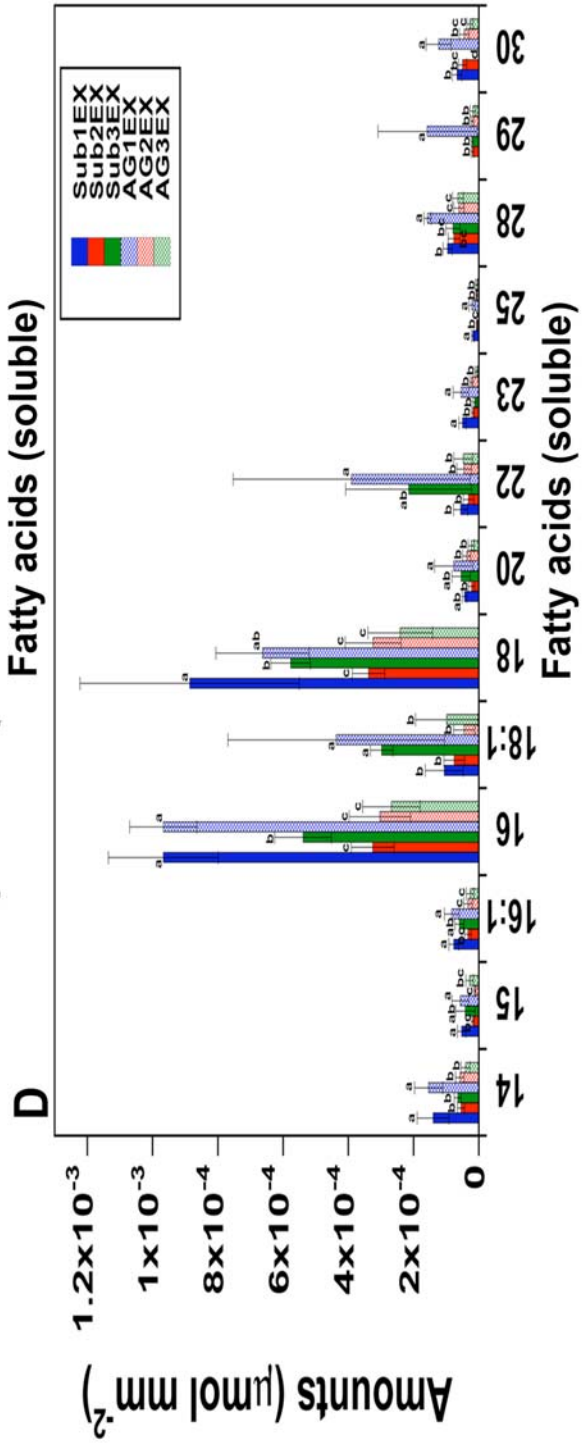
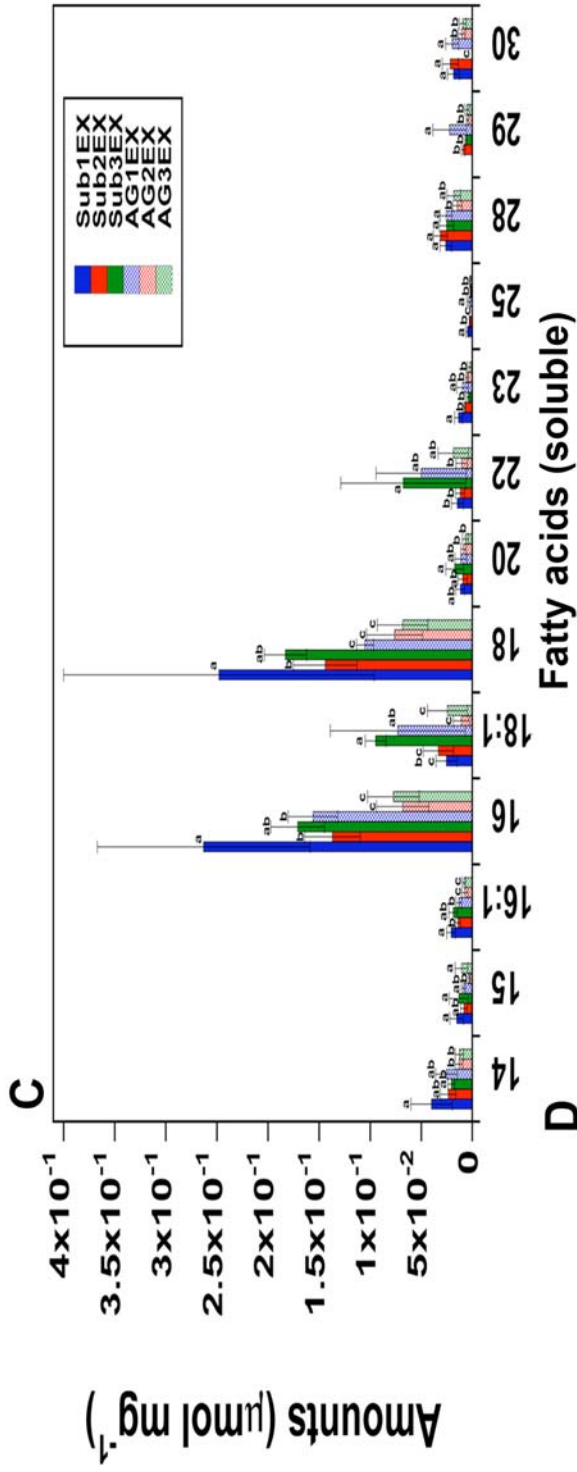


Table 4.2 Percent composition of the soluble fraction of *Iris germanica*'s exodermal suberin at different maturation zones. Sub 1EX = submerged tissue with 1 mature exodermal layer; Sub 2EX = submerged tissue with 2 mature exodermal layers; Sub 3EX = submerged tissue with 3 mature exodermal layers; AG 1EX = air gap-exposed tissue with 1 mature exodermal layer; AG 2EX = air gap-exposed tissue with 2 mature exodermal layers; AG 3EX = air gap-exposed tissue with 3 mature exodermal layers.

Monomer class	Sub 1EX (%)	Sub 2EX (%)	Sub 3EX (%)	AG 1EX (%)	AG 2EX (%)	AG 3EX (%)	Avg. (%)
Fatty acids	81	67.5	66	61	56	76.5	68
Alkanes	14	26.5	31	32	38	14.5	26
Fatty alcohols	3	2	1	2	2	3	2
Ferulic acid	2	4	2	5	4	6	4
Sum	100	100	100	100	100	100	100

The fatty acid group was composed of thirteen different monomers, with the most abundant being C16 and C18. Amounts of the C16 and C18 fatty acids in submerged tissue were abundant with maturation of the first exodermal layer, but declined and leveled off in the second and third layers (Fig. 4.10C). In air gap tissue, C16 and C18 amounts were high with one mature exodermal layer, but tended to decline with the maturation of the second and third layers (Fig. 4.10C). Accumulation of C16 and C18 fatty acids in submerged tissue was high in the first exodermal layer, followed by a sharp decrease in the second layer, and a subsequent sharp increase in the third layer (Fig. 4.10D). In air gap tissue, C16 and C18 accumulation was high in the first exodermal layer, but was reduced in the second and third layers (Fig. 4.10D).

The next most abundant fatty acids were C18:1 and C22. Amounts of these two monomers in submerged tissue were low with the maturation of two exodermal layers, but increased when the third layer matured (Fig. 4.10C). In air gap tissue, abundance was high with the maturation of the first exodermal layer, but was scaled back as the second and third layers matured (Fig. 4.10C). In submerged tissue, accumulation was fairly low in the first and second exodermal layers, but was markedly increased in the third layer (Fig. 4.10D). Conversely, in air gap tissue, C18:1 and C22 had abundantly accumulated in the first exodermal layer followed by a reduction in the second and third layers (Fig. 4.10D).

The trends in accumulation for the other, less abundant fatty acids were variable and not consistent. In general, monomer amounts were either steady across exodermal layers, or were high in the first layer followed by reductions in underlying layers. (For the changes in

accumulation between maturing exodermal layers for the different fatty acid monomers, see Supplementary Fig. 4.5.)

Alkanes. Alkanes were relatively abundant, comprising an average of 26% of the soluble fraction (Table 4.2). The trends in alkane amounts across exodermal layers differed substantially between submerged and air gap-exposed root tissues. In submerged tissue, the amount of alkanes increased significantly with the maturation of each additional exodermal layer (Fig. 4.11A). Conversely, in air gap tissue, alkane amounts were abundant when only one exodermal layer was mature, but then decreased significantly as additional layers matured (Fig. 4.11A). Alkane accumulation in the first and second exodermal layers of submerged tissue was low and uniform, but tended to increase in the third layer (Fig. 4.11B). On the other hand, in air gap tissue, alkanes accumulated in abundance in the first exodermal layer, but were significantly and progressively reduced in the two underlying layers (Fig. 4.11B). In fact, with only one mature exodermal layer, the amounts and accumulation of alkanes were on average 2.5-fold and 4-fold greater, respectively, in air gap tissue compared with submerged tissue. These accumulation trends were similar to trends in the changes to alkane accumulation between maturing exodermal layers (Fig. 4.9).

The alkane group was composed of five different monomers, with the most abundant being C27. Trends in abundance and accumulation were virtually the same for each monomer (Fig. 4.11C,D), and hence, were similar to the overall alkane trends (as described above). (For the changes in accumulation between maturing exodermal layers for the different alkane monomers, see Supplementary Fig. 4.6.)

Fatty alcohols. The fatty alcohols were the least abundant of the soluble monomers, accounting for only an average of 2% of the soluble fraction (Table 4.2). Fatty alcohol abundance in submerged tissue was high when one exodermal layer was mature, but declined significantly with the maturation of the additional layers (Fig. 4.12A). Interestingly, in air gap tissue, fatty alcohol amounts were steady as more exodermal layers matured.

Accumulation of fatty alcohols in submerged tissue was abundant in the first exodermal layer, and significantly reduced in the two underlying layers (Fig. 4.12B). The accumulation of fatty alcohols in air gap tissue was essentially the same as for submerged tissue (Fig. 4.12B). The change in fatty alcohol accumulation between maturing exodermal layers was greatest in the first layer, slightly reduced in the third layer, but vastly reduced in the second layer for both submerged and air gap-exposed tissue (Fig. 4.9).

The fatty alcohol group was composed of four different monomers, all of similar abundance except for C16 which was not detected in submerged tissue. The accumulation of C14, C16, and C18 fatty alcohols was similar to the overall fatty alcohol trends, as described above (Fig. 4.12C,D). (For the changes in accumulation between maturing exodermal layers for the different fatty alcohol monomers, see Supplementary Fig. 4.7.)

Ferulic acid. Ferulic acid comprised an average of only 4% of the soluble fraction (Table 4.2). The accumulation of ferulic acid across exodermal layers in submerged tissue was uniform (Fig. 4.13A,B). However, in air gap-exposed tissue, ferulic acid abundance was high in the first exodermal layer, but was later reduced as more layers matured (Fig. 4.13A). Furthermore, accumulation was greatest in the first exodermal layer, followed by significant reductions in the second and third layers (Fig. 4.13B). Similar trends were observed for the

Figure 4.11 Accumulation of alkanes in the soluble wax fraction of *Iris germanica*'s exodermal suberin. Data are displayed per unit of tissue mass (A & C, in $\mu\text{mol mg}^{-1}$) and per unit of suberized surface area (B & D, in $\mu\text{mol mm}^{-2}$) for each mature exodermal layer under different growth conditions (legend insets). (A,B) Total alkanes. (C,D) Individual alkane monomers. Values are means \pm standard deviation. Different lowercase letters within the total alkanes (A,B) or within each monomer chain length (C,D) indicate a significant difference ($P \leq 0.05$). Abbreviations: Sub1EX = submerged tissue with one mature exodermal layer; Sub2EX = submerged tissue with two mature exodermal layers; Sub3EX = submerged tissue with three mature exodermal layers; AG1EX = air gap-exposed tissue with one mature exodermal layer; AG2EX = air gap-exposed tissue with two mature exodermal layers; AG3EX = air gap-exposed tissue with three mature exodermal layers.

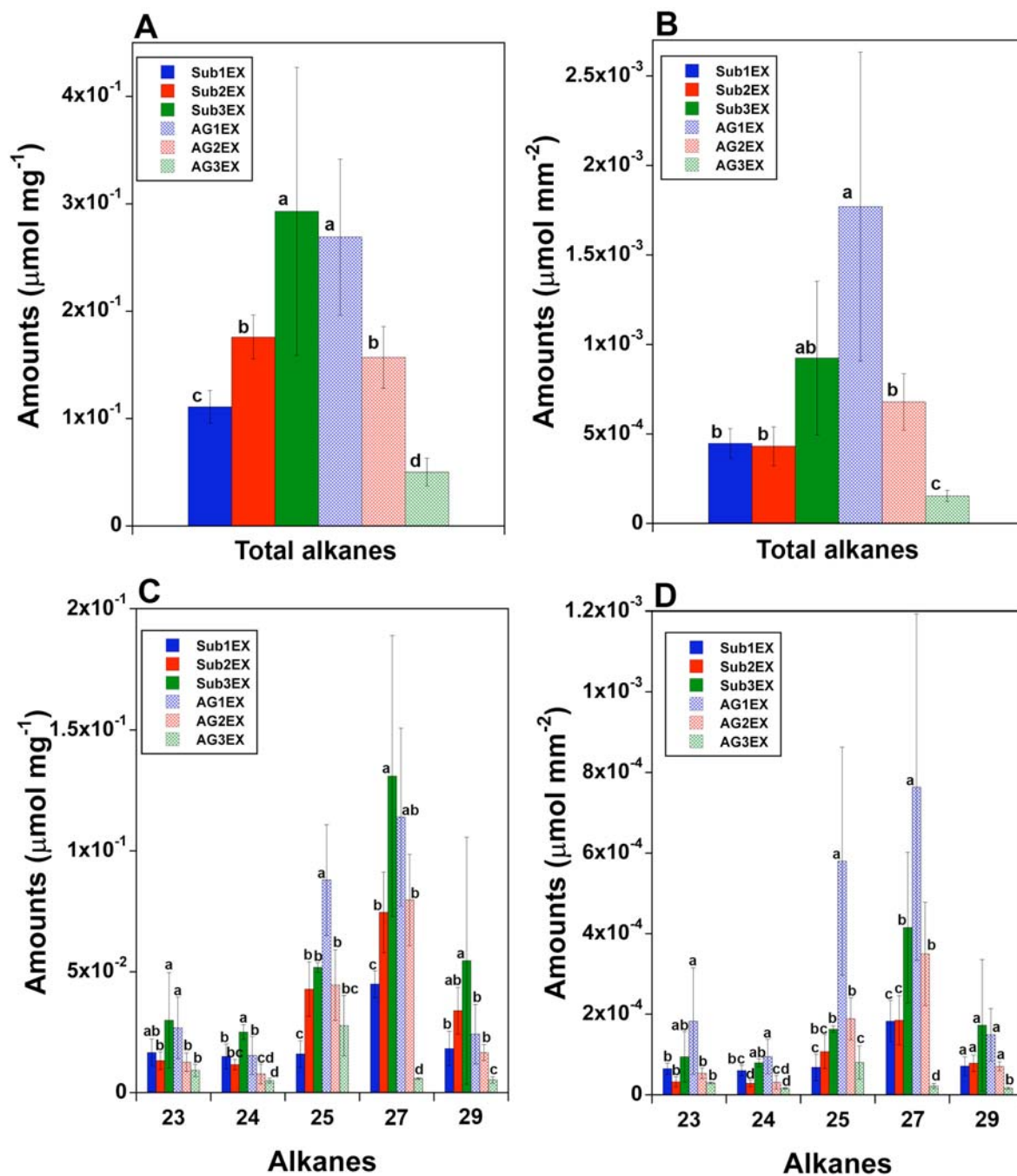


Figure 4.12 Accumulation of fatty alcohols in the soluble fraction of *Iris germanica*'s exodermal suberin. Data are displayed per unit of tissue mass (A & C, in $\mu\text{mol mg}^{-1}$) and per unit of suberized surface area (B & D, in $\mu\text{mol mm}^{-2}$) for each mature exodermal layer under different growth conditions (legend insets). (A,B) Total fatty alcohols. (C,D) Individual fatty alcohol monomers. Values are means \pm standard deviation. Different lowercase letters within the total fatty alcohols (A,B) or within each monomer chain length (C,D) indicate a significant difference ($P \leq 0.05$). Abbreviations: Sub1EX = submerged tissue with one mature exodermal layer; Sub2EX = submerged tissue with two mature exodermal layers; Sub3EX = submerged tissue with three mature exodermal layers; AG1EX = air gap-exposed tissue with one mature exodermal layer; AG2EX = air gap-exposed tissue with two mature exodermal layers; AG3EX = air gap-exposed tissue with three mature exodermal layers.

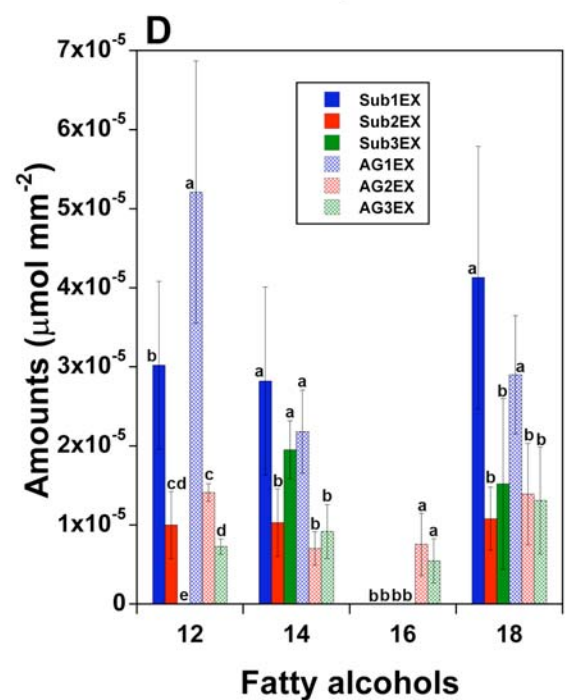
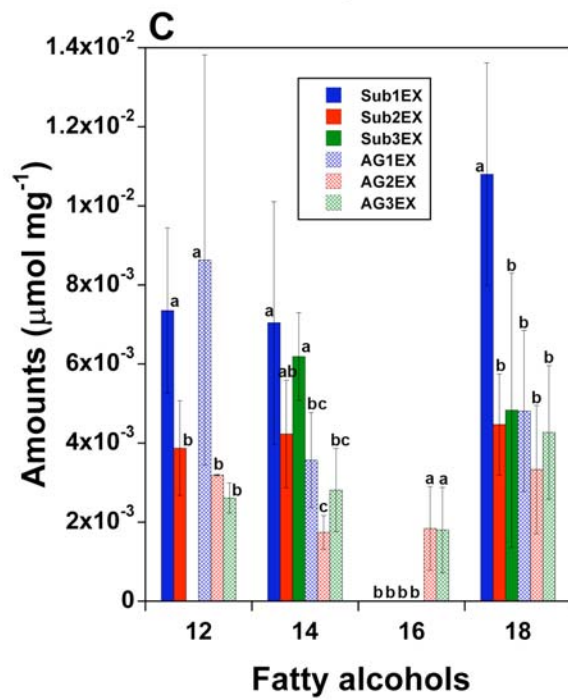
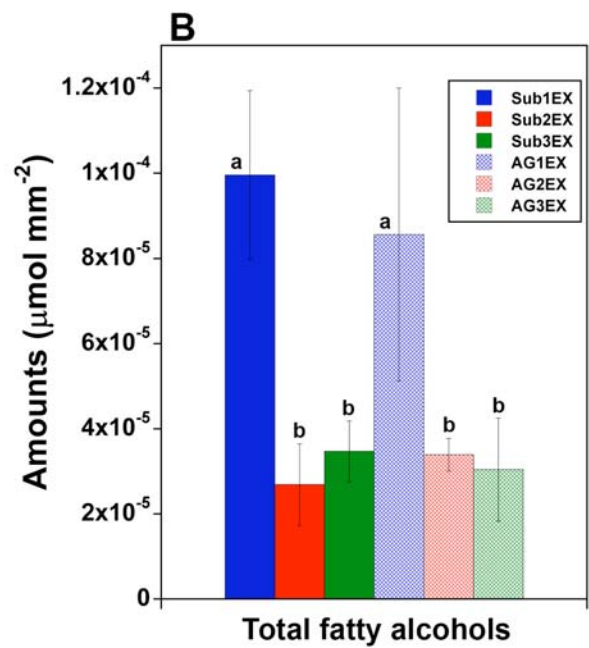
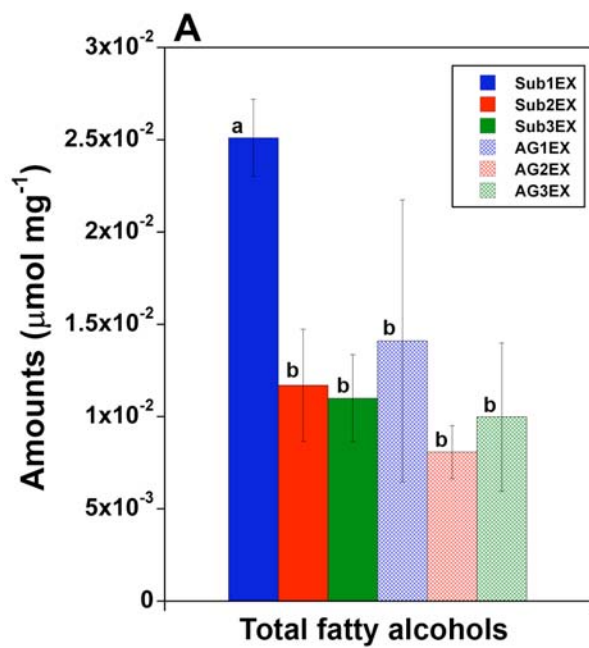
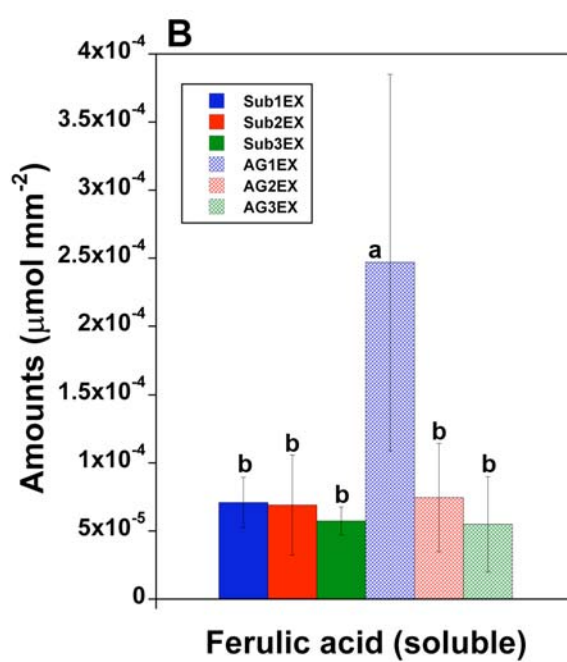
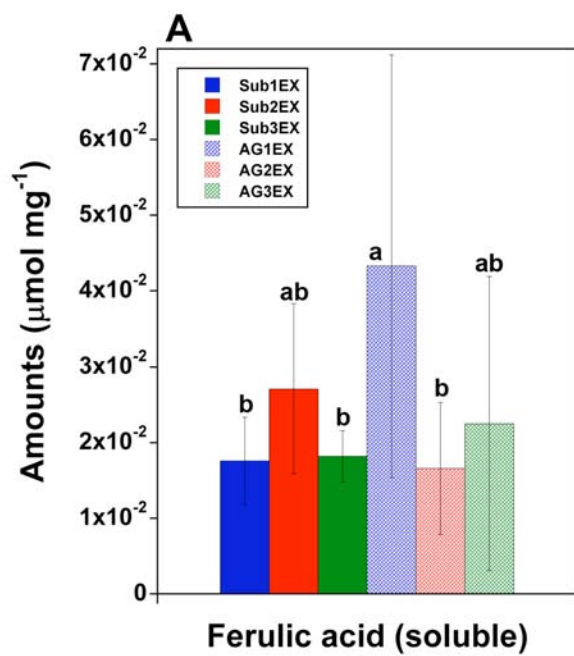


Figure 4.13 Accumulation of ferulic acid in the soluble fraction of *Iris germanica*'s exodermal suberin. Data are displayed per unit of tissue mass (A, in $\mu\text{mol mg}^{-1}$) and per unit of suberized surface area (B, in $\mu\text{mol mm}^{-2}$) for each mature exodermal layer under different growth conditions (legend insets). Values are means \pm standard deviation. Different lowercase letters within each graph indicate a significant difference ($P \leq 0.05$).

Abbreviations: Sub1EX = submerged tissue with one mature exodermal layer; Sub2EX = submerged tissue with two mature exodermal layers; Sub3EX = submerged tissue with three mature exodermal layers; AG1EX = air gap-exposed tissue with one mature exodermal layer; AG2EX = air gap-exposed tissue with two mature exodermal layers; AG3EX = air gap-exposed tissue with three mature exodermal layers.



change in ferulic acid accumulation between maturing exodermal layers. In submerged tissue, ferulic acid accumulation was similar in each exodermal layer. On the other hand, in air gap-exposed tissue, the majority of the ferulic acid was deposited in the first layer with less deposited in the second and third layers (Fig. 4.9; see Supplementary Fig. 4.8).

4.5 Discussion

The adventitious roots of *Iris germanica* proved to be excellent subjects for analyzing suberin composition, abundance and deposition in the Casparian bands and suberin lamellae of a maturing multiseriate exodermis (MEX). MEX maturation occurred as expected in submerged and humid air gap growth conditions (Meyer et al. 2009; see Chapters 2 and 3) and, therefore, root segments could be sampled one-at-a-time at specific maturation stages. Plus, due to the wide diameter of *I. germanica* roots and the large amounts of exodermal suberization, mechanical separation of the exodermis from the underlying tissues was feasible.

The suberin poly(aliphatic) domain (SPAD) composition for the most abundant insoluble monomer classes of *I. germanica*'s MEX includes α,ω -dioic acids (53%) and ω -OH fatty acids (19%) (see Table 4.1). This composition was similar to the composition of *S. tuberosum* tuber periderm, where α,ω -dioic acids and ω -OH fatty acids comprise 54% and 25% of the insoluble aliphatics, respectively (not including glycerol or unidentified compounds; Graça and Pereira 2000b; Schreiber et al. 2005a). But, SPAD composition often varies between species. For example, *A. thaliana* roots included mainly ω -OH fatty acids (48%) and α,ω -dioic acids (28%) in the insoluble fraction (not including unidentified

compounds; Franke et al. 2005). In another example, *Q. suber* stem periderm is composed mainly of ω -OH acids (41%) and epoxides (31%) (Holloway 1983). Nonetheless, for the majority of tested species, including those listed above, the α,ω -dioic acids and ω -OH fatty acids are always detected and typically the C18:1 monomers are the most abundant (Holloway 1983; Matzke and Riederer 1991).

Interestingly, for *I. germanica*'s MEX, there was very little difference in the percent composition of the insoluble suberin fraction between exodermal maturation stages and between growth conditions (see Table 4.1). Such compositional data is relative, meaning each monomer class is a proportion of the sum of all monomer classes, and is not representative of the actual amount of monomer production and deposition. Hence, even though the percent composition of the insoluble fraction between exodermal maturation stages and between growth conditions did not change, the actual amounts of monomer production and deposition did change significantly (see below).

Insoluble suberin monomer production and deposition were influenced by the exodermal maturation stage and the growth condition. Production of insoluble α,ω -dioic acids, ω -OH fatty acids, and fatty acids increased steadily and significantly as more exodermal layers matured in both submerged and air gap-exposed root tissue. However, there was significantly greater production at the second exodermal layer of air gap-exposed tissue, compared with submerged tissue (see Figs. 4.4, 4.5). Deposition of these monomers was fairly uniform across exodermal layers, but was significantly greater in the first two layers of air gap-exposed tissue compared with submerged tissue (see Figs. 4.3 - 4.5). From these results it was evident that a large and rapid induction of insoluble suberin monomer production and

deposition occurred in the first and second exodermal layers when roots were exposed to a dehydrating air gap. Increases in insoluble monomer amounts were also measured in *S. tuberosum* tuber periderms that were held in nearly 100% humid storage conditions for 7-30 days (Kolattukudy and Dean 1974; Schreiber et al. 2005a).

The two most abundant SPAD monomers in *I. germanica*'s MEX were the C18:1 α,ω -dioic acid and the C18:1 ω -OH fatty acid; both are characteristic of suberin. Interestingly, these monomers were not detected in the soluble fraction. Yang and Bernards (2006) similarly measured these monomers in abundance in the insoluble fraction, and only in trace amounts in the soluble fraction of *S. tuberosum* tuber periderm – the authors provided two possible explanations. 1) Once ω -OH fatty acids and α,ω -dioic acids are synthesized, they are rapidly transferred into the apoplast and then immediately incorporated into the SPAD. 2) Fatty acids may be transferred to the apoplast and incorporated into the SPAD, where they are then ω -hydroxylated into ω -OH fatty acid, and possibly oxidized into α,ω -dioic acid. These explanations still need to be tested. Nevertheless, it is probable that the increased production of C18:1 α,ω -dioic acid and ω -OH fatty acid, especially in dehydrating conditions, is the result of an up-regulation in the synthesis and/or activity of enzymes involved in SPAD monomer biosynthesis. Such enzymes include the units in the fatty acid elongation complex (including β -ketoacyl-CoA synthase [KCS]), fatty acid desaturases, cytochrome P450 monooxygenases (P450), ω -hydroxyacid dehydrogenases, and possibly SPAD polymerizing enzymes such as polyester synthases (including glycerol-3-phosphate acyltransferase5 [GPAT5]) (Kolattukudy and Dean 1974; Kolattukudy 1980; Bernards 2002; Franke and Schreiber 2007; see section 1.4.2, Chapter 1 for more details). Functional

characterization of such enzymes is ongoing (KCS: Franke et al. 2009; Lee et al. 2009; Serra et al. 2009a; P450: Höfer et al. 2008; Compagnon et al. 2009; Serra et al. 2009b; GPAT5: Beisson et al. 2007; Li et al. 2007; see section 6.12, Chapter 6 for more details). The up-regulation of SPAD monomer biosynthesis in dehydrating conditions may partially allow *I. germanica*'s MEX to better retard water loss. However, one must take into account results from the soluble fraction before drawing physiological conclusions.

Total soluble monomer accumulation varied between growth conditions and within the air gap growth condition. Specifically, in air gap-exposed tissue, production and accumulation of soluble monomers were very high in the first exodermal layer but were significantly lower in the second and third layers (see Figs. 4.8, 4.9). Such trends pointed to a targeted effect on the outermost exodermal layer of air gap tissue.

The percent composition of the soluble fraction changed between exodermal maturation stages and between growth conditions. Particularly, the changes between the relative contributions of fatty acids and alkanes were notable (see Table 4.2). In submerged tissue, as more exodermal layers matured, the contribution of fatty acids declined while the alkane contribution increased. In air gap-exposed tissue, the fatty acid contribution decreased across the first two exodermal layers, while the alkane contribution increased. Then, in the third exodermal layer, fatty acid contribution increased as alkane contribution decreased (see Figs. 4.9 - 4.11). Importantly, in the first exodermal layer of air gap-exposed tissue, the alkane contribution was more than double that of the corresponding layer in submerged tissue. Furthermore, the measured abundance and accumulation of alkanes in the outermost exodermal layer of air gap tissue were on average 2.5-fold and 4-fold greater, respectively,

than in the same layer of submerged tissue (see Figs. 4.9, 4.11). Therefore, in response to the dehydrating air gap, the rate of alkane synthesis was greatly increased and accumulation was diverted toward the outermost exodermal layer.

A combination of the high alkane/wax accumulation, and high α,ω -dioic acid and ω -OH fatty acid deposition in the outermost exodermal layer of air gap-exposed tissue may be the key factor in restricting water loss from the underlying tissues. Previous work has shown that as *I. germanica*'s MEX matures in a humid air gap, radial water permeability is reduced (see Chapter 3). However, the overall number of suberized exodermal layers may not necessarily enhance impermeability. This counter-intuitive statement is supported by the following three examples. 1) North and Nobel (1995) measured radial water permeability in *Agave deserti* root regions that had the same number of exodermal layers but were exposed to either well-watered or drought conditions. The tissue exposed to drought was significantly less permeable than the well-watered subjects. 2) In another example, Vogt et al. (1983) measured water permeability across the multiseriate periderm of *S. tuberosum* tubers. Permeability across the periderm from freshly harvested tubers was greater by about one order of magnitude compared with periderm of tubers that were harvested and then stored in humid air for only 5 d. 3) Lastly, Schreiber et al. (2005a) added to Vogt et al.'s (1983) work by comparing the water permeability of old, 'native' periderm to newly-developed, 'wound-induced' periderm. In native periderm, there were consistently 8 ± 2 phellem cell layers present during the 30 d of storage out of soil. Water permeability decreased significantly during the first 3 d of storage, but there was no change to the permeability between days 3-28. In wound periderm, the number of cell layers increased to 6 during 30 d in storage, and

its water permeability progressively decreased during that time. However, the permeability of wound periderm at 30 d was more than two orders of magnitude greater than that of the native periderm. These differences in water permeability are known to be caused, in part, by the suberin-associated waxes within the periderm of *S. tuberosum* tubers (Soliday et al. 1979; Vogt et al. 1983; Schreiber et al. 2005a). Intriguingly, while there were no major differences in the suberin composition between native and wound periderm, the native periderm contained 40-50% more suberin and wax monomers than wound periderm (Schreiber et al. 2005a). Then, after solvent extraction of the waxes, water permeability increased by a factor of 100 in native periderm and by a factor of 2 to 10 in wound periderm (Schreiber et al. 2005a). It is not known if the waxes were evenly distributed through the periderm or if they were targeted to specific phellem layers. For the MEX of *I. germanica*, the up-regulation of wax synthesis and accumulation in the outermost layer of air gap-exposed tissue indicates that this layer is likely to be the most physiologically important factor for the retention of water inside the root. In addition, the concomitant induction of C18:1 α,ω -dioic acid and ω -OH fatty acid synthesis and deposition would increase the lipophilicity of the suberin and, perhaps more importantly, act as a scaffold for the prolific wax accumulation in the outermost exodermal layer. It is postulated that this localized and abundant monomer accumulation in the first mature exodermal layer is more important for radial water impermeability than the overall number of mature exodermal layers.

Lastly, the accumulation of the soluble fatty acids is notable as this monomer class comprised the majority of the soluble fraction. The abundance of C16 and C18 primary fatty acids was more uniform across exodermal layers in submerged tissue compared with air gap

tissue in which monomers were targeted mainly to the first exodermal layer (see Fig. 4.10). Short-chained primary fatty acids, particularly C16, C18 and C18:1, are most likely components of membrane phospholipids (which would be liberated as methyl esters during MeOH/HCl treatment), but may also be biosynthetic precursors for SPAD monomers and waxes (including long chain fatty acids, alkanes and fatty alcohols) (Galliard 1973; Yang and Bernards 2006).

In conclusion, acceleration in the maturation of *I. germanica*'s MEX when exposed to a humid air gap was detected chemically as an up-regulation in the synthesis and deposition of fatty acids, α,ω -dioic acids, ω -OH fatty acids, and ferulic acids in the SPAD, with the associated accumulation of soluble compounds (made up of alkanes, fatty acids, fatty alcohols, and ferulic acid), especially in the outermost exodermal layer. The percent monomer composition of the SPAD changed very little between exodermal maturation stages and between growth conditions. The two most abundant SPAD monomers were the C18:1 α,ω -dioic acid and the C18:1 ω -OH fatty acid. Interestingly, these monomers were produced and deposited in significantly greater amounts in the first two exodermal layers of air gap-exposed tissue compared with the corresponding layers of submerged tissue. The composition of the SPAD of *I. germanica* is similar to that of *S. tuberosum* tuber periderm. The percent composition of soluble compounds from *I. germanica* suberin changed significantly between exodermal maturation stages and between growth conditions, exemplified by an increased alkane accumulation in the first exodermal layer of air gap-exposed tissue. Targeted production and deposition of alkanes, α,ω -dioic acids and ω -OH fatty acids in the outermost exodermal layer probably function synergistically to retain water

inside the root when it is exposed to dehydrating growth conditions. The abundance and deposition of these key lipophilic monomers in specific tissue locations is likely more important for enhancing water retention than the overall number of suberized exodermal layers.

4.6 Supplementary data

See Appendix B for Supplementary Figures 4.1 – 4.8. Supplementary Figure 4.1 - Change in amounts of α,ω -dioic acids in the SPAD of the maturing MEX in *Iris germanica* roots.

Supplementary Figure 4.2 - Change in amounts of ω -OH fatty acids in the SPAD of the

maturing MEX in *Iris germanica* roots. Supplementary Figure 4.3 - Change in amounts of

fatty acids in the SPAD of the maturing MEX in *Iris germanica* roots. Supplementary Figure

4.4 - Change in amounts of ferulic acid in the SPAD of the maturing MEX in *Iris germanica*

roots. Supplementary Figure 4.5 - Change in amounts of fatty acids in the soluble suberin

fraction of the maturing MEX in *Iris germanica* roots. Supplementary Figure 4.6 - Change in

amounts of alkanes in the soluble suberin fraction of the maturing MEX in *Iris germanica*

roots. Supplementary Figure 4.7 - Change in amounts of fatty alcohols in the soluble suberin

fraction of the maturing MEX in *Iris germanica* roots. Supplementary Figure 4.8 - Change in

amounts of ferulic acid in the soluble suberin fraction of the maturing MEX in *Iris*

germanica roots.

Chapter 5

Suberin biosynthesis in *Allium cepa*'s maturing exodermis

5.1 Overview

Suberin is a complex biopolymer composed of a poly(aliphatic) domain (SPAD) and a poly(phenolic) domain (SPPD). These two domains are covalently linked but are also spatially distinct with the SPPD thought to be embedded in the cell wall and the SPAD located between the wall and plasma membrane. Suberin is typically confined to specialized cell types including root exodermal cells, but its synthesis in a maturing exodermis is still not well understood. For the current work, hydroponically grown *Allium cepa* roots were used as models to analyze SPAD and SPPD synthesis in a maturing uniseriate exodermis. Roots were divided into four maturation zones based on the growth rate and the deposition of suberin lamellae in maturing exodermal cells as determined by histochemical analyses. Exodermal and epidermal cell layers were separated from the underlying layers in each maturation zone, and then soxhlet-extracted with chloroform/methanol to remove the soluble monomer fraction of suberin. Then, the tissue was either transesterified with methanolic HCl to depolymerize the SPAD or hydrolyzed with alkaline nitrobenzene to depolymerize the SPPD. All monomers were quantified and identified by GC-MS. Temporal patterns for the synthesis of the SPAD, but not for the SPPD, were revealed upon resolution of the soluble and insoluble suberin metabolite profiles. The composition of the soluble fraction was essentially unchanged as the exodermis matured. In contrast, the SPAD composition differed during maturation, mainly due to significant increases in the deposition of two key SPAD monomers

(C18:1 α,ω -dioic acid and C18:1 ω -OH fatty acid). It is proposed that the exodermal maturation zones with corresponding suberin metabolite profiles be used as targets for the functional enzymatic characterization of suberin biosynthetic pathways.

5.2 Introduction

Suberin is a complex biopolymer that, in a suberin lamella, is composed of two spatially distinct but covalently-linked domains. 1) The poly(phenolic) domain (SPPD) is proposed to be embedded in the primary cell wall, and 2) the poly(aliphatic) domain (SPAD) is located between the cell wall and plasma membrane (after Bernards 2002; Mattinen et al. 2009). Typical monomeric compositions of the two domains have been determined through analyses of depolymerized compounds isolated from mature tissues, primarily from *Solanum tuberosum* tuber periderm (reviewed in Kolattukudy 1980, 1984; Bernards 2002). SPPD is rich in hydroxycinnamic acid derivatives with less relative amounts of amides and monolignols. Key derivatives released after hydrolysis of the SPPD include *p*-hydroxybenzaldehyde, vanillin and syringin (Borg-Olivier and Monties 1993; Negrel et al. 1996; see also Bernards and Lewis 1998). The location and chemical nature of the SPPD establishes it as a structure restrictive to microbial infection (Kolattukudy 1980, 1984; Lulai and Corsini 1998). SPAD is thought to be a glycerol-bridged, three dimensional polymer that is rich in fatty acid derivatives including ω -hydroxy fatty acids, α,ω -dicarboxylic acids, mid-chain oxidized fatty acids, and long-chain fatty acids. The ω -hydroxy fatty acids and α,ω -dicarboxylic acids are typically the two most abundant monomer classes that are deposited in the SPAD. Other commonly found monomer classes include intercalated alkanes and

esterified hydroxycinnamic acids. The location and chemical nature of the SPAD establishes it as a structure restrictive to radial water and solute transport (Kolattukudy and Dean 1974; Soliday et al. 1979; Vogt et al. 1983; Evert et al. 1985; Zimmermann et al. 2000; Hose et al. 2001; Schreiber et al. 2005a; see Chapter 3). The amounts of all these monomers and the relative composition of the SPAD can vary between different species (Kolattukudy and Dean 1974; Kolattukudy 1980, 1984; Holloway 1983; Matzke and Riederer 1991; Zeier and Schreiber 1998, 1999; Zeier et al. 1999a, b; Graça and Pereira 2000a, b; Bernards 2002, and references therein). These typical SPAD and SPPD monomer profiles have been used, in conjunction with genetic and functional enzymatic information, to predict how suberin lamellae are synthesized.

Recent developmental time-course investigations into suberin biosynthesis have begun to reveal the dynamic nature of these metabolic processes. Previously, Yang and Bernards (2006) used developing wound-induced periderm from *Solanum tuberosum* tuber to measure the changes in composition and abundance for monomers that were organic solvent-extractable (soluble fraction), and monomers polymerized in the SPAD (insoluble fractions). Three days after wound periderm formation was started, ω -OH fatty acids, α,ω -dioic acids, and fatty acids ($>C_{20}$) were detected in the insoluble fraction. The abundance of these monomers increased progressively for three more days. On the other hand, in the soluble fraction, the ω -OH fatty acids and α,ω -dioic acids were detected in only trace amounts, but $>C_{20}$ fatty acids and alkanes were present in increased amounts as the periderm developed. In another example, Thomas et al. (2007) measured the composition and abundance of the soluble fraction and insoluble SPAD and SPPD fractions in the maturing endodermis of

Glycine max roots. They measured marked increases of α,ω -dioic acids, ω -OH fatty acids, primary fatty acids, alkanes, vanillin, and syringin as half of the endodermal cells became encrusted with suberin lamellae (160 mm from the root tip). The data obtained by Yang and Bernards (2006) and Thomas et al. (2007) could not have been determined without analyzing tissue specimens at multiple stages of maturation; in other words, developmental time-course analyses were necessary.

Allium cepa root anatomy and physiology have been well studied (Moon et al. 1984; Peterson and Perumalla 1984; Perumalla and Peterson 1986; Barnabas and Peterson 1992; Melchior and Steudle 1993; Stasovski and Peterson 1993; Barrowclough and Peterson 1994; Kamula et al. 1994; Taleisnik et al. 1999; Barrowclough et al. 2000; Ma and Peterson 2000, 2001a, b; Cholewa and Peterson 2001; Waduwara et al. 2008). In particular, the steps in the maturation (meaning concurrent deposition of Casparian bands and suberin lamellae) of the exodermis of *A. cepa* is known. The exodermis is single-layered (uniseriate) and dimorphic meaning there are two distinct cell lengths – referred to as short and long cells (von Guttenberg 1968; Shishkoff 1986; Perumalla et al. 1990; Kamula et al. 1994). Casparian bands are deposited in all exodermal cells regardless of cell length. In 100-mm-long, hydroponically grown *A. cepa* roots, exodermal Casparian bands are located 50-65 mm from the root tip (Perumalla and Peterson 1986; Barrowclough and Peterson 1994). Suberin lamellae, on the other hand, are first deposited in the long cells concurrent with or soon after Casparian band deposition (60-70 mm from the root tip; Perumalla and Peterson 1986; Barrowclough and Peterson 1994). The majority of short cells are not encrusted with suberin lamellae in early stages of development; those short cells that lack suberin lamellae function

as passage cells (Esau 1965; von Guttenberg 1968; Kamula et al. 1994; Peterson and Enstone 1996). With the deposition of suberin lamellae, plasmodesmata are severed and the cells die shortly thereafter (Ma and Peterson 2000). The importance of the exodermis as a physiological sheath has often been overlooked, but more than 90% of tested angiosperms have roots with an exodermis (Peterson and Perumalla 1990; Perumalla et al. 1990; Meyer et al. 2009; see Chapter 2). For the current work, roots of *A. cepa* were used to study suberin monomer deposition in the peripheral cell layers, including the epidermis but mainly the Casparian bands and suberin lamellae of a uniseriate exodermis, at multiple stages of maturation.

End point-analyses of the suberin from the mature exodermis of *A. cepa* roots have been conducted previously. Zeier and Schreiber (1998) calculated the total yield of exodermal aliphatic suberin (approximately $23 \mu\text{g mg}^{-1}$) and phenolic monomers (approximately $35 \mu\text{g mg}^{-1}$) at a single mature region in *A. cepa* roots. These roots were hydroponically grown and were at least 300 mm in length at harvest. It is assumed that the measured monomer amounts corresponded to an exodermis that had been fully mature for about 14 days. To extend this previous work, an objective for the current work was to analyze the suberin monomer composition at multiple stages of exodermal maturation in tissue between 0-5 days old.

In the current work, hydroponically grown *A. cepa* adventitious roots were used as a model to analyze the insoluble and soluble monomer compositions and quantities for both the SPAD and SPPD in the maturing peripheral cell layers. These cell layers included the maturing uniseriate exodermis and the epidermis. *Allium cepa* roots were amenable to these tests because many roots are generated per bulb in hydroponic conditions, and the roots

produce very few or no lateral roots under ideal growing conditions. Furthermore, since *A. cepa*'s exodermal maturation is similar between roots grown in vermiculite or hydroponics, maturation has been proposed to be under a stringent genetic regulation (Peterson and Perumalla 1984; Perumalla and Peterson 1986; Stasovski and Peterson 1993; Barrowclough and Peterson 1994; Kamula et al. 1994; Ma and Peterson 2000, 2001a). It was hypothesized that as the exodermis matured, the SPAD and SPPD compositions would change and that the incorporation of key SPAD and SPPD monomers into the polymer would increase. It was expected that the findings of this work would lead to a more complete understanding of the dynamics of suberin monomer synthesis during the maturation of a uniseriate exodermis.

5.3 Materials and methods

5.3.1 Growth conditions and plant material

Adventitious root growth from *Allium cepa* (cv. Wolf) bulbs was initiated and maintained in aerated hydroponic culture. A 16 L hydroponic tank was partitioned in half and each compartment filled with nutrient solution (0.7 mM K₂SO₄, 0.5 mM Ca(NO₃)₂, 0.5 mM MgSO₄, 0.1 mM KCl, 0.1 mM KH₂PO₄, 0.01 mM Fe(III)-EDTA, 1.0 μM H₃BO₃, 0.5 μM MnSO₄, 0.5 μM ZnSO₄, and 0.2 μM CuSO₄). This solution was continuously aerated using bubbling stones connected to an aquarium pump. To reduce light intensity in the root zone, the tank walls were covered with opaque plastic wrap and the top was covered with two layers of shading cloth. The tank was located in a greenhouse with supplemental lighting (18 hrs d⁻¹). *Allium cepa* bulbs (approximately 80 mm in diameter) were peeled to remove the

outer dried epidermal scales, and then placed on two stacked styrofoam sheets that floated on the nutrient solution inside the filled hydroponic tank. Each styrofoam sheet (215 mm long x 195 mm wide x 10 mm thick) had two holes (65 mm diameter) cut into them allowing only the basal part of two bulbs to be submerged in solution (Fig. 5.1). New roots began to emerge from the bulb after 5-7 d.

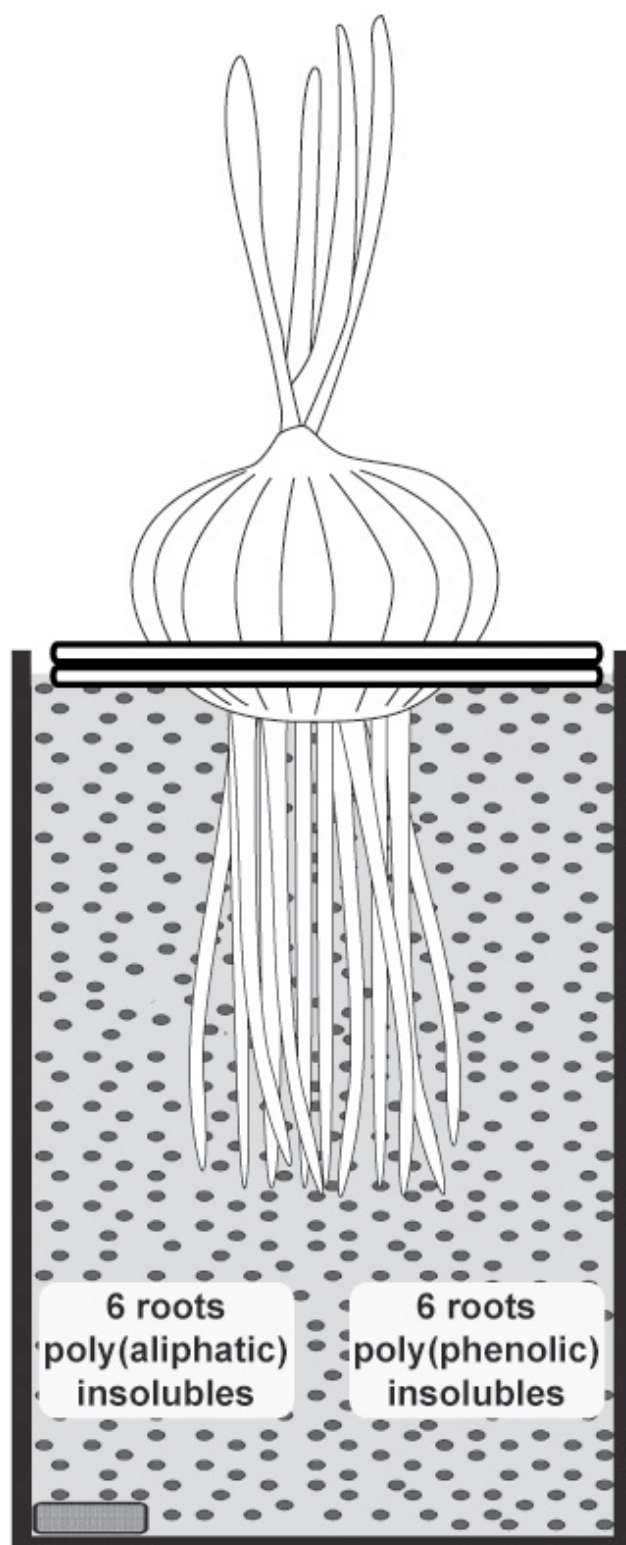
5.3.2 Root growth rate measurements

Root growth rates were measured during two separate periods, using six bulbs with 12 roots total in the first period and four bulbs with 11 roots total in the second period. The lengths of selected roots were measured initially (>20 mm) followed by a second measurement 2-3 d later.

5.3.3 Exodermal maturation

Exodermal maturation refers to the concurrent deposition of Casparian bands and suberin lamellae. To observe this process, roots that were 120 mm or slightly longer were freehand-cross sectioned with razor blades at several measured distances from the root tip. Sections were stained with Sudan Red 7B for aliphatic suberin (Brundrett et al. 1991), or Toluidine blue O as a general polychromatic dye (O'Brien et al. 1964). Stained specimens were observed with a Zeiss Axiophot epifluorescence microscope using only white light (Carl Zeiss Inc., Canada). Photomicrographs were taken with a Q-Imaging digital camera (Retiga 2000R, Fast 1394, Cooled Mono, 12-bit; Quorum Technologies Inc., Canada).

Figure 5.1 Illustration of the hydroponic system used to initiate and maintain *Allium cepa* root growth (not to scale). Nutrient solution was constantly aerated with atmospheric air using a bubbling stone (small grey rectangle). The bulb was placed on two stacked styrofoam sheets so it could float on the solution's surface. The basal end of the bulb, submerged in solution, was the location of root emergence. From each bulb, 12 roots (each 120 mm in length) were used for suberin monomer analyses; 6 roots pooled for the poly(aliphatic) insoluble fraction analysis (1 replicate) and 6 roots pooled for the poly(phenolic) insoluble fraction analysis (1 replicate). A total of 6 bulbs were cultured, hence there were 6 repetitions available for both the poly(aliphatic) and poly(phenolic) fractions.



5.3.4 Root tissue isolation

When six or more roots per bulb had grown to lengths of 120 mm or slightly longer, they were individually excised from the base of the bulb for isolation of the peripheral cell layers (including the epidermis, exodermis, and some unmodified central cortex parenchyma) that comprised the outer part of the root (OPR). Each root was divided into four segments based on the mean growth rate per day and observations of exodermal maturation. Root segment diameters (1.0-1.5 mm) were measured with a digital caliper in order to calculate root surface area. Then, from each root segment, the OPR was stripped from the inner tissues using a wire stripping tool (AWG = 20-30; Mastercraft Canada). The stripped tissue was flash frozen by quickly placing it in a 1.5 mL eppendorf tube that was floating in liquid nitrogen. Frozen tissue was stored at -20°C prior to suberin monomer extraction. Root regions that were not stripped were freehand-cross sectioned and stained (as described above) to verify the stage of exodermal maturation. Stripped segments were stained with TBO or cross sectioned and stained to verify that the stripping method removed only the outermost root tissue layers.

Stripped tissue was pooled with the equivalent segments of six roots that originated from the same bulb, hence comprising one replicate for each of the four maturation zones. This was repeated for an additional six roots from the same bulb; therefore, a total of two replicates for each zone were collected per bulb. Lastly, six bulbs were cultured totaling 12 replicates: 6 replicates for each of the poly(aliphatic) and poly(phenolic) insoluble fraction analyses, as described below (see Fig. 5.1).

5.3.5 Suberin monomer extraction and analysis

Soluble compound extraction. Frozen OPR tissue was quickly placed into chloroform/methanol (2:1) filled cellulose extraction thimbles (Whatman Ltd., Maidstone, England). Thimbles now containing the OPR tissue were placed into a micro-soxhlet extractor, which was used to extract soluble compounds (including unpolymerized suberin monomers, waxes, and membrane components). Extraction included two 3.5 h treatments with 2:1 CHCl₃/CH₃OH, followed by an overnight treatment with CHCl₃. Following each treatment, the solvent containing the soluble extracts was pooled and concentrated by evaporating the solvent with a rotary evaporator (Buchi, Switzerland) under vacuum. With little volume remaining, the solvent was transferred to a 5 mL glass vial to complete the drying with a stream of N₂. This dried soluble residue was then hydrolyzed in 2 M MeOH/HCl (Supelco/Sigma-Aldrich, USA) at 80°C for 2 h, yielding the methyl esters of free carboxylic acids. Vials were removed from the heat, and NaCl-saturated water was added to each to stop the reaction. Internal standard (10 µL of 1 mg/mL triacontane) was added and the aliphatics extracted with hexane (three times). Each time, after the solvents were allowed to separate, the upper hexane phase was pipetted into a clean vial. The pooled hexane phases containing the soluble extracts were dried down under a stream of N₂ gas. Then the remaining free alcohols within the dried residue were trimethylsilylated (TMS) using 50 µL each of pyridine and 99% BSTFA + 1% TMS (Supelco/Sigma-Aldrich, USA), at 70°C for 40 min.

Insoluble poly(aliphatic) compound extraction. Soxhlet extracted-OPR tissue was recovered from the cellulose thimbles as it still contained the insoluble fraction (i.e.,

polymerized suberin monomers). This tissue was rinsed with acetone, dried at room temperature, and stored at 4°C. Prior to further processing, the dried OPR tissue weight was recorded (1-2 mg). Then half of the samples, or six replicates per maturation zone, were selected for MeOH/HCl transesterification in order to depolymerize the SPAD. Tissue was submerged in 0.5 mL of 2 M MeOH/HCl and incubated at 80°C for 2 h to allow hydrolysis and transesterification of ester-linked fatty acids (adapted from Browse et al. 1986). Note that the subsequent steps for this method were identical to those used for working-up the soluble extracts, specifically hexane partitioning and TMS derivatization (see above).

Gas chromatography-mass spectrometry. The methyl ester/TMS ether derivatives from the soluble and insoluble poly(aliphatic) monomer fractions were quantified with a Varian CP-3800 Gas Chromatograph equipped with a flame ionization detector (GC-FID). Monomer identification was accomplished with a Saturn 2000 ion trap Mass Spectrometer (GC-MS). A pair of CP-Sil 5 CB low bleed MS columns (WCOT silica 30 m x 0.25 mm ID) were installed in the GC, with one column directed to the FID and the other to the MS. The temperature of the injector oven was 250°C, and the FID oven was set to 300°C. After a 1 µL sample injection into each column (splitless mode), monomers were eluted using the following program: 70°C held for 2 min, ramped up to 200°C at 40°C min⁻¹ and held for 2 min, ramped up to 300°C at 3°C min⁻¹ and held for 9.42 min, for a total run time of 50 min. High purity helium was used as the carrier gas with a flow rate of 1 mL min⁻¹.

Insoluble poly(phenolic) compound extraction. The remaining six repetitions per maturation zone of soxhlet extracted-OPR tissue were chemically treated using nitrobenzene oxidation (NBO) for the hydrolysis of the SPPD (adapted from Meyer et al. 1998). SPPD

was first saponified by incubating the tissue samples in 0.5 mL of 1 M sodium hydroxide at 37°C for 24 h. Then the NaOH was pipetted off and the tissue rinsed three times with dH₂O, followed by a single rinse with 80% methanol, and finished with a 30 min soak in 100% acetone. The acetone was pipetted off and the tissue allowed to air-dry overnight. Dried tissue was then transferred to 2 mL ampoules and submerged in 500 µL of 2 M NaOH and 30 µL of nitrobenzene (Sigma-Aldrich, USA). Ampoules were sealed using an Ampulmatic sealer (Model 29001, Bioscience Inc., USA), and then placed in a 160°C oven for 3 h. After this incubation, ampoules were cooled to room temperature, opened, and 5 µL of 3-ethoxy-4-hydroxybenzaldehyde (5 mg/mL) dissolved in pyridine was added to each sample as the internal standard. Samples were transferred to 4 mL collecting vials using two 1 mL volumes of dH₂O. The NBO hydrolysate was partitioned twice with 1 mL volumes of dichloromethane; the lower, organic phase was pipetted off and discarded. The remaining aqueous phase was acidified to pH 2 using concentrated hydrochloric acid. This phase was then partitioned twice with 900 µL volumes of ethyl ether. The ether phases were pipetted off and pooled into a clean, collecting vial for each sample. Anhydrous sodium sulphate was added, in small amounts, to each sample vial to capture residual water. Then the dried ether was transferred into small, clean vials and evaporated off under a stream of nitrogen. The dried residue was TMS derivatized using 50 µL each of pyridine and 99% BSTFA + 1% TMS (Supelco/Sigma-Aldrich, USA), at 70°C for 40 min. Samples were analysed on the same GC-MS equipment as above, but using the following parameters: initial oven temperature at 140°C for 1 min, then ramped up to 300°C at 12.5°C min⁻¹, for a total time of 16.4 min.

Data analysis. Soluble and insoluble monomers were identified using their retention time, retention index, and by matching the measured mass spectra to the spectra of authentic standards. These same monomers were then quantified from their peaks on the GC-FID chromatograms and with the internal standard and standard calibration curves. Then the monomer amounts were calculated per root segment surface area ($\mu\text{mol mm}^{-2}$), in order to reveal trends in monomer deposition and accumulation in the maturing exodermis. Data were then statistically analyzed within monomer classes and between exodermal maturation zones by first using an Analysis of Variance (ANOVA). If significant differences were noted, then a Least Significant Difference post-hoc test (LSD) was used, where $P \leq 0.05$. Also calculated was the percent contribution of each monomer class, within each exodermal maturation zone, to the total compound fraction.

5.4 Results

5.4.1 *Allium cepa* root growth, anatomy, and exodermal maturation

Each *A. cepa* adventitious root was segmented into four zones based on the mean growth rate per day and the sequence of exodermal maturation. Root growth rate data from the two independent measurement periods were pooled to calculate a mean growth rate of $23.89 \pm 4.64 \text{ mm d}^{-1}$ (mean \pm standard deviation, $n = 23$, data not shown). Next, zones of exodermal maturation were mapped in relation to the distance from the root tip and tissue age (Fig. 5.2). Starting near the root tip, the length of the first zone equalled one and a half days of growth (0.5-2 d old tissue and 10-48 mm from the tip; Fig. 5.2A). This first zone was called the

'Immature zone' since there was no visible suberin lamellae deposition in the exodermis (Fig. 5.3A). The lengths of the remaining three zones each corresponded to one day of growth. For the second zone, the tissue was 2-3 d old and 48-72 mm from the tip (Fig. 5.2B). This zone was termed 'Transition zone 1' because it corresponded to the position along the root where exodermal suberin lamellae deposition was first detected (Fig. 5.3B). For the third zone, the tissue was 3-4 d old and 72-96 mm from the tip (Fig. 5.2C). This zone was called 'Transition zone 2' because although suberin lamellae continued to be deposited in more exodermal cells, it was not deposited in all cells at the same age or distance from the root tip (Fig. 5.3C). In the fourth and final zone, the tissue was 4-5 d old and 96-120 mm from the tip (Fig. 5.2D). This oldest zone was termed the 'Mature zone' because the majority of exodermal cells were now encrusted with suberin lamellae, with the exception of very few passage cells (Fig. 5.3D). Diffuse suberin was detected in epidermal cells between Transition zone 1 and the Mature zone (Fig. 5.3B-D).

The root-stripping device (i.e., a wire stripping tool) worked well for separating the outer part of the root (OPR) from the underlying tissue layers. When comparing cross sections of unstripped and stripped roots, it was clear that the stripping device had removed the epidermis, exodermis, and some central cortex layers (Fig. 5.3E,F). Furthermore, when viewing the TBO-stained surface of a partially stripped root, the absence of the epidermis and exodermis from the stripped region was unmistakable due to the differential staining reaction of the exodermis and central cortex (Fig. 5.3G).

Figure 5.2 Diagram of the key exodermal maturation zones in *Allium cepa* adventitious roots. The scale on the left refers to distance from the root tip. The scale on the right refers to root tissue age from the tip, based on the mean growth rate. Horizontal dashed lines separate the key maturation zones. (A) Immature zone = 10-48 mm from the root tip, 0.5-2 d old. (B) Transition zone 1 = 48-72 mm from the tip, 2-3 d old. (C) Transition zone 2 = 72-96 mm from the tip, 3-4 d old. (D) Mature zone = 96-120 mm from the tip, 4-5 d old. Vertical dashed grey lines (in B and C) = exodermal suberin lamellae deposition in progress. Vertical solid grey lines (in D) = majority of exodermal cells have suberin lamellae (i.e., very few passage cells remained).

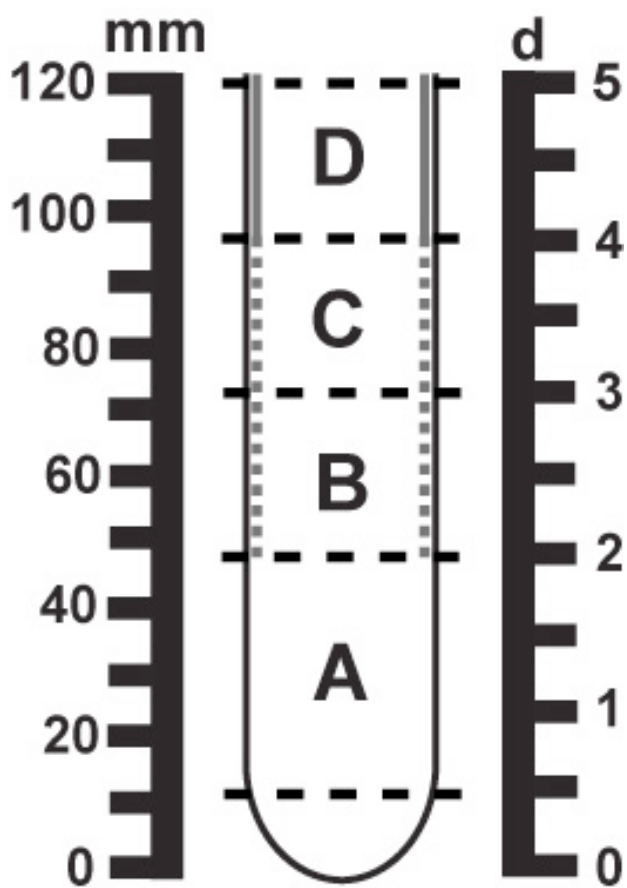
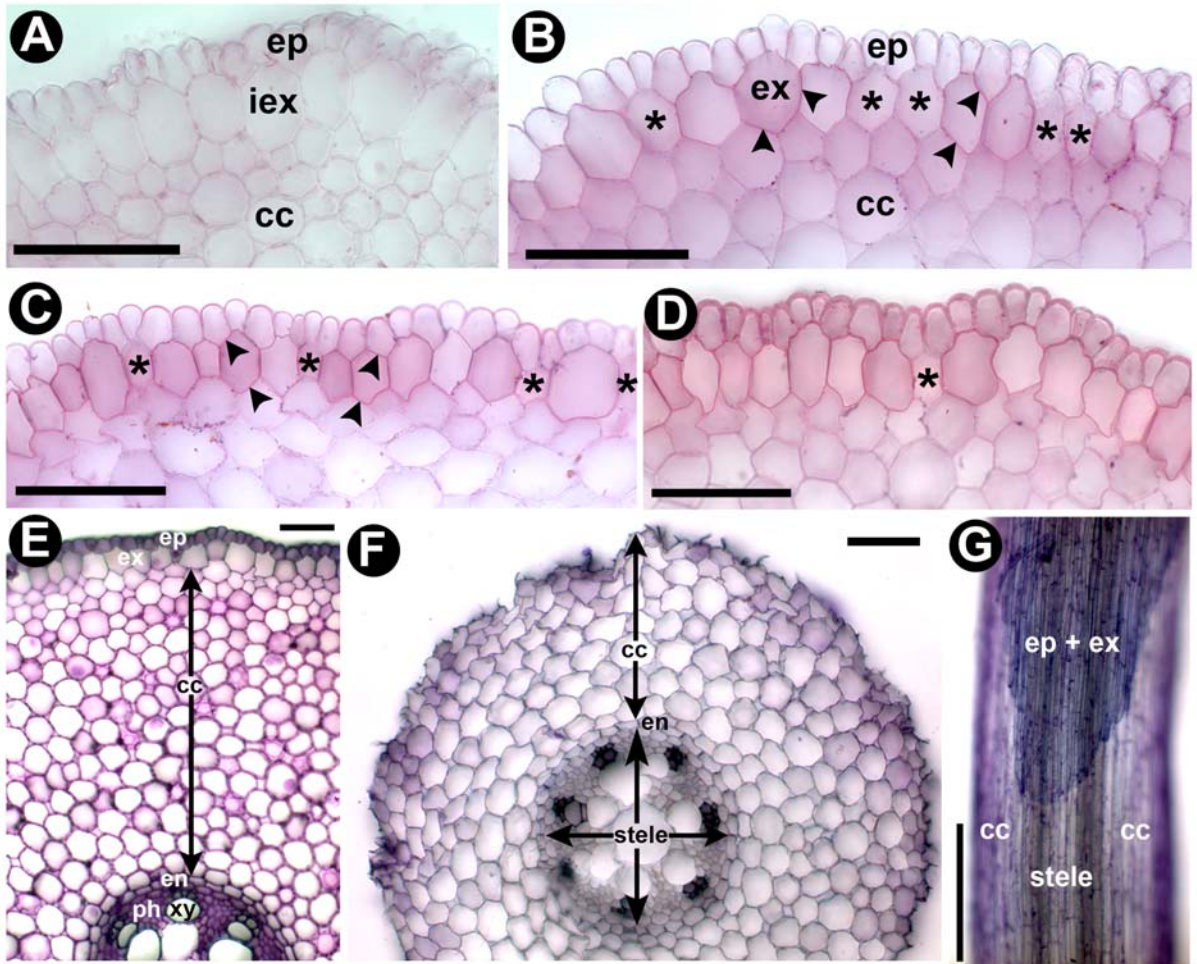


Figure 5.3 Photomicrographs of *Allium cepa* adventitious roots in cross section (A-F) and surface view (G). (A-D) Sections stained with Sudan red 7B; suberin lamellae appeared as red outlines in exodermal cells (arrowheads). (A) Immature zone, 30 mm from the root tip. (B) Transition zone 1, 60 mm from the root tip. (C) Transition zone 2, 80 mm from the root tip. (D) Mature zone, 110 mm from the root tip. (E-G) Specimens stained with TBO. (E) Unstripped root section with all tissue layers, 80 mm from the tip. (F) Stripped root section missing the epidermis, exodermis and some central cortex layers, 60 mm from the tip. (G) Root segment with an unstripped region (stained blue) and a stripped region (transparent and stained purple). The stele underlies the central cortex. Abbreviations: ep = epidermis; iex = immature exodermis; ex = exodermis; cc = central cortex; en = endodermis; ph = phloem; xy = xylem. Asterisks = exodermal cells without suberin lamellae. Scale bars for A-F = 100 μm ; scale bar for G = 500 μm .



5.4.2 Suberin chemistry

5.4.2.1 Poly(aliphatic) insoluble fraction

Total poly(aliphatic) insoluble fraction. The total poly(aliphatic) insoluble fraction includes all the monomers that were released from the SPAD following its depolymerization (transesterification) with MeOH/HCl. In general, the deposition of insoluble monomers gradually increased as the exodermis matured (Fig. 5.4A). From the immature zone to transition zone 2, deposition of suberin monomers increased slightly, albeit not significantly. However, with complete maturation of the exodermis, monomer deposition increased sharply and significantly. This increased deposition was on average nearly 2-fold greater than the rate of deposition in transition zone 2 (Fig. 5.4A). The composition of the poly(aliphatic) insoluble fraction changed substantially as the exodermis matured (see the following sections for more details). The components of the poly(aliphatic) insoluble fraction included C18:1 α,ω -dioic acid, ω -OH fatty acids (C16, C18:1, and C22), fatty acids (C16, C18, and C24), 2-OH fatty acids (C22 and C24), a C22 fatty alcohol, and ferulic acid (Table 5.1, Fig. 5.4B).

C18:1 α,ω -dioic acid. The C18:1 α,ω -dioic acid was the only dioic acid detected in the poly(aliphatic) insoluble fraction. Nonetheless, its deposition in the exodermis was intriguing. The amount of C18:1 α,ω -dioic acid was very low in the immature zone, but increased significantly into transition zone 2. Then, with the completed maturation of the exodermis (mature zone), the deposition of this monomer increased approximately 6-fold (Fig. 5.4B). The contribution of this monomer to the total poly(aliphatic) insoluble fraction

was only 2-4% from the immature zone to transition zone 1, but it increased radically to 10.5% in transition zone 2 and then up to 31% in the mature zone (Table 5.1).

ω-OH fatty acids. Three different ω-OH fatty acid monomers were detected (16:0, 18:1 and 22:0), with deposition of the C18:1 monomer showing the most significant developmental changes. The amount of the C18:1 ω-OH fatty acid was very low in the immature zone through to transition zone 1 (Fig. 5.4B); thereafter the amount of this monomer deposited in the SPAD began to increase significantly, from transition zone 2 through to the mature exodermal zone. In fact, the increase in deposition of this monomer from transition zone 2 to the mature zone was on average about 6-fold (Fig. 5.4B). As for the remaining two ω-OH fatty acids (C16 and C22), their deposition was fairly uniform across maturation zones (Fig. 5.4B). The total amount of ω-OH fatty acids accounted for an average of 12% of the poly(aliphatic) insoluble fraction in the immature zone, but increased to 21% in the mature zone (Table 5.1).

Fatty acids. The fatty acid group was composed of three monomers. Deposition of C16 and C18 fatty acids was low in the immature zone, but increased in transition zone 1 and then was unchanged through to the mature zone. However, the deposition of C24 was uniform across exodermal maturation zones but at lower amounts than C16 and C18 (Fig. 5.4B). The fatty acid group comprised an average of 32% of the poly(aliphatic) insoluble fraction in the immature zone, but decreased to 16.5% in the mature exodermal zone (Table 5.1).

2-OH fatty acids. There were two 2-OH fatty acid monomers detected, both with similar patterns of deposition. Deposition of C22 and C24 2-OH fatty acids in the SPAD increased from the immature zone to transition zone 1, but then decreased into transition zone 2, and

Figure 5.4 Total and individual insoluble SPAD monomers in the OPR of *Allium cepa*. (A) Total insoluble monomers. (B) Deposition of the different insoluble monomers. Data are displayed per unit of root segment surface area (in $\mu\text{mol mm}^{-2}$) for each maturation zone (legends inset). Values are means \pm standard deviation. Different lowercase letters within the total insolubles (A) or within each monomer class (B) indicate a significant difference ($P \leq 0.05$).

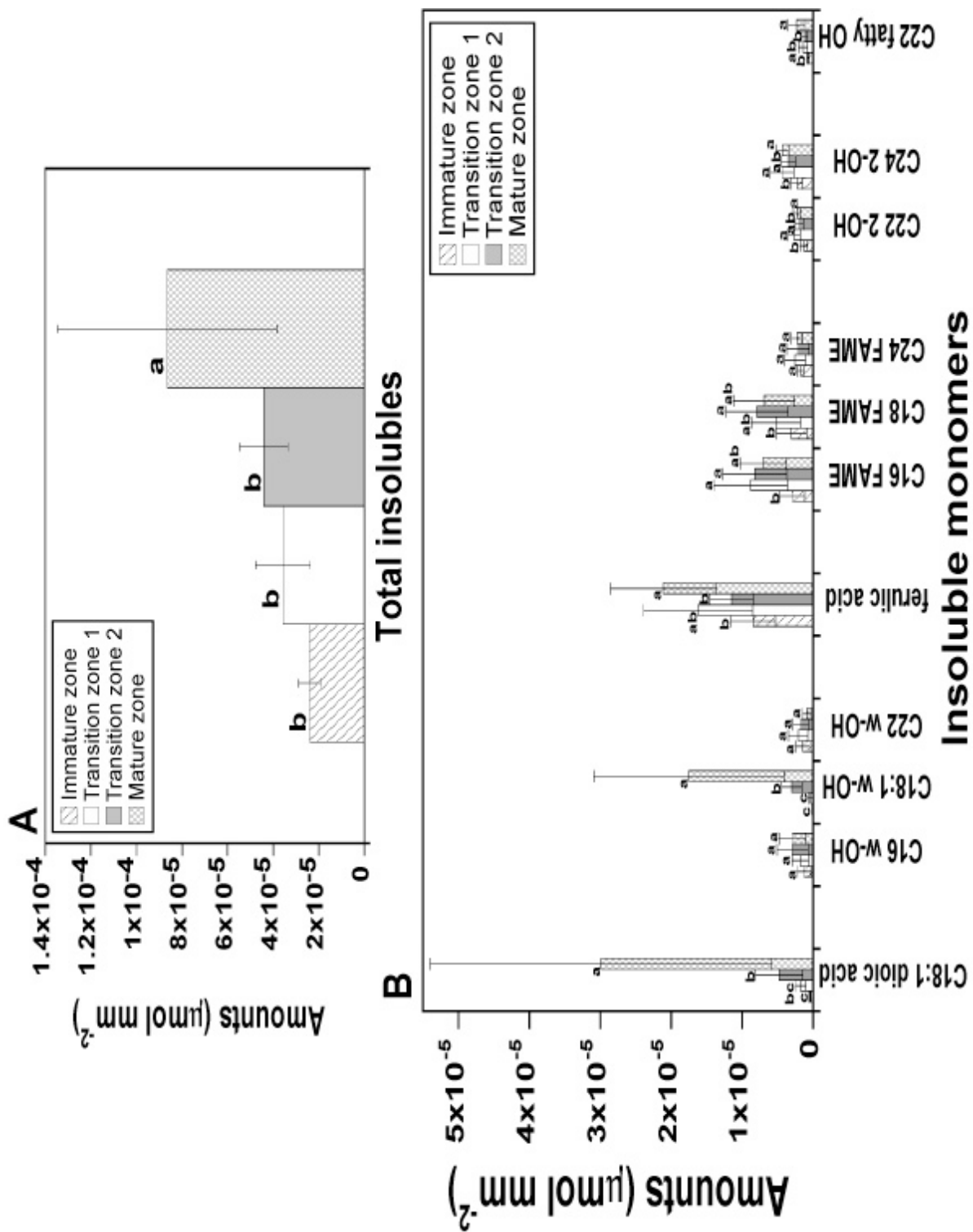


Table 5.1 Percent composition of the OPR of *Allium cepa*'s SPAD at the different exodermal maturation zones.

Compounds	Immature zone (%)	Transition zone 1 (%)	Transition zone 2 (%)	Mature zone (%)
C18:1 α,ω -dioic acid	2	4	10.5	31
ω -OH fatty acids	12	9	13.5	21
Ferulic acid	35	34	24	22
Fatty acids	32	35	38.5	16.5
2-OH fatty acids	16	15	11	6.5
C22 fatty alcohol	3	3	2.5	3
Sum	100	100	100	100

then did not change through to the mature zone (Fig. 5.4B). The 2-OH fatty acids accounted for an average of 16% of the poly(aliphatic) insoluble fraction in the immature exodermal zone, but this was reduced to 6.5% in the mature zone as other monomers were incorporated into the SPAD (Table 5.1).

C22 fatty alcohol. The C22 fatty alcohol monomer was the only fatty alcohol detected in the poly(aliphatic) insoluble fraction. Its deposition increased gradually from the immature zone to the mature zone (Fig. 5.4B). This fatty alcohol made up an average of just 3% of the poly(aliphatic) insoluble fraction across all exodermal maturation zones (Table 5.1).

Ferulic acid. Esterified ferulic acid deposition was substantial in the immature zone and gradually increased as the exodermis matured (Fig. 5.4B). Ferulic acid was detected in an average of 35% of the poly(aliphatic) insoluble fraction in the immature zone, but was reduced to 22% in the mature exodermal zone (Table 5.1).

5.4.2.2 Soluble fraction

Total soluble fraction. The total soluble fraction includes all the monomers that were not cross-linked to either the SPAD or SPPD. In general, the accumulation of soluble monomers showed no statistical differences along the developmental axis. However, there was a gradual decrease in accumulation from the immature zone to transition zone 2, followed by an increase in accumulation at the mature zone (Fig. 5.5). There was very little change in the percent composition of the soluble fraction as the exodermis matured (see the following sections for more details). The composition of the soluble fraction included fatty acids (C14 - C28), alkanes (C21 - C29), fatty alcohols (C14 - C28), ω -OH fatty acids (C20 - C24), and 2-OH fatty acids (C22 - C26) (Table 5.2, Figs. 5.6-5.10).

Figure 5.5 Total soluble monomer fraction in the OPR of *Allium cepa*. Data are displayed per unit of root segment surface area (in $\mu\text{mol mm}^{-2}$) for each maturation zone (legend inset). Values are means \pm standard deviation. Different lowercase letters within each graph indicate a significant difference ($P \leq 0.05$).

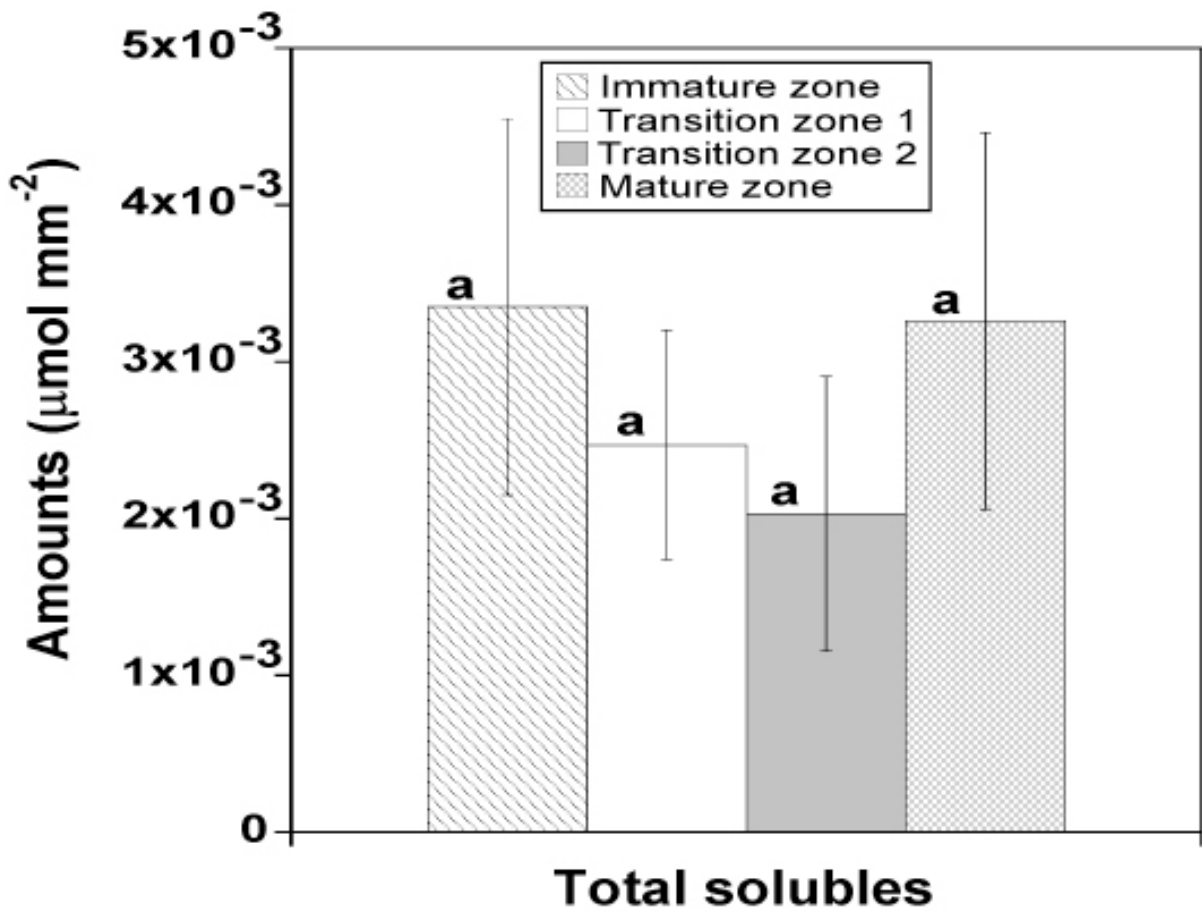


Table 5.2 Percent composition of the soluble monomer fraction in the OPR of *Allium cepa* at the different exodermal maturation zones.

Compounds	Immature zone (%)	Transition zone 1 (%)	Transition zone 2 (%)	Mature zone (%)
Fatty acids	52	45.5	44.5	47
Alkanes	37	37.5	36	35
Fatty alcohols	7	11	12	12
ω -OH fatty acids	3	5	5	5
2-OH fatty acids	1	1	1.5	1
Sum	100	100	100	100

Fatty acids. Soluble fatty acids were the most abundant group of monomers, comprising an average of 52% of the total soluble fraction in the immature exodermal zone, and declining slightly to 47% in the mature zone (Table 5.2). Fatty acid accumulation was uniform across the exodermal maturation zones (Fig. 5.6A).

The fatty acid group was composed of 13 different monomers, with the most abundant being the C16 and C18. Accumulation of C16 and C18 resembled the corresponding trends for the total fatty acid group. Briefly, for both C16 and C18 fatty acids, their accumulation was statistically uniform as the exodermis matured (Fig. 5.6B). Similarly, for the remaining, less abundant fatty acids, their accumulation was uniform across maturation zones. However, the C18:2 had a low accumulation in the immature zone followed by a sharply increased accumulation in transition zone 1 that then leveled off in the subsequent two maturation zones (Fig. 5.6B).

Alkanes. Alkanes were relatively abundant, comprising an average of 36% of the soluble fraction across exodermal maturation zones (Table 5.2). Alkane accumulation was uniform in each exodermal maturation zone (Fig. 5.7A).

The alkane group was composed of seven different monomers, with a fairly even abundance for each. Accumulation patterns were similar for all alkane monomers, as well as similar to the total alkane group trends (Fig. 5.7B).

Fatty alcohols. Fatty alcohols accounted for an average of 7% of the soluble fraction in the immature zone, increasing slightly to 12% in the mature zone (Table 5.2). Although there were no statistical differences in fatty alcohol accumulation between exodermal maturation

Figure 5.6 Accumulation of fatty acids in the soluble fraction in the OPR of *Allium cepa*. (A) Total fatty acids. (B) Accumulation of the different fatty acid monomers. Data are displayed per unit of root segment surface area (in $\mu\text{mol mm}^{-2}$) for each maturation zone (legends inset). Values are means \pm standard deviation. Different lowercase letters within the total fatty acids (A) or within each monomer chain length (B) indicate a significant difference ($P \leq 0.05$).

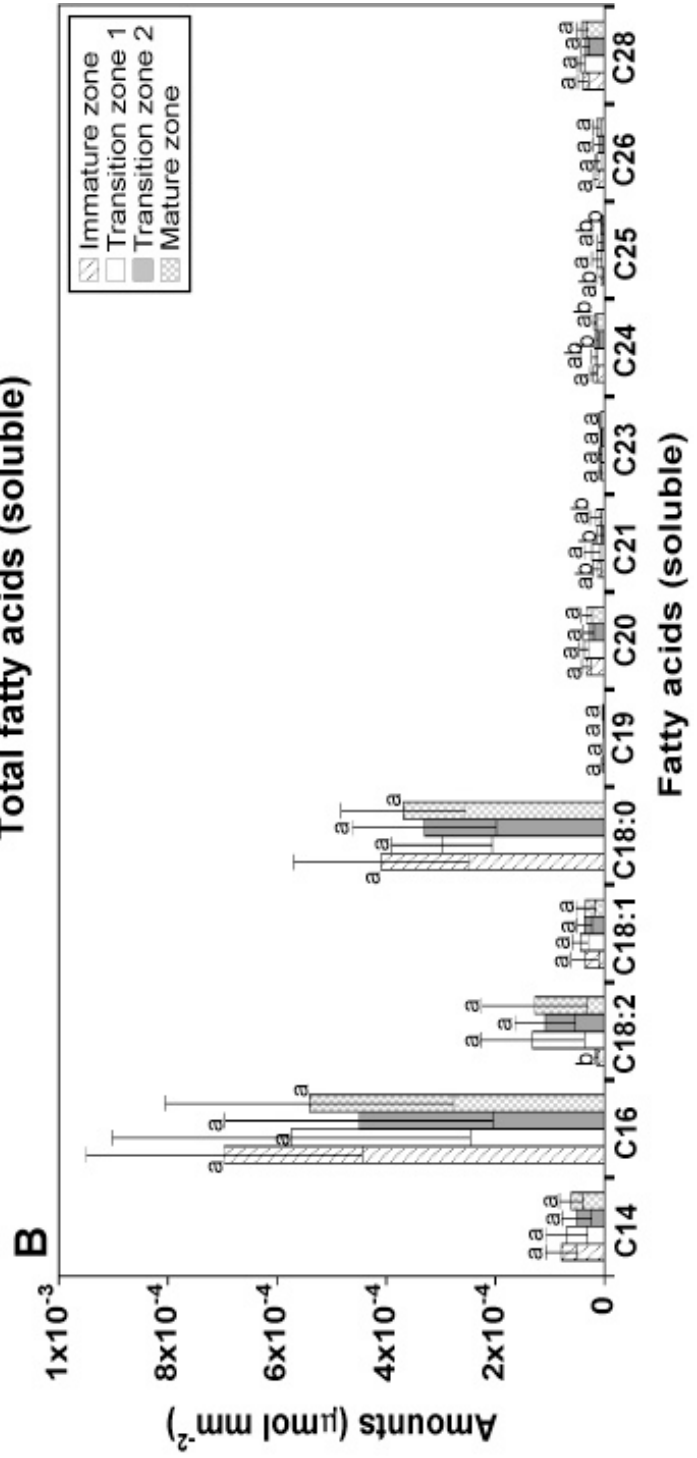
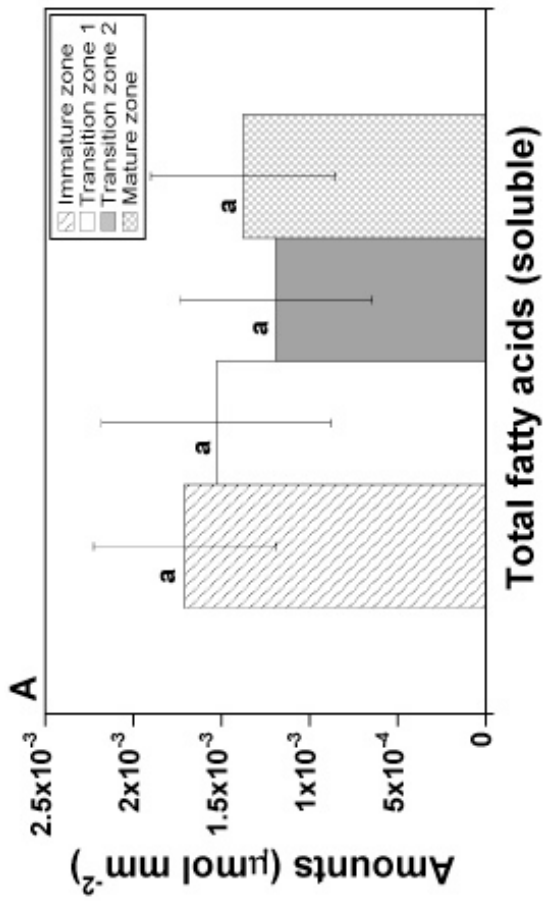
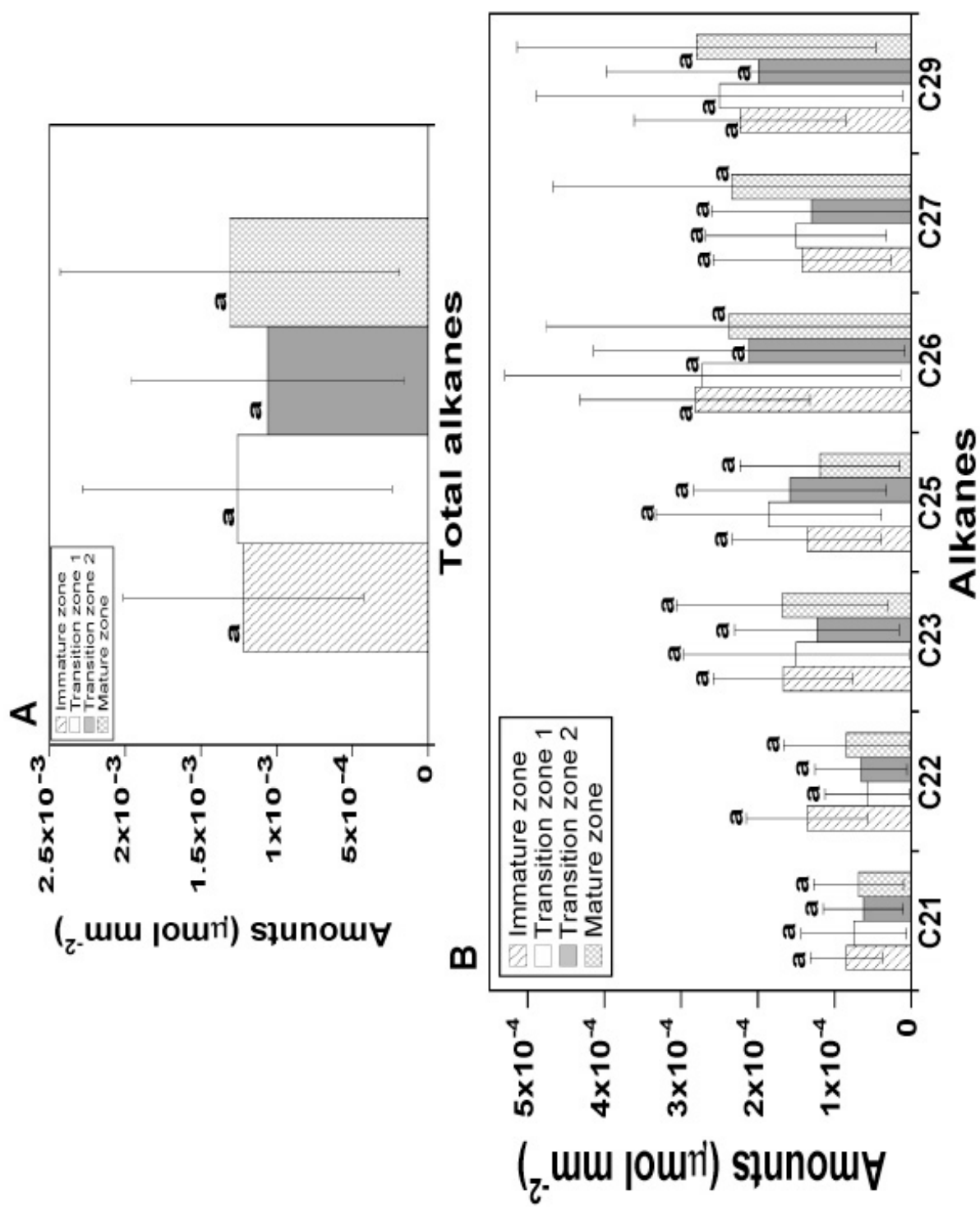


Figure 5.7 Accumulation of alkanes in the soluble fraction in the OPR of *Allium cepa*. (A) Total alkanes. (B) Accumulation of the different alkane monomers. Data are displayed per unit of root segment surface area (in $\mu\text{mol mm}^{-2}$) for each maturation zone (legends inset). Values are means \pm standard deviation. Different lowercase letters within the total alkanes (A) or within each monomer chain length (B) indicate a significant difference ($P \leq 0.05$).



zones, the accumulation tended to increase only from the immature zone to transition zone 1 (Fig. 5.8A).

The fatty alcohol group was composed of 12 different monomers, with C22 and C28 as the most abundant. The accumulation of C22 and C28 fatty alcohols started in the immature zone and increased significantly in transition zone 1 to a level that was maintained as the exodermis finished maturing (Fig. 5.8B). Similar accumulation trends, at a reduced scale, were observed for C14, C16, C18, C20, C23, C24, and C26. Of the remaining three fatty alcohol monomers, C19 and C25 each had a uniform accumulation pattern across the maturation zones, whereas the C21 accumulation increased significantly in the mature zone (Fig. 5.8B).

ω-OH fatty acids. The ω-OH fatty acids were detected in relatively low abundance and accounted for only an average of 5% of the soluble fraction across exodermal maturation zones (Table 5.2). Accumulation patterns for this group of monomers resembled that for fatty alcohols, but at a much lower scale. The accumulation of ω-OH fatty acids was statistically uniform as the exodermis matured. However, the trend was toward a slight increase in accumulation between the immature zone and transition zone 1, followed by a very gradual decline through to the mature zone (Fig. 5.9A).

The ω-OH fatty acid group was composed of 4 different monomers, with C22 and C24 being the most abundant. Similar trends in accumulation were observed between the individual monomers (Fig. 5.9B).

2-OH fatty acids. The 2-OH fatty acids were the least abundant monomers, comprising an average of only 1% of the soluble fraction across exodermal maturation zones (Table 5.2).

Monomer accumulation was uniform across the exodermal maturation zones (Fig. 5.10A).

The 2-OH fatty acid group was composed of 4 different monomers, with C24 being the most abundant. Monomer accumulation was mostly uniform across maturation zones (Fig. 5.10B).

5.4.2.3 Poly(phenolic) insoluble fraction

Total poly(phenolic) insoluble fraction. The total poly(phenolic) insoluble fraction includes monomers that were released from the SPPD following its depolymerization with NBO.

Poly(phenolic) monomer amounts increased by an average of nearly 2-fold from the immature zone to transition zone 1, and then remained steady through to the mature exodermal zone (Fig. 5.11A). The poly(phenolic) monomers that were detected in the insoluble fraction included syringin, vanillic acid, and vanillin (Table 5.3).

Syringin. Syringin deposition was steady through the first three maturation zones, but then increased by an average of 2-fold in the mature zone (Fig. 5.11B). The contribution of syringin to the total poly(phenolic) fraction was 40% in the immature zone, lowered to 20 and 28% in transition zones 1 and 2, but then increased to 47% in the mature zone (Table 5.3).

Vanillic acid. Deposition of vanillic acid was statistically uniform across exodermal maturation zones. However, it was clear from the mean trends that the deposition increased between the immature zone and transition zone 1 by an average of more than 2-fold, followed by a very gradual decline to the mature zone (Fig. 5.11C). The contribution of

Figure 5.8 Accumulation of fatty alcohols in the soluble fraction in the OPR of *Allium cepa*.

(A) Total fatty alcohols. (B) Accumulation of the different fatty alcohol monomers. Data are displayed per unit of root segment surface area (in $\mu\text{mol mm}^{-2}$) for each maturation zone (legends inset). Values are means \pm standard deviation. Different lowercase letters within the total fatty alcohols (A) or within each monomer chain length (B) indicate a significant difference ($P \leq 0.05$).

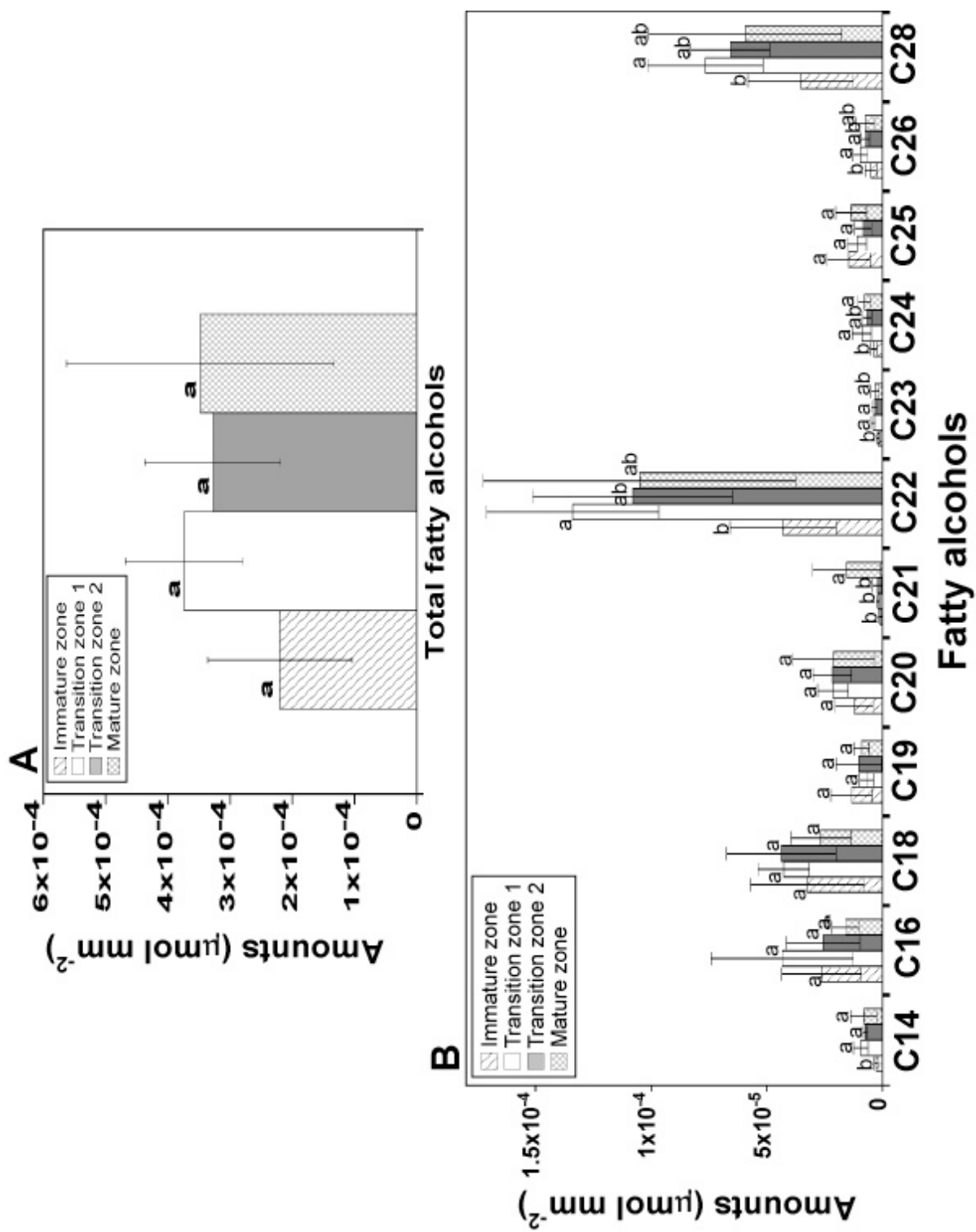


Figure 5.9 Accumulation of ω -OH fatty acids in the soluble fraction in the OPR of *Allium cepa*. (A) Total ω -OH fatty acids. (B) Accumulation of the different ω -OH fatty acid monomers. Data are displayed per unit of root segment surface area (in $\mu\text{mol mm}^{-2}$) for each maturation zone (legends inset). Values are means \pm standard deviation. Different lowercase letters within the total ω -OH fatty acids (A) or within each monomer chain length (B) indicate a significant difference ($P \leq 0.05$).

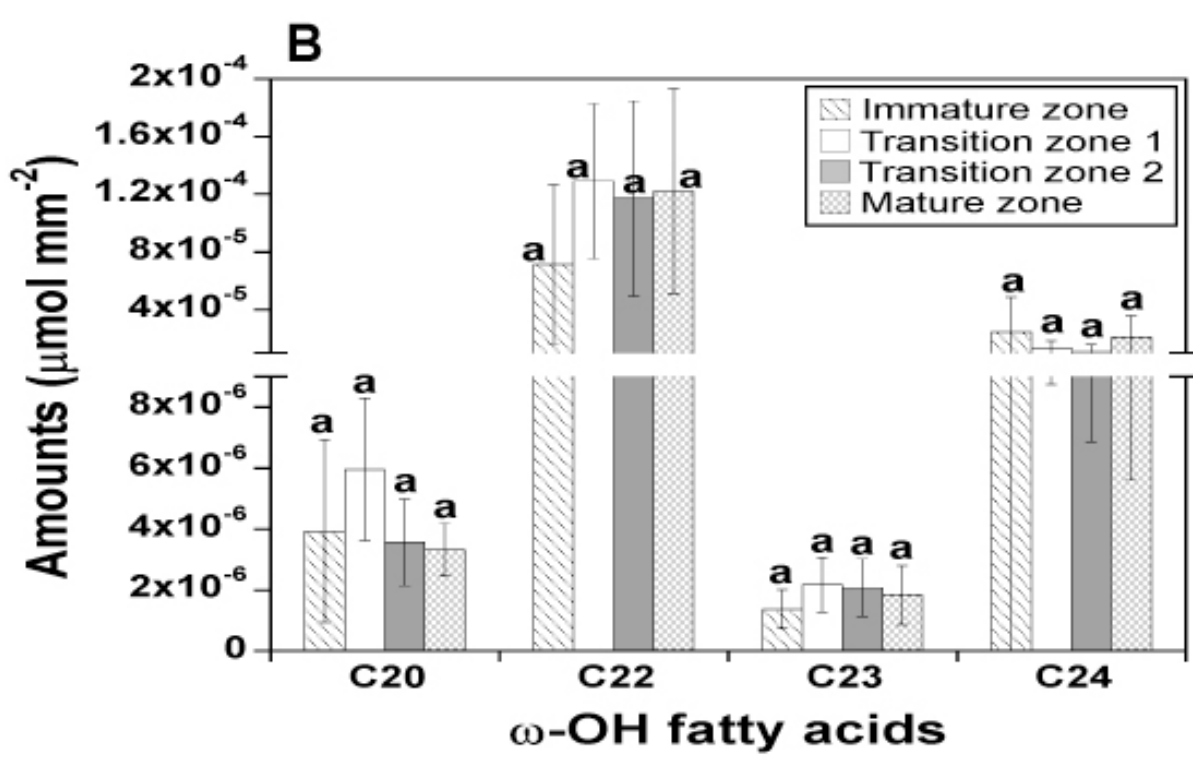
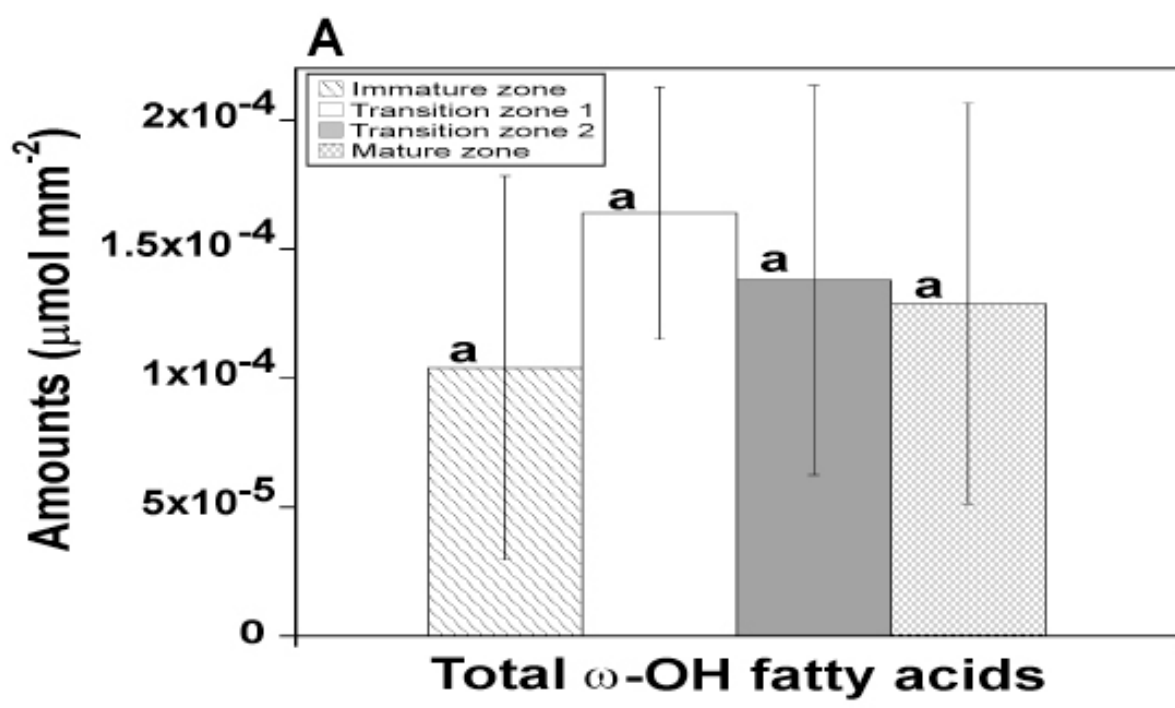


Figure 5.10 Accumulation of 2-OH fatty acids in the soluble fraction in the OPR of *Allium cepa*. (A) Total 2-OH fatty acids. (B) Accumulation of the different 2-OH fatty acid monomers. Data are displayed per unit of root segment surface area (in $\mu\text{mol mm}^{-2}$) for each maturation zone (legends inset). Values are means \pm standard deviation. Different lowercase letters within the total 2-OH fatty acids (A) or within each monomer chain length (B) indicate a significant difference ($P \leq 0.05$).

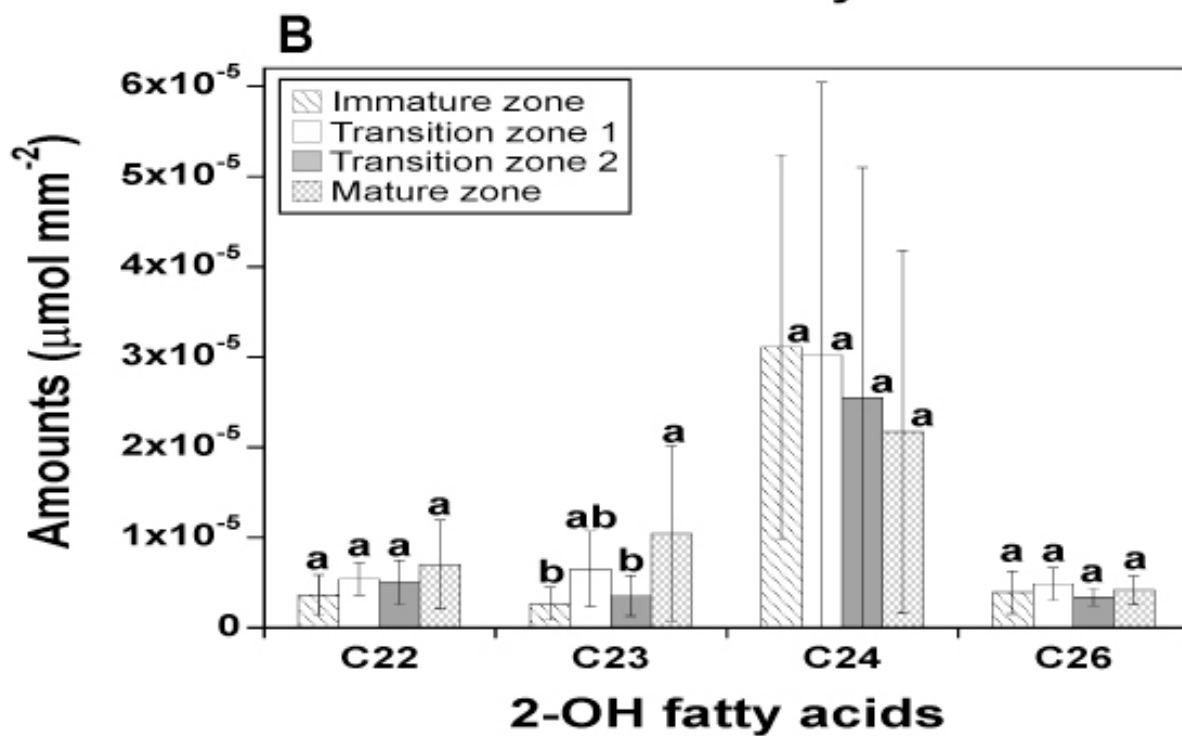
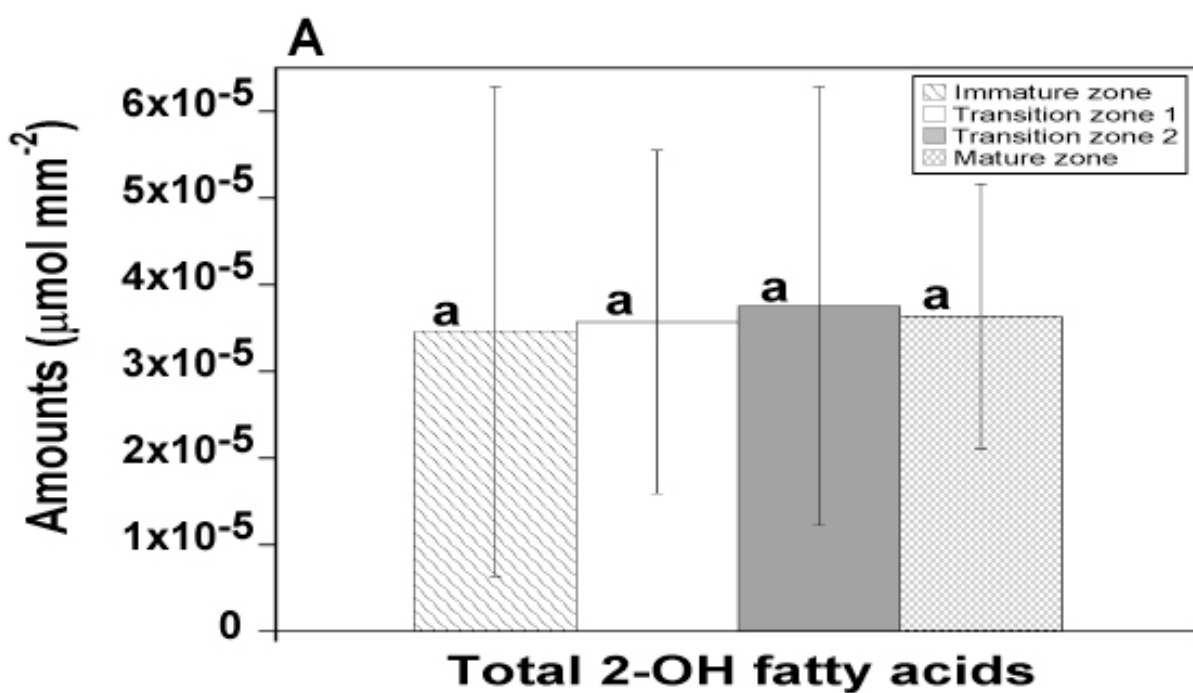


Figure 5.11 Total and individual insoluble SPPD monomer deposition in the OPR of *Allium cepa*. (A) Total SPPD fraction. (B) Syringin deposition. (C) Vanillic acid deposition. Data are displayed per unit of root segment surface area (in $\mu\text{mol mm}^{-2}$) for each maturation zone (legends inset). Values are means \pm standard deviation. Different lowercase letters within each graph indicate a significant difference ($P \leq 0.05$).

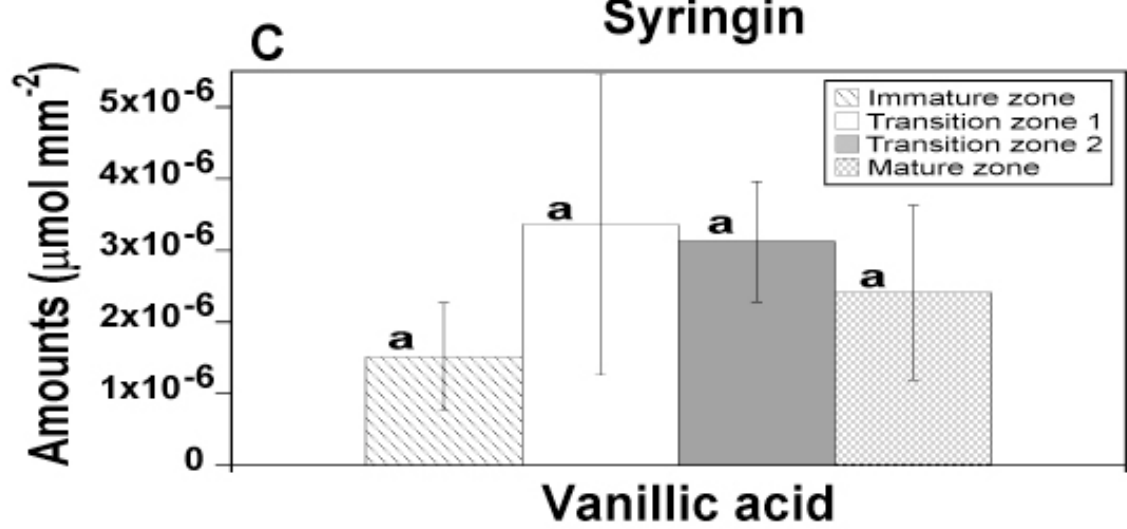
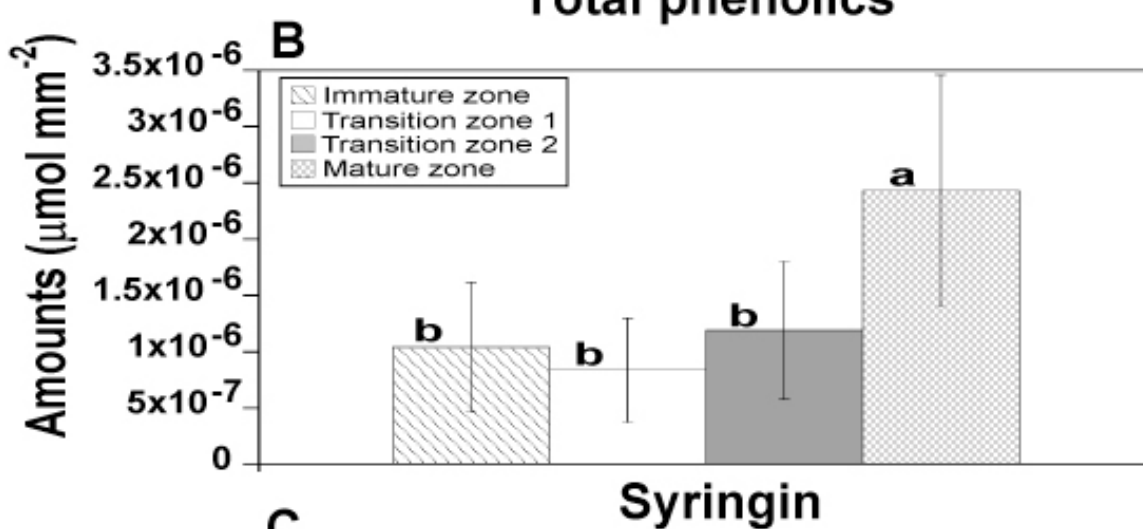
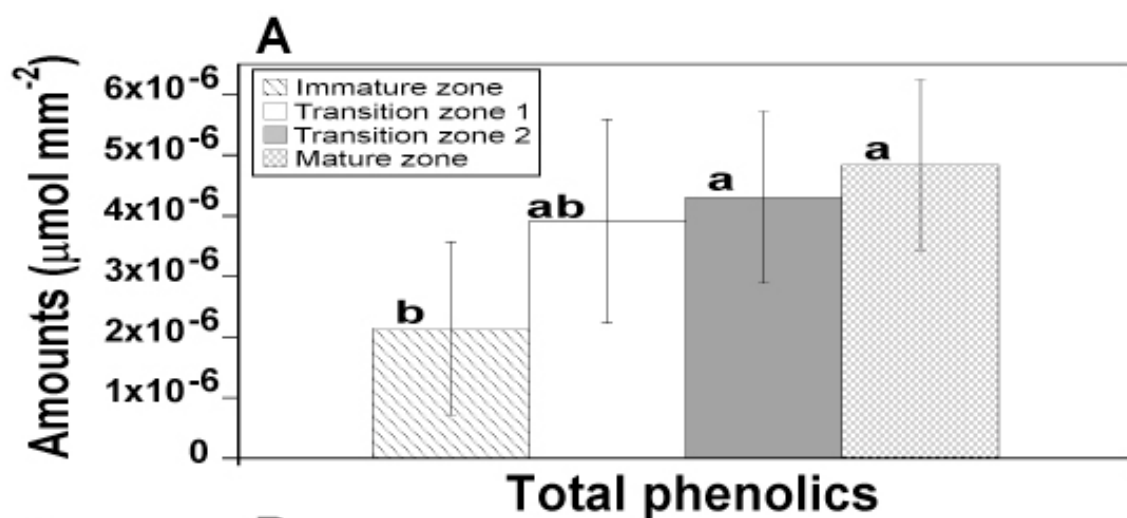


Table 5.3 Percent composition in the OPR of *Allium cepa*'s SPPD at the different exodermal maturation zones.

Compounds	Immature zone (%)	Transition zone 1 (%)	Transition zone 2 (%)	Mature zone (%)
Syringin	40	20	28	47
Vanillic acid	60	80	72	53
Vanillin	trace	trace	trace	trace
Sum	100	100	100	100

vanillic acid to the total poly(phenolic) fraction increased from 60 to 80% between the immature zone and transition zone 1. But, as the amounts of syringin started to increase, vanillic acid contribution fell to 72% in transition zone 2, and then 53% in the mature zone (Table 5.3).

Vanillin. Detection of vanillin was expected because it is a common product of the SPPD after NBO degradation. However, in the gas chromatograms, vanillin overlapped with other contaminating compounds, so its abundance and deposition could not be quantified. Hence, vanillin is reported as being detected in trace amounts (Table 5.3).

5.5 Discussion

Using *Allium cepa* roots as a model for suberin biosynthesis in the uniseriate, dimorphic exodermis was favourable for several reasons. Importantly, the sequence of exodermal maturation was well known from previous work, and these roots generated very few or no lateral roots that could potentially alter the chemical analyses (Peterson and Perumalla 1984; Perumalla and Peterson 1986; Stasovski and Peterson 1993; Barrowclough and Peterson 1994; Kamula et al. 1994; Ma and Peterson 2000, 2001a). Furthermore, according to histochemical studies, exodermal maturation is consistent and may be controlled by a tight developmental program, regardless of the growth conditions thus far tested (Perumalla and Peterson 1986; Barrowclough and Peterson 1994). In the current work, *A. cepa* root growth in hydroponics and the exodermal maturation sequence occurred as expected based on the earlier work (cited above).

Suberin-associated compounds were isolated from the outer part of *A. cepa* roots (OPR). In other words, the measured suberin amounts included monomers deposited in exodermal Casparian bands and suberin lamellae. With the concurrent development of these two structures in exodermal cells, it is not possible to separate them for chemical analysis. However, such separation is possible with the endodermis, as demonstrated for *Clivia miniata*, *Monstera deliciosa*, and *G. max* (Schreiber et al. 1994; Schreiber 1996; Zeier and Schrieber 1997, 1998; Thomas et al. 2007; see section 6.10, Chapter 6 for more details). Furthermore, most suberin analyses of the exodermis also include diffuse suberin from epidermal cells because separation of the exodermis from the epidermis is very difficult, even after enzymatic digestion (Zeier et al. 1999a; reviewed in Ma and Peterson 2003). Diffuse or non-lamellar suberin was first described by Peterson et al. (1978), and has been detected in the epidermis of many species including *A. cepa* and *G. max* (Peterson et al. 1978; Wilson and Peterson 1983; Brundrett et al. 1988; Thomas et al. 2007; Ranathunge et al. 2008). In general, deposition of diffuse suberin occurs close to the root tip; the phenolic component (detected by ultra-violet autofluorescence) is deposited about 10-15 mm from the tip, and the aliphatic component (detected with Fluorol yellow 088 staining) is deposited 20 mm from the tip (Peterson et al. 1978; Thomas et al. 2007). The function of diffuse suberin is not to regulate water transport (Peterson et al. 1993; Steudle and Peterson 1998), but instead to potentially act as a first line of partial resistance to pathogen infection, especially in the absence of an exodermis (see Thomas et al. 2007; Ranathunge et al. 2008). Interestingly, the amount of diffuse suberin deposited in the epidermis is very low. For example, in *G. max* roots, the amounts of poly(aliphatic) and poly(phenolic) suberin monomers in a relatively

well-developed epidermis (90-160 mm from the tip) were about 2-fold lower than the monomer amounts in only endodermal Casparian bands (0-70 mm from the tip). Then, the amount of epidermal diffuse suberin became about 3.5-fold lower following the deposition of suberin lamellae in only half of the endodermal cells (90-160 mm from the tip) (Thomas et al. 2007). Presumably, the density of suberin monomers is much greater when deposited in cell wall-modifying structures compared with diffuse accumulation. Therefore, in the current work, it was assumed that the measured amounts of deposited suberin monomers in the OPR of *A. cepa* roots were mainly the result of deposition in the Casparian bands and suberin lamellae of the maturing exodermis.

Using developmental time-course analyses to study suberin biosynthesis are necessary for detecting marked changes, or lack thereof, in the abundances of key suberin monomers as tissues mature. By employing a time course-based study, important changes to the composition of *A. cepa*'s exodermal SPAD were measured (as discussed in the next section). Also, Yang and Bernards (2006) were able to pin-point the times when SPAD monomers were deposited in newly-developing *S. tuberosum* tuber periderm (see Introduction). Similarly, Krishnamurthy et al. (2009) measured increased amounts of SPAD compounds as the exodermis matured in hydroponically grown *Oryza sativa* roots. This increase was mostly caused by the increase in fatty acid and ω -OH fatty acid amounts; there was little to no change in α,ω -dioic acid amounts. In contrast, Zeier et al. (1999b) measured very little change in the SPAD composition of *Zea mays*' maturing exodermis. Specifically, they detected slight increases (of approximately 10%) in ω -OH fatty acid amounts and corresponding decreases in fatty acid amounts as the exodermis matured. However,

according to Zeier et al. (1999b), the basal regions of their hydroponically grown *Z. mays* roots were “located above the surface of the nutrient solution and therefore exposed to an appreciably lower water potential than the submerged parts”. It is known that a humid air gap growth condition accelerates exodermal suberization in *Z. mays* (Enstone and Peterson 1998) and *I. germanica* (Meyer et al. 2009; see Chapters 2-4), hence maturation becomes less patchy or more uniform along the length of the root. This may partially explain why there was little change to the SPAD composition in the maturing exodermis of *Z. mays*.

The suberin poly(aliphatic) domain (SPAD) composition changed significantly as the exodermis of *A. cepa* matured. These changes were mainly due to increases in the amounts of both the C18:1 α,ω -dioic acid and C18:1 ω -OH fatty acid, which are characteristic SPAD monomers in the most mature tissue (see Table 5.1). The deposition of these two monomers increased by an average of 6-fold when the exodermis was completing its maturation (i.e., in tissue regions at least 4 d old or 96 mm from the root tip) (see Fig. 5.4). Such changes would have been impossible to detect using only histochemical tests or chemical analyses on only fully mature tissues. In addition, fatty acids were detected in the SPAD in relatively abundant amounts in zones where the exodermis was still immature and had just started maturing. Then, fatty acid abundance declined or remained steady as ω -OH fatty acid and α,ω -dioic acid abundances increased (see Fig. 5.4). It is likely that these fatty acids acted as the biosynthetic precursors for the production of ω -OH fatty acids and α,ω -dioic acids. Furthermore, it is possible that an up-regulation in the synthesis and/or activity of cytochrome P450 monooxygenases, ω -hydroxyacid dehydrogenases, and ω -oxoacid dehydrogenases occurred when the exodermis was completing its maturation (see section

1.4.2, Chapter 1 for more details). These enzymatic factors could have been the driving force behind the significant increases in the synthesis of C18:1 ω -OH fatty acids and C18:1 α,ω -dioic acids. The functional characterization of such enzymes is still required to assess the legitimacy of the previous statement, but some candidates are starting to be revealed (see Höfer et al. 2008; Compagnon et al. 2009; Serra et al. 2009b; see section 6.12, Chapter 6 for more details). It is recommended that the exodermal maturation zones, with corresponding suberin metabolite profiles, described here for *A. cepa* roots, may be used as targets for future work on the functional enzymatic characterization of suberin biosynthetic pathways in the exodermis.

Intriguingly, C18:1 α,ω -dioic acids and C18:1 ω -OH fatty acids were absent from the soluble fraction. Thomas et al. (2007) also did not detect these monomers in the soluble fraction from *G. max* endodermis, while Yang and Bernards (2006) detected only trace amounts of these monomers in *S. tuberosum* periderm. All of the above results, including the results discussed in the previous section, support the possibility that C18:1 fatty acids are first transported across the plasma membrane, which is hypothesized to occur via vesicle exocytosis or through an ATP-binding cassette transporter (see Franke and Schreiber 2007), and then polymerized into the SPAD. It is following polymerization when the fatty acids may be hydroxylated into ω -OH fatty acids and subsequently oxidized into α,ω -dioic acids (Yang and Bernards 2006). This hypothesis would require that specific fatty acid ω -hydroxylases be associated with the plasma membrane instead of the endoplasmic reticulum. It is also noteworthy that ω -hydroxyacid dehydrogenase and ω -oxoacid dehydrogenase (required for ω -OH fatty acids to be oxidized to α,ω -dioic acids; see Fig. 1.14, Chapter 1) were previously

detected in the soluble enzyme fractions from the wound-induced periderm of *S. tuberosum* tubers (Agrawal and Kolattukudy 1977). However, fatty acid ω -hydroxylases are known traditionally to be endoplasmic reticulum-associated (see Kolattukudy 1980, 1984; Franke and Schreiber 2007), and in the current work, there were examples of ω -OH and 2-OH fatty acids being present in both the soluble and insoluble fractions (see below). Therefore, an alternative hypothesis is that the ω -hydroxylases associated with the endoplasmic reticulum are in close proximity to the plasma membrane, allowing efficient transport of fatty acid derivatives into the cell wall. More functional enzymatic evidence is required in order to judge these hypotheses.

The relative composition of the most abundant insoluble monomer classes in the SPAD varies between species and tissue types, but such variation is common (Holloway 1983; Matzke and Riederer 1991; Zeier and Schreiber 1998, 1999; Zeier et al. 1999a, b). In the present work, the main composition of the SPAD in the mature exodermis of *A. cepa* includes α,ω -dioic acids (31%), ω -OH fatty acids (21%), and fatty acids (16.5%) (see Table 5.1). For the multiseriate exodermis of *I. germanica*, the SPAD composition included mainly α,ω -dioic acids (53%), ω -OH fatty acids (19%), and fatty acids (17%) (see Table 4.1, Chapter 4). Similar to *I. germanica*, the SPAD composition of tuber periderm from *S. tuberosum* included mainly α,ω -dioic acids (54%) and ω -OH fatty acids (25%) (not including glycerol or unidentified compounds; Graça and Pereira 2000b; Schreiber et al. 2005a). In contrast, the SPAD composition measured in the mature endodermis of *G. max* included ω -OH fatty acids (51-62%), fatty acids (31-46%), and α,ω -dioic acids (3-6%) (Thomas et al. 2007). Nevertheless, in most species so far tested, α,ω -dioic acids and ω -OH fatty acids are

usually present in the SPAD, with the most abundant monomer often being the C18:1 for both classes (Holloway 1983; Matzke and Riederer 1991).

The soluble monomer fraction of the exodermal suberin of *A. cepa* had a chemical composition that changed very little as the exodermis matured. The main compound classes in the soluble monomer fraction of the mature exodermis included fatty acids (47%) and alkanes (36%) (see Table 5.2). In contrast, the composition of *I. germanica*'s exodermal soluble fraction differed as the multiseriate exodermis matured (see Table 4.2, Chapter 4). Nonetheless, the most abundant monomer classes that were detected were fatty acids and alkanes.

Soluble fatty acid accumulation was uniform across exodermal maturation zones in *A. cepa*. This trend was especially evident for C16 and C18:0, which were the two most abundant fatty acids (see Fig. 5.6). The accumulation trends for short-chained fatty acids (especially C16 and C18) were as expected based on the assumption that they are derived from both membrane phospholipids as well as being biosynthetic precursors for SPAD monomers and waxes (including long chain fatty acids, alkanes and fatty alcohols) (Galliard 1973; Yang and Bernards 2006).

The remaining soluble fraction was composed of alkanes, fatty alcohols, and lower amounts of long chain ω -OH fatty acids and 2-OH fatty acids. Alkanes accumulated uniformly from immature zones (i.e., before the start of SPAD polymerization) into the mature exodermal zone, but were detected in only in the soluble fraction; this is consistent with their being part of the suberin-associated wax component (see Fig. 5.7; Soliday et al. 1979; Schreiber et al. 2005a; Yang and Bernards 2006). As a part of the waxes, alkanes may

function with the SPAD to enhance water retention synergistically (Soliday et al. 1979; Vogt et al. 1983; Schreiber et al. 2005a; see Chapters 3-4). For the fatty alcohols, soluble ω -OH fatty acids, and soluble 2-OH fatty acids, the accumulation trends were similar (see Figs. 5.8-5.10). In general, the accumulation of these monomers was highest in the first two maturation zones, and then less so as the exodermis matured. Some of the monomers within these three classes could be a part of the wax component, or were potentially biosynthetic precursors for the SPAD. Specifically, the C22 fatty alcohol, C22 ω -OH fatty acid, and C22 and C24 2-OH fatty acids were likely precursors as they were detected in both the soluble and insoluble fractions. The presence of these monomers in both suberin fractions indicate that reduction and oxidation reactions were catalyzed by endoplasmic reticulum-associated enzymes. Following reduction or oxidation, these suberin monomer derivatives would have been transported across the plasma membrane and incorporated into the SPAD.

The suberin poly(phenolic) domain (SPPD) composition changed as the exodermis of *A. cepa* matured. In zones where the exodermis was just starting to mature, deposition of vanillic acid increased but syringin levels remained constant. As the exodermis matured, syringin deposition increased while vanillic acid decreased. Nonetheless, the amount of vanillic acid was always greater than the amount of syringin (see Fig. 5.11). These changes to the SPPD composition may be the result of alterations to the rate of enzyme synthesis and/or activity involved in monomer synthesis or polymerization. Phenolic monomer synthesis is initiated when the shikimate pathway yields phenylalanine. Phenylalanine is the biosynthetic precursor for hydroxycinnamic acids that are then hydroxylated and methylated into SPPD monomers (Held et al. 1993; Dixon et al. 2001; see Fig. 1.17, Chapter 1). In *S. tuberosum*,

polymerization of these monomers into the SPPD is hypothesized to be driven by a suberin-associated peroxidase that requires a source of hydrogen peroxide from a plasma membrane-bound oxidase. It is believed that the monomers may first activate the membrane oxidase leading to the production of hydrogen peroxide. The hydrogen peroxide then activates a peroxidase in the cell wall, which catalyzes the monomer polymerization (Kolattukudy 1980, 1984; Bernards et al. 1999; Razem and Bernards 2003; see Bernards et al. 2004).

To estimate the total SPPD monomer composition, alkaline nitrobenzene oxidation (NBO) was used to hydrolyze the robust ether and C–C bonds that cross-link the SPPD (see Bernards 2002; Thomas et al. 2007). In using NBO, the structural identity of the SPPD is lost, meaning that the released phenolics simply provide clues about the actual SPPD compounds. For example, vanillic acid is a proxy for guaiacyl-substituted compounds and syringin is a proxy for syringyl-substituted units that were polymerized in the SPPD. However, due to the limited amount of syringin and vanillic acid in the exodermis of *A. cepa*, the current data set probably does not represent the whole SPPD. Perhaps the amount of exodermal tissue used per sample (1-2 mg) was too low for the detection of other monomers that were expected to be released by NBO, such as *p*-hydroxybenzaldehyde or syringic acid.

Previously, SPPD deposition in the cell wall was shown to begin prior to the start of SPAD deposition, helping to anchor the SPAD in place. This sequence of domain deposition was demonstrated using histochemical and chemical analyses of *S. tuberosum* tuber periderm (Lulai and Corsini 1998; Yang and Bernards 2007). In the present work, syringin and vanillic acid were detected in early maturation zones prior to the visible start of exodermal SPAD formation. The origin of these phenolics in young zones could have been from the walls of

the epidermis or immature exodermis. However, due to the limited monomer yields from the SPPD, it is not possible to state conclusively whether or not SPPD deposition started before SPAD deposition.

In conclusion, by analyzing the suberin monomer composition and abundance during the maturation of the uniseriate exodermis of *A. cepa*, it was possible to determine the approximate locations where key biosynthetic steps occurred, especially for the SPAD fraction. The SPAD monomer composition changed as the exodermis matured. Interestingly, the marked increases in the deposition of C18:1 α,ω -dioic acid and C18:1 ω -OH fatty acid (two key SPAD monomers) were targeted to the later stages of exodermal maturation. Fatty acid deposition in the SPAD increased during early exodermal maturation, but decreased or remained steady in the later stages. One interesting observation, that C18:1 α,ω -dioic acids and C18:1 ω -OH fatty acids were detected in only the insoluble fraction, supports the idea that C18:1 fatty acids are polymerized into the SPAD prior to their ω -hydroxylation and oxidation into ω -OH fatty acids and α,ω -dioic acids, respectively. On the other hand, ω -hydroxylases are known to be endoplasmic reticulum-associated and may be located very close to the plasma membrane, allowing efficient and rapid transport of C18:1 α,ω -dioic acids and ω -OH fatty acids into the cell wall. The composition of the soluble monomer fraction did not change significantly as the exodermis matured. This soluble fraction was composed of suberin-associated alkanes (which may function in enhancing water retention), long-chained fatty acids (>C18), fatty alcohols, long chain (C22, C24) ω -OH fatty acids and 2-OH fatty acids (as SPAD biosynthetic precursors), and short-chained fatty acids (C14 - C18), some of which were probably derived from membrane phospholipids. The SPPD

monomer composition changed as the exodermis matured. However, due to the low yield of monomers, this data set may not be a reliable indicator of the total SPPD composition.

Ultimately, the exodermal maturation zones described here, with their corresponding suberin metabolite profiles, can be used as targets for future work on the functional characterization of enzymes found in suberin biosynthetic pathways. Additional future work could involve testing whether or not tolerance to various abiotic stresses, such as a humid air gap, salt stress, or osmotic stress, is enhanced by changes in exodermal SPAD composition and abundance.

Chapter 6

General discussion

The thesis work has focused on the maturation of *Iris germanica* roots, particularly the multiseriate exodermis (MEX), under differing growth conditions, and how its maturation affected radial water and solute permeability. Also, suberin metabolite profiles were established for the maturing MEX of *I. germanica* and the maturing uniseriate exodermis of *Allium cepa*. The uniqueness of the present work is in its multidisciplinary approach, combining exodermal development with physiological and suberin biochemical studies. This comprehensive research is the first of its kind on a maturing MEX.

6.1 Exodermal development

Development of an exodermis has been observed in more than 90% of the angiosperm species so far examined (Perumalla et al. 1990; Peterson and Perumalla 1990). The majority of these species have a uniseriate or single-layered exodermis, including *A. cepa*, *Zea mays*, and *Oryza sativa*. Within the uniseriate exodermal layer, typical Casparian bands are deposited in only the anticlinal walls while the suberin lamellae are encrusted on the inner surface of all the walls. The exodermis in *A. cepa* adventitious roots is dimorphic meaning that it is composed of cells with two distinct lengths. Suberin lamella deposition typically occurs in the long exodermal cells first, but is delayed in the short passage cells (von Guttenberg 1968; Shishkoff 1986; Perumalla et al. 1990; Kamula et al. 1994).

In contrast to uniseriate exodermal development, the development of a multiseriate exodermis (MEX) occurs in approximately 18% of tested angiosperms with an exodermis (Meyer et al. 2009; see Chapter 2). In the detailed investigation of *I. germanica* root structure, the constitutive development of an unusual Casparian band was observed in the both the anticlinal and tangential cell walls of the MEX (Meyer et al. 2009; Chapter 2). This atypical structure was unbroken around the root circumference and was termed a “continuous circumferential Casparian band” (ccCb). A ccCb has also been observed in the MEX of *Typha* spp. (Seago and Marsh 1989; Seago et al. 1999) and *Phragmites australis* (Soukup et al. 2002, 2007). Furthermore, all of *I. germanica*'s MEX cells possessed suberin lamellae. There was no sign of exodermal passage cells even though *I. germanica* had a characteristic 'mixed MEX', meaning the outermost layer was dimorphic and all underlying layers were uniform (after Kroemer 1903).

Development of the immature MEX near the root apical meristem determines how the cells are oriented relative to each other. This is important because the shape of the exodermal wall continuum defines the shape of the ccCb. For example, in the roots of *Typha glauca* and *T. angustifolia* with tiered root apical meristems, the MEX was formed by successive, orderly and centripetal periclinal cell divisions. In transverse section, the wall continuum was H-shaped and consequently acted as a scaffold for its H-shaped ccCb (Seago and Marsh 1989; Seago et al. 1999; Heimsch and Seago 2008). However, not all species with a MEX have only an H-shaped ccCb. In particular, because *I. germanica* had an open root apical meristem, its immature MEX cell divisions were ambiguous and caused the shape of the wall continuum to be variable. Hence, *I. germanica*'s MEX was only partially arranged radially so

that its ccCb appeared both H and Y-shaped in cross section (Meyer et al. 2009; see Chapter 2). Similarly, *P. australis* also has a combination of an H and Y-shaped ccCb in its MEX (Soukup et al. 2002, 2007) indicative of ambiguous cell divisions in the immature MEX.

Recent studies of root radial patterning have begun to reveal the mechanisms behind the development of a single-layered endodermis in the roots of nearly all plant species. The results of such work may be analogous to uniseriate and multiseriate exodermal development as discussed below. Interestingly, Cui et al. (2007) have demonstrated the importance of a direct interaction between scarecrow (SCR) and short-root (SHR) proteins for the development of a uniseriate endodermis in *Arabidopsis thaliana* roots. SHR was previously shown to induce an asymmetric cell division of cortical initials and was necessary for endodermal specification (Helariutta et al. 2000). In subsequent work, Cui et al. (2007) reported that SCR sequestered SHR in an endodermal cell nucleus, preventing SHR from flowing into the central cortex. Furthermore, the SHR-SCR protein complex drives the transcription of *SCR* genes to ensure a steady and large supply of SCR for the interaction with and sequestration of SHR (i.e., a positive feedback loop). When SCR production was reduced in RNA interference mutants, SHR was not sequestered and supernumerary endodermal layers were formed. Therefore, the interaction of these proteins prevented the differentiation of additional endodermal layers (Cui et al. 2007). Based on these results, it is speculated that similar mechanisms are involved in the development of uniseriate and multiseriate exodermal layers. Perhaps an SHR-like protein is generated in the protoderm cells (that later form the epidermis), which then interacts with an SCR-like protein in immature exodermal cells. Species with roots that have a uniseriate exodermis may have an

SCR-SHR developmental mechanism similar to that observed for the endodermis. For roots with a MEX, either a lack of SCR-like protein or an excess of SHR-like protein could induce additional periclinal cell divisions in underlying ground meristem cells. In roots that lack an exodermis, such as *A. thaliana* and *Glycine max*, the genes expressing SCR-like and SHR-like proteins may be absent or repressed. In the future, it would be interesting to elucidate the molecular mechanisms that regulate exodermal development.

6.2 Lateral root emergence

Lateral root emergence from the primary root and the subsequent sealing of the damaged exodermis are interesting phenomena. Lateral roots function in maximizing water and nutrient uptake from substrates by increasing the surface area of the whole root system. In the current work with *I. germanica*, lateral root emergence was minimal but it still occurred (Meyer et al. 2009; see Chapter 2). Lateral root primordia were initiated at the pericycle and grew through the central cortex in the wake of a digestive pocket. But upon reaching the MEX, the lateral root physically broke through in order to emerge. Wounded exodermal regions around the lateral root were sealed with a collar of suberized and lignified cells. (This type of wound reaction is typical for monocots; specifically the deposition of aliphatic and phenolic compounds into pre-existing walls [Esau 1965; Lipetz 1970].) This collar prevented both ferric ions and berberine from permeating into the root (data not shown). The formation of a sealing collar around the emerged lateral root and the collar's impermeability to apoplastic tracers was similarly noted for *A. cepa* (Peterson and Moon 1993), *Z. mays* (McCully and Mallett 1993), and *P. australis* (Soukup et al. 2002). A fascinating trait in the

primary roots of some species is the presence of so-called “windows” in the mature exodermis. Exodermal windows are essentially groups of cells in mature zones of the root that do not contain suberin lamellae and are located where lateral roots will emerge; it is unknown whether or not these cells contain Casparian bands. The ubiquitousness of these windows in the angiosperms is not known, but they have been observed in the roots of species that live at least part of their life cycle in submerged conditions, including *P. australis* and *O. sativa* (Soukup et al. 2002; Armstrong and Armstrong 2005). The exodermal windows in aquatic roots provide low resistance pathways for radial water influx, but are also susceptible to radial oxygen loss which is detrimental for survival in submerged, oxygen-deficient conditions (Armstrong et al. 2000). Such windows were absent from *I. germanica* (Meyer et al. 2009; see Chapter 2), but may not be necessary since this species naturally inhabits well-drained, drought-prone soils and produces far fewer lateral roots than *P. australis* and *O. sativa*.

6.3 Hydraulic conductivity measurements

Direct measurements of hydraulic water permeability (L_p) in roots is achieved using root pressure probes and/or pressure chambers. When testing narrow roots, L_p values are often similar between the pressure probe and pressure chamber (Rüdinger et al. 1994; Zimmermann and Steudle 1998) because the water storage capacity of the central cortex is low (*Z. mays* has 8-9 central cortex layers and *A. cepa* has 7-12 layers, pers. obs.). On the other hand, in *I. germanica* roots, L_p values as measured with the pressure probe were significantly greater than the values measured with the pressure chamber (see Chapter 3).

This was due to the substantial storage capacity of *I. germanica*'s thick central cortex of 12-18 cell layers. It was this storage capacity that dampened the pressure pulses induced with the pressure probe; consequently, the measured L_p values pertained to only the innermost tissues including the endodermis. Conversely, the pressure chamber moved water across all root tissues under steady-state conditions. Hence, the true contribution of *I. germanica*'s exodermis to water permeability was resolved only with the pressure chamber (see below).

6.4 Exodermal suberin lamellae deposition reduces water permeability

According to the composite transport model, all cell layers work in series contributing to the resistance to radial water flow (Steudle and Peterson 1998). Most of the resistance is typically caused by the suberin lamellae in mature exodermal and endodermal cell layers (Zimmermann et al. 2000; Hose et al. 2001; Enstone et al. 2003). In the current work, the high hydraulic resistance of *I. germanica*'s MEX was measured by conducting experiments with the pressure chamber (see Chapter 3). As the MEX matured, its permeability to water decreased by more than 2-fold. In terms of the composite transport model, the contribution of the MEX and endodermis to hydraulic resistance were 75% and 25%, respectively.

Radial water permeability across roots typically decreases following the deposition of exodermal suberin lamellae. For example, as the MEX of *I. germanica* matured, the radial water permeability fell from 0.9×10^{-7} to $0.4 \times 10^{-7} \text{ m s}^{-1} \text{ MPa}^{-1}$, emphasizing the importance of the MEX as a highly hydraulically resistant tissue (see Chapter 3). Similar reductions to water permeability were noted for the exodermis of *Z. mays* (Clarkson et al. 1987;

Zimmermann and Steudle 1998), *Agave deserti* (North and Nobel 1991), and *Sorghum bicolor* (Cruz et al. 1992). Furthermore, as the exodermis of hydroponically grown *A. cepa* roots matured, their radial water permeability decreased from 2.8×10^{-7} to $0.7 \times 10^{-7} \text{ m s}^{-1} \text{ MPa}^{-1}$ (Melchior and Steudle 1993). (These water permeability values are greater than those measured for *I. germanica*.) A dimorphic uniseriate exodermis, like *A. cepa*'s, has long cells with suberin lamellae that may function in water retention, and short passage cells that function in water absorption (von Guttenberg 1968; Kamula et al. 1994). In contrast, even though *I. germanica*'s outermost exodermal layer is dimorphic, it lacks passage cells and is better suited for water retention rather than water absorption.

The development of multiple files of exodermal or phellem cell layers does not necessarily enhance the water retention properties of the whole exodermis or periderm, respectively. This counter-intuitive statement is supported by experimental data with *Solanum tuberosum* and *A. deserti* (Vogt et al. 1983; North and Nobel 1995; Schreiber et al. 2005a; see Chapter 4 for more details). Instead, suberin-associated wax accumulation is known to have a marked influence on water impermeability as measured in *S. tuberosum* tuber periderm (Soliday et al. 1979; Vogt et al. 1983; Schreiber et al. 2005a). Intriguingly, in the current work, alkane waxes accumulated in abundance in *I. germanica*'s outermost exodermal layer when it was exposed to a humid air gap. This increase in alkane accumulation, in unison with the increased deposition of key suberin aliphatic monomers, probably functioned synergistically in *I. germanica*'s MEX to restrict radial water and solute flow (see Chapters 3 and 4).

6.5 The role of aquaporins

Aquaporin abundance and activity are also important for regulating radial water permeability in roots. Aquaporins are water channels, located in the plasma membrane and tonoplast, that facilitate radial water flow through the root via the transcellular pathway (Maurel et al. 2008). These channels are known to close in reaction to abiotic stress, consequently reducing radial water flow. Such reactions have been measured in *Chara corallina* internodes (osmotic stress) and *A. thaliana* roots (salt stress) (Ye et al. 2004; Boursiac et al. 2005). In fact, hyperosmolarity may be more important than ion toxicity for causing aquaporins to close in the early stages of a response to salinity (see Boursiac et al. 2005). Although aquaporin activity was not directly measured in *I. germanica*, it would probably have been affected by the variable growth conditions and by the NaCl osmotic permeability tests (see Chapter 3).

6.6 Cell viability and the symplastic pathway with respect to ion transport

Root cell viability is supported by an intact symplast between neighbouring cells, connected by plasmodesmata. In *A. cepa*'s dimorphic exodermis, suberin lamellae deposition in the long cells severs their plasmodesmata (Ma and Peterson 2000). (Suberin lamella deposition is delayed in the short exodermal cells so their plasmodesmata remain intact.) The severing of plasmodesmata interrupts the symplastic path, and those exodermal cells soon die. However, suberin lamellae do not always sever the plasmodesmata and can be deposited around these channels, as is the case for *Z. mays*' uniform exodermis (Clarkson et al. 1987; Wang et al. 1995) and in general for the endodermis of all species examined to date (Ma and Peterson

2000, and references therein). Although *I. germanica*'s outermost exodermal layer is dimorphic, deposition of suberin lamellae was not delayed in the short cells (i.e., there were no exodermal passage cells). Nonetheless, the presence of living epidermal cells and the continued development of all the MEX cells, indicates the presence of plasmodesmata linking the epidermis to the central cortex (see below).

Cell viability in root tissues must be considered when interpreting physiological data because it can have significant effects on radial ion transport. In exodermal roots, an ion would initially enter the apoplast at the outer tangential wall of a living epidermal cell (see Fig. 1.5, Chapter 1). If the ion is then paired with an appropriate transmembrane transporter in the plasma membrane of this cell, the ion is shunted into the symplast compartment through which it flows radially into the root, moving through the cytoplasm of neighbouring cells connected by plasmodesmata. However, in the absence of an appropriate transporter, the ion will be prevented from crossing the plasma membrane and thus it is confined to the apoplast. The inward movement of such an ion would be blocked by the exodermal Casparian bands (see Fig. 1.5, Chapter 1). But, if the epidermal cells die, their plasma membranes deteriorate and no longer mediate ion transport into the symplast. In roots with a dimorphic exodermis (*A. cepa*) or with patchy exodermal development (*Z. mays*), the living exodermal cells that lack suberin lamellae have an accessible plasma membrane along the outer tangential walls for ion transport into the symplast (Kamula et al. 1994). These unsuberized exodermal cells are important for ion transport because epidermal death is common in *A. cepa* and *Z. mays* roots (Barrowclough and Peterson 1994; Enstone and Peterson 1998). On the other hand, in the roots of *I. germanica*, the epidermal cells must be

alive for symplastic ion flow to occur because all the MEX cells contain a ccCb and suberin lamellae. (The ccCb blocks apoplastic ion flow, and the poly(aliphatic) domain of suberin lamellae restricts access to the exodermal plasma membrane [see Fig. 3.1, Chapter 3].) Perhaps this is why in *I. germanica* approximately half of the epidermal cells retained their viability after a 14 day exposure to a humid air gap, whereas epidermal cells of *A. cepa* and *Z. mays* died within two days under similar conditions (Barrowclough and Peterson 1994; Enstone and Peterson 1998). It is currently unknown if the robustness of the epidermal cells of *I. germanica* represents a special case or if it is a common feature among species with a MEX. In summary, radial ion flow through roots is regulated by a combination of four main factors: 1) the presence or absence of appropriate transmembrane transporters, 2) the impermeability of the plasma membrane itself to ions, 3) the impermeability of the Casparian band to ions, and 4) the presence of suberin lamellae controlling access to the symplast by preventing ions from contacting the plasma membrane.

6.7 How do roots tolerate salt stress?

Understanding the role of roots in salt exclusion is essential for determining a species' tolerance to salt stress. This is important because high NaCl concentrations (100-200 mM) in a growth substrate can be toxic for many plants, including some staple agricultural cereals such as *O. sativa* (rice), *Triticum turgidum* ssp *durum* (durum wheat), *T. aestivum* (bread wheat), and *Hordeum vulgare* (barley) (see Munns and Tester 2008). Some of the more recent work on salt tolerance has focused on Na⁺ transport across the plasma membrane and the tonoplast. Briefly, Na⁺ can cross the plasma membrane passively through non-selective

cation channels, entering the cytoplasm. In response, the cell can use Na^+/H^+ antiporters to pump the Na^+ either back into the apoplast or into the vacuole. While sequestered in the vacuole, the Na^+ may, in fact, return to the cytoplasm passively through non-selective cation channels, but it is then pumped back into the vacuole. Vacuolar sequestration of Na^+ is known to improve salt tolerance by reducing the concentration of Na^+ in the cytoplasm (reviewed in Munns and Tester 2008).

The current work shows that root tolerance to salt stress could also be facilitated by the presence of exodermal Casparian bands and suberin lamellae. For example, in *I. germanica* roots, the blockage of Na^+ flow across the MEX was achieved through a combination of three factors. First, it is hypothesized that in living epidermal cells, Na^+ was either unable to traverse the plasma membrane or was sequestered in the vacuole. Secondly, the infiltration of the anticlinal and tangential cell walls with the ccCb prevented apoplastic Na^+ flow past the MEX. Lastly, the deposition of the poly(aliphatic) domain of suberin lamellae (SPAD) between the wall and plasma membrane of all MEX cells prevented Na^+ from contacting the exodermal plasma membrane (see Fig. 3.1, Chapter 3). Based on these three factors and the quantitative results, it is concluded that the MEX of *I. germanica* is highly restrictive to Na^+ flow.

The abundance of SPAD monomers in roots typically increases after exposure to saline-stressed conditions compared with salt-free substrates. For example, when soil-grown *A. thaliana* roots were exposed to 100 mM of NaCl for 24 days, the abundance of SPAD monomers was doubled compared with roots that were not exposed to NaCl (Franke et al. 2009). In another example, Krishnamurthy et al. (2009) detected significantly greater

amounts of ω -hydroxy fatty acids in the exodermis of a salt-tolerant cultivar of *O. sativa* when exposed to salt stress (50-100 mM NaCl) for 7 days, compared with non-stressed plants. Lastly, Schreiber et al. (2005c), using *Ricinus communis* roots, measured increased SPAD deposition in the exodermis of NaCl-stressed roots (100 mM, 30 days) compared with non-stressed counterparts. In all the above examples, SPAD composition and chain length distribution did not differ between control and NaCl-exposed roots. The increased density of monomers in the Casparian bands and suberin lamellae could enhance the restriction of Na^+ flow by clogging more of the intermicrofibrillar spaces, by blocking access to plasma membranes, or possibly severing plasmodesmata. This enhanced restriction to Na^+ flow would be beneficial for roots of *Z. mays* or *O. sativa* because the uniseriate exodermis of these species are not nearly as resistant to Na^+ flow as the MEX of *I. germanica* (Steudle et al. 1993; Ranathunge et al. 2003; see Chapter 3).

It is also noteworthy that when plants are grown in high salinity substrates, root growth rates are often reduced. In this situation, if the rate of exodermal maturation remains steady or is accelerated, more of the root surface area would have a uniformly mature exodermis, hence younger regions close to the tip would be better able to block Na^+ flow (Wilcox 1962; Perumalla and Peterson 1986; Enstone et al. 2003, and references therein). Clearly, exclusion of Na^+ at the peripheral cell layers of the root in exodermal species is important for preventing the influx of salt into deeper tissue regions, including the stele; ergo, Casparian bands and suberin lamellae should always be observed when evaluating of a species' tolerance to salt.

6.8 Additional responses of roots to abiotic stress

Root responses to stress are not limited to the exodermis. Other tissue processes that can be involved include accelerated endodermal maturation, dormancy of lateral root primordia, and die-back or sloughing off of outer tissue layers such as the epidermis and central cortex (see Enstone et al. 2003, and references therein). Also, the reduction in both activity and abundance of aquaporins would definitely play a role in lowering root water permeability under stress (Maurel et al. 2008). Therefore, reactions of roots to changes in substrate conditions are multi-structural and multi-functional, occurring at different temporal and spatial scales as required to optimize the survival of the plant in an adverse environment. It would be interesting to study in *I. germanica* the role of abscisic acid and other phytohormones in abiotic stress tolerance, as well as how small RNAs are involved in the regulation of expression of stress-related genes. Information from these additional factors would add to our understanding of the coordinated responses to particular abiotic stresses.

6.9 The two-domain model of suberin lamellae

A suberin lamella is a complex biopolymer with a poly(aliphatic) domain (SPAD) and a poly(phenolic) domain (SPPD) that are spatially distinct but covalently linked (reviewed in Bernards 2002; see Fig. 1.10, Chapter 1). This two-domain model was developed following the culmination of many independent analyses (see Bernards 2002, and references therein). Recently, Mattinen et al. (2009) supported this model using several approaches, but the most revealing evidence came from their differential scanning calorimeter (DSC) measurements. When samples containing the complete suberin polymer were analyzed with the DSC, two

distinct peaks at 45°C and 59°C were detected, suggesting that the polymer had two distinct domains. Then, when samples that contained isolated SPPD were analyzed, only one distinct peak at 59°C was detected. Hence, the 45°C peak from the former experiment corresponded to the SPAD (Mattinen et al. 2009). Small molecules such as water and glycerol can lower the temperature required for a phase transition in the DSC. Since glycerol acts as the primary linker between monomers in the SPAD (Graça and Pereira 2000a, b), it makes sense that the DSC detected the SPAD at a lower temperature than the SPPD.

Each suberin lamella domain has a unique chemical composition and location in the cell wall, both of which are indicative of the domain's primary function. For instance, the SPAD and its associated waxes are hydrophobic and are located between the primary cell wall and plasma membrane. These features establish the SPAD as a structure that restricts water and solute flow through the transcellular pathway (Kolattukudy and Dean 1974; Soliday et al. 1979; Vogt et al. 1983; Evert et al. 1985; Zimmermann et al. 2000; Hose et al. 2001; Schreiber et al. 2005a; see Fig. 1.5, Chapter 1 or Fig. 3.1, Chapter 3). Conversely, the SPPD is composed of phenolic compounds that are embedded in the cell wall, establishing this domain as a structure restrictive to apoplastic microbial penetration (Kolattukudy 1980, 1984; Lulai and Corsini 1998).

6.10 A revised chemical model for the Casparian band

The chemical structure of the Casparian band is not considered within the chemical model for suberin lamellae, which was produced mainly from analyses of suberin in *S. tuberosum* tuber periderm. (To the best of this author's knowledge, the presence of a Casparian band in

the periderm has never been tested with berberine-aniline blue staining, so it is not possible to state whether or not the periderm lacks a Casparian band.) Nevertheless, in any analysis of exodermal or endodermal cells with suberin lamellae, the Casparian band will always be included, based on the strict sequence of developmental states (Van Fleet 1961; Esau 1965; and Robards et al. 1973; see Chapter 1). However, it is possible to obtain endodermal cells with only a Casparian band, which can be utilized to determine its chemical composition. For example, Zeier and Schreiber (1997, 1998), inspired by Schreiber et al. (1994) and Schreiber (1996), isolated the endodermal Casparian bands in two monocotyledonous species (*Clivia miniata* and *Monstera deliciosa*) and identified primarily phenolic compounds (5-6% w/w) with trace amounts of aliphatics (0.1-1% w/w). Interestingly, after the endodermis was exposed to an enzyme mixture of cellulase and pectinase for 14 days, only the Casparian band remained. In longitudinal view, the intact mass of endodermal Casparian bands had a net-like appearance (Schreiber et al. 1994; Schreiber 1996). Presumably, the only way for the Casparian bands of several cells to hold together in the net-like sheet following pectinase treatment would be if the Casparian bands of neighbouring cells were cross-linked across the pectic acid-rich middle lamellae. An alternative way to isolate at least part of the Casparian bands involves sulphuric acid digestion which reportedly destroys phenolics but spares aliphatics (Johansen 1940). Perumalla et al. (1990) exposed the uniseriate exodermis of 156 different angiosperm species to concentrated sulphuric acid. The epidermis and exodermis remained attached to each other indicating that at least parts of the walls had been retained presumably including the Casparian bands and suberin lamellae of the exodermis and diffuse

suberin of the epidermis. For Casparian bands to remain intact following acid digestion, the aliphatic region would need to be located at least partially in the middle lamellae.

Based on all of the above-mentioned work, a revised but tentative model for the Casparian band is presented here. It was reported previously that both the phenolic and aliphatic components of the Casparian band were embedded in the intermicrofibrillar spaces of anticlinal cell walls (Schreiber 1996; see Steudle and Peterson 1998). For the revised Casparian band model, it is predicted that only the phenolic component (comprising 5-6% w/w) infiltrates the intermicrofibrillar spaces and that the aliphatic component (comprising only 0.1-1% w/w) is located at the middle lamella where it is cross-linked to the aliphatic component of neighbouring Casparian bands. Furthermore, cell walls that are targeted for Casparian band deposition are limited to the anticlinal walls in the endodermis and a uniseriate exodermis, but include the anticlinal and some tangential walls in a multiseriate exodermis. The precise arrangement of the Casparian band's phenolic and aliphatic components described in the revised model requires experimental verification. Further, the interactions between the phenolic region of the Casparian bands and the poly(phenolic) domain of suberin lamellae are still unknown.

6.11 Time course-based suberin metabolite analyses

When using analytical targeted analyses, metabolite profiling is conducted in great detail because optimized methods are used for monomer extraction, identification and quantification (see Hall 2006). But, a targeted analysis alone is not enough to reveal the dynamic nature of suberin synthesis. By using time course-based targeted metabolite

analyses, monomer composition and abundance can be profiled in tissues at multiple stages of maturation. In the current work, time course-based suberin metabolite analyses were used successfully to determine whether or not the production of specific monomers changed during exodermal maturation and under differing growth conditions (see Chapters 4 and 5). It is recommended that the suberin metabolite profiles resolved for the maturing MEX of *I. germanica* and the maturing uniseriate exodermis of *A. cepa* be used in future studies when determining the functional properties of specific enzymes in the suberin biosynthetic pathway.

6.12 Suberin biosynthetic enzymes

Suberin biosynthetic pathways are composed of many hypothesized enzymatic steps (reviewed by Kolattukudy 1980, 1984; Bernards 2002; Franke and Schreiber 2007; see Figs. 1.14, 1.15, Chapter 1). The identity and function of these enzymes are now beginning to be characterized. In the current work, after resolving the suberin metabolite profiles for the maturing exodermis in *I. germanica* and *A. cepa*, it was suggested that in order to increase the production of key SPAD monomers that the abundance and/or activity of some biosynthetic enzymes would have had to increase. This would have been especially important for the increase in production of C18:1 ω -OH fatty acids and C18:1 α,ω -dioic acids when *I. germanica*'s MEX was exposed to the humid air gap, and when *A. cepa*'s exodermis was completing its maturation (see Chapters 4 and 5, respectively). The enzyme families of particular importance include 1) cytochrome P450 monooxygenases (P450s) for fatty acid ω -

hydroxylation and perhaps 2) β -ketoacyl-CoA synthase (KCS) for fatty acid elongation. Each of these enzyme families function in separate metabolism pools, as described below.

For the synthesis of key SPAD derivatives, plastid-synthesized C18 fatty acids are desaturated, ω -hydroxylated into C18:1 ω -OH fatty acid, and then potentially oxidized into C18:1 α,ω -dioic acid (Kolattukudy 1980, 1984; Yang and Bernards 2006; see Fig. 1.14, Chapter 1 for more details). Fatty acid ω -hydroxylation is catalyzed by NADPH-dependent P450s (Duan and Schuler 2005). Höfer et al. (2008) identified a root-specific P450 (CYP86A1) in *A. thaliana* that proved to be necessary for ω -hydroxylation of fatty acids with chain lengths less than C20. Compagnon et al. (2009) identified another P450 (CYP86B1) that was required for ω -hydroxylation of fatty acids between C22 and C24. Lastly, Serra et al. (2009b) identified a P450 (CYP86A33) in *S. tuberosum* tuber periderm that, when down-regulated, produced 60% less aliphatic suberin compared with the wildtype. In particular, C18:1 ω -OH fatty acid and α,ω -dioic acid amounts were significantly lower in the mutant (70% and 90% lower, respectively). These above-mentioned results indicate that specific P450s target particular monomer chain lengths.

The ω -hydroxylation and oxidation reactions that produce suberin fatty acid derivatives are known to occur on the endoplasmic reticulum (see Kolattukudy 1980, 1984; Franke and Schreiber 2007; Höfer et al. 2008; Compagnon et al. 2009), but it has been hypothesized recently that these reactions may also occur at the plasma membrane. In the current work, some ω -OH and 2-OH fatty acids were present in both the soluble and insoluble suberin fractions, demonstrating that the hydroxylation reactions occurred on the endoplasmic reticulum. Alternatively, the reactions to produce C18:1 ω -OH fatty acids and α,ω -dioic acids

may occur after the polymerization of C18:1 primary fatty acids into the SPAD. The basis for this hypothesis was from the insoluble and soluble suberin monomer profiles for *S. tuberosum* tuber periderm (Yang and Bernards 2006), and for the exodermis of *I. germanica* and *A. cepa* (see Chapters 4 and 5). For the three tested species, C18:1 ω -OH fatty acids and C18:1 α,ω -dioic acids were detected in abundance in the polymerized, insoluble fraction from mature tissue. However, these same two SPAD monomers were absent from the soluble fraction in *I. germanica* and *A. cepa*, and were detected in only trace amounts in the soluble fraction of *S. tuberosum*. For this hypothesis to be true, the specific ω -hydroxylases would have to be associated with the plasma membrane rather than the endoplasmic reticulum. On the other hand, it is possible that endoplasmic reticulum-associated ω -hydroxylases are in close proximity to the plasma membrane, allowing efficient and rapid transport of C18:1 ω -OH fatty acids and α,ω -dioic acids into the cell wall. Therefore, these specific fatty acid derivatives may have been transported across the plasma membrane rapidly and then polymerized quickly into the SPAD. Specific functional enzymatic evidence is required to test these hypotheses.

In a different metabolism pool, SPAD fatty acid derivatives are elongated to C20 - C30, and either reduced into primary alcohols, decarboxylated into *n*-alkanes, or oxidized into ω -OH and 2-OH fatty acids (Kolattukudy 1980, 1984; Yang and Bernards 2006; see Fig. 1.15, Chapter 1 for more details). Fatty acid elongation occurs through a microsomal malonyl-CoA dependent pathway, as demonstrated in the primary roots of *Z. mays* (Schreiber et al. 2005b). The first step in elongation is catalyzed by a KCS. Franke et al. (2009) identified a KCS (DAISY) in *A. thaliana* roots that was necessary for elongation of C20 fatty acid derivatives.

Serra et al. (2009a) identified a KCS (StKCS6) in *S. tuberosum* tuber periderm that was necessary for elongation of fatty acids with chain lengths of C28 and greater. Lastly, Lee et al. (2009) generated an *A. thaliana* *kcs20 kcs2/daisy-1* double mutant and measured significantly lower abundances for only C22 and C24 fatty acid suberin precursors, with a concomitant accumulation of C20 compounds. The results listed above suggest that specific KCSs target particular fatty acid chain lengths.

Information about the transport and polymerization of suberin-specific fatty acid derivatives is currently hypothetical. Following the synthesis of the derivatives, they may be transported in vesicles to the plasma membrane. The derivatives traverse the membrane potentially by exocytosis or through an ATP-binding cassette transporter. Lastly, polymerization of the derivatives into the SPAD is possibly catalyzed by polyester synthases including GPAT5 (Franke and Schreiber 2007; Beisson et al. 2007; Li et al. 2007).

The functional characterization of suberin biosynthetic enzymes is underway, but there are still many enzymes to be investigated. As additional enzymes are characterized, the complete biosynthetic pathways will eventually be determined. According to the work mentioned above that demonstrates how specific P450s and KCS enzymes target particular monomer chain lengths, there will certainly be several members that comprise the suite of enzymes involved in suberin synthesis. Although enzyme characterization was not conducted in the current work, the resolved suberin metabolite profiles can guide researchers toward certain enzyme families to help search for specific members involved in the key reactions of exodermal suberin synthesis. In particular, it would be of great interest to characterize the specific P450s, ω -hydroxyacid dehydrogenases, and ω -oxoacid dehydrogenases involved in

the synthesis of C18:1 ω -OH fatty acids and C18:1 α,ω -dioic acids. Additionally, the response of these enzymes to differing abiotic stresses would be valuable to better understand stress tolerance.

6.13 Conclusions

Changes in substrate conditions can have substantial effects on exodermal maturation, in turn affecting the radial water and solute permeability across the root. It was found that the maturation of *I. germanica*'s MEX, with concurrent deposition of the ccCb and suberin lamellae, was delayed if the roots were grown completely submerged in hydroponic culture compared with soil-grown roots. However, MEX maturation was accelerated by exposing the basal part of the hydroponically grown root to a humid air gap (Meyer et al. 2009; see Chapter 2). The acceleration of MEX maturation in air gap-exposed tissue was also detected chemically. Specifically, the concomitant increase in 1) the deposition of two key suberin poly(aliphatic) domain (SPAD) monomers (C18:1 α,ω -dioic acids and C18:1 ω -OH fatty acids) in the first two exodermal layers, and 2) the accumulation of alkane waxes in the outermost exodermal layer were detected (see Chapter 4). Consequently, in these air gap-exposed root segments, radial water permeability rates were markedly reduced and radial NaCl flow was immeasurable (see Chapter 3). Thus, the MEX is responsive to differing substrate conditions, and it is a very hydraulically resistant tissue layer. The functional properties of *I. germanica*'s MEX are compatible with a previously proposed function for the MEX of *Carex arenaria* roots; specifically that the MEX functions to protect the stele against unfavourable situations but concurrently reduces its permeability to water and ions (Robards

et al. 1979). The MEX is one of many important evolutionary specializations that some species have developed to tolerate both drought-prone and saline habitats.

Occasionally, changes in substrate conditions do not noticeably affect root tissue maturation, as detected histochemically. This was the case for the maturation of *A. cepa*'s exodermis, as detected previously (Perumalla and Peterson 1986; Barrowclough and Peterson 1994; Kamula et al. 1994). The consistent exodermal maturation sequence for *A. cepa* makes it an excellent model for studying suberin biosynthesis in a uniseriate exodermis. In the present work, *A. cepa*'s maturing exodermis had progressively increasing amounts of SPAD monomers. But, it was only when the exodermis was completing its maturation that the incorporation of two key SPAD monomers (C18:1 α,ω -dioic acid and C18:1 ω -OH fatty acid) into the polymer increased significantly (see Chapter 5). It is recommended that the suberin metabolite profiles established for the maturing uniseriate exodermis of *A. cepa*, as well as the maturing MEX of *I. germanica*, be used in future work when determining the functional properties of specific suberin biosynthetic enzymes.

Appendices

Appendix A – Supplementary Tables for Chapter 2

Supplementary Table 2.1 List of the 25 *Iris germanica* cultivars observed for their root anatomy. All cultivars had identical root anatomy.

Species	Cultivar
<i>Iris germanica</i>	Florentina
	Paradise
	Renaissance fair
	Riot of dreams
	Rollercoaster
	Skyblaze
	Strawberry field
	Startler
	St. Louis blues
	Tropical night
	Titan's glory
	Tigershark
	Thriller
	Theatre
	Temple spire
	Witching
	Winterscape
	Winter adventure
	Wild jasmine
	Westland gold
	Wedding candles
	Warrior King
	Wakeup call
	Wabash
	Vivien

Supplementary Table 2.2 Monocot species with a uniseriate exodermis and various growth substrates.

Order	Family	Genus and species	Soil type	
Alismatales	Alismataceae	* <i>Sagittaria sagittifolia</i> L.	Wet	
	Araceae	* <i>Amorphophallus konjac</i> K. Koch	Moist but well-drained	
		^ <i>Anthurium andraeanum</i> Linden	Moist but well-drained	
		^ <i>Anthurium scherzerianum</i> Schott	Moist but well-drained	
		^ <i>Arisaema triphyllum</i> (L.) Schott	Moist but well-drained	
		* <i>Arum italicum</i> Mill.	Well-drained	
		* <i>Calla palustris</i> L.	Wet	
		^ <i>Dieffenbachia amoena</i> hort. ex Gentil	Moist but well-drained	
		^ <i>Dieffenbachia oerstedii</i> Schott	Well-drained	
		^ <i>Dieffenbachia seguine</i> (Jacq.) Schott	Well-drained	
		^ <i>Philodendron</i> <i>bipennifolium</i> Schott	Moist but well-drained	
		^ <i>Philodendron scandens</i> fo <i>micans</i> (Klotzsch ex K. Koch) Bunting	Moist but well-drained	
		^ <i>Syngonium podophyllum</i> Schott	Well-drained	
		Butomaceae	* <i>Butomus umbellatus</i> L.	Wet
		Cymodoceaceae	* <i>Cymodocea nodosa</i> (Ucria) Asch.	Wet
Hydrocharitaceae	* <i>Elodea canadensis</i> Michx.	Wet		
	* <i>Najas marina</i> L.	Wet		
Juncaginaceae	* <i>Triglochin palustris</i> L.	Wet		
Potamogetonaceae	* <i>Potamogeton perfoliatus</i> L.	Wet		
Zosteraceae	* <i>Zostera marina</i> L.	Wet		
Arecales	Arecaceae	^ <i>Caryota mitis</i> Lour.	Moist but well-drained	
Asparagales	Alliaceae	^ <i>Allium cernuum</i> Roth	Well-drained	
		† <i>Allium cepa</i> L.	Moist but well-drained	
		^ <i>Allium christophii</i> Trautv.	Moist but well-drained	
		^ <i>Allium moly</i> L.	Well-drained	
		^ <i>Allium neapolitanum</i>	Moist but well-drained	

	Cirillo	
	^ <i>Allium porrum</i> L.	Moist but well-drained
	^ <i>Allium schoenoprasum</i> L.	Well-drained
	^ <i>Allium tricoccum</i> Aiton	Moist but well-drained
Agavaceae	^ <i>Agave americana</i> L.	Dry
	^ <i>Cordyline indivisa</i> Hook. f.	Moist but well-drained
Amaryllidaceae	^ <i>Galanthus nivalis</i> L.	Moist but well-drained
	^ <i>Hippeastrum vittatum</i> (L'Hér.) Herb.	Moist but well-drained
	^ <i>Lycoris radiata</i> (L'Hér.) Herb.	Well-drained
Asphodelaceae	^ <i>Aloe jucunda</i> G. Reyn.	Dry
	^ <i>Aloe vera</i> (L.) Burm. f.	Dry
	* <i>Asphodelus fistulosus</i> L.	Well-drained
	^ <i>Haworthia radula</i> Haw.	Dry
	^ <i>Haworthia truncata</i> Schönland	Dry
Hemerocallidaceae	^ <i>Dianella revoluta</i> R. Br.	Well-drained
Hyacinthaceae	* <i>Hyacinthus orientalis</i> L.	Well-drained
	* <i>Lachenalia aloides</i> hort.	Moist but well-drained
	^ <i>Ornithogalum arabicum</i> L.	Moist but well-drained
	^ <i>Ornithogalum</i> <i>longibracteatum</i> Jacq.	Moist but well-drained
	* <i>Ornithogalum narbonense</i> L.	Well-drained
Iridaceae	^ <i>Crocus ancyrensis</i> (Herb.) Maw	Moist but well-drained
	^ <i>Crocus chrysanthus</i> Herb.	Well-drained
	^ <i>Crocus sativus</i> L.	Well-drained
	* <i>Gladiolus communis</i> L.	Well-drained
	† <i>Iris hexagona</i> Walt.	Wet
	† <i>Iris pseudacorus</i> L.	Wet
	^ <i>Iris reticulata</i> M.Bieb.	Well-drained
	† <i>Iris sibirica</i> L.	Wet
	† <i>Iris spuria</i> L.	Wet
	† <i>Iris versicolor</i> L.	Wet
	‡ <i>Iris virginica</i> L.	Wet
	^ <i>Sisyrinchium montanum</i> Greene	Well-drained
Orchidaceae	^ <i>Epipactis helleborine</i> (L.) Crantz	Well-drained

	Ruscaceae	^ <i>Beaucarnea recurvata</i> Lem.	Dry	
		^ <i>Maianthemum canadense</i> Desf.	Moist but well-drained	
		^ <i>Maianthemum stellatum</i> (L.) Link	Moist but well-drained	
		^ <i>Sansevieria grandis</i> L.	Dry	
		^ <i>Sansevieria trifasciata</i> Prain	?	
	Themidaceae	^ <i>Milla bivalvis</i> Baker	?	
Commelinales	Commelinaceae	^ <i>Commelina erecta</i> L.	Moist but well-drained	
		^ <i>Cyanotis somaliensis</i> C.B.Clarke	Well-drained	
		^ <i>Tradescantia fluminensis</i> Vell.	Moist but well-drained	
Dioscoreales	Dioscoreaceae	* <i>Dioscorea batatas</i> Decne.	Well-drained	
Liliales	Colchicaceae	^ <i>Uvularia grandiflora</i> Sm.	Moist but well-drained	
	Liliaceae	^ <i>Erythronium americanum</i> Ker Gawl.	Moist but well-drained	
		^ <i>Fritillaria uva-vulpis</i> Cornu ex G�r�me & Labroy	Well-drained	
		* <i>Gagea lutea</i> (L.) Ker Gawl.	Moist but well-drained	
		* <i>Lilium longiflorum</i> Thunb.	Well-drained	
		* <i>Lilium martagon</i> L.	Well-drained	
		* <i>Tricyrtis hirta</i> (Thunb.) Hook.	Moist but well-drained	
		* <i>Tulipa gesneriana</i> L.	Well-drained	
		* <i>Tulipa silvestris</i> L.	Well-drained	
		Melanthiaceae	^ <i>Trillium erectum</i> L.	Moist but well-drained
			^ <i>Trillium grandiflorum</i> (Michx.) Salisb.	Moist but well-drained
	^ <i>Trillium luteum</i> (Muhl.) Harb.		Moist but well-drained	
		Smilacaceae	* <i>Smilax aspera</i> L.	Moist but well-drained
			* <i>Smilax rotundifolia</i> L.	Moist but well-drained
Poales	Anarthriaceae	* <i>Anarthria laevis</i> R.Br.	Wet	
	Cyperaceae	* <i>Carex acutiformis</i> Ehrh.	Wet	
		* <i>Carex disticha</i> Huds.	Wet	
		^ <i>Cyperus alternifolius</i> L.	Wet	
	Poaceae	* <i>Bambusa multiplex</i> (Lour.) Schult. & Schult.f.	Moist but well-drained	

	* <i>Bambusa vulgaris</i> Schrad. ex J.C. Wendl.	Moist but well-drained
	* <i>Echinochloa crus-galli</i> (L.) P.Beauv.	Well-drained
	^ <i>Fargesia nitida</i> (Mitford) Keng f. ex T.P. Yi	Moist but well-drained
	‡ <i>Glyceria grandis</i> S. Watson	Wet
	‡ <i>Glyceria maxima</i> (Hartm.) Holmb.	Wet
	‡ <i>Glyceria striata</i> (Lam.) Hitc.	Wet
	* <i>Holcus mollis</i> L.	Well-drained
	* <i>Molinia caerulea</i> (L.) Moench	Wet
	† <i>Oryza sativa</i> L.	Wet
	* <i>Phyllostachys bambusoides</i> Siebold & Zucc.	Moist but well-drained
	* <i>Phyllostachys edulis</i> (Carriere) J.Houz.	Moist but well-drained
	* <i>Phyllostachys nigra</i> (Lodd. ex Lindl.) Munro	Moist but well-drained
	* <i>Pseudosasa japonica</i> (Zucc. ex Steud.) Makino ex Nakai	Moist but well-drained
	*^ <i>Saccharum officinarum</i> L.	Varietal differences ?
	* <i>Secale cereale</i> L.	Well-drained
	* <i>Sorghum bicolor</i> (L.) Moench.	Well-drained
	*† <i>Zea mays</i> L.	Well-drained
Restionaceae	* <i>Chaetanthus leptocarpoides</i> R. Br.	?
	* <i>Elegia deusta</i> (Rottb.) Kunth	?
	* <i>Hypodiscus willdenowia</i> (Nees) Mast.	?
	* <i>Leptocarpus chilensis</i> Mast.	Wet?
	* <i>Leptocarpus ciliaris</i> Nees	?
	* <i>Lepyrodia scariosa</i> R.Br.	Wet?
	* <i>Lyginia barbata</i> R. Br.	?
	* <i>Restio complanatus</i> R.Br.	Wet?

		* <i>Restio amblycoleus</i>	?
		F.Muell.	
		* <i>Thamnochortus fruticosus</i>	?
		P.J. Bergius	
		* <i>Willdenowia humilis</i> Nees	?
		ex Mast.	
Zingiberales	Musaceae	^ <i>Musa X paradisiaca</i> L.	Moist but well-drained
	Zingiberaceae	^ <i>Alpinia zerumbet</i> (Pers.) B.L. Burtt & R.M. Sm.	Well-drained
		* <i>Elettaria cardamomum</i> (L.) Maton	Moist but well-drained

*Kroemer (1903); ^Perumalla et al. (1990); ‡Stevens (2003); †pers. obs.

Taxonomic information referenced from the Angiosperm Phylogeny Group (Stevens 2001 onwards) and Tropicos.org websites.

Habitat information referenced from the Kemper Center PlantFinder and Plants for a Future websites.

Supplementary Table 2.3 Eudicot species with a uniseriate exodermis and various growth substrates.

Order	Family	Genus and species	Soil type
Asterales	Asteraceae	* <i>Anaphalis margaritacea</i> (L.) Benth. & Hook.f.	Well-drained
		* <i>Anthemis nobilis</i> L.	Well-drained
		* <i>Artemisia absinthium</i> L.	Well-drained
		* <i>Bellis perennis</i> L.	Well-drained
		* <i>Carlina vulgaris</i> L.	Well-drained
		* <i>Eupatorium cannabinum</i> L.	Wet
		^ <i>Eurybia macrophylla</i> (L.) Cass.	Well-drained
		^ <i>Helianthus annuus</i> L.	Well-drained
		* <i>Lactuca sativa</i> L.	Well-drained
		* <i>Petasites hybridus</i> (L.) P.Gaertn., B.Mey. & Scherb.	Wet
		* <i>Senecio articulatus</i> (L.f.) Sch.Bip.	Well-drained
		* <i>Senecio vulgaris</i> L.	Well-drained
		^ <i>Solidago flexicaulis</i> L.	Well-drained
		^ <i>Solidago rugosa</i> Mill.	Varietal differences ?
		^ <i>Symphotrichum cordifolium</i> (L.) G.L. Nesom	Well-drained
		^ <i>Symphotrichum dumosum</i> (L.) G.L. Nesom	Moist to wet
		^ <i>Symphotrichum ericoides</i> (L.) G.L. Nesom	Well-drained
		^ <i>Symphotrichum foliaceum</i> (Lindl. ex DC.) G.L. Nesom	Well-drained
		^ <i>Symphotrichum lanceolatum</i> (Willd.) G.L. Nesom	Moist to wet
		^ <i>Symphotrichum lateriflorum</i> (L.) A 4. Löve & D. Löve	Well-drained
		^ <i>Symphotrichum novae-angliae</i> (L.) G.L. Nesom	Moist to wet
		^ <i>Symphotrichum</i>	Dry

		<i>oblongifolium</i> (Nutt.) G.L. Nesom	
		^ <i>Symphyotrichum patens</i> (Aiton) G.L. Nesom	Dry
		^ <i>Symphyotrichum pilosum</i> (Willd.) G.L. Nesom	Dry to wet
		^ <i>Symphyotrichum</i> <i>puniceum</i> (L.) A 4. Löve & D. Löve	Wet
		^ <i>Symphyotrichum</i> <i>spathulatum</i> (Lindl.) G.L. Nesom	Moist but well-drained
		^ <i>Symphyotrichum</i> <i>urophyllum</i> (Lindl. ex DC.) G.L. Nesom	Dry
		* <i>Tanacetum vulgare</i> L.	Well-drained
		* <i>Taraxacum officinale</i> Weber ex Wiggers	Well-drained
	Campanulaceae	* <i>Lobelia inflata</i> L.	Moist but well-drained
Brassicales	Brassicaceae	^ <i>Cardamine diphylla</i> (Michx.) Alph. Wood	Moist but well-drained
		* <i>Cardamine pratensis</i> L.	Wet
Caryophyllales	Cactaceae	^ <i>Brasilicactus graessneri</i> (K. Schum.) Backeb.	Dry
		* <i>Cereus napoleonis</i> Graham	Dry
		* <i>Cereus rostratus</i> Lem.	Dry
		^ <i>Echinopsis ancistrophora</i> Speg.	Dry
		^ <i>Nopalxochia</i> <i>phyllanthoides</i> (DC.) Britton & Rose	Dry
		^ <i>Pereskia grandiflora</i> Pfeiff.	Dry
	Caryophyllaceae	^ <i>Arenaria capillaris</i> Poir.	Dry
	Phytolaccaceae	^ <i>Rivina humilis</i> L.	Moist but well-drained
Cornales	Cornaceae	* <i>Cornus sanguinea</i> L.	Moist but well-drained
Cucurbitales	Begoniaceae	^ <i>Begonia albopicta</i> W. Bull	Moist but well-drained
		^ <i>Begonia maculata</i> Raddi	Moist but well-drained
	Curcubitaceae	* <i>Luffa aegyptiaca</i> Mill.	Well-drained
Dilleniales (or 'unassigned')	Dilleniaceae	^ <i>Hibbertia cuneiformis</i> Labill.	Moist but well-drained
Ericales	Balsaminaceae	^† <i>Impatiens capensis</i>	Wet

		Meerb.	
		‡ <i>Impatiens glandulifera</i>	Moist but well-drained
		Royle	
		‡ <i>Impatiens pallida</i> Nutt.	Wet
		^ <i>Impatiens walleriana</i>	Moist but well-drained
		Hook. f.	
	Primulaceae	^ <i>Primula japonica</i> A. Gray	Moist but well-drained
	Theaceae	* <i>Camellia japonica</i> L.	Moist but well-drained
Fagales	Fagaceae	* <i>Fagus sylvatica</i> L.	Well-drained
		* <i>Quercus cerris</i> L.	Moist but well-drained
Gentianales	Apocynaceae	^ <i>Carissa macrocarpa</i>	Moist but well-drained
		(Eckl.) A. DC.	
		^ <i>Catharanthus roseus</i> (L.)	Well-drained
		G. Don	
		^ <i>Hoya australis</i> R. Br. ex J.	??
		Traill	
		^ <i>Hoya bella</i> Hook.	??
		^ <i>Hoya carnososa</i> R. Br.	Well-drained
		^ <i>Hoya cinnamomifolia</i>	??
		Hook.	
		^ <i>Hoya globulosa</i> Hook. f.	??
		^ <i>Hoya longifolia</i> Wall. ex	??
		Wight	
		^ <i>Nerium oleander</i> L.	Well-drained
		^ <i>Stapelia gigantea</i> N.E. Br.	Well-drained
		^ <i>Vinca minor</i> L.	Well-drained
	Rubiaceae	^ <i>Apomuria punctata</i>	Well-drained
		(Vatke) Bremek.	
Geraniales	Geraniaceae	^ <i>Pelargonium peltatum</i>	Well-drained
		(L.) L'Hér.	
Lamiales	Acanthaceae	^ <i>Aphelandra aurantiaca</i>	??
		(Scheidw.) Lindl.	
		^ <i>Aphelandra squarrosa</i>	Well-drained
		Nees	
		^ <i>Justicia fulvicoma</i> Schltl.	Well-drained
		& Cham.	
	Bignoniaceae	* <i>Campsis radicans</i> (L.)	Moist but well-drained
		Bureau	
		^ <i>Pithecoctenium</i>	??
		<i>crucigerum</i> (L.) A.H.	
		Gentry	
	Lamiaceae	* <i>Galeopsis segetum</i> Neck.	Moist but well-drained
		^ <i>Mentha aquatica</i> L.	Wet
		^ <i>Mentha x dumetorum</i> H.	??

		Perrier	
		^ <i>Mentha x gracilis</i> Sole	Moist but well-drained
		^ <i>Mentha spicata</i> L.	Wet
		* <i>Satureja hortensis</i> L.	Well-drained
		^ <i>Solenostemon repens</i> (Gürke) J.K. Morton	??
		^ <i>Solenostemon scutellarioides</i> (L.) Codd	Moist but well-drained
	Oleaceae	^ <i>Jasminum magnificum</i> Lingelsh.	Well-drained
	Scrophulariaceae	* <i>Antirrhinum majus</i> L.	Well-drained
Laurales	Lauraceae	* <i>Laurus nobilis</i> L.	Well-drained
Malpighiales	Euphorbiaceae	^ <i>Euphorbia pulcherrima</i> Willd. ex Klotzsch	Well-drained
		* <i>Mercurialis perennis</i> L.	Moist but well-drained
		* <i>Ricinus communis</i> L.	Moist but well-drained
	Linaceae	* <i>Linum usitatissimum</i> L.	Well-drained
	Passifloraceae	* <i>Passiflora gracilis</i> J. Jacq. ex Link	Well-drained
		^ <i>Passiflora quadrangularis</i> L.	Moist but well-drained
	Phyllanthaceae	^ <i>Phyllanthus grandifolius</i> L.	??
	Violaceae	* <i>Viola canina</i> L.	Well-drained
		* <i>Viola odorata</i> L.	Moist but well-drained
Malvales	Malvaceae	* <i>Malva alcea</i> L.	Moist but well-drained
Myrtales	Lythraceae	* <i>Cuphea lanceolata</i> W. T. Aiton	Moist but well-drained
		† <i>Decodon verticillatus</i> (L.) Elliott	Wet
		† <i>Lythrum alatum</i> Pursh	Wet
		† <i>Lythrum hyssopifolia</i> L.	Wet
		† <i>Lythrum salicaria</i> L.	Wet
	Myrtaceae	^ <i>Callistemon rigidus</i> R.Br	Moist but well-drained
		^ <i>Myrtus communis</i> L.	Well-drained
	Onagraceae	† <i>Chamerion angustifolium</i> (L.) Holub	Well-drained
		† <i>Epilobium ciliatum</i> Raf.	Well-drained
		† <i>Epilobium hirsutum</i> L.	Moist but well-drained
		† <i>Epilobium parviflorum</i> Schreb.	Wet
	Trapaceae	* <i>Trapa natans</i> L.	Wet
Nymphaeales	Nymphaeaceae	‡ <i>Nymphaea odorata</i> Aiton	Wet
		* <i>Victoria amazonica</i>	??

		(Poepp.) Sowerby	
Oxalidales	Oxalidaceae	* <i>Oxalis acetosella</i> L.	Moist but well-drained
		^ <i>Oxalis adenophylla</i> Gillies ex Hook. & Arn.	Well-drained
		^ <i>Oxalis purpurea</i> L.	Well-drained
Piperales	Aristolochiaceae	^ <i>Aristolochia littoralis</i> D. Parodi	Moist but well-drained
	Piperaceae	^ <i>Peperomia obtusifolia</i> (L.) A. Dietr.	Moist but well-drained
Ranunculales	Berberidaceae	* <i>Berberis vulgaris</i> L.	Well-drained
		^ <i>Podophyllum peltatum</i> L.	Well-drained
	Fumariaceae	* <i>Corydalis cava</i> (L.) Schweig. & Köerte.	Well-drained
	Ranunculaceae	^ <i>Anemonoides blanda</i> Holub	Well-drained
Rosales	Moraceae	^ <i>Ficus altissima</i> Blume	Well-drained
		* <i>Ficus barbata</i> Warb.	Well-drained
		^ <i>Ficus benjamina</i> L.	Well-drained
	Rosaceae	* <i>Filipendula ulmaria</i> (L.) Maxim.	Wet
		^ <i>Fragaria virginiana</i> Duchesne	Well-drained
		^ <i>Malus pumila</i> Mill.	Well-drained
		* <i>Potentilla palustris</i> (L.) Scop.	Wet
		^ <i>Rosa gallica</i> L.	Well-drained
		^ <i>Waldsteinia fragarioides</i> Tratt.	Well-drained
		Urticaceae	^ <i>Pilea cadierei</i> Gagnep. & Guillaumin
Sapindales	Rutaceae	^ <i>Citrus maxima</i> (Burm. ex Rumph.) Merr.	Moist but well-drained
		^ <i>Citrus paradisi</i> Macfad.	Moist but well-drained
		* <i>Ruta graveolens</i> L.	Well-drained
Solanales	Convolvulaceae	^ <i>Calystegia sepium</i> (L.) R. Br.	Well-drained
		* <i>Cuscuta epilinum</i> Weihe	Well-drained
	Solanaceae	^ <i>Atropa belladonna</i> L.	Well-drained
		* <i>Datura stramonium</i> L.	Well-drained
		*^ <i>Hyoscyamus niger</i> L.	Well-drained
Solanaceae	^ <i>Solanum betaceum</i> Cav.	Moist but well-drained	
	^ <i>Solanum lycopersicum</i> L.	Moist but well-drained	

Vitales	Vitaceae	<i>*Solanum nigrum</i> L.	Well-drained
		<i>*Cissus discolor</i> Blume	Moist but well-drained
		<i>*Cissus sulcicaulis</i> (Baker) Planch.	Well-drained
		<i>*Parthenocissus quinquefolia</i> (L.) Planch.	Moist but well-drained
		<i>^Vitis riparia</i> Michx.	Well-drained

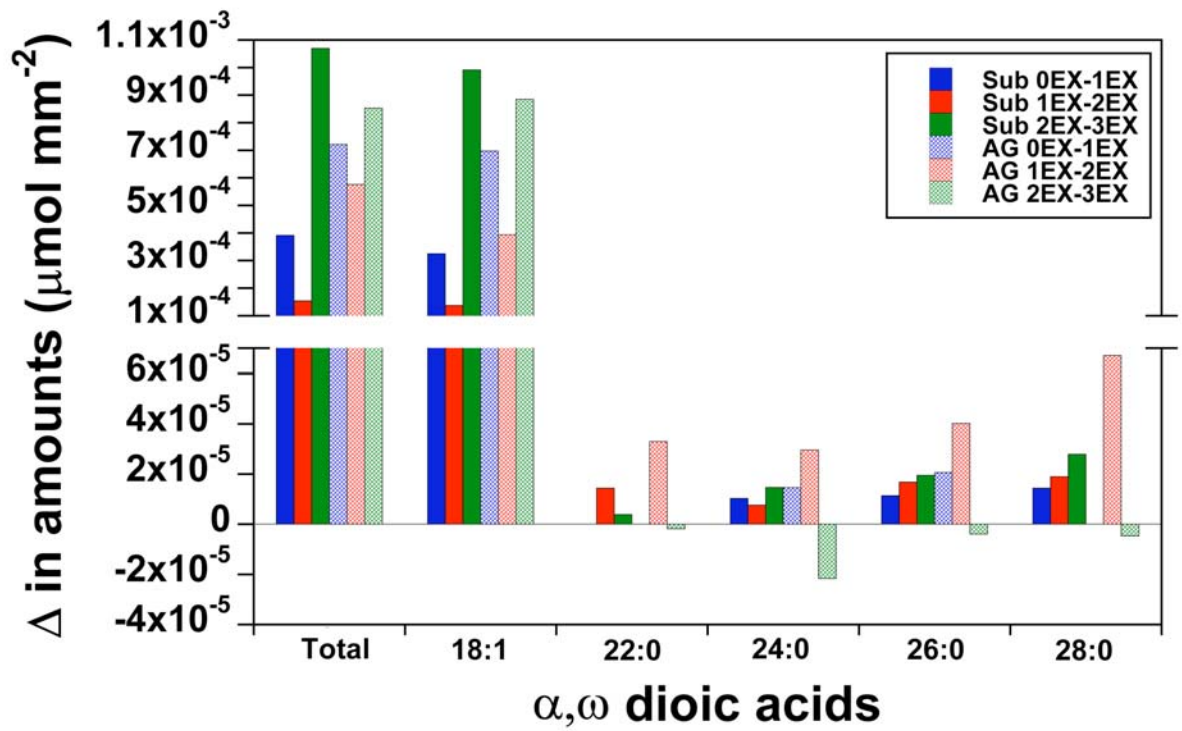
*Kroemer (1903); ^Perumalla et al. (1990); ‡Seago et al. (2000); †Stevens (2003).

Taxonomic information referenced from the Angiosperm Phylogeny Group (Stevens 2001 onwards) and Tropicos.org websites.

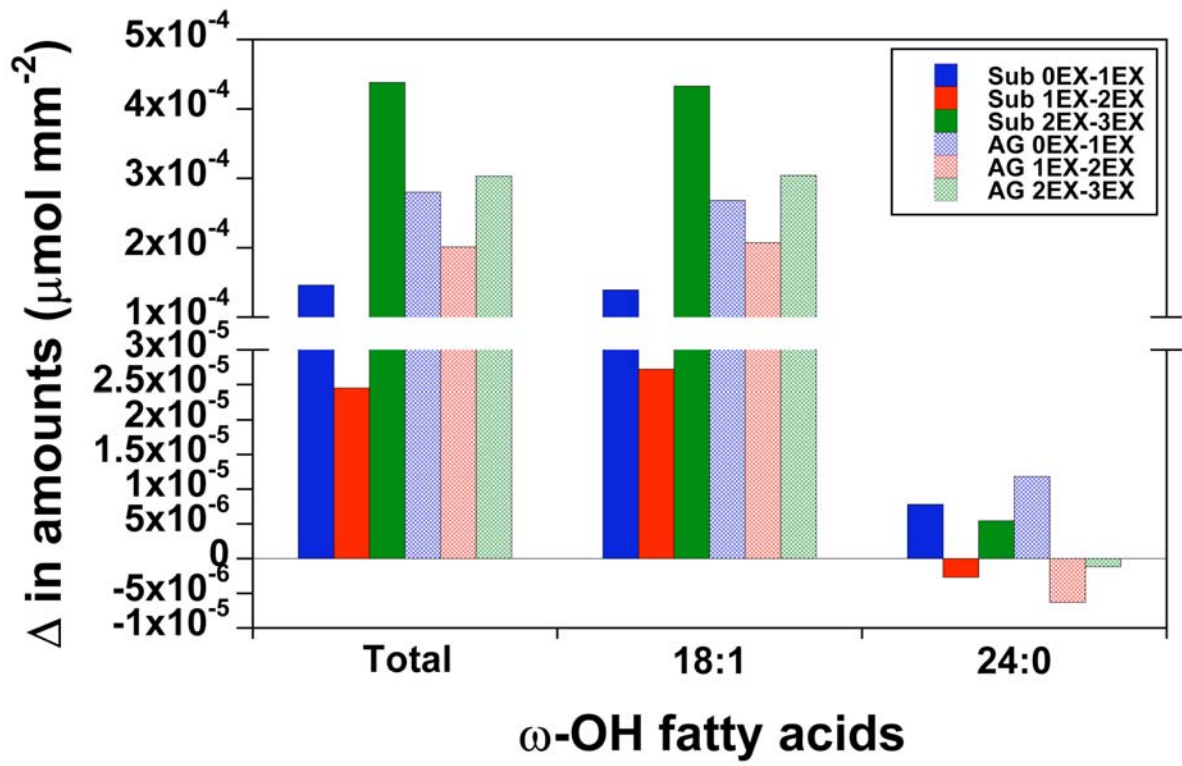
Habitat information referenced from the Kemper Center PlantFinder and Plants for a Future websites.

Appendix B – Supplementary Figures for Chapter 4

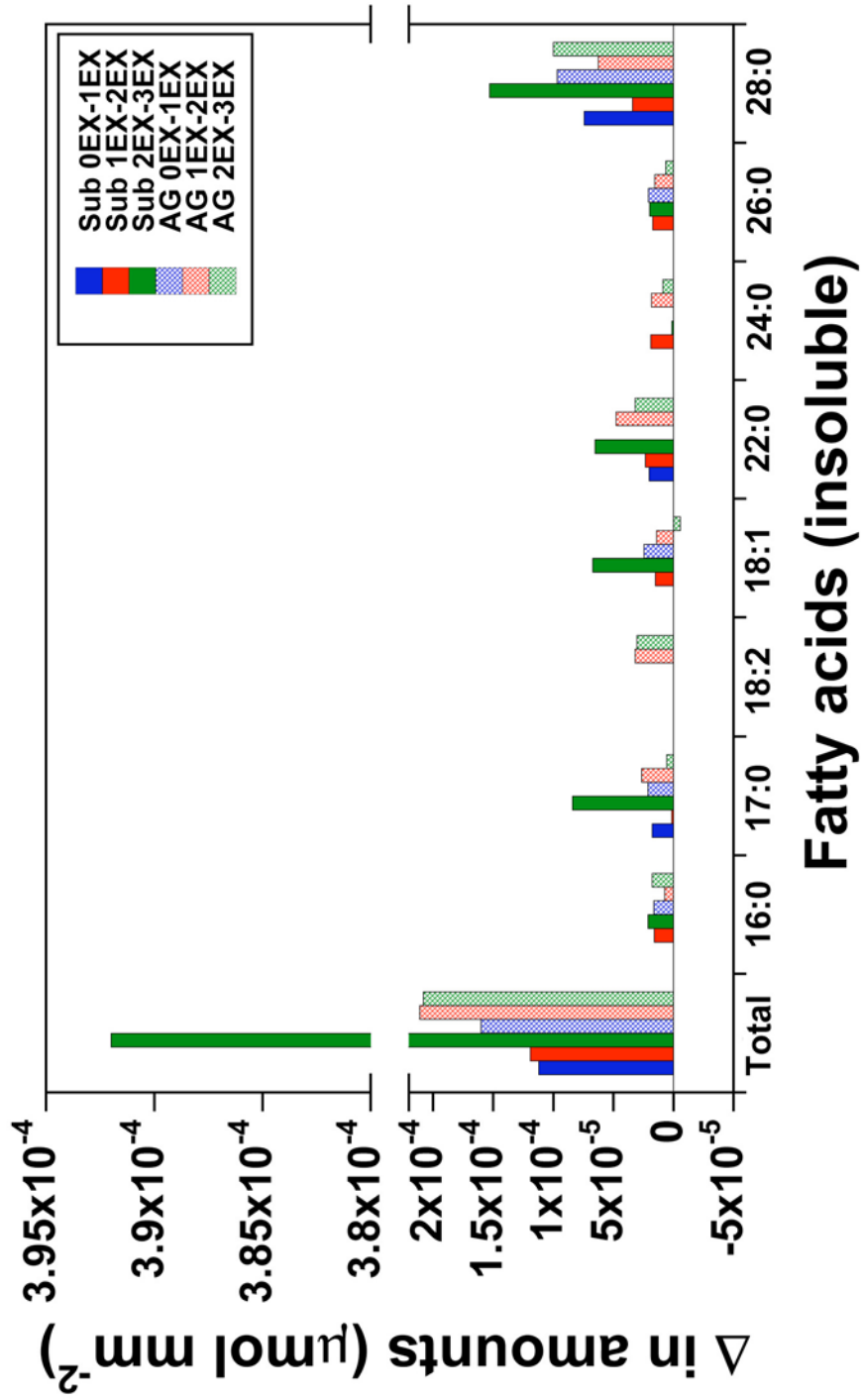
Supplementary Figure 4.1 Change in amounts of α,ω -dioic acids in the SPAD of the maturing MEX in *Iris germanica* roots. Data are displayed per root segment surface area ($\mu\text{mol mm}^{-2}$), and refer to the change in monomer amounts from one exodermal maturation stage to the next, under different growth conditions (legend inset). See section 4.3.2, Chapter 4, for data calculation details. Abbreviations: Sub 0EX-1EX = submerged tissue, monomer amounts in the first exodermal layer; Sub 1EX-2EX = submerged tissue, change in amounts between exodermal layers one and two; Sub 2EX-3EX = submerged tissue, change in amounts between exodermal layers two and three; AG 0EX-1EX = air gap-exposed tissue, monomer amounts in the first exodermal layer; AG 1EX-2EX = air gap-exposed tissue, change in amounts between exodermal layers one and two; AG 2EX-3EX = air gap-exposed, change in amounts between exodermal layers two and three.



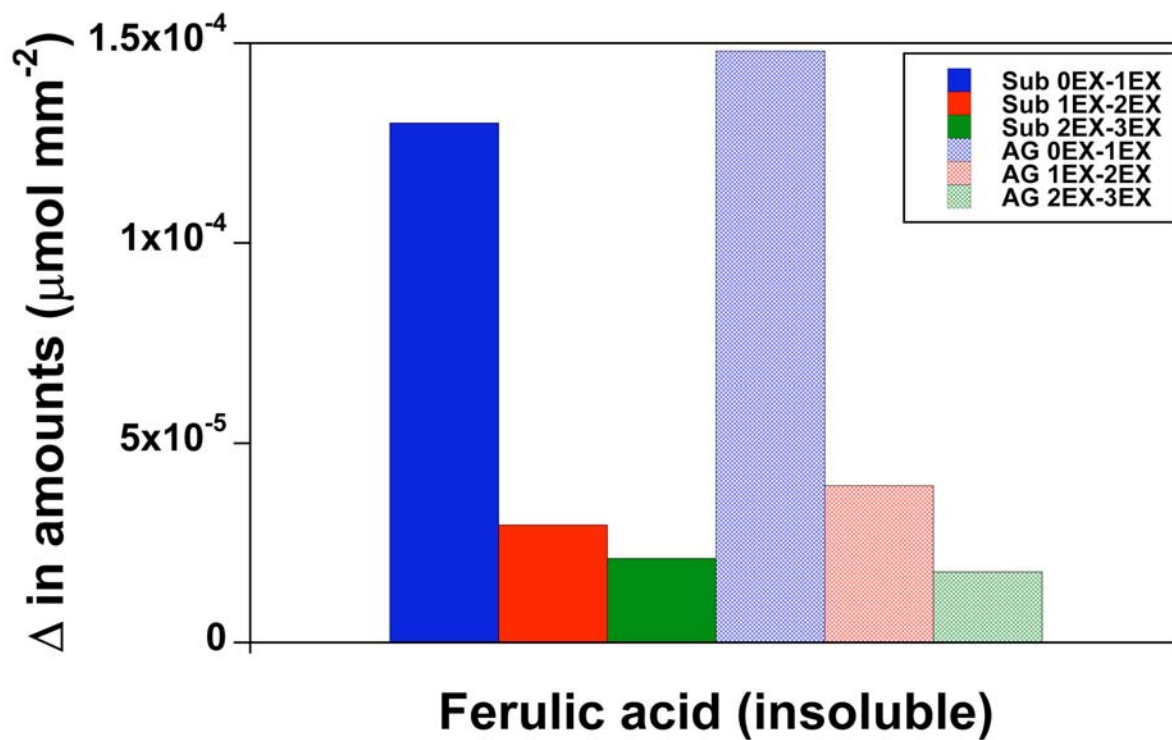
Supplementary Figure 4.2 Change in amounts of ω -OH fatty acids in the SPAD of the maturing MEX in *Iris germanica* roots. Data are displayed per root segment surface area ($\mu\text{mol mm}^{-2}$), and refer to the change in monomer amounts from one exodermal maturation stage to the next, under different growth conditions (legend inset). See section 4.3.2, Chapter 4, for data calculation details. Abbreviations: Sub 0EX-1EX = submerged tissue, monomer amounts in the first exodermal layer; Sub 1EX-2EX = submerged tissue, change in amounts between exodermal layers one and two; Sub 2EX-3EX = submerged tissue, change in amounts between exodermal layers two and three; AG 0EX-1EX = air gap-exposed tissue, monomer amounts in the first exodermal layer; AG 1EX-2EX = air gap-exposed tissue, change in amounts between exodermal layers one and two; AG 2EX-3EX = air gap-exposed, change in amounts between exodermal layers two and three.



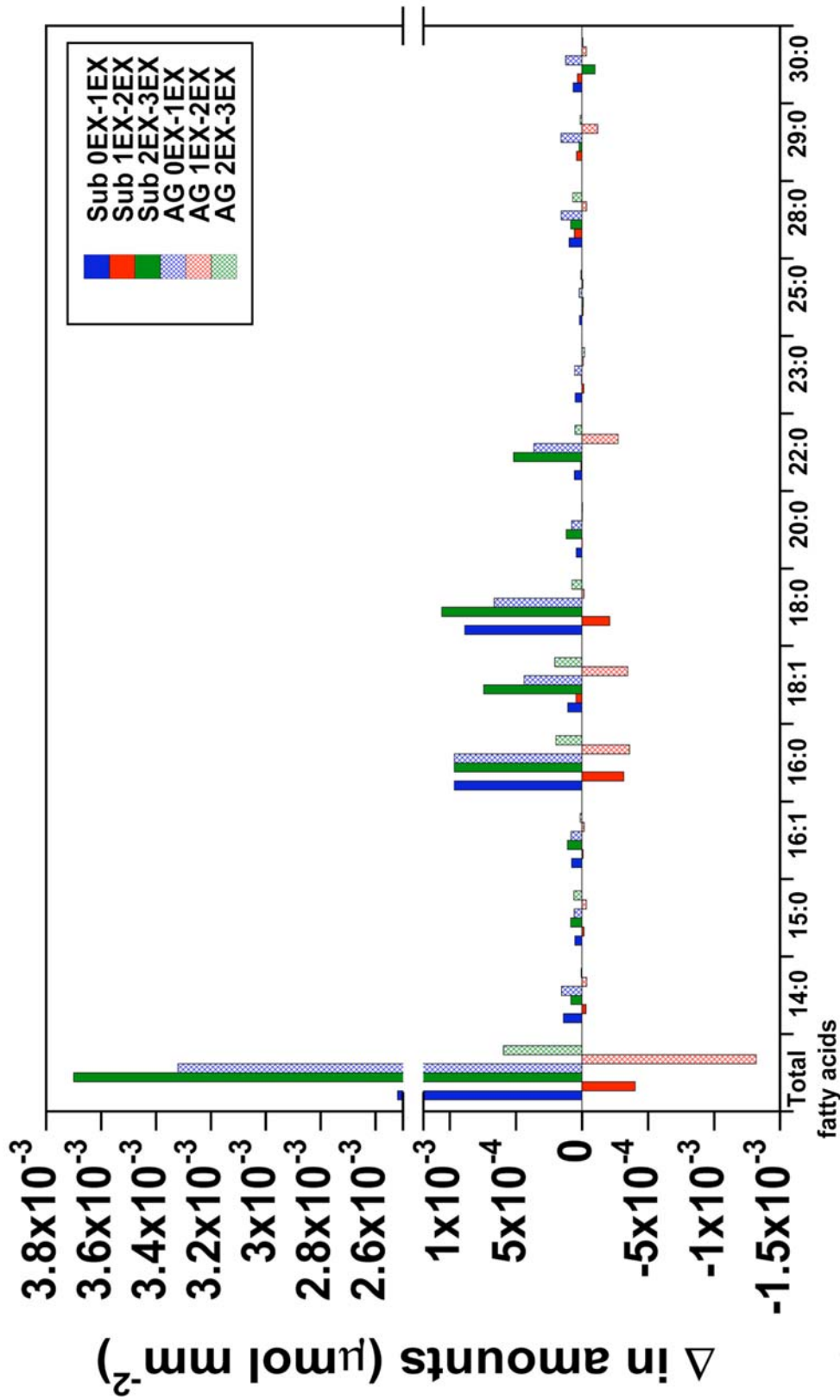
Supplementary Figure 4.3 Change in amounts of fatty acids in the SPAD of the maturing MEX in *Iris germanica* roots. Data are displayed per root segment surface area ($\mu\text{mol mm}^{-2}$), and refer to the change in monomer amounts from one exodermal maturation stage to the next, under different growth conditions (legend inset). See section 4.3.2, Chapter 4, for data calculation details. Abbreviations: Sub 0EX-1EX = submerged tissue, monomer amounts in the first exodermal layer; Sub 1EX-2EX = submerged tissue, change in amounts between exodermal layers one and two; Sub 2EX-3EX = submerged tissue, change in amounts between exodermal layers two and three; AG 0EX-1EX = air gap-exposed tissue, monomer amounts in the first exodermal layer; AG 1EX-2EX = air gap-exposed tissue, change in amounts between exodermal layers one and two; AG 2EX-3EX = air gap-exposed, change in amounts between exodermal layers two and three.



Supplementary Figure 4.4 Change in amounts of ferulic acid in the SPAD of the maturing MEX in *Iris germanica* roots. Data are displayed per root segment surface area ($\mu\text{mol mm}^{-2}$), and refer to the change in monomer amounts from one exodermal maturation stage to the next, under different growth conditions (legend inset). See section 4.3.2, Chapter 4, for data calculation details. Abbreviations: Sub 0EX-1EX = submerged tissue, monomer amounts in the first exodermal layer; Sub 1EX-2EX = submerged tissue, change in amounts between exodermal layers one and two; Sub 2EX-3EX = submerged tissue, change in amounts between exodermal layers two and three; AG 0EX-1EX = air gap-exposed tissue, monomer amounts in the first exodermal layer; AG 1EX-2EX = air gap-exposed tissue, change in amounts between exodermal layers one and two; AG 2EX-3EX = air gap-exposed, change in amounts between exodermal layers two and three.

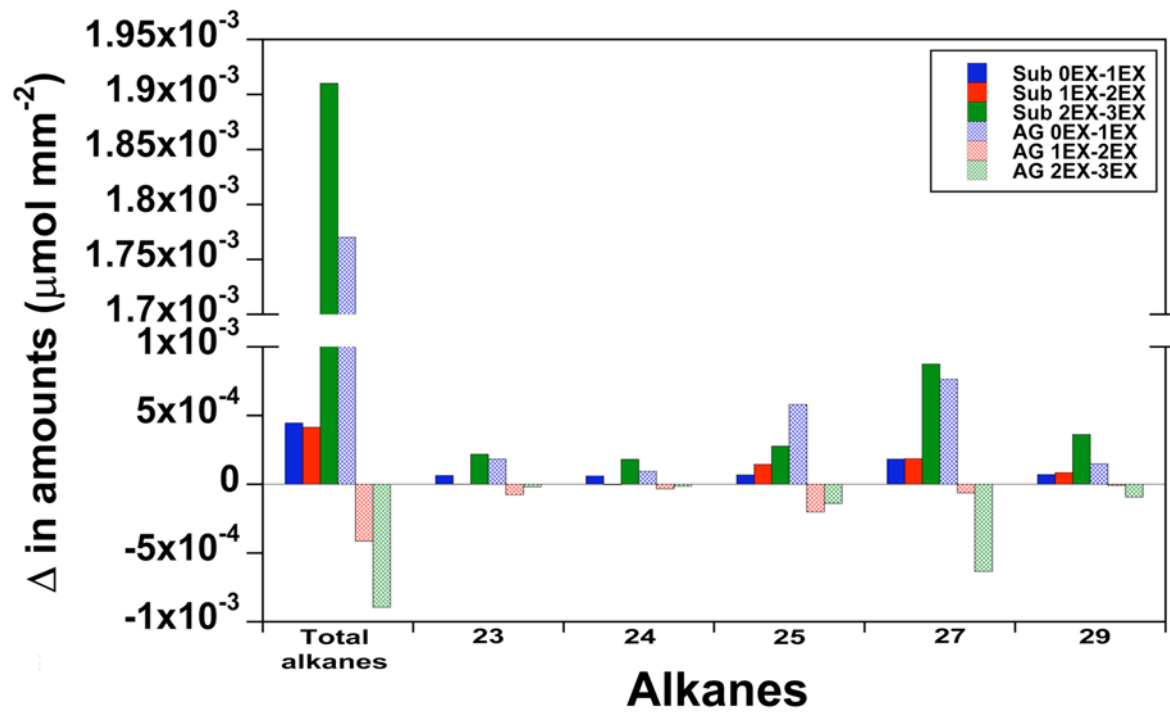


Supplementary Figure 4.5 Change in amounts of fatty acids in the soluble suberin fraction of the maturing MEX in *Iris germanica* roots. Data are displayed per root segment surface area ($\mu\text{mol mm}^{-2}$), and refer to the change in monomer amounts from one exodermal maturation stage to the next, under different growth conditions (legend inset). See section 4.3.2, Chapter 4, for data calculation details. Abbreviations: Sub 0EX-1EX = submerged tissue, monomer amounts in the first exodermal layer; Sub 1EX-2EX = submerged tissue, change in amounts between exodermal layers one and two; Sub 2EX-3EX = submerged tissue, change in amounts between exodermal layers two and three; AG 0EX-1EX = air gap-exposed tissue, monomer amounts in the first exodermal layer; AG 1EX-2EX = air gap-exposed tissue, change in amounts between exodermal layers one and two; AG 2EX-3EX = air gap-exposed, change in amounts between exodermal layers two and three.

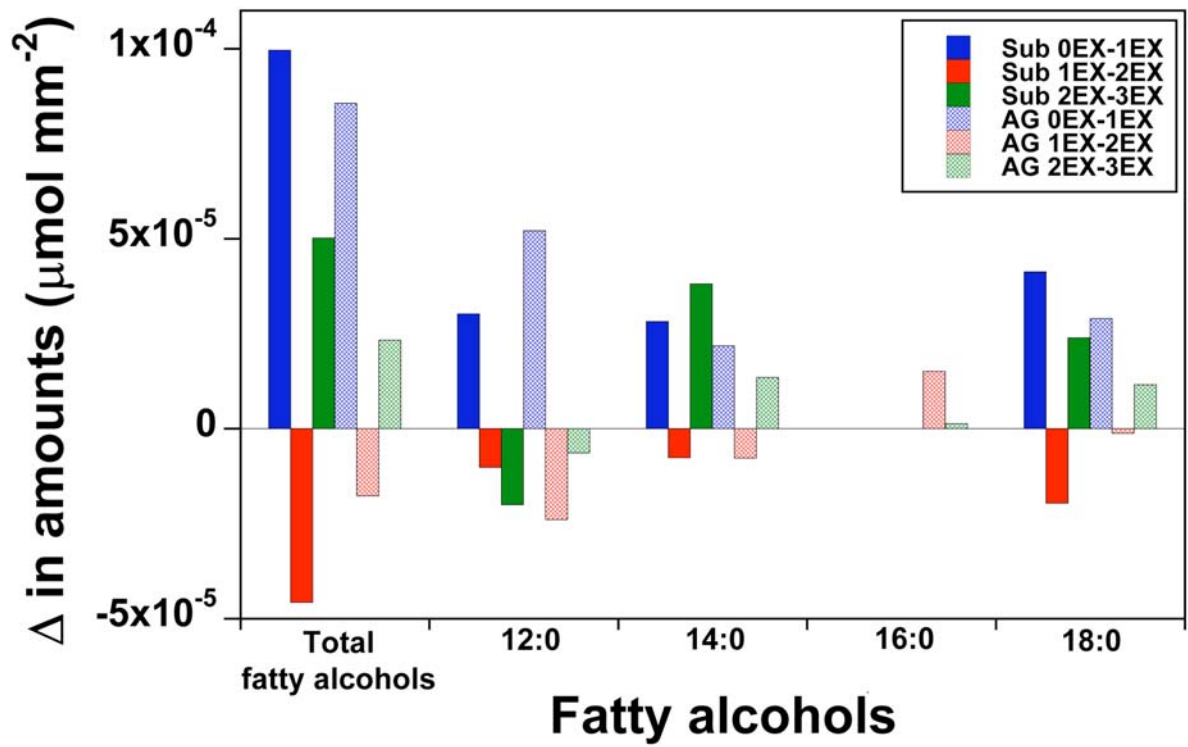


Fatty acids (soluble)

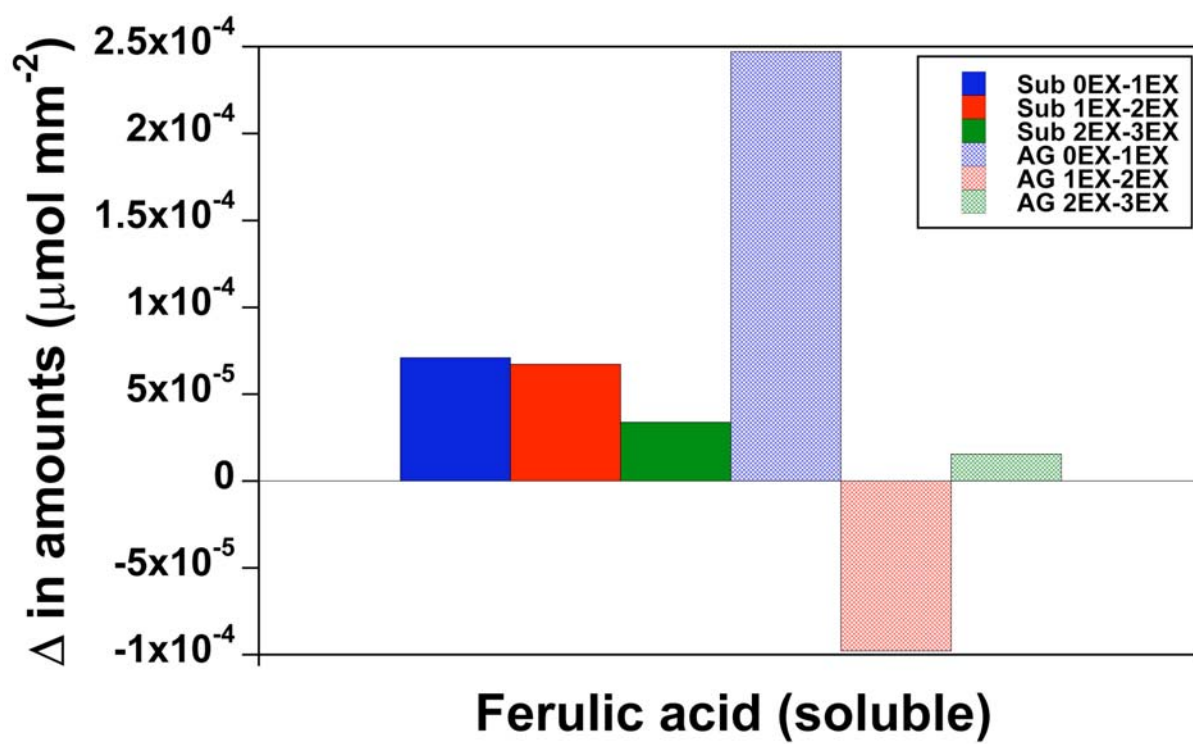
Supplementary Figure 4.6 Change in amounts of alkanes in the soluble suberin fraction of the maturing MEX in *Iris germanica* roots. Data are displayed per root segment surface area ($\mu\text{mol mm}^{-2}$), and refer to the change in monomer amounts from one exodermal maturation stage to the next, under different growth conditions (legend inset). See section 4.3.2, Chapter 4, for data calculation details. Abbreviations: Sub 0EX-1EX = submerged tissue, monomer amounts in the first exodermal layer; Sub 1EX-2EX = submerged tissue, change in amounts between exodermal layers one and two; Sub 2EX-3EX = submerged tissue, change in amounts between exodermal layers two and three; AG 0EX-1EX = air gap-exposed tissue, monomer amounts in the first exodermal layer; AG 1EX-2EX = air gap-exposed tissue, change in amounts between exodermal layers one and two; AG 2EX-3EX = air gap-exposed, change in amounts between exodermal layers two and three.



Supplementary Figure 4.7 Change in amounts of fatty alcohols in the soluble suberin fraction of the maturing MEX in *Iris germanica* roots. Data are displayed per root segment surface area ($\mu\text{mol mm}^{-2}$), and refer to the change in monomer amounts from one exodermal maturation stage to the next, under different growth conditions (legend inset). See section 4.3.2, Chapter 4, for data calculation details. Abbreviations: Sub 0EX-1EX = submerged tissue, monomer amounts in the first exodermal layer; Sub 1EX-2EX = submerged tissue, change in amounts between exodermal layers one and two; Sub 2EX-3EX = submerged tissue, change in amounts between exodermal layers two and three; AG 0EX-1EX = air gap-exposed tissue, monomer amounts in the first exodermal layer; AG 1EX-2EX = air gap-exposed tissue, change in amounts between exodermal layers one and two; AG 2EX-3EX = air gap-exposed, change in amounts between exodermal layers two and three.



Supplementary Figure 4.8 Change in amounts of ferulic acid in the soluble suberin fraction of the maturing MEX in *Iris germanica* roots. Data are displayed per root segment surface area ($\mu\text{mol mm}^{-2}$), and refer to the change in monomer amounts from one exodermal maturation stage to the next, under different growth conditions (legend inset). See section 4.3.2, Chapter 4, for data calculation details. Abbreviations: Sub 0EX-1EX = submerged tissue, monomer amounts in the first exodermal layer; Sub 1EX-2EX = submerged tissue, change in amounts between exodermal layers one and two; Sub 2EX-3EX = submerged tissue, change in amounts between exodermal layers two and three; AG 0EX-1EX = air gap-exposed tissue, monomer amounts in the first exodermal layer; AG 1EX-2EX = air gap-exposed tissue, change in amounts between exodermal layers one and two; AG 2EX-3EX = air gap-exposed, change in amounts between exodermal layers two and three.



Appendix C – Declaration of research collaborations

This thesis is a compilation of four articles, each of which include different research work. Most of the work was carried out by myself independently at the University of Waterloo (UW) with Dr. Carol A. Peterson, the University of Bayreuth (Bayreuth) with Dr. Ernst Steudle, and the University of Western Ontario (UWO) with Dr. Mark A. Bernards.

The majority of experiments in Chapter 2 were conducted by myself at UW. The root apical meristem work was carried out and interpreted by Dr. James L. Seago at SUNY, Oswego. I wrote the manuscript with input from Drs. Peterson (UW) and Seago.

All experimental work in Chapter 3 was conducted by myself at Bayreuth. Interpretation of the results was a collaborative effort with Drs. Steudle (Bayreuth) and Peterson. I wrote the manuscript with input from Drs. Steudle and Peterson.

All experimental work in Chapters 4 and 5 was conducted by myself at UW and UWO. Interpretation of the results was a collaborative effort with Dr. Bernards (UWO). I wrote the manuscripts with input from Drs. Bernards and Peterson.

References

- Agrawal V, Kolattukudy P. 1977.** Biochemistry of suberization: ω -hydroxyacid oxidation in enzyme preparations from suberizing potato tuber disks. *Plant Physiology* **59**: 667-672.
- Agrawal V, Kolattukudy P. 1978a.** Purification and characterization of a wound-induced ω -hydroxyfatty acid:NADP oxidoreductase from potato tuber disks (*Solanum tuberosum* L.). *Archives of Biochemistry and Biophysics* **191**: 452-465.
- Agrawal V, Kolattukudy P. 1978b.** Mechanism of action of a wound-induced ω -hydroxy fatty acid:NADP oxidoreductase isolated from potato tubers (*Solanum tuberosum* L.). *Archives of Biochemistry and Biophysics* **191**: 466-478.
- Aloni R, Enstone DE, Peterson CA. 1998.** Indirect evidence for bulk water flow in root cortical cell walls of three dicotyledonous species. *Planta* **207**: 1-7.
- Angeles G, Bond B, Boyer JS, Brodribb T, Brooks JR, Burns MJ, Cavender-Bares J, Clearwater M, Cochard H, Comstock J, Davis SD, Domec JC, Donovan L, Ewers F, Gartner B, Hacke U, Hinckley T, Holbrook NM, Jones HG, Kavanagh K, Law B, Lopez-Portillo J, Lovisolo C, Martin T, Martinez-Vilalta J, Mayr S, Meinzer FC, Melcher P, Mencuccini M, Mulkey S, Nardini A, Neufeld HS, Passioura J, Pockman WT, Pratt RB, Rambal S, Richter H, Sack L, Salleo S, Schubert A, Schulte P, Sparks JP, Sperry J, Teskey R, Tyree M. 2004.** The cohesion-tension theory. *New Phytologist* **163**: 451-452.
- Armstrong J, Armstrong W. 2001.** Rice and *Phragmites*: effects of organic acids on growth, root permeability, and radial oxygen loss to the rhizosphere. *American Journal of Botany* **88**: 1359-1370.
- Armstrong J, Armstrong W. 2005.** Rice: sulfide-induced barriers to root radial oxygen loss, Fe^{2+} and water uptake, and lateral root emergence. *Annals of Botany* **96**: 625-638.
- Armstrong W, Cousins D, Armstrong J, Turner DW, Beckett PM. 2000.** Oxygen distribution in wetland plant roots and permeability barriers to gas-exchange with the rhizosphere: a microelectrode and modelling study with *Phragmites australis*. *Annals of Botany* **86**: 687-703.
- Baker DA. 1971.** Barriers to the radial diffusion of ions in maize roots. *Planta* **98**: 285-293.
- Barnabas A, Peterson C. 1992.** Development of Casparian bands and suberin lamellae in the endodermis of onion roots. *Canadian Journal of Botany* **70**: 2233-2237.
- Barrowclough DE, Peterson CA. 1994.** Effects of growing conditions and development of the underlying exodermis on the vitality of the onion root epidermis. *Physiologia Plantarum* **92**: 343-349.
- Barrowclough DE, Peterson CA, Steudle E. 2000.** Radial hydraulic conductivity along developing onion roots. *Journal of Experimental Botany* **51**: 547-557.

- Beisson F, Li Y, Bonaventure G, Pollard M, Ohlrogge JB. 2007.** The acyltransferase GPAT5 is required for the synthesis of suberin in seed coat and root of *Arabidopsis*. *The Plant Cell* **19**: 351-368.
- Bernards MA. 2002.** Demystifying suberin. *Canadian Journal of Botany* **80**: 227-240.
- Bernards MA, Fleming WD, Llewellyn DB, Priefer R, Yang X, Sabatino A, Plourde GL. 1999.** Biochemical characterization of the suberization-associated anionic peroxidase of potato. *Plant Physiology* **121**: 135-46.
- Bernards MA, Lewis NG. 1998.** The macromolecular aromatic domain in suberized tissue: a changing paradigm. *Phytochemistry* **47**: 915-933.
- Bernards MA, Lopez M, Zajicek J, Lewis N. 1995.** Hydroxycinnamic acid-derived polymers constitute the polyaromatic domain of suberin. *Journal of Biological Chemistry* **270**: 7382-7386.
- Bernards MA, Summerhurst D, Razem F. 2004.** Oxidases, peroxidases and hydrogen peroxide: the suberin connection. *Phytochemistry Reviews* **3**: 113-126.
- Bonnett HT, Jr. 1968.** The root endodermis: fine structure and function. *The Journal of Cell Biology* **37**: 199-205.
- Borg-Olivier O, Monties B. 1993.** Lignin, suberin, phenolic acids and tyramine in the suberized, wound-induced potato periderm. *Phytochemistry* **32**: 601-606.
- Boursiac Y, Chen S, Luu DT, Sorieul M, van den Dries N., Maurel C. 2005.** Early effects of salinity on water transport in *Arabidopsis* roots. Molecular and cellular features of aquaporin expression. *Plant Physiology* **139**: 790-805.
- Bray EA, Bailey-Serres J, Weretilnyk E. 2000.** Responses to abiotic stresses. In: Buchanan BB, Gruissem W, Jones RL, eds. *Biochemistry and Molecular Biology of Plants*. Rockville, Maryland: American Society of Plant Physiologists, 1158-1203.
- Browse J, McCourt PJ, Somerville CR. 1986.** Fatty acid composition of leaf lipids determined after combined digestion and fatty acid methyl ester formation from fresh tissue. *Analytical Biochemistry* **152**: 141-145.
- Brundrett MC, Enstone DE, Peterson CA. 1988.** A berberine-aniline blue fluorescent staining procedure for suberin, lignin and callose in plant tissue. *Protoplasma* **146**: 133-142.
- Brundrett MC, Kendrick B, Peterson CA. 1991.** Efficient lipid staining in plant material with Sudan red 7B or Fluorol yellow 088 in polyethylene glycol-glycerol. *Biotechnic and Histochemistry* **66**: 111-116.
- Cholewa E, Peterson CA. 2001.** Detecting exodermal Casparian bands in vivo and fluid-phase endocytosis in onion (*Allium cepa* L.) roots. *Canadian Journal of Botany* **79**: 30-37.
- Cholewa E, Peterson CA. 2004.** Evidence for symplastic involvement in the radial movement of calcium in onion roots. *Plant Physiology* **134**: 1793-1802.

- Clarkson DT. 1996.** Root structure and sites of ion uptake. In: Waisel Y, Eshel A, Kafkafi U, eds. *Plant Roots: The Hidden Half, 2nd Ed.* New York: Marcel Dekker, Inc, 483-510.
- Clarkson DT, Robards AW, Stephens JE, Stark M. 1987.** Suberin lamellae in the hypodermis of maize (*Zea mays*) roots; development and factors affecting the permeability of hypodermal layers. *Plant, Cell and Environment* **10**: 83-93.
- Colombo SJ, Asselstine MF. 1989.** Root hydraulic conductivity and root growth capacity of black spruce (*Picea mariana*) seedlings. *Tree Physiology* **5**: 73-81.
- Compagnon V, Diehl P, Benveniste I, Meyer D, Schaller H, Schreiber L, Franke R, Pinot F. 2009.** CYP86B1 is required for very long chain ω -hydroxyacid and α,ω -dicarboxylic acid synthesis in root and seed suberin polyester. *Plant Physiology* **150**: 1831-1843.
- Cruz RT, Jordan WR, Drew MC. 1992.** Structural changes and associated reduction of hydraulic conductance in roots of *Sorghum bicolor* L. following exposure to water deficit. *Plant Physiology* **99**: 203-212.
- Cui H, Levesque MP, Vernoux T, Jung JW, Paquette AJ, Gallagher KL, Wang JY, Blilou I, Scheres B, Benfey PN. 2007.** An evolutionarily conserved mechanism delimiting SHR movement defines a single layer of endodermis in plants. *Science* **316**: 421-425.
- Dainty J. 1963.** Water relations of plant cells. *Advances in Botanical Research* **1**: 279-326.
- Damus M, Peterson RL, Enstone DE, Peterson CA. 1997.** Modifications of cortical cell walls in roots of seedless vascular plants. *Botanica Acta* **110**: 190-195.
- Dean B, Kolattukudy PE. 1977.** Biochemistry of suberization: incorporation of [1-¹⁴C]oleic acid and [1-¹⁴C]acetate into the aliphatic components of suberin in potato tuber disks (*Solanum tuberosum*). *Plant Physiology* **59**: 48-54.
- de Rufz de Lavison M. 1910.** Du mode de pénétration de quelques sels dans la plante vivante. Role de l'endoderme. *Revue Générale de Botanique* **22**: 225-240.
- De Simone O, Haase K, Muller E, Junk WJ, Hartmann K, Schreiber L, Schmidt W. 2003.** Apoplasmic barriers and oxygen transport properties of hypodermal cell walls in roots from four Amazonian tree species. *Plant Physiology* **132**: 206-217.
- Dixon H, Joly J. 1894.** On the ascent of sap. *Proceedings of the Royal Society of London* **57**: 3-5.
- Dixon RA, Chen F, Guo D, Parvathi K. 2001.** The biosynthesis of monolignols: a "metabolic grid", or independent pathways to guaiacyl and syringyl units? *Phytochemistry* **57**: 1069-1084.
- Duan H, Schuler MA. 2005.** Differential expression and evolution of the Arabidopsis CYP86A subfamily. *Plant Physiology* **137**: 1067-1081.
- Enstone DE, Peterson CA. 1992.** The apoplastic permeability of root apices. *Canadian Journal of Botany* **70**: 1502-1512.

- Enstone DE, Peterson CA. 1997.** Suberin deposition and band plasmolysis in the corn (*Zea mays* L.) root exodermis. *Canadian Journal of Botany* **75**: 1188-1199.
- Enstone DE, Peterson CA. 1998.** Effects of exposure to humid air on epidermal viability and suberin deposition in maize (*Zea mays* L.) roots. *Plant, Cell and Environment* **21**: 837-844.
- Enstone DE, Peterson CA. 2005.** Suberin lamella development in maize seedling roots grown in aerated and stagnant conditions. *Plant, Cell and Environment* **28**: 444-455.
- Enstone DE, Peterson CA, Ma F. 2003.** Root endodermis and exodermis: structure, function, and responses to the environment. *Journal of Plant Growth Regulation* **21**: 335-351.
- Esau K. 1965.** *Plant anatomy, 2nd Ed.* New York: John Wiley and Sons.
- Evert RF, Botha CEJ, Mierzwa RJ. 1985.** Free-space marker studies on the leaf of *Zea mays* L. *Protoplasma* **126**: 62-73.
- Franke R, Briesen I, Wojciechowski T, Faust A, Yephremov A, Nawrath C, Schreiber L. 2005.** Apoplastic polyesters in *Arabidopsis* surface tissues - a typical suberin and a particular cutin. *Phytochemistry* **66**: 2643-2658.
- Franke R, Höfer R, Briesen I, Emsermann M, Efremova N, Yephremov A, Schreiber L. 2009.** The DAISY gene from *Arabidopsis* encodes a fatty acid elongase condensing enzyme involved in the biosynthesis of aliphatic suberin in roots and the chalaza-micropyle region of seeds. *Plant Journal* **57**: 80-95.
- Franke R, Schreiber L. 2007.** Suberin - a biopolyester forming apoplastic plant interfaces. *Current Opinion in Plant Biology* **10**: 252-259.
- Fiscus EL. 1975.** The interaction between osmotic- and pressure-induced water flow in plant roots. *Plant Physiology* **55**: 917-922.
- Galliard T. 1973.** Lipids of potato tubers. I. lipid and fatty acid composition of tubers from different varieties of potato. *Journal of the Science of Food and Agriculture* **24**: 617-622.
- Graça J, Pereira H. 2000a.** Methanolysis of bark suberins: analysis of glycerol and acid monomers. *Phytochemical Analysis* **11**: 45-51.
- Graça J, Pereira H. 2000b.** Suberin structure in potato periderm: glycerol, long-chain monomers, and glyceryl and feruloyl dimers. *Journal of Agricultural and Food Chemistry* **48**: 5476-5483.
- Guerinot ML, Yi Y. 1994.** Iron: nutritious, noxious, and not readily available. *Plant Physiology* **104**: 815-820.
- Grymaszewska G, Golinowski W. 1987.** The structure of the endodermis during the development of wheat (*Triticum aestivum* L.) roots. *Acta Societatis Botanicorum Poloniae* **56**: 3-10.

- Haas DL, Carothers ZB. 1975.** Some ultrastructural observations on endodermal cell development in *Zea mays* roots. *American Journal of Botany* **62**: 336-348.
- Hall RD. 2006.** Plant metabolomics: from holistic hope, to hype, to hot topic. *New Phytologist* **169**: 453-468.
- Heimsch C, Seago JL, Jr. 2008.** Organization of the root apical meristem in angiosperms. *American Journal of Botany* **95**: 1-21.
- Helariutta Y, Fukaki H, Wysocka-Diller JW, Nakajima K, Jung J, Sena G, Hauser MT, Benfey PN. 2000.** The *SHORT-ROOT* gene controls radial patterning of the *Arabidopsis* root through radial signaling. *Cell* **101**: 555-567.
- Held B, Wang H, Wurtele E, Colbert J. 1993.** An mRNA putatively coding for an *O*-methyltransferase accumulates preferentially in maize roots and is located predominantly in the region of the endodermis. *Plant Physiology* **102**: 1001-1008.
- Holloway P. 1983.** Some variations in the composition of suberin from the cork layers of higher plants. *Phytochemistry* **22**: 495-502.
- Hose E, Clarkson DT, Steudle E, Schreiber L, Hartung W. 2001.** The exodermis - a variable apoplastic barrier. *Journal of Experimental Botany* **52**: 2245-2264.
- Höfer R, Briesen I, Beck M, Pinot F, Schreiber L, Franke R. 2008.** The *Arabidopsis* cytochrome P450 CYP86A1 encodes a fatty acid ω -hydroxylase involved in suberin monomer biosynthesis. *Journal of Experimental Botany* **59**: 2347-2360.
- Javot H, Maurel C. 2002.** The role of aquaporins in root water uptake. *Annals of Botany* **90**: 301-313.
- Jensen WA. 1962.** *Botanical histochemistry – principles and practice*. San Francisco: W.H. Freeman.
- Johansen DA. 1940.** *Plant microtechnique*. New York: McGraw-Hill.
- Joshi A, Knipfer T, Steudle E. 2009.** Effects of water storage in the stele on measurements of the hydraulics of young roots of corn and barley. *New Phytologist* **184**: 631-643.
- Kamula SA, Peterson CA, Mayfield CI. 1994.** The plasmalemma surface area exposed to the soil solution is markedly reduced by maturation of the exodermis and death of the epidermis in onion roots. *Plant, Cell and Environment* **17**: 1183-1193.
- Karahara I, Shibaoka H. 1992.** Isolation of Casparian strips from pea roots. *Plant and Cell Physiology* **33**: 555-561.
- Kemper Center PlantFinder.** Missouri Botanical Garden. 27 Jun 2008
<<http://www.mobot.org/gardeninghelp/plantfinder/Search.asp>>
- Knipfer T, Das D, Steudle E. 2007.** During measurements of root hydraulics with pressure probes, the contribution of unstirred layers is minimized in the pressure relaxation mode: comparison with pressure clamp and high-pressure flowmeter. *Plant, Cell and Environment* **30**: 845-860.

- Knipfer T, Steudle E. 2008.** Root hydraulic conductivity measured by pressure clamp is substantially affected by internal unstirred layers. *Journal of Experimental Botany* **59**: 2071–2084.
- Kolattukudy PE. 1980.** Biopolyester membranes of plants: cutin and suberin. *Science* **208**: 990-1000.
- Kolattukudy PE. 1984.** Biochemistry and function of cutin and suberin. *Canadian Journal of Botany* **62**: 2918-2933.
- Kolattukudy PE. 2001.** Polyesters in higher plants. In: Scheper T, ed. *Advances in biochemical engineering biotechnology. Vol. 71: Biopolyesters*. Berlin: Springer-Verlag, 1–19.
- Kolattukudy PE, Dean B. 1974.** Structure, gas chromatographic measurement, and function of suberin synthesized by potato tuber tissue slices. *Plant Physiology* **54**: 116-121.
- Krishnamurthy P, Ranathunge K, Franke R, Prakash HS, Schreiber L, Mathew MK. 2009.** The role of root apoplastic transport barriers in salt tolerance of rice (*Oryza sativa* L.). *Planta* **230**: 119-134.
- Kroemer K. 1903.** Wurzelhaut, Hypodermis und Endodermis der Angiospermenwurzel. *Bibliotheca Botanica* **59**: 1-148.
- Kunst L, Samuels A. 2003.** Biosynthesis and secretion of plant cuticular wax. *Progress in Lipid Research* **42**: 51-80.
- Kurdyukov S, Faust A, Trenkamp S, Bär S, Franke R, Efremova N, Tietjen K, Schreiber L, Saedler H, Yephremov A. 2006.** Genetic and biochemical evidence for involvement of HOTHEAD in the biosynthesis of long-chain α,ω -dicarboxylic fatty acids and formation of extracellular matrix. *Planta* **224**: 315-329.
- Lee S, Jung S, Go Y, Kim H, Kim J, Cho H, Park OK, Suh M. 2009.** Two *Arabidopsis* 3-ketoacyl CoA synthase genes, KCS20 and KCS2/DAISY, are functionally redundant in cuticular wax and root suberin biosynthesis, but differentially controlled by osmotic stress. *Plant Journal* **60**: 462-475.
- Lehmann H, Stelzer R, Holzamer S, Kunz U, Gierth M. 2000.** Analytical electron microscopical investigations on the apoplastic pathways of lanthanum transport in barley roots. *Planta* **211**: 816-822.
- Li Y, Beisson F, Ohlrogge J, Pollard M. 2007.** Monoacylglycerols are components of root waxes and can be produced in the aerial cuticle by ectopic expression of a suberin-associated acyltransferase. *Plant Physiology* **144**: 1267-1277.
- Lipetz J. 1970.** Wound healing in higher plants. *International Review of Cytology* **27**: 1–28.
- Lopes MH, Gil AM, Silvestre ADJ, Neto CP. 2000a.** Composition of suberin extracted upon gradual methanolysis of *Quercus suber* L. cork. *Journal of Agricultural and Food Chemistry* **48**: 383–391.

- Lopes MH, Sarychev A, Neto CP, Gil AM. 2000b.** Spectra editing of ¹³C CP/MAS NMR spectra of complex systems: application to the structural characterization of cork cell walls. *Solid State NMR* **16**: 109–121.
- Lu F, Ralph J. 1997.** Derivatization followed by reductive cleavage (DFRC Method), a new method for lignin analysis: protocol for analysis of DFRC monomers. *Journal of Agricultural and Food Chemistry* **45**: 2590-2592.
- Lulai E, Corsini D. 1998.** Differential deposition of suberin phenolic and aliphatic domains and their roles in resistance to infection during potato tuber (*Solanum tuberosum* L.) wound-healing. *Physiological and Molecular Plant Pathology* **53**: 209-222.
- Lulai EC, Morgan WC. 1992.** Histochemical probing of potato periderm with neutral red: a sensitive cytofluorochrome for the hydrophobic domain of suberin. *Biotechnic and Histochemistry* **67**: 185–195.
- Lux A, Morita S, Abe J, Ito K. 2005.** An improved method for clearing and staining free-hand sections and whole-mount samples. *Annals of Botany* **96**: 989-996.
- Ma F, Peterson CA. 2000.** Plasmodesmata in onion (*Allium cepa* L.) roots: a study enabled by improved fixation and embedding techniques. *Protoplasma* **211**: 103–115.
- Ma F, Peterson CA. 2001a.** Development of cell wall modifications in the endodermis and exodermis of *Allium cepa* roots. *Canadian Journal of Botany* **79**: 621-634.
- Ma F, Peterson C. 2001b.** Frequencies of plasmodesmata in *Allium cepa* L. roots: implications for solute transport pathways. *Journal of Experimental Botany* **52**: 1051-1061.
- Ma F, Peterson C. 2003.** Current insights into the development, structure, and chemistry of the endodermis and exodermis of roots. *Canadian Journal of Botany* **81**: 405–421.
- Mattinen M, Filpponen I, Jarvinen R, Li B, Kallio H, Lehtinen P, Argyropoulos D. 2009.** Structure of the polyphenolic component of suberin isolated from potato (*Solanum tuberosum* var. Nikola). *Journal of Agricultural and Food Chemistry* **57**: 9747-9753.
- Matzke K, Riederer M. 1991.** A comparative study into the chemical constitution of cutins and suberins from *Picea abies* (L.) Karst., *Quercus robur* L., and *Fagus sylvatica* L. *Planta* **185**: 233-245.
- Maurel C. 1997.** Aquaporins and water permeability of plant membranes. *Annual Review of Plant Physiology and Plant Molecular Biology* **48**: 399–429.
- Maurel C, Verdoucq L, Luu DT, Santoni V. 2008.** Plant aquaporins: membrane channels with multiple integrated functions. *Annual Review of Plant Biology* **59**: 595–624.
- McCully ME. 1999.** Roots in soil: unearthing the complexities of roots and their rhizospheres. *Annual Review of Plant Physiology and Plant Molecular Biology* **50**: 695-718.
- McCully ME, Mallett JE. 1993.** The branch roots of *Zea*. 3, vascular connections and bridges for nutrient recycling. *Annals of Botany* **71**: 327-341.

- Melchior W, Steudle E. 1993.** Water transport in onion (*Allium cepa* L.) roots. *Plant Physiology* **101**: 1305-1315.
- Meyer CJ, Seago JL, Peterson CA. 2009.** Environmental effects on the maturation of the endodermis and multiseriate exodermis of *Iris germanica* roots. *Annals of Botany* **103**: 687–702.
- Meyer CJ, Steudle E, Peterson CA. 2007.** Patterns and kinetics of water uptake by soybean seeds. *Journal of Experimental Botany* **58**: 717-732.
- Meyer K, Shirley AM, Cusumano JC, Bell-Lelong DA, Chapple C. 1998.** Lignin monomer composition is determined by the expression of a cytochrome P450-dependent monooxygenase in *Arabidopsis*. *Proceedings of the National Academy of Sciences* **95**: 6619-6623.
- Miyamoto N, Steudle E, Hirasawa T, Lafitte R. 2001.** Hydraulic conductivity of rice roots. *Journal of Experimental Botany* **52**: 1835-1846.
- Moon G, Peterson C, Peterson R. 1984.** Structural, chemical, and permeability changes following wounding in onion roots. *Canadian Journal of Botany* **62**: 2253–2259.
- Munns R, Tester M. 2008.** Mechanisms of salinity tolerance. *Annual Review of Plant Biology* **59**: 651–681.
- Negrel J, Pollet B, Lapierre C. 1996.** Ether-linked ferulic acid amides in natural and wound periderms of potato tuber. *Phytochemistry* **43**: 1195–1199.
- Nightingale ER. 1959.** Phenomenological theory of ion solvation. Effective radii of hydrated ions. *Journal of Physical Chemistry* **63**: 1381-1387.
- Nobel PS. 2005.** *Physicochemical and environmental plant physiology, 3rd Ed.* San Diego: Elsevier Academic Press.
- North GB, Nobel PS. 1991.** Changes in hydraulic conductivity and anatomy caused by drying and rewetting roots of *Agave deserti* (Agavaceae). *American Journal of Botany* **78**: 906-915.
- North GB, Nobel PS. 1995.** Hydraulic conductivity of concentric root tissues of *Agave deserti* Engelm. under wet and drying conditions. *New Phytologist* **130**: 47-57.
- Nye PH, Tinker PB. 1977.** *Solute movement in the soil-root system.* Oxford: Blackwell Scientific.
- O'Brien TP, Feder N, McCully ME. 1964.** Polychromatic staining of plant cell walls by Toluidine Blue O. *Protoplasma* **59**: 369-373.
- Pearse AG. 1968.** *Histochemistry (theoretical and applied).* London: J & A Churchill Ltd.
- Perumalla CJ, Peterson CA. 1986.** Deposition of Casparian bands and suberin lamellae in the exodermis and endodermis of young corn and onion roots. *Canadian Journal of Botany* **64**: 1873-1878.

Perumalla CJ, Peterson CA, Enstone DE. 1990. A survey of angiosperm species to detect hypodermal Casparian bands. I. Roots with a uniseriate hypodermis and epidermis. *Botanical Journal of the Linnean Society* **103**: 93-112.

Peterson CA. 1987. The exodermal Casparian band of onion blocks apoplastic movement of sulphate ions. *Journal of Experimental Botany* **32**: 2068–2081.

Peterson CA. 1997. The exodermis and its interactions with the environment. In: Flores HE, Lynch JP, Eissenstat D, eds. *Radical Biology: Advances and Perspectives on the Function of Plant Roots. Proceedings of the 11th Annual Penn State Symposium in Plant Physiology May 22-24, 1997*. Rockville, Maryland: American Society of Plant Biologists, 131-138.

Peterson CA, Enstone DE. 1996. Functions of passage cells in the endodermis and exodermis of roots. *Physiologia Plantarum* **97**: 592-598.

Peterson CA, Lefcourt BEM. 1990. Development of endodermal Casparian bands and xylem in lateral roots of broad bean. *Canadian Journal of Botany* **68**: 2729–2735.

Peterson CA, Moon GJ. 1993. The effect of lateral root outgrowth on the structure and permeability of the onion root exodermis. *Botanica Acta* **106**: 411-418.

Peterson CA, Murrmann M, Steudle E. 1993. Location of the major barriers to water and ion movement in young roots of *Zea mays* L. *Planta* **190**: 127-136.

Peterson CA, Perumalla CJ. 1984. Development of the hypodermal Casparian band in corn and onion roots. *Journal of Experimental Botany* **35**: 51-57.

Peterson CA, Perumalla CJ. 1990. A survey of angiosperm species to detect hypodermal Casparian bands. II. Roots with a multiseriate hypodermis or epidermis. *Botanical Journal of the Linnean Society* **103**: 113-125.

Peterson CA, Peterson RL, Robards AW. 1978. A correlated histochemical and ultrastructural study of the epidermis and hypodermis of onion roots. *Protoplasma* **96**: 1–21.

Plants for a Future. The Field, Penpol, Lostwithiel, Cornwall, PL22 0NG, UK. 27 Jun 2008 <<http://www.pfaf.org>>

Ranathunge K, Kotula L, Steudle E, Lafitte R. 2004. Water permeability and reflection coefficient of the outer part of young rice roots are differently affected by closure of water channels (aquaporins) or blockage of apoplastic pores. *Journal of Experimental Botany* **55**: 433-448.

Ranathunge K, Steudle E, Lafitte R. 2003. Control of water uptake by rice (*Oryza sativa* L.): role of the outer part of the root. *Planta* **217**: 193-205.

Ranathunge K, Steudle E, Lafitte R. 2005a. Blockage of apoplastic bypass-flow of water in rice roots by insoluble salt precipitates analogous to a Pfeffer cell. *Plant, Cell and Environment* **28**: 121-133.

Ranathunge K, Steudle E, Lafitte R. 2005b. A new precipitation technique provides evidence for the permeability of Casparian bands to ions in young roots of corn (*Zea mays* L.) and rice (*Oryza sativa* L.). *Plant, Cell and Environment* **28**: 1450-1462.

- Ranathunge K, Thomas RH, Fang X, Peterson CA, Gijzen M, Bernards MA. 2008.** Soybean root suberin and partial resistance to root rot caused by *Phytophthora sojae*. *Phytopathology* **98**: 1179-1189.
- Raven PH, Evert RF, Eichhorn SE. 1999.** *Biology of plants, 6th Ed.* New York: WH Freeman and Company.
- Razem FA, Bernards MA. 2003.** Reactive oxygen species production in association with suberization: evidence for an NADPH-dependent oxidase. *Journal of Experimental Botany* **54**: 935-941.
- Riederer M, Schönherr J. 1986.** Quantitative gas chromatographic analysis of methyl esters of hydroxy fatty acids derived from plant cutin. *Journal of Chromatography A* **360**: 151-161.
- Robards AW, Clarkson DT, Sanderson J. 1979.** Structure and permeability of the epidermal/hypodermal layers of the sand sedge (*Carex arenaria* L.). *Protoplasma* **101**: 331-347.
- Robards AW, Jackson SM, Clarkson DT, Sanderson J. 1973.** The structure of barley roots in relation to the transport of ions into the stele. *Protoplasma* **77**: 291-311.
- Rüdinger M, Hallgren SW, Steudle E, Schulze ED. 1994.** Hydraulic and osmotic properties of spruce roots. *Journal of Experimental Botany* **45**: 1413-1425.
- Samuels L, Kunst L, Jetter R. 2008.** Sealing plant surfaces: cuticular wax formation by epidermal cells. *Annual Review of Plant Biology* **59**: 683-707.
- Sands R, Fiscus EL, Reid CPP. 1982.** Hydraulic properties of pine and bean roots with varying degrees of suberization, vascular differentiation and mycorrhizal infection. *Australian Journal of Plant Physiology* **9**: 559-569.
- Schreiber L. 1996.** Chemical composition of Casparian strips isolated from *Clivia miniata* Reg. roots: evidence for lignin. *Planta* **199**: 596-601.
- Schreiber L, Breiner H, Riederer M, Düggelin M, Guggenheim R. 1994.** The Casparian strip of *Clivia miniata* Reg. roots: isolation, fine structure and chemical nature. *Botanica Acta* **107**: 353-361.
- Schreiber L, Franke R, Hartmann K. 2005a.** Wax and suberin development of native and wound periderm of potato (*Solanum tuberosum* L.) and its relation to peridermal transpiration. *Planta* **220**: 520-530.
- Schreiber L, Franke R, Lessire R. 2005b.** Biochemical characterization of elongase activity in corn (*Zea mays* L.) roots. *Phytochemistry* **66**: 131-138.
- Schreiber L, Franke R, Hartmann K. 2005c.** Effects of NO₃ deficiency and NaCl stress on suberin deposition in rhizo- and hypodermal (RHCW) and endodermal cell walls (ECW) of castor bean (*Ricinus communis* L.) roots. *Plant and Soil* **269**: 333-339.
- Schreiber L, Hartmann K, Skrabs M, Zeier J. 1999.** Apoplastic barriers in roots: chemical composition of endodermal and hypodermal cell walls. *Journal of Experimental Botany* **50**: 1267-1280.

- Seago JL, Jr., Marsh LC. 1989.** Adventitious root development in *Typha glauca*, with emphasis on the cortex. *American Journal of Botany* **76**: 909-923.
- Seago JL, Jr., Peterson CA, Enstone DE, Scholey CA. 1999.** Development of the endodermis and hypodermis of *Typha glauca* Godr. and *Typha angustifolia* L. roots. *Canadian Journal of Botany* **77**: 122-134.
- Seago JL, Jr., Peterson CA, Kinsley LJ, Broderick J. 2000.** Development and structure of the root cortex in *Caltha palustris* L. and *Nymphaea odorata* Ait. *Annals of Botany* **86**: 631-640.
- Serra O, Soler M, Hohn C, Franke R, Schreiber L, Prat S, Molinas M, Figueras M. 2009a.** Silencing of StKCS6 in potato periderm leads to reduced chain lengths of suberin and wax compounds and increased peridermal transpiration. *Journal of Experimental Botany* **60**: 697-707.
- Serra O, Soler M, Hohn C, Sauveplane V, Pinot F, Franke R, Schreiber L, Prat S, Molinas M, Figueras M. 2009b.** CYP86A33-targeted gene silencing in potato tuber alters suberin composition, distorts suberin lamellae, and impairs the periderm's water barrier function. *Plant Physiology* **149**: 1050-1060.
- Shishkoff N. 1986.** *The dimorphic hypodermis of plant roots: its distribution in the angiosperms, staining properties, and interaction with root-invading fungi.* PhD Thesis, Cornell University, USA.
- Soliday CL, Kolattukudy PE, Davis RW. 1979.** Chemical and ultrastructural evidence that waxes associated with the suberin polymer constitute the major diffusion barrier to water vapor in potato tuber (*Solanum tuberosum* L.). *Planta* **146**: 607-614.
- Soukup A, Armstrong W, Schreiber L, Franke R, Votrubová O. 2007.** Apoplastic barriers to radial oxygen loss and solute penetration: a chemical and functional comparison of the exodermis of two wetland species, *Phragmites australis* and *Glyceria maxima*. *New Phytologist* **173**: 264-278.
- Soukup A, Votrubová O, Čížková H. 2002.** Development of anatomical structure of roots of *Phragmites australis*. *New Phytologist* **153**: 277-287.
- Stadelmann EJ, Kinzel H. 1972.** Vital staining of plant cells. In: Prescott VDM, ed. *Methods in Cell Physiology*. New York: Academic Press, 325-372.
- Stark RE, Garbow JR. 1992.** Nuclear magnetic resonance relaxation studies of plant polyester dynamics. 2. Suberized potato cell wall. *Macromolecules* **25**: 149-154.
- Stasovski E, Peterson CA. 1993.** Effects of drought and subsequent rehydration on the structure, vitality, and permeability of *Allium cepa* adventitious roots. *Canadian Journal of Botany* **71**: 700-707.
- Steudle E. 2001.** The cohesion-tension mechanism and the acquisition of water by plant roots. *Annual Review of Plant Physiology and Plant Molecular Biology* **52**: 847-875.

- Steudle E, Brinckmann E. 1989.** The osmometer model of the root: water and solute relations of *Phaseolus coccineus*. *Botanica Acta* **102**: 85–95.
- Steudle E, Frensch J. 1989.** Osmotic responses of maize roots. *Planta* **177**: 281–295.
- Steudle E, Jeschke WD. 1983.** Water transport in barley roots. *Planta* **158**: 237–248.
- Steudle E, Meshcheryakov AB. 1996.** Hydraulic and osmotic properties of oak roots. *Journal of Experimental Botany* **47**: 387–401.
- Steudle E, Murrmann M, Peterson CA. 1993.** Transport of water and solutes across maize roots modified by puncturing the endodermis. Further evidence for the composite transport model of the root. *Plant Physiology* **103**: 335–349.
- Steudle E, Oren R, Schulze ED. 1987.** Water transport in maize roots. Measurement of hydraulic conductivity, solute permeability, and of reflection coefficients of excised roots using the root pressure probe. *Plant Physiology* **84**: 1220–1232.
- Steudle E, Peterson CA. 1998.** How does water get through roots? *Journal of Experimental Botany* **49**: 775–788.
- Steudle E, Tyerman SD. 1983.** Determination of permeability coefficients, reflection coefficients, and hydraulic conductivity of *Chara corallina* using the pressure probe: effects of solute concentration. *Journal of Membrane Biology* **75**: 85–96.
- Stevens KJ. 2003.** *The role of root system characteristics in plant responses to flooding and drought*. PhD Thesis, University of Guelph, Canada.
- Stevens PF. 2001 onwards.** Angiosperm Phylogeny Website. Version 9, June 2008 [and more or less continuously updated since].
<<http://www.mobot.org/MOBOT/research/APweb/>>
- Taleisnik E, Peyrano G, Cordoba A, Arias C. 1999.** Water retention capacity in root segments differing in the degree of exodermis development. *Annals of Botany* **83**: 19–27.
- Taylor JA, West DW. 1980.** The use of Evan's blue stain to test the survival of plant cells after exposure to high salt and high osmotic pressure. *Journal of Experimental Botany* **31**: 571–576.
- Thomas R, Fang X, Ranathunge K, Anderson TR, Peterson CA, Bernards MA. 2007.** Soybean root suberin: anatomical distribution, chemical composition, and relationship to partial resistance to *Phytophthora sojae*. *Plant Physiology* **144**: 299–311.
- Trethewey JAK, Campbell LM, Harris PJ. 2005.** (1→3),(1→4)-β-D-glucans in the cell walls of the Poales (sensu lato): an immunogold labelling study using a monoclonal antibody. *American Journal of Botany* **92**: 1660–1674.
- Tropicos.org.** Missouri Botanical Garden. 27 Jun 2008 <<http://www.tropicos.org>>
- Tyerman SD, Bohnert HJ, Maurel C, Steudle E, Smith JAC. 1999.** Plant aquaporins: their molecular biology, biophysics and significance for plant water relations. *Journal of Experimental Botany* **50**: 1055–1071.

- Tyerman SD, Niemietz CM, Bramley H. 2002.** Plant aquaporins: multifunctional water and solute channels with expanding roles. *Plant Cell and Environment* **25**: 173–194.
- Tyree MT, Patino S, Bennink J, Alexander J. 1995.** Dynamic measurements of root hydraulic conductance using a high-pressure flowmeter in the laboratory and field. *Journal of Experimental Botany* **46**: 83–94.
- Tyree MT, Yang S, Cruiziat P, Sinclair B. 1994.** Novel methods of measuring hydraulic conductivity of tree root systems and interpretation using AMAIZED. *Plant Physiology* **104**: 189–199.
- Van Fleet DS. 1961.** Histochemistry and function of the endodermis. *The Botanical Review* **27**: 165–221.
- Vogt E, Schönherr J, Schmidt HW. 1983.** Water permeability of periderm membranes isolated enzymatically from potato tubers (*Solanum tuberosum* L.). *Planta* **158**: 294–301.
- von Guttenberg H. 1968.** Der primäre Bau der Angiospermenwurzeln. In: Linsbauer K, ed. *Handbuch der Pflanzenanatomie, Vol. 8*. Berlin: Gebrüder Borntraeger, 141–159.
- Waduwara CI, Walcott SE, Peterson CA. 2008.** Suberin lamellae of the onion root endodermis: their pattern of development and continuity. *Canadian Journal of Botany* **86**: 623–632.
- Wang Y. 2002.** Ecological, physiological and molecular responses of *Iris hexagona* to salinity stress. PhD thesis, University of Louisiana, Lafayette, Louisiana, USA.
- Wang XL, McCully ME, Canny MJ. 1995.** Branch roots of *Zea V*: structural features that may influence water and nutrient transport. *Botanica Acta* **108**: 209–219.
- Wilcox H. 1962.** Growth studies of the root of incense cedar, *Libocedrus decurrens*. I. The origin and development of primary tissues. *American Journal of Botany* **49**: 221–236.
- Wilson CA, Peterson CA. 1983.** Chemical composition of the epidermal, hypodermal, endodermal and intervening cortical cells walls of various plant roots. *Annals of Botany* **51**: 759–769.
- Wilson AJ, Robards AW. 1978.** The ultrastructural development of mechanically impeded barley roots. Effects on the endodermis and pericycle. *Protoplasma* **95**: 255–265.
- Yang WL, Bernards MA. 2006.** Wound-induced metabolism in potato (*Solanum tuberosum*) tubers. *Plant Signaling & Behavior* **1**: 59–66.
- Yang WL, Bernards MA. 2007.** Metabolite profiling of potato (*Solanum tuberosum* L.) tubers during wound-induced suberization. *Metabolomics* **3**: 147–159.
- Ye Q, Wiera B, Steudle E. 2004.** A cohesion/tension mechanism explains the gating of water channels (aquaporins) in *Chara* internodes by high concentration. *Journal of Experimental Botany* **55**: 449–461.

Zeier J, Goll A, Yokoyama M, Karahara I, Schreiber L. 1999a. Structure and chemical composition of endodermal and rhizodermal/hypodermal walls of several species. *Plant, Cell and Environment* **22**: 271-279.

Zeier J, Ruel K, Ryser U, Schreiber L. 1999b. Chemical analysis and immunolocalisation of lignin and suberin in endodermal and hypodermal/rhizodermal cell walls of developing maize (*Zea mays* L.) primary roots. *Planta* **209**: 1-12.

Zeier J, Schreiber L. 1997. Chemical composition of hypodermal and endodermal cell walls and xylem vessels isolated from *Clivia miniata*: identification of the biopolymers lignin and suberin. *Plant Physiology* **113**: 1223–1231.

Zeier J, Schreiber L. 1998. Comparative investigation of primary and tertiary endodermal cell walls isolated from the roots of five monocotyledoneous species: chemical composition in relation to fine structure. *Planta* **206**: 349-361.

Zeier J, Schreiber L. 1999. Fourier transform infrared-spectroscopic characterisation of isolated endodermal cell walls from plant roots: chemical nature in relation to anatomical development. *Planta* **209**: 537-542.

Zimmermann HM, Hartmann K, Schreiber L, Steudle E. 2000. Chemical composition of apoplastic transport barriers in relation to radial hydraulic conductivity of corn roots (*Zea mays* L.). *Planta* **210**: 302-311.

Zimmermann HM, Steudle E. 1998. Apoplastic transport across young maize roots: effect of the exodermis. *Planta* **206**: 7-19.